The University Of Sheffield.

Thesis Title

In Vitro Modelling of Neuroblastoma Development using Human Pluripotent Stem Cells

Ingrid Maricel Saldaña Guerrero

A thesis submitted in partial fulfilment of the requirements for the degree of Doctor of Philosophy

The University of Sheffield
Faculty of Science
Biomedical Science

Submission Date
07/06/2021

Acknowledgements:

I can hardly believe I am writing this text that will be one of the first pages of my PhD thesis. This is truly a dream come true. I cannot either believe how much the course of my PhD changed since the moment I arrived, but I am undoubtedly very happy and thankful about it. In addition, this is when I want to thanks enormously to my supervisor Dr Anestis Tsakiridis. Thank you for giving me the opportunity to be part of your laboratory, for believing in me. I know this might be a cliché but in my case, I found myself lost within the first year of my PhD thinking that maybe I had made a big mistake by coming to the United Kingdom to study. Thank you for offering me a chance, even when you had no idea who I was and how it was going to be. For all the effort, time and money you invested in me, for always trying to make sure I was being supported. I have truly given my best and I have enjoyed all this time, even when experiments sometimes would not cooperate.

I also want to thank my advisors, Kai Erdmann and Vincent Cunliffe and Freek van Eeden, which gave me their professional guidance but also, offered me support in the moments where I needed it the most. Thank you for helping me to turn this PhD into something I truly enjoyed.

To my lab mates, my friends Matthew and Antigoni. thank you for all the help in the moments of stress, for the guidance, the advice and all the good laughs and pints downed in the pub on a Friday after a very long week. The lab would not have been the same without you guys.

To Neveen, the sister I did not know I had on the other side of the world. Thank you for all those hours of coffee, the long talks, the laughs, the meals and the tears, for being always one of my biggest supports in these 4 years. Thank you for being there for me in the brightest and darkest moments. Your friendship is something I am taking with me for the rest of my life.

To my Latin gang, Brenda and Ernesto, thank you for all those crazy adventures we have had, all the hours of dance in cubanas, all the laughs, the comforting talks, the support and the good company.

To my family, that even when they are 8,000 km away from here, they are always in my heart and mind. Thank you for supporting me even when most of the time you have no idea what I am doing for a living. I know I will always have a place to call home because of you.

To Dylan Stavish. I do not think I can have enough words to let you know how much you have been a support for me. Thank you for all the hours in the lab listening to music, for all your advice, for teaching me countless techniques, for helping me to see science from so many perspectives, for showing me what a good lab mate should be, for giving me the example of hard work, for being such a good influence in my life. You have filled my days with bright light even when I was unable to find the switch. Thank you for being my personal cheerleader, for convincing me that I can do all things I want to do, for being my travel pal, for seeing and tasting the whole world with me. I hope many more adventures come for both of us!

Finally, I want to thank the University of Sheffield, for all the support they have offered me since the moment I arrived in the United Kingdom. For granting me not only an extension to finish my PhD but also a studentship to do it.

Abstract

Neuroblastoma is one of the most common cancers that appear in early childhood. It affects 1 in 8000 live births and accounts for 12%-15% of all deaths in childhood related to cancer. It develops in the sympathetic nervous system and is thought to be derived from trunk neural crest (NC) cells or their sympathoadrenal derivatives during embryonic development. Tumours present different degrees of differentiation and common genetic aberrations associated with poor prognosis in neuroblastoma include amplification of the MYCN gene and chromosome 17q. Current popular models for examining the origins of neuroblastoma involve the use of transgenic mouse lines/primary explants or established human neuroblastoma-derived cell lines. Here I describe the development of a tractable human pluripotent stem cell (hPSC) differentiation *in vitro* system that allows the temporal dissection of the early events associated with neuroblastoma initiation. This involves the efficient generation of the cell types that give rise to neuroblastoma i.e. trunk NC and sympathoadrenal cells from hPSCs. I exploited this system to characterise hPSC lines that harbour neuroblastoma-relevant aberrations such as 17q amplification as well as a line I generated with an inducible MYCN overexpression cassette. I was able to highlight the impact of these aberrations on both cellular specification and cancer-related cellular dynamics along a sympathoadrenal trajectory. The overexpression of MYCN leads to both differentiation blockage and the presentation of cancer hallmarks, whereas 17q amplification presented an undocumented differential response to WNT signalling during trunk axial specification, leading to downstream differentiation defects. My data provides the basis for an *in vitro* model that might fully recapitulate the onset and progression of neuroblastoma in a physiologically relevant context.

Table of Abbreviations

Abbreviation	Meaning
2nd Only	Secondary only antibody staining
BMP	Bone Morphogenetic Protein
BSA	Bovine Serum Albumin
CHIR	CHIR99021 (GSK3β inhibitor)
Ct value	Cycle threshold value
DMEM	Dulbecco's Modified Eagle Medium
EFS	Event-free Survival
ESC	Embryonic Stem Cells
FACS	Fluorescence Activated Cell Sorting
FCS	Fetal Calf Serum
FGF	Fibroblast Growth Factor
GSK3β	Glycogen Synthase Kinase 3 beta
iPS	Induced Pluripotent Stem cell
NMP	Neuromesodermal Progenitor
NC	Neural Crest
SAP	Sympathoadrenal Progenitor
SN	Sympathetic Neurons
PSC	Pluripotent Stem Cells
qPCR	Quantitative Polymerase Chain Reaction

Contents

TABLE OF FIGURES

1 Chapter1: Introduction

1.1 Neuroblastoma

Neuroblastoma is the most common extracranial tumour in early childhood. This malignancy may appear as localised or metastatic tumours, showing a heterogeneous clinical resolution as it can spontaneously regress or progress despite exhaustive therapy (Maris et al., 2007).

The physician Rudolf Virchow that called the tumours “gliomas” first described this malignancy in 1864(Virchow, 1864). In 1891, Marchand noted similarities between tumours derived from the sympathetic nervous system and the adrenal medulla (Marchand, 1891). In 1910, James Homer Wright decided to call them “neuroblastomas” as they resembled those “immature” cells from which the sympathetic nervous system and adrenal medulla arise (Wright, 1910). Later in 1926, these perceptions would be somehow corroborated, as Harvey Cushing and Burt Wolbach reported the spontaneous loss of proliferation and differentiation of a tumour into ganglion cells (Cushing and Wolbach, 1927).

1.2 Diagnosis

Neuroblastoma represents around 10% of childhood malignancies and 15% of cancer deaths in infants. It is normally diagnosed within the first year of life when around 30% of the total incidence is observed. Then, its occurrence decreases with age as 50% of the cases are reported between 1 to 4 years old, and 20% is only found between the ages of 5 to 14(Stiller and Parkin, 1992).

As clinical heterogeneity has been observed in neuroblastoma patients, a classification system has been established with the aim to predict the tumour behaviour and, therefore, provide the best treatment possible for each particular case(Cohn et al., 2009, Brodeur et al., 1993). The extent of the disease is determined by the invasion profile of the tumour, defining the disease stage as local (L1 and L2) or metastatic (M and MS)(Monclair et al., 2009). Around 50% of the patients have a localised mass, commonly this presents in the abdomen with 40% occurring in the adrenal gland and 15% presenting elsewhere in the abdomen. Further sites include regions in thoracic (15%), cervical (5%) and pelvic sympathetic ganglia (5%)(Alexander, 2000, Schulte and Eggert, 2015). Metastases occur in approximately half of the patients and it frequently spreads to bone marrow (70.5%), bone (55.7%), lymph nodes (30.9%), liver (29.6%), and intracranial and orbital sites (18.2%)(DuBois et al., 1999).

The diagnosis of Neuroblastoma requires a variety of tests such as histological assessment of the tumour, imaging studies, metastatic evaluation and laboratory tests. High levels of catecholamines can be detected in nearly all cases of neuroblastoma and they have been related to the degree of

maturation of the tumour(Strenger et al., 2007). The levels of other serum markers such as ferritin and lactate dehydrogenase are also informative(Cangemi et al., 2012).

The age of the patient is one of the most significant factors to determine the disease phenotype. It has been seen that localised primary tumours of patients under 18 months are more likely to undergo spontaneous maturation and regression than in older children (Maris, 2010). This also applies to metastasis when this is restricted to skin, liver and bone marrow (Evans et al., 1980). Other significant factors are combined to determine the disease stage including the grade of tumour differentiation, the status of MYCN and DNA ploidies (Cohn et al., 2009).

Neuroblastoma tumours normally present as large masses consisting of 2 type of cells: The neural type and the schwannian-type. The neural-type cells exhibit varying levels of maturity consisting of primitive neuroblast, differentiating neuroblasts and maturing ganglion cells. The Schwannian-type cells comprise of immature and mature Schwann cells. The balance between neural versus Schwannian has been used to classify predictive outcomes by the INPC (The International Neuroblastoma Pathology Classification) with the most aggressive type containing higher proportions of neural type cells predominantly, primitive neuroblasts(Shimada et al., 1999). These tumours fall in the undifferentiated classification. Undifferentiated neuroblastoma normally exhibits small cells with large nucleoli, this morphology is associated with poor prognosis and the presence of MYC oncogene(Wang et al., 2013a). Histological analysis should be complemented with immunohistochemistry for markers such as tyrosine hydroxylase, cyclin D1, neuron-specific enolase among others, to confirm neuroblastoma identity.

1.3 Genetic factors driving Neuroblastoma

1.3.1 MYCN

In 1983, MYCN was first isolated from homogeneously staining regions (gene amplification signature) in human neuroblastoma cell lines. Then, it was found that it shared certain homology to myc oncogene and it could be amplified more than 100 times(Kohl et al., 1983, Schwab et al., 1985). A few years later, *MYCN* amplification demonstrated to correlate with poor prognosis(Brodeur et al., 1984, Seeger et al., 1985), becoming an important factor to determine the stage of the tumour.

Currently, MYCN belongs to the MYC proto-oncogene family of transcription factors, the other two members are c-MYC and MYCL(Westermark et al., 2011). The amplification/mutation of *MYCN* has not only been correlated with neuroblastoma but also in other cancers such as Wilm's tumour(Nisen et al., 1986), medulloblastoma(Rouah et al., 1989), retinoblastoma(Lee et al., 1984) and

glioblastoma(Hui et al., 2001). All these cancers originate from groups of cells where MYCN is normally involved in the normal development of the tissues.

MYCN, as a member of MYC transcription factor family, exerts control on the expression of genes involved in varied processes within the cell. These include proliferation, migration, synthesis of proteins, metabolism, differentiation and apoptosis(Eilers and Eisenman, 2008). Given its broad influence in regular processes, dysregulation of MYCN can lead to the disruption of vital processes such as differentiation, uncontrolled cell division, metastasis, angiogenesis, modulation of the immune system and apoptosis(Huang and Weiss, 2013).

In 1985, Seeger et al observed that in patients whose tumours harboured more than 10 copies of MYCN, their probability of progression-free survival at 18 months after being diagnosed fell up to 5% compared to 70% of those who only carried an extra copy. Furthermore, if patients were in an advanced stage of the disease, their probability dropped to 0 per cent (Seeger et al., 1985). In a more recent study, using data from 2660 patients, tumours were analysed and their MYCN status correlated to the event-free survival probability. Although all patients harboured low-stage tumours, those with *MYCN* amplification showed less favourable event-free survival (EFS) (53%) versus non-amplified ones (72%)(Bagatell et al., 2009). Therefore, MYCN is a prognosis factor for tumour progression and aggressiveness in patients despite the age and the stage of the disease.

Increased MYC protein expression has also been observed in neuroblastoma. In a cohort of tumours, cells were found to express either MYCN (19%) or MYC (11%). Cells showed unfavourable histology and considerable levels of MKI (Mitosis-Karyorrhexis Index) and both cohorts presented significantly low 3-year event-free survivals (MYCN -46.2%. MYC- 43.4%) (Wang et al., 2015).

1.3.2 ALK

Initially, neuroblastoma had been proposed to be a predisposed event triggered by an initial germline mutation(Knudson and Strong, 1972). However, familial cases of neuroblastoma are exceedingly rare, accounting for 1-2% of the cases (Mossé et al., 2008, Friedman et al., 2005). In 2008, Mosse et al identified a germline mutation in the cell-surface kinase ALK (anaplastic lymphoma kinase) gene, localised in 2p23-24 in the vicinity to *MYCN* gene (2p24). This mutation renders a constitutively active version of the kinase, bolstering the overall penetrance in the hereditable disease. When ALK mRNA was downregulated in neuroblastoma cell lines that harboured either amplifications or mutations of this gene, a significant reduction in proliferation was observed. Furthermore, mutations in ALK were also found in around 11% of tumours harbour amplifications of *MYCN*(Bresler et al., 2014).

ALK gene amplification has been observed in a frequency of 2-4%, and it normally occurs simultaneously with *MYCN* amplification(Subramaniam et al., 2009). This might be explained by their

proximity in the chromosome region. Concomitant expression of ALK/MYCN has been linked with a decrease in overall survival in neuroblastoma (Wang et al., 2013b)

1.3.3 PHOX2B

The paired-like homeobox 2B (PHOX2B) is a protein that participates in the development of the autonomic nervous system. PHOX2B alterations are present in the central hypoventilation syndrome (CCHS)(Amiel et al., 2003), but germline mutations consisting of a loss of function mutation on PHOX2B have also been observed in around 10% of the familial neuroblastoma cases (Mosse et al., 2004, Trochet et al., 2004, Raabe et al., 2008). Although rare, both ALK and PHOX2B mutations result in high penetrance in familial neuroblastoma (Matthay et al., 2016).

1.3.4 LIN28B

Let-7 is a switch gene responsible for the timing of the developmental events (Ambros, 1989). When Let-7 is dysregulated, events specific to a certain stage of development are either omitted or repeated (Ambros and Horvitz, 1984). LIN28B or Lin-28 homolog B is a protein that binds RNA and that negatively regulates the biogenesis of let-7 (miRNA). These proteins are abundantly expressed in stem cells where LIN28 is a master regulator of pluripotency (Yu et al., 2007). LIN28 are also present in tissues in development(Moss et al., 1997). Furthermore, amplifications and overexpression of these proteins have been associated with poor outcome in different types of malignancies (Viswanathan et al., 2009, Wang et al., 2010), therefore their participation as an oncogene was suspected.

Polymorphic alleles in the LIN28B locus are related to high risk in neuroblastoma (Diskin et al., 2012). Additionally, Molenaar et al 2012 showed that high-risk neuroblastomas overexpressed LIN28B, and this was an independent factor associated with poor prognosis. Moreover, when LIN28B was knockdown in neuroblastoma cell lines let-7 levels significantly increased and cell viability diminished. Interestingly, MYCN protein also decreased when LIN28B was downregulated, suggesting that let-7 inhibits the translation of MYCN(Molenaar et al., 2012). Furthermore, it was shown that LIN28B promotes neuroblastoma proliferation through a signalling network with RAN GTPase and Aurora Kinase (Schnepp et al., 2015) and very recently, Chen et al 2020 demonstrated that LIN28B is also a driver of neuroblastoma metastasis aided by PDZ binding kinase (PBK), which promotes self-renewal and migration (Chen et al., 2020). Overall, the interplay between LIN28B, let-7 and MYCN seems to have an important role in the progression of neuroblastoma.

1.3.5 Chromosomal aberrations in neuroblastoma

Almost all high-risk neuroblastomas frequently show segmental chromosomal alterations such as gain and losses of whole and/or segments of chromosomes. And from these, segmental chromosome aberrations are associated with poor prognosis (Janoueix-Lerosey et al., 2009). The recurrent

segmental changes in neuroblastoma are the loss of 1p, 3p, 11q (Spitz et al., 2003, Caron et al., 1996, Attiyeh et al., 2005). Whilst gains normally occur in 1q, 2p and 17q (Diskin et al., 2009, Szewczyk et al., 2019, Hirai et al., 1999).

The gain of chromosome 17q is the most common genetic aberration in neuroblastoma, as it is normally found in more than 50% of the cases (Bown et al., 1999b). Additionally, the presence of 17q aberration is related to adverse clinical outcome, as patients harbouring 17q trisomy showed a significant decrease in their overall survival (Bown et al., 1999b, Bown et al., 2001). It is also associated with the amplification of *MYCN* and older age (Theissen et al., 2014). Trisomy 17q normally presents as an unbalanced translocation in neuroblastoma tumours and although it translocates to a wide range of chromosomes, it has shown a preference for translocation to chromosome 1(Van Roy et al., 1997, Meddeb et al., 1996, Lastowska et al., 1997, Savelyeva et al., 1994, McConville et al., 2001, Stark et al., 2003, Stallings et al., 2004).

Hirai et al 1999 analysed neuroblastoma samples and they observed that, from those in the most advanced stage of the disease, 50% showed a gain at 1q21-25. Additionally, the aberration was also present in all cases showing resistance to chemotherapy treatment.

Loss of 1p36 has been reported in around one-third of neuroblastoma cases and this aberration strongly correlates with *MYCN* amplification. Additionally, 1p36 loss has been associated with a decrease in overall survival, even when patients showed low-risk characteristics (Attiyeh et al., 2005).

Another frequent genetic alteration is the deletion of the chromosome 11q, especially the region 11q23 (Guo et al., 1999). This aberration is found in approximately 35%-45% of neuroblastoma tumours and its presence is almost mutually exclusive with *MYCN* amplification (Guo et al., 1999, Carén et al., 2010, Plantaz et al., 2001). Furthermore, around 80% of the neuroblastoma tumours in the most advanced stage harbour either *MYCN* amplification or deletion of 11q, both strongly correlating to poor prognosis (8 years- OS-35%) (Carén et al., 2010).

1.4 The cell of origin of neuroblastoma

The “cell of origin” in cancer is normally defined as the first normal cell that gains mutations that will eventually lead to the development of cancer. Two models try to explain how this cell of origin progresses. The first theory posits that the heterogeneity within a tumour arises from a common cell type that has suffered multiple mutations resulting in different cellular phenotypes. The second theory proposes that different cells along a differentiation trajectory undergo a mutational event, generating different subtypes within the tumour (Visvader, 2011).

The exact cellular origin of neuroblastoma is still a matter of debate. Its presence in the adrenal glands and its presentation in early development points to the sympathetic lineage and its precursors. However, the precise time of initiation during embryogenesis remains elusive.

Latter stages of sympathetic neuron development have been investigated as the potential cell of origin. Several studies support this notion as the overexpression of the *MYCN* oncogene, driven by the tyrosine hydroxylase promoter (TH), induces tumour formation in an *in vivo* model (Weiss et al., 1997). However, in a separate study, the overexpression of *MYCN* in sympathoadrenal progenitor explants increased proliferation, but it was not sufficient to cause tumour formation (Mobley et al., 2015).

This opens the possibility that initiation might happen at an earlier stage. When MYCN was exogenously expressed in primary neural crests from mice and zebrafish and re-introduce in developing embryos, tumour formation was observed (Olsen et al., 2017, Zhu et al., 2012). Conversely, Yang et al 2020, have claimed that neural crest cells might not be the cell of origin, as human neuroblastoma tumours commonly lack the expression of the neural crest SOX10 expression.

Given that some controversy around the potential cell of origin still exists, understanding the role of all the elements such as precursor states and signalling dynamics involved in the specification of the sympathoadrenal lineage is mandatory to further dissect the mechanisms of neuroblastoma initiation.

1.4.1 Trunk neural crest and the specification of the sympathoadrenal lineage

The elongation of the body axis is generated by a population of bipotent progenitors. These cells possess the capacity to generate neural and mesodermal cell types and they are referred to as Neuromesodermal progenitors (NMPs) or axial progenitors (Tzouanacou et al., 2009b). During early development, at the onset of somitogenesis, NMPs are located in the node streak border and the caudal lateral epiblast (Cambray and Wilson, 2007, Wilson and Beddington, 1996). This population is able to self-regenerate and, while doing so, they fuel the elongation of the posterior axis of the embryo (Tzouanacou et al., 2009a). In mice, NMPs have been found within the Chordoneural Hinge region of the tail bud, showing the capacity of the population to maintain their identity until axial elongation has been fully achieved (Cambray and Wilson, 2002, Tzouanacou et al., 2009a).

The NMP population is normally identified by the co-expression of T(BRACHYURY) (mouse homologue of TBXT) and SOX2 markers (Tsakiridis et al., 2014, Olivera-Martinez et al., 2012). The expression of these markers is maintained through a dynamic signalling network involving WNT and FGF to preserve the NMP population (Amin et al., 2016, Gouti et al., 2014). BRACHYURY expression is activated through WNT signalling and simultaneously, the expression of WNT ligands are induced by BRACHYURY, therefore creating a positive feedback loop (Yamaguchi et al., 1999) (Martin and Kimelman, 2008). On the other hand, the expression of SOX2 is regulated through the N-1 enhancer, which is induced when

the neural plate development starts and remaining active until the posterior neural plate extension has concluded. FGF and WNT signalling are both involved in the activation of the N-1 enhancer (Takemoto et al., 2006).

During the anterior to posterior elongation, the NMP population acquires different positional identities governed by the induction of specific domains of HOX genes. HOX genes are organised in 4 separated clusters (HOXA-HOXB-HOXC-HOXD). The clusters contain genes ordered 1 to 13, which are activated in descending order (anterior to posterior) (Deschamps et al., 1999) and their expression domains are broadly split into hindbrain (HOX1-3), cervical (HOX3-5), branchial (HOX6-7), thoracic (HOX8-9) and lumbosacral (HOX10-13) **(Figure 1)** (reviewed in Mallo et al 2010) .

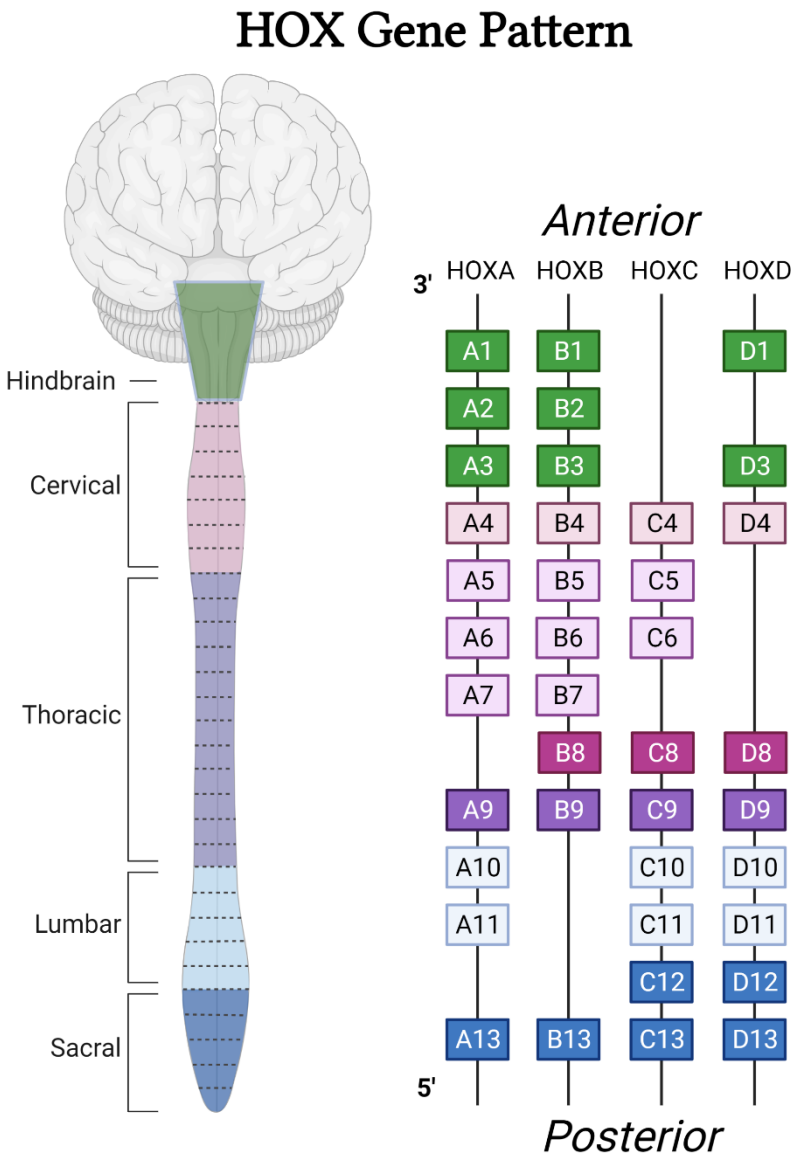

Figure 1: HOX Gene Patterning

Representation of HOX gene clusters patterns and their approximate positions anterior to posterior.

When HOX genes are sufficiently activated, their expression is maintained by Polycomb and trithorax proteins, which mark and sustain their axial identity throughout development (Deschamps et al., 1999). Activation of the WNT signalling leads to the expression of CDX genes (1, 2 and 4), which in turn regulates the expression of posterior HOX genes (Chawengsaksophak et al., 2004, van den Akker et al., 2002, Young et al., 2009). The sole loss of CDX2 disrupts the axial patterning causing axial truncation (Chawengsaksophak et al., 2004).

Therefore, a balancing act between WNT and FGF signalling in a regulatory loop with BRA and SOX2, maintains the NMP bipotent state, simultaneously orchestrated by CDX and HOX proteins to maintain the NMP pool while fuelling the elongation of the posterior axis of the body (Neijts et al., 2014).

The bipotent NMP population, as aforementioned, provides a constant supply of cells to promote the elongation of the postcranial axis of the neural plate. Later, this population will contribute to the formation of the neural tube, somites and notochord(Cambray and Wilson, 2007, Cambray and Wilson, 2002, McGrew et al., 2008, Henrique et al., 2015, Steventon and Martinez Arias, 2017).

1.4.2 Neural crest specification

The initiation of the neural crest specification starts during the gastrulation period when the neural plate border becomes specified. In this neural plate border territory inhabits a precursor of the neural crest(Meulemans and Bronner-Fraser, 2002, Sauka-Spengler and Bronner-Fraser, 2008), a multipotent population from which other cell types also arise such as, among others, the sensory neurons of the central nervous system(Groves and LaBonne, 2014).

The specification of the neural plate border is triggered by a combination of inductive and repressing signals involving the WNT and BMP pathways. WNT and BMP activating signals are found on the lateral region of the embryo, where the presumptive non-neural ectoderm tissue will develop. Whilst WNT and BMP antagonist are expressed in the future neural ectoderm area. This creates a gradient with intermediates levels of WNT/BMP activity, which combined with FGF and NOTCH signals, will give rise to the neural plate border (Reviewed in (Groves and LaBonne, 2014)). The combination of WNT, BMP, FGF and NOTCH results in the activation of genes related to the neural plate border domain called “neural plate border specifiers” which include but are not restricted to TFAP2A, MSX1, ZIC1, GBX2, *PAX3*/7. These genes interact with each other, promoting and sustaining their expression (Monsoro-Burq et al., 2005, Sato et al., 2005, Nikitina et al., 2008, Bhat et al., 2013).

While the neural plate is folding, neural crest specifiers become activated within the neural plate border, the latter is now transitioning towards the pre-migratory neural crest. *PAX3*/7, *MSX1 and ZIC1*

are essential neural plate border genes (Bae et al., 2014, Plouhinec et al., 2014, Barembaum and Bronner, 2013), which co-operate to activate the neural crest specifiers FOXD3, ETS1 (cranial neural crest specific (Théveneau et al., 2007)) and SNAI1/2 (Khudyakov and Bronner-Fraser, 2009a). Although these neural crest specifiers are distinctive for the neural crest progenitors, these cells retain plasticity, thus being able to generate neural crest or ectodermal cells (Selleck and Bronner-Fraser, 1995). To further promote the neural crest specification, WNT signalling is required. The precise mechanisms are still not fully understood. However, it has been demonstrated in chick and frog embryos to drive the expression of SNAI2, FOXD3, ZIC1 and *PAX3* (García-Castro et al., 2002, Sato et al., 2005).

Genes belonging to the neural crest specification stage coordinate in a positive regulatory loop to consolidate their expression. Stable expression leads to the activation of the next set of neural crest specifiers: in the frog, SNAI1/2 encourages the expression of TWIST, FOXD3 and SOX9 (Aybar et al., 2003). In mouse, SNAI2 is activated by SOX10 (Honoré et al., 2003) which in turn is promoted by FOXD3 (Dottori et al., 2001). At this point, the neural plate has folded to form the neural tube, and the neural crest cells reside within the dorsal region of this structure. At this stage, the full complement of neural crest specifiers has been established, and they, in turn, will orchestrate the cellular changes such as EMT, required to promote neural crest delamination.

The migratory neural crest maintains the expression of some of the premigratory neural crest specifiers. These, however, can be regulated by different enhancers (Simões-Costa et al., 2012). SOX10 expression, for example, is driven by two different enhancers depending on whether cells migrate from cranial or trunk regions (Betancur et al., 2010). Other factors have been shown to be important in neural crest migration. During early events of neural crest migration oxygen availability is low because vascularisation has not been completed, therefore hypoxia-inducible factors (HIF) are activated (Dunwoodie, 2009). It has been shown that (HIF)-1α is implicated in the correct specification and delamination of cranial neural crest (Scully et al., 2016). Recently, trunk neural crest, which specification and migration occurs at later stages of development when oxygen levels are higher, have been shown to rely on (HIF)-2α rather than (HIF)-1α. Dysregulation of the expression has been seen to affect trunk neural crest development, self-renewal capacity and the total number of migrating cells (Niklasson et al., 2021). **(Figure 2a)**

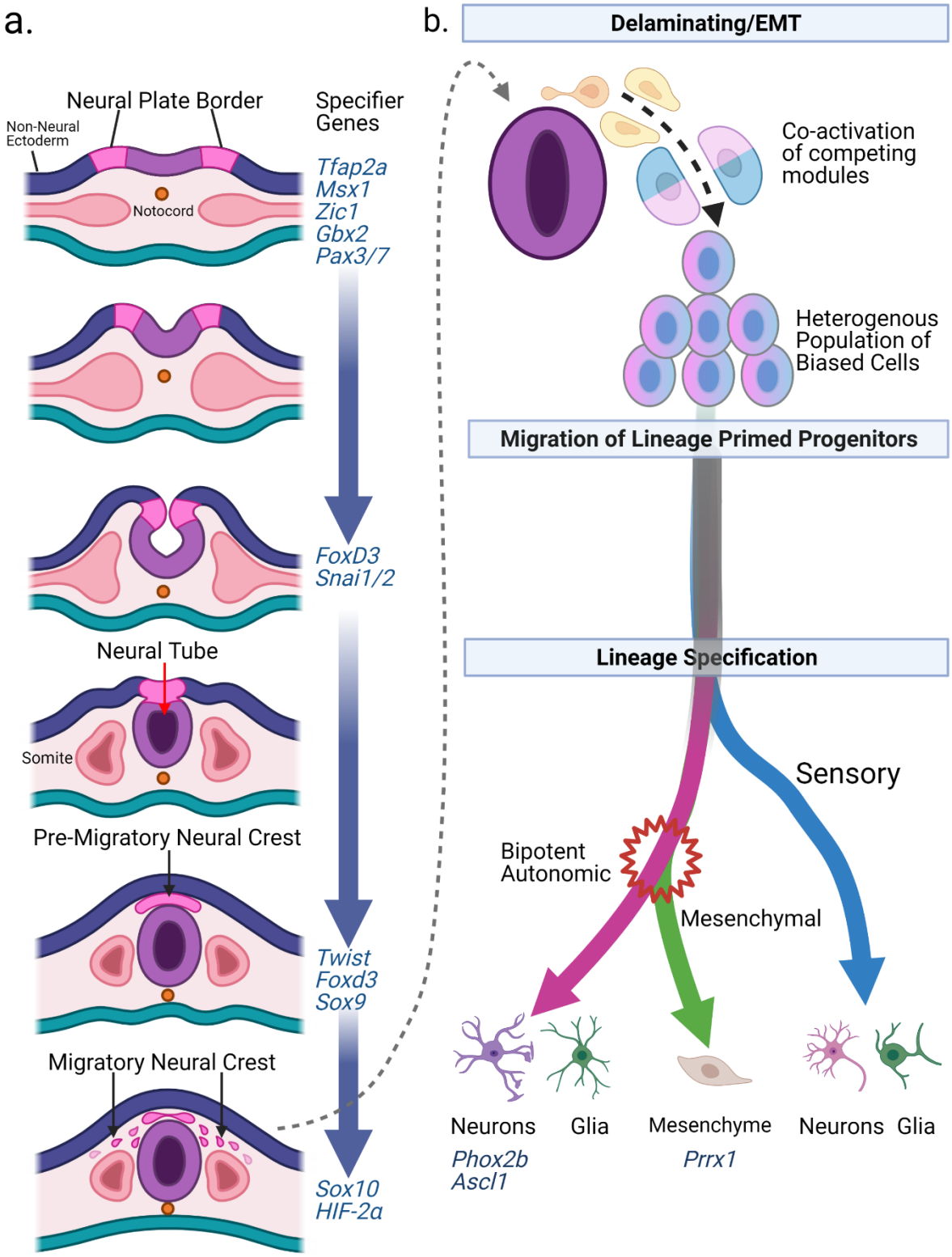

Figure 2: Neural crest and sympathetic specification.

a) A schematic representing the development of the neural crest cells from neural plate border specification through to migration. Important genes involved during the process are annotated. B) Figure adapted from (Soldatov et al., 2019). A representation of the different fate decisions of migrating neural crests towards their final lineage. Specific markers for sympathetic neurons and mesenchyme are shown.

1.4.3 Sympathoadrenal specification

Once neural crest cells have started their migration process, lineage-specific pathways become activated. Differences in the neural crest migratory fates rely on their particular transcription state and their interaction with the environmental signals. In mouse, the migrating neural crest population is heterogeneous, with lineage-primed transcriptional profiles active. Whereas cranial neural crest cells have a bias towards mesenchymal lineage, trunk neural crest cells tend to produce cells of the sensory and autonomic lineages (Soldatov et al., 2019). The first separation within the migrating neural crests leads to the creation of the sensory lineage and an autonomic-mesenchymal progenitor. From the second bifurcation, Phox2b marks a bipotent population that gives rise to the autonomic and mesenchymal cell types. Committed mesenchymal cells will express Prrx1, whilst Ascl1/Phox2b expression is restricted to the autonomic progenitor population (Soldatov et al., 2019) **(Figure 2b).**

Cells committed to the neural fate are pre-specified before delamination and this is reflected by the expression of transcription factors Foxd3, Sox9 and Snai1/2 (Krispin et al., 2010). Foxd3 in particular is required for self-renewal and multipotency of neural crest cells whilst inhibiting mesenchymal fates by promoting neural potential (Stewart et al., 2006).

The neural crest cells that have delaminated from the dorsal part of the neural tube, and are destined to become part of the sympathoadrenal nervous system will follow a ventral pathway through the somites (Serbedzija et al., 1990). As has been aforementioned, SOX10 plays a crucial role in the delaminating neural crest. However, further in development it also impacts upon the sympathetic lineage specification by activating PHOX2B and ASCL1 (Kim et al., 2003). This is supported by the environmental signals cells receive later during migration.

These migrating cells express the chemokine receptor CXCR4 (Kasemeier-Kulesa et al., 2010), and thus they are attracted to the dorsal part of the aorta by chemoattractants stromal cell-derived factor-1 (SDF 1) and Neuregulin 1(NRG1) (Saito et al., 2012). There, the cells receive BMP signals from the dorsal aorta, some of them would then differentiate into the para-vertebral ganglia of the sympathetic trunk (neurons and glia)(Vogel and Weston, 1990), others will continue towards the adrenal gland. BMP2, BMP4 and BMP7 signals emanating from the dorsal aorta specify the sympathetic ganglia, this has been demonstrated in neural crest cell culture and the chick embryo (Varley and Maxwell, 1996, Varley et al., 1995, Reissmann et al., 1996, Shah et al., 1996).

BMP signals will elicit differentiation by further activating key transcription factors such as Phox2b and Ascl1, previously initiated by SOX10. This activation happens in a smad-independent and dependent fashion for Phox2b and Ascl1 respectively (Morikawa et al., 2009b). It has also been reported that

Sonic hedgehog (Shh) is important for appropriate timing and patterning of this stage of the sympathetic nervous system development (Morikawa et al., 2009a).

In the chick embryo, the activation of Phox2b and Ascl1 leads to sequential activation of transcription factors for further development and maintenance of the sympathoadrenal progenitors. The first set of transcription factors activated are Hand2, Phox2a and Gata2 these have been linked with cell survival, differentiation and proliferation (reviewed in (Rohrer, 2011)). Subsequently, upon further maturation, enzymes involved in catecholamine and dopamine biosynthesis, Tyrosine hydroxylase (TH) and Dopamine beta-hydroxylase (*DBH*) are expressed (Xu et al., 2003, Rychlik et al., 2003). This process is aided by the signalling of NGF and BDNF (Hickman et al., 2018, Kasemeier-Kulesa et al., 2015).

A proportion of cells will not remain in the para-aortic region and will continue their way towards the adrenal gland, this fate decision is governed by smad-dependant BMP signalling (Saito et al., 2012). Cells are guided by NRG1, mainly, coming from the adrenal cortex (Vogel and Weston, 1990, Saito et al., 2012). Once they have entered the adrenal medulla, they are exposed to glucocorticoids inducing their further differentiation towards chromaffin cells (Vogel and Weston, 1990, Huber, 2015).

1.4.4 Generation of sympathetic neurons *in vitro*

The cues and key signalling factors involved in the onset and progression towards sympathetic neuron development have been slowly but steadily revealed through the extensive *in vivo* work on developing embryos of different species. One of the founding discoveries that would open the possibilities of the *in vitro*-derived neural crest cells was an experiment that bridged *in vivo* and *in vitro* work. Basch et al 2006 discovered that only a specific part of the chick embryo epiblast generates neural crest and, that this specification can be disrupted by blocking BMP and WNT signals (Basch et al., 2006). A year earlier, sympathetic neurons were generated from human pluripotent stem cells (hPSC) in an *in vitro* system co-culturing with stromal mouse cells. Although the signals involved were not fully understood, this experiment was the proof of principle that neural crest and subsequently sympathetic neurons could be generated *in vitro (Pomp et al., 2005)*. From these discoveries, others started to walk a path to further understand and refine the signals involved in the generation of neural crest cells(Lee et al., 2007, Chambers et al., 2009, Bajpai et al., 2010, Menendez et al., 2011, Mica et al., 2013, Leung et al., 2016, Tchieu et al., 2017). It was not until the integration of the top-down inhibition technique, developed by Hackland in 2017, that highly efficient and reproducible induction of neural crest cells was achieved. The top-down inhibition technique relies on the controlled level of BMP signalling by saturating with endogenous BMP ligands whilst titrating the input signal with an inhibitor of a major BMP receptor.

The differentiations developed up to this point were mainly focused on the production of cranial/anterior neural crest and thus, were not permissive for the development of cell lines of the sympathetic lineage. As the sympathetic lineage stem from the trunk rather than cranial cells, the necessity to develop more posterior neural crest cells was evident. *In vivo* experiments suggested that trunk neural crest arises from NMPs (Schoenwolf et al., 1985, Rodrigo Albors et al., 2018, Wymeersch et al., 2016). Further Metzis et al 2018 showed that cells acquire an axial identity before committing to their neural fate.

Denham et al 2015, created an *in vitro* protocol to generate "caudal" neural crest cells, these cells were first exposed to WNT signalling to induce de expression of TBXT (Brachyury) whilst retaining the expression of SOX2, resembling the traditional markers for NMPs(Denham et al., 2015). Frith et al 2018 developed a new protocol for the derivation of trunk neural crest cells by firstly inducing an NMP state following the protocol set up by Gouti et al 2014 and subsequently incorporation the top-down inhibition approach for neural crest specification detailed by Hackland et al 2017. These cells expressed posterior markers such as HOXC9 as well as specific neural crest markers such as SOX10 and SNAI1/2 (Frith et al., 2018). Then their potential to generate sympathetic neural lineages was confirmed when cells were grown in conditions modified from Oh et al 2016 protocol. Cells showed the expression of early sympathetic markers such as ASCL1/PHOX2B when exposed to BMP and SHH signalling, and more mature markers such as TH and *DBH* were shown after maturation in the presence of GDNF, BDNF and NGF (Oh et al., 2016). This protocol allows for the robust generation of trunk neural crest and this establishes a platform to dissect the development of the sympathetic lineages and model the progression of diseases associated with this lineage such as neuroblastoma.

1.5 Disease modelling with pluripotent stem cells

Understanding the development of human diseases is necessary not only to increase our knowledge about their onset and natural progression but also to generate new targeted treatments. Many different approaches have been developed, and all of them have their advantages and flaws. Primary cultures derived from patients are very useful to characterise cellular and molecular dynamics, however, they have limited expansion capacity *in vitro*. In cancer patients, tumours cells are extracted and although they can be grown indefinitely in culture, they only represent an advanced stage of the disease progression. This could hinder the discovery of the disease origin. Animal modelling also represents an attractive approach to understand disease progression. Although useful, human development processes do not always overlap with those seen in the different models. Therefore, the need for a human viable approach was desired.

Since their derivation in 1998 (Thomson et al., 1998), human embryonic stem cells (hESC) became an attractive tool as they fulfil several of the culture characteristics required, such as indefinite self-renewal capacity, and the ability to form any of the cells from the three germ layers, rendering the possibility to direct their development into the cell type desired. Nonetheless, the use of hESC still raises ethical concerns preventing its widespread usage. Yamanaka circumvented this in 2007 after he announced a method to induce pluripotency in human cells, now called induced pluripotent stem cells (iPSC). This approach would open a world of possibilities as it would allow reprogramming any cell of the body, avoiding difficult tissue biopsies. Also, the cells could be patient-specific, including those carrying disease-related mutations.

Having precious tools such as hESC and iPSC, collectively termed human pluripotent stem cells (hPSC), many protocols have been generated in an attempt to emulate disease development *in vitro*. One of the earliest examples of the use of hESC was in 2004 when Urbach et al used homologous recombination to mutate the HPRT1 gene which is the cause of Lesch-Nyhan disease, a malady characterised by excessive production of uric acid, triggering symptoms similar to gout, the presence of urinary stones and neurological problems. Although it did not fully recapitulate the disease, it did demonstrate the potential for using hESC to dissect disease-related mechanisms and provide a platform for disease modelling and drug screening.

Since then, hPSC have been used to model many diseases (reviewed in (Avior et al., 2016)), covering diseases from heart diseases, neurodevelopmental up to blood disorders (Stein et al., 2020, Georgomanoli and Papapetrou, 2019, Telias and Ben-Yosef, 2014). The approaches have also become more sophisticated as protocols have developed to differentiate the cells to the disease-specific cell type.

More specifically with respect to cancer modelling, a wide range of approaches has been developed (reviewed in (Zhang et al., 2020). These broadly split into three categories. One is the use of normal hPSC which are genetically modified, using techniques such as CRISPR/CAS9, to introduce mutations that are normally found in the cancer type. Terada et al 2019, used the CRISPR/CAS9 system to knock out the TP53 gene and SMARCB1, the loss of the latter is a well-established marker for Atypical teratoid/rhabdoid tumour (AT/RT). The authors differentiated these cells into neural progenitor-like cells (NPLCs) and transplanted them into mice. Cells lacking SMARCB1 readily generated tumours that resemble those observed in AT/RT (Terada et al., 2019). A second approach for cancer modelling is using somatic cells from patients harbouring germline mutations. For example, Susanto et al 2020 reprogrammed cells from a patient with Gorlin syndrome, carrying a mutation in PTCH1, a sonic hedgehog (SHH) receptor. By generating neuroepithelial stem cells (NES), they were able to identify

gene interactions that are also found in a subgroup of medulloblastoma patients. This study not only demonstrated that iPSC from a patient can successfully be used to model the onset and progression of medulloblastoma but also, can be used to identify putative targets normally found in the disease(Susanto et al., 2020). Lee et al 2015 developed another in vitro model using this approach. In this system, they derived hiPSC from the somatic cells of patients with Li-Fraumeni Syndrome (LFS) to investigate the participation that the germline mutation of p53 has in the development of osteosarcoma (OS). Differentiation of these hiPSC towards osteoblasts recapitulated the characteristics observed in OS, and they were able to highlight previously unreported imprinting activity in the development of OS in LFS patients (Lee et al., 2015b).

Finally, tumour-derived cells can be reprogrammed to pluripotent stem cells in an attempt to recapitulate cancer progression in a line harbouring all cancer "hits". Kim et al, 2013 induced pancreatic ductal adenocarcinoma (PDAC) tumour samples towards pluripotency. These cells were then engrafted into immune-deficient mice forming neoplasias that ultimately developed into an invasive stage. Cells from these neoplasias were used to generate pancreatic organoids, allowing them to identify biomarkers and pathways that could be used to detect this disease in early stages (Kim et al., 2013).

In the area of neuroblastoma, a few approaches exist using hPSC. Cohen et al 2020 generated a line with inducible expression of MYCN and an ALK mutation, both associated with high-risk neuroblastoma. They were able to induce tumour formation in mice, resembling those found in patients, these tumours also triggered common immune response seen in the disease (Cohen et al., 2020). Much like many of the models described above, this relies upon a mouse host to guide the cells into the disease/cell type. Although these approaches provide a very useful tool, the feasibility to adapt this technique across all labs is challenging, as it requires permissions and facilities for animal study. Recently, iPSC have been derived from neuroblastoma patients, opening further possibilities of modelling this disease (Marin Navarro et al., 2019).

1.6 Project aims

Current popular models for examining the origins of neuroblastoma involve the use of transgenic mouse lines/primary explants or established human neuroblastoma-derived cell lines. Although these approaches have provided useful insights, they fail to recapitulate the mechanisms that drive the emergence of neuroblastoma from "untransformed" embryonic cells. Here we describe the development of a tractable human pluripotent stem cell (hPSC) differentiation system that allows the temporal dissection of the early events associated with neuroblastoma initiation. This involves the efficient *in vitro* generation of the cell types that give rise to neuroblastoma i.e. trunk NC and

sympathoadrenal cells from hPSCs. Using this approach, we describe the generation and characterisation of hPSC lines that harbour neuroblastoma-relevant aberrations such as 17q amplification and an inducible *MYCN* overexpression cassette.

Aims

1. Dissect the influence that a gain of 17q chromosome has in the development of the sympathoadrenal lineage from human pluripotent stem cells *in vitro*

In this aim, I attempt to recapitulate from hPSC the key transitional stages of development towards the sympathetic lineage in vitro, whilst assessing the impact that a gain of 17q chromosome could have on specification at each of these stages. This is analysed by RNA expression and immunofluorescence analysis. This could shed light on the contribution that a 17q aberration has in neuroblastoma development and, particularly, whether 17q alters cells fate decisions.

2. Elucidate the impact of MYCN overexpression on a line harbouring a 17q gain at specific time-points during sympathoadrenal specification from hPSC *in vitro*.

Building on the work of aim one, this aim focuses on examining whether the overexpression of MYCN at different time points can modify the differentiation route characterised in aim one. Further to this, assessing whether MYCN overexpression has the same impact along the whole differentiation or its impact is temporally dependant.

3. Assess the development of cancer-associated traits during the differentiation to sympathoadrenal lineages in cells harbouring the 17q aberration in the presence or absence of MYCN overexpression.

Aim three attempts to further characterise the works from aim one and two by assessing phenotypic traits normally associated with cancer development. The aim goes beyond lineage tracing characterisation and focuses on the identification of early hints of malignant transformation.

2 Chapter 2: Materials and methods

2.1 Cell lines

Wild type (H7) A kind gift from Peter Andrews and Ivana Barbaric. Karyotypically normal, female human embryonic stem cell line originally derived in Thomson et al 1998. We used the H7 S14 subline published in Draper et al 2004.

(H7) 17q A kind gift from Peter Andrews, Ivana Barbaric and Christopher Price. A subline of H7 published in Draper et al 2004. Female human embryonic stem cell line carrying a gain in chromosome 17q (region q27q11) via an unbalanced translocation with chromosome 6.

(H7) 17q-MYCN This cell line is a derivative of **17q** described above**.** This cell line was transfected with a TetOn-PiggyBac plasmid carrying the wild-type version of the *MYCN* gene (Randolph et al., 2017). After transfection, the cell line was sent to be karyotyped and it was discovered that it had acquired a duplication of the long arm of chromosome 1 via an unbalanced translocation with the second chromosome 1. The region gained spans from 1q21 to 1q terminal.

2.2 Cell Culture

hPSC cell lines were grown in feeder-free conditions, using Vitronectin (Thermo Fisher) as an attachment factor. Cells were cultured in E8 media (following the recipe published by **Chen et al, 2011** (Chen et al., 2011)) complemented with GlutaMax (Thermo Fisher). Flasks of hPSC were placed during culture in humidified incubators at 37°C and 5%CO_2.

2.2.1 Coating

2.2.1.1 Vitronectin

Flasks were coated using Vitronectin (rhVTN-N) (Thermo Fisher), resuspended at 1:100 in PBS (without Ca+, Mg++). The solution was pipetted in flask/plates and incubated for 45 minutes at 37°C. Flasks were used or stored in the fridge (4°C) up to one week after coating.

2.2.1.2 Geltrex

Undiluted geltrex was defrosted on ice. Geltrex was diluted 1:10 in Dulbecco's Modified Eagle Medium (DMEM) (Sigma-Aldrich). 1ml aliquots were stored at -80°C. When coating was required, each aliquot was defrosted by adding 1ml of cold DMEM. Once it was defrosted, 8 ml of DMEM were added to have a final volume of 10 ml. Diluted geltrex was added to flasks/plates and incubated for 2 hours at 37°C. Coated Flasks/Plates were used or stored in the fridge (4°C) up to one week after coating (keeping the surface properly hydrated).

2.2.2 Media Preparation

2.2.2.1 E8 Media

E8 medium was made following a recipe published by Chen et al, 2011, with solely the replacement of standard glutamine for GlutaMax (Thermofisher) to increase its stability in the incubator. Batches of 50X E8 concentrate were prepared and aliquoted (10 ml each). Aliquots were stored at -20°C. To prepare media, aliquots were defrosted and diluted by adding 490 ml of DMEM/F12 without glutamine. Media was filtered using a stericup (Millipore) 0.22 µm pore size filter.

Table 1

E8 MEDIUM RECIPE				
Component	50X concentrate	Final concentrations per 1 Litre of E8	Company	Catalogue Number
DMEM/F12	-	-	Sigma	D6421
L-ascorbic acid	3200mg/L	64mg/L	Sigma	A8960
Sodium selenium	700µg/L	14µg/L	Sigma	S5261
Insulin	970mg/L	19.4mg/L	ThermoFisher	A11382IJ
$NaHCO_3$	27.15g/L	543mg/L	Sigma	S5761
Transferrin	535mg/L	10.7mg/L	Sigma	T0665
Glutamax	50X	10ml/L	ThermoFisher	35050038
FGF2	5mg/L	100µg/L	Peprotech	100-18B
TGFβ1	100µg/L	2µg/L	Peprotech	100-21

In order to improve our E8 media, the recipe was adapted following Weiwei Liu et al, 2018(Liu et al., 2018a) and by changing the regular FGF2 for a more stable version. The stable E8 recipe can be found in Table 2.

Table 2

STABLE E8 MEDIUM RECIPE				
Component	50X concentrate	Final concentrations per 1 Litre of E8	Company	Catalogue Number
DMEM/F12	348 ml	-	Sigma	D6421

L-ascorbic acid	3200mg/L	64mg/L	Sigma	A8960
Sodium selenium	700µg/L	14µg/L	Sigma	S5261
Insulin	970mg/L	19.4mg/L	ThermoFisher	A11382IJ
$NaHCO_3$	69.15g/L	1383mg/L	Sigma	S5761
Transferrin	535mg/L	10.7mg/L	Sigma	T0665
Glutamax	50X	10ml/L	ThermoFisher	35050038
FGF2	1mg/L	20µg/L	ThermoFisher	PHG0360
TGFβ1	100µg/L	2µg/L	Peprotech	100-21

2.2.2.2 Neuro-mesodermal progenitor induction Medium

Neuro-mesodermal progenitor media (NMP media) (Gouti et al., 2014) consists in N2B27 medium(Brewer et al., 1993), supplemented with 20ng/ml of FGF (R&D, cat no:233-FB/CF) and 3µm-4 µm of CHIR (Tocris).

Table 3

Component	For 200 ml (1X)	Company	Catalogue Number
DMEM/F12	100ml	Sigma	D6421
Neurobasal	100ml	Invitrogen	21103049
N-2 Supplement (100X)	2ml	Invitrogen	17502048
B-27 serum-free supplement (50X)	4ml	Invitrogen	17504044
MEM Non-essential AA (100X)	2ml	ThermoFisher	11140050
GlutaMax (100X)	2ml	Thermofisher	35050061
FGF2	20ng/ml	R&D	233-FB/CF
CHIR 99021	3µm-4µm	Tocris	4423

2.2.2.3 Trunk Neural Crest Induction Medium

Neural Crest Medium was developed by Hackland et al 2017 and then was adapted to generate trunk neural crest by Frith et al 2018**.** The neural crest recipe is presented in Table 4.

Table 4

Component	For 50ml (1X)	Company	Catalogue Number
DMEM/F12	48.5ml	Sigma	D6421
N-2 Supplement (100X)	500µl	Invitrogen	17502048
MEM Non-essential AA (100X)	500µl	ThermoFisher	11140050
GlutaMax (100X)	500µl	Thermofisher	35050061
SB431542	2µM	Tocris	1614
CHIR99021	1µM	Tocris	4423
DMH1	1µM	Tocris	4126
BMP4	15ng/ml	Gibco	PHC9534

2.2.2.4 Sympathoadrenal Progenitor induction medium

Sympathoadrenal Progenitors medium was developed by Frith et al 2018, adapting a method developed by Oh et al, 2016. Sympathoadrenal Progenitors medium is showed in Table 5.

Table 5

Component	For 50 ml (1X)	Company	Catalogue Number
BrainPhys	47.5ml	Stem Cell Technologies	05790
N-2 Supplement (100X)	500µl	Invitrogen	17502048
B-27 or B-27 plus serum-free supplement (50X)	1ml	Invitrogen	17504044
MEM Non-essential AA (100X)	500µl	ThermoFisher	11140050
GlutaMax (100X)	500µl	Thermofisher	35050061
BMP4	50ng/ml	Gibco	PHC9534
Purmorphamine	1.5µM	Sigma	SML0868
Sonic Hedgehog C24II N-terminus	50ng/ml	R&D	1845-SH-025

2.2.2.5 Sympathetic Neuron induction Medium

The sympathetic neuron medium was developed by Frith et al 2018, adapting a method developed by Oh et al, 2016. The sympathetic Neuron medium is showed in Table 6.

Table 6

Component	For 50 ml (1X)	Company	Catalogue Number
BrainPhys	47.5ml	Sigma	D6421
N-2 Supplement (100X)	500µl	Invitrogen	17502048
B-27 serum-free supplement (50X)	1ml	Invitrogen	17504044
MEM Non-essential AA (100X)	500µl	ThermoFisher	11140050
GlutaMax (100X)	500µl	Thermofisher	35050061
Recombinant Human NGF	10ng/ml	Peprotech	450-01
Recombinant Human BDNF	10ng/ml	Peprotech	450-02
Recombinant Human GDNF	10ng/ml	Peprotech	450-10

2.2.3 Routine cell passaging

Human pluripotent stem cells (hESC) were grown and maintained in E8 media (described in **2.2.2.1.).** When cells were around 80% of confluence, they were passaged to a new flask coated with vitronectin. First, old E8 media was removed from the flask, then 1 ml of ReLeSR (Stemcell technologies) was added to the flask. The flask was rocked back and forth to ensure the ReLeSR was covering the whole surface, then, it was left for 20 seconds. After that time, ReLeSR was removed and the flask was left to "dry" for 2-4 minutes. Once the time passed, 1ml of fresh E8 was added. Flask was tapped until cells were released from the surface of the flask. Then, as the normal ratios of passaging are between 1:4 and 1:8, fresh E8 media was added to equal either 4 ml or 8ml. Cells were then, gently pipetted up and down in order to break colonies into smaller conglomerates. Once the suspension was homogenised, equal parts of 1ml were distributed into new flasks previously coated with vitronectin and containing 1.5 ml of warm E8 media.

2.2.4 Stem Cell freezing

In order to be frozen, cells were detached using ReLeSR, following the same steps as described in **2.2.3.** Once the cells were released from the surface of the flask, 1ml of DMEM media was added to collect them. Then, cells were further suspended in 9ml of DMEM, to dilute the concentration of ReLeSR. Cells were then centrifuged at 1000 rpm for 3-4 minutes. Once pelleted, the supernatant was aspirated and, very gently, the pellet was resuspended in 1ml of Stem-Cell Banker (Zenoaq). Half of the suspension of cells were transferred to cryovials, to be then immediately placed in Mr Frosty (Thermofisher) (previously filled with 100% isopropyl alcohol). Mr Frosty containing the cryovials was

placed at -80°C. After 24 hours, cryovials with cells were then transferred to the liquid nitrogen dewar for long term storage.

2.2.5 Stem Cell thawing

To defrost the cells that have been in liquid nitrogen, 1ml of warm media (E8) was added to the vial. Defrost should occur very quickly otherwise vial was placed in the water bath for a few seconds. Once the cells have defrosted, they were transferred to a 15ml falcon tube containing 10 ml of warm fresh E8. Cells were then centrifuged at 1000 rpm for 4 min. After this time, the supernatant was removed and cells were resuspended very gently in 1 ml of warm E8 or mTeSR (StemCell Technologies, Catalog #85850) containing Rock inhibitor (Y-27632) at a concentration of 10µM. Cells were then transferred to a flask previously coated with Geltrex and incubated at 37°C in 5% CO_2. After 24 hours, the media was replaced with fresh E8 media or mTeSR without Rock inhibitor addition.

2.2.6 Preparation of Single-cell suspension

In order to count cells or at any time a single cell suspension was required, media was removed from flasks/plates and StemPro Accutase (Gibco) was added into the flask/plates. Flask/plates with the accutase were then incubated at 37°C at 5% CO_2 for 10 min. Once the time has passed, cells were resuspended in DMEM to have a final volume of 10 ml. Then, cells were centrifuged at 1300 rpm for 5 min to pellet the cells.

2.2.7 Counting cells

After cells have been treated with Accutase (Gibco) and left for 10 min at 37°C as has been described in **2.2.6**, cells were resuspended in DMEM to have a final volume of 10ml. The tube containing the cells was inverted at least twice in order to homogenise the suspension of cells. Once this was done, 10µl of the suspension was taken and placed on a haemocytometer. Haemocytometer was placed under the microscope and cells inside the four corners were counted and the average was calculated. The value obtained was multiplied by 10 000. This result corresponds to the concentration of cells per microliter. This concentration is then multiplied by the total volume (10ml) of the media in order to obtain the final total cell number.

2.3 Differentiation Protocols

2.3.1 Neuro-mesodermal progenitor differentiation

1. **Day 0.** Plates were coated with Vitronectin (2.2.1.1.1.). Cells were harvested (2.2.6), counted (2.2.7), and plated at 60 000 cells/cm2 in NMP media (3 or 4µM CHIR) (2.2.2.2) with 10µM of

Rock Inhibitor (Y-27632). The volume of media was 300µl/cm2. Plates were placed in an incubator at 37°C and 5%CO2.

2. **Day 1.** 24 hours later, media was refreshed removing Rock Inhibitor.
3. **Day3.** Plates kept the same media until cells were harvested/fixed on the third day of differentiation.

2.3.2 Trunk Neural Crest Differentiation

1. **Day 3.** Plates were coated with Geltrex (2.2.1.1.2.). Following NMP differentiation (2.3.1.1), cells were harvested (2.2.6), counted (2.2.7), and plated at 50-80 000 cells/cm^2 in NC media (2.2.2.3) with 10µM of Rock Inhibitor (Y-27632). The volume of media was 300µl/cm2. Plates were placed in an incubator at 37°C and 5%CO2.
2. **Day 5.** Media was replaced removing Rock Inhibitor after 48 hours.
3. **Day 7.** The media was refreshed.
4. **Day 8.** The media was refreshed.
5. **Day 9.** Cells were harvested/fixed on the fifth day of NC differentiation (ninth day of total differentiation).

2.3.3 Sympathoadrenal Progenitors Differentiation

1. **Day 9.** Plates were coated with Geltrex (2.2.1.1.2.). Following Trunk Neural Crest Differentiation (2.3.2.2), cells were harvested (2.2.6), counted (2.2.7), and plated at 100 000 cells/cm2 in Sympathoadrenal Progenitor media (2.2.2.4.) supplemented with B-12 plus with 10 µM of Rock Inhibitor (Y-27632). The volume of media was 125µl/cm2. Plates were placed in an incubator at 37°C and 5% CO2.
2. **Day 10.** The media was refreshed removing Rock Inhibitor after 24 hours. The volume of media used was 125µl/cm2
3. **Day 11.** The media was refreshed. The volume of media was increased from this day on up to 250 µl/cm2.
4. **Day 12.** The media was refreshed.
5. **Day 13.** The media was refreshed.
6. **Day 14.** Cells were harvested/fixed on the fifth day of Sympathoadrenal progenitor differentiation (Fourteenth day of total differentiation).

2.3.4 Sympathetic Neurons Differentiation

1. **Day 14.** Remove Sympathoadrenal progenitors medium and switch to Sympathetic Neuron Differentiation medium (2.2.2.5.). The volume of media required was 250 µl/cm2
2. **Day 15.** The media was refreshed, increasing the amount given to 300 µl/cm2. Media was changed every day until desired time point (Day 19).

2.4 Immunostaining

2.4.1 Antibodies

A broad selection of antibodies was used along with the project in order to identify types of cells, stages of differentiation and cell single intensity for specific proteins. All the antibodies used were for intracellular markers. All of them acquired from companies that specialised in their production. Normally, we follow the manufacturer's recommendation for antibody dilution. In the case where dilution was not provided by the manufacturer, the antibodies were titrated, assessing a range from 1:50 to 1:1000. The list of the antibodies used is shown in table 4.

Table 7 Primary Antibodies

Antibody	Antigen	Isotype	Host Species	Dilution	Company	Catalogue Number
SOX10 (D5V9L)	SOX10	IgG	Rabbit	1:500	Cell Signalling	89356S
Anti-HOXC9	HOXC9	IgG2b	Mouse	1:50	Abcam	Ab50839
CDX2	CDX2	MIgG1	Mouse	1:100	DSHB	PCRP-CDX2-1A3
BRACHYURY	Brachyury	IgG	Rabbit	1:1000	Abcam	Ab209665
SOX2	SOX2	IgG	Rabbit	1:400	Abcam	Ab92494
MYCN	MYCN	IgG2a	Mouse	1:100	Santa Cruz	Sc-53993
MASH1	MASH1	IgG	Rabbit	1:100	Abcam	Ab211327
MASH1	MASH1	IgG2a	Mouse	1:500	Santa Cruz	SC-374104
yH2AX	Phospho-Histone H2A.X (Ser139)	IgG	Rabbit	1:400	Cell signalling	S139/9718S
PHOX2B	PHOX2B	IgG1	Mouse	1:500	Santa Cruz	SC-376997

PERIPHERIN	PERIPHERIN	Polyclonal	Rabbit	1:400	Sigma-millipore	AB1530
TH	TH	IgG2a	Mouse	1:500	Santa Cruz	25269
Anti-Ki-67	Ki-67	IgG2b	Mouse	1:100	Abcam	Ab238020

Table 8 Secondary Antibodies

Antibody	Specificity	Fluorophore	Dilution	Source
Goat anti Mouse	IgG + IgM (H+L)	AlexaFluor 647	1:500	Stratech (Jackson ImmunoResearch)
Donkey anti Rabbit	IgG (H+L)	AlexaFluor 488	1:1000	Invitrogen-Thermofisher

2.4.2 Fixation process

In order to start the immunofluorescence, cells were first required to be fixed. Media was removed from the wells. Cells were washed once with PBS (without Ca+, Mg++) to remove any possible remain of death cells that could interfere in the analysis. PBS was removed and 4% PFA was then added to the wells for 10 min at room temperature. Once this time has passed, PFA was removed and cells were washed twice with PBS to remove traces of PFA. Wells were filled with PBS to keep cells moistened.

2.4.3 Permeabilisation

As the antibodies used are intracellular, we permeabilised the cellular membrane using 0.5% Triton X-100 buffer. PBS was removed from the wells, and then 0.5% Triton X-100 buffer was added leaving the cells in incubation for 10 min at room temperature. Once this time has passed, the buffer was removed and cells were washed once with PBS.

2.4.4 Blocking

After cells have been fixed and permeabilised, cells need to be "blocked", so unspecific interactions between primary antibodies and cells are less likely to occur. Cells were incubated in Blocking buffer for 2 hours at room temperature. Blocking buffer consists of PBS with 10% FCS and 0.1% BSA. After blocking time concluded, the buffer was removed and wells were filled with PBS to preserve cells moistened.

2.4.5 Cellular Staining

Primary antibodies were diluted in PBS with 10% FCS and 0.1% BSA following the ratios shown in Table 7. If two or more antibodies were intended to be analysed in the same well, it was important to only mix antibodies from different species, i.e. SOX10/Rabbit with MYCN/Mouse. Primary antibodies dilutions were added to the wells containing the cells and left incubated at 4°C on an orbital shaker overnight. Then, primary dilutions were removed and wells were washed the first time with blocking buffer, and the second time with PBS. After washings, secondary antibody was added to the wells. Secondary antibodies were diluted following the ratios from Table 8. Also, Hoechst 33342 (Invitrogen. Cat number H3570) was added at a ratio of 1:1000 to the secondary antibodies' mixture. Hoechst was used to distinguish nuclei in the cells as it binds to double-stranded DNA. Plates containing the secondary antibody mixture were then incubated at 4°C for 2 hours on an orbital shaker. Once this time has passed, wells were washed once with blocking buffer and a second time with PBS. Wells then were filled with PBS in order to keep cells moistened. Plates were either imaged immediately or stored at 4°C for posterior analysis. The capture of the images was done using InCell analyzer 2200 (GE Healthcare), at a 20X amplification. Images were processed for the generation of the pictures using Image J software. Thresholding was set based on wells stained with secondary antibodies only. To determine single cell intensity, images were processed by Cell Profiler and histogram and density plots were made using FlowJo software.

2.5 Intracellular Flow cytometry staining

Cells were detached and resuspended as single cells using accutase (2.2.6) and then counted (2.2.7). Next, 10 million of cells per millilitre were resuspended in 4%PFA at room temperature for 10 minutes. Then cells were washed once with PBS (without Ca+, Mg++) and pelleted at 200g. Cells were resuspended in PBS at 10million/ml and 200ul were taken for each antibody staining. 300ul of permeabilisation buffer (0.5% Triton X-100 buffer in PBS with 10% FCS and 0.1%BSA) was added to each sample and incubated at room temperature for 10 minutes. Samples were then washed once with staining buffer (PBS with 10% FCS and 0.1% BSA) and pelleted at 200g. Then samples were resuspended in staining buffer containing pre-diluted primary antibody (ratios in table 7) or no primary antibody for the secondary control. The samples were left incubated at 4°C on an orbital shaker overnight. Then, primary dilutions were removed and samples were washed two times with staining buffer. After washings, staining buffer with pre-diluted secondary antibody was added to the samples and incubated at 4°C for 2 hours. Secondary antibodies were diluted following the ratios from Table 8. Finally, samples were washed once with staining buffer and resuspended in 500ul staining buffer and run on the BD FacsJAZZ for analysis. The secondary only sample was used to set the baselines.

2.6 qPCR analysis

2.6.1 RNA extraction

Cells that were going to be analysed for RNA expression, were harvested on the desired stage/day using Accutase as it has been described in **1.2.6**. Then, cells were centrifuged at 1300 rpm for 5 min. The supernatant was removed and pellets were processed either immediately or stored at -80°C. For RNA extraction, pellets were processed using RNA Clean-Up and Concentration Kit (NORGEN BIOTEK CORP) following the instructions of the manufacturer. The amount of RNA extract was quantified using NanoDrop Lite (Thermo Scientific), measuring first the blank which consisted of the liquid used to dilute the sample in the very last step of the RNA clean-up and concentration protocol. Once the blank was set, samples were measured. Results were given in ng/µl. The purity of the sample was acceptable between 1.85-2.10 A260/280.

2.6.2 cDNA generation

For the conversion of RNA into cDNA, the RNA sample was processed using a High-Capacity cDNA reverse transcription Kit (ThermoFisher) following the instructions of the manufacturer. Typically, 2000 ng of cDNA were converted.

2.6.3 qPCR assay

Once cDNA was made. qPCR mix was prepared following the instructions of TaqMan Fast Universal PCR master mix (Applied Biosystems). This mix contains the TaqMan master mix, the primers specifics for the gene we want to quantify, water and a probe specific to the sequence (**Table 9**). Then, in a 384 well PCR plate (alpha laboratories), 2µl of the cDNA at a concentration of 5ng/µl was pipetted into each well, followed by 8 µl of the qPCR mix into the wells. Plates were analysed using QuantStudio 12k Flex (ThermoFisher). The machine was programmed to undergo 40 cycles of amplification, each of one consisting in 2 minutes 50°C, 10 minutes at 95°C, 15 seconds 95°C, followed by 1 min at 60°C.

Table 9 qPCR Primer/Probe List

Gene	Forward	Reverse	Roche UPL Probe
ASCL1	cgacttcaccaactggttctg	atgcaggttgtgcgatca	38
CDX2	atcaccatccggaggaaag	tgcggttctgaaaccagatt	34
DBH	tctccatgcactgcaacaa	ggctgcaggttccattca	30
GAPDH	agccacatcgctcagacac	gcccaatacgaccaaatcc	60
GATA2	ttgtgcaaattgtcagacgac	tcatggtcagtggcctgtta	77
GATA3	gcttcggatgcaagtcca	gccccacagttcacacact	8
HOXB1	ccagctagggggcttgtc	atgctgcggaggatatgg	39
HOXB2	aatccgccacgtctcctt	gctgcgtgttggtgtaagc	70
HOXB4	ctggatgcgcaaagttcac	agcggttgtagtgaaattcctt	62
HOXB5	aagcttcacatcagccatga	cggttgaagtggaactcctttt	1
HOXC8	tcccagcctcatgtttcc	tgataccggctgtaagtttgc	86
HOXC9	gcagcaagcacaaagagga	cgtctggtacttggtgtaggg	85
MYCN	ccacaaggccctcagtacc	tcttcctcttcatcatcttcatca	55
PAX3	aggaggccgacttggaga	cttcatctgattggggtgct	13
PHOX2a	cactaccccgacatttacacg	gctcctgtttgcggaactt	17
PHOX2b	ctaccccgacatctacactcg	ctcctgcttgcgaaacttg	17
SOX1	gaagcccagatggaaatacg	ggacaaggaagggtgttgag	66
SOX10	ggctcccccatgtcagat	ctgtcttcggggtggttg	21
SOX2	atgggttcggtggtcaagt	ggaggaagaggtaaccacagg	19
SOX9	gtacccgcacttgcacaac	tctcgctctcgttcagaagtc	61
TBXT	gctgtgacaggtacccaacc	catgcaggtgagttgtcag	23
TH	acgccaaggacaagctca	agcgtgtacgggtcgaact	42

2.6.4 Data analysis

The Ct values generated during the qPCR assay were analysed as it has been suggested by Schmittgen and Livak 2008. Therefore, ΔCT and 2^-ΔΔCt values were generated, where ΔCt= data normalised against internal control= (Ct Gene of Interest – Ct internal control). 2^-ΔΔCt= fold change= [(Ct gene of interest - CT internal control) sample A-(Ct gene of interest - Ct internal control) sample B)].

2.7 Cell cycle analysis

2.7.1 Edu

In order to evaluate the cell cycle profile the cells had during the different stages of the differentiation protocol, we decided to use the EdU Flow Cytometry Assay Kit. This technique uses the "EdU" (5-ethynyl-2´-deoxyuridine) which is a nucleoside analogue to thymidine and therefore, it is incorporated into DNA during the DNA synthesis. The advantage of the EdU engineering is that it allows us to use it in normal culture conditions without the need to denature (and possibly damage) the DNA for the "EdU" to gain access, and therefore, having fewer problems detecting the cell cycle distribution.

The EdU assay was performed following the manufacturer's instructions (Thermofisher, C10633 Alexa Fluor 488). They recommend adapting the concentration/exposure time of the EdU to your own culture. The optimal concentration for my cells was 10µM for 2 hours.

Cells were analysed in the flow cytometer (BD FACSJazz) using the 405 nm laser to detect the Hoechst staining and 488 nm to detect the Edu staining.

2.7.2 Ki-67

Ki-67 antigen has been observed in every phase of the cell cycle, although it is not expressed in cells in the G0 phase (reviewed in Jurikova, 2016). These characteristics made this protein a convenient marker to determine if cells were proliferating in a given population. Its biological function is still not well understood, nonetheless, it is believed it has a role in cell division as cell proliferation arrests when Ki-67 is blocked (Starborg et al., 1996). In addition, it has been shown its participation in the stabilisation and maintenance of the mitotic spindle in mitosis (Vanneste et al., 2009).

Taking advantage of Ki-67 characteristics, we analysed the presence of this protein throughout the differentiation protocol, in the presence or in absence of MYCN overexpression. In order to do this, an anti-Ki-67 antibody was purchased (Abcam, #Ab238020). Cells were fixed and immunostained (2.4) at different time points, including its expression in embryonic stem cells. The image analysis was

performed using a pipeline in Cell Profiler that allowed us to detect and quantify Ki-67 protein expression.

2.8 DNA damage

Cells are continuously under stress posing the risk for DNA damage. Double strand breaks (DSBs) are among the most aggressive DNA lesions that a cell can undergo (Karagiannis and El-Osta, 2004b, Sedelnikova et al., 2003) and ultimately, if the DNA repair machinery fails, they can lead to the acquisition of mutations and compromising the cell genomic stability, all potentially contributing to tumorigenesis. A prompt response of the cell to DSBs is the phosphorylation on the Ser-139 of the histone H2AX. This phosphorylation and its link to DNA damage and repair have been well characterised (Sedelnikova et al., 2002, Karagiannis and El-Osta, 2004b).

In order to know the level of damage that the different cell lines had along the whole differentiation process, we decided to assess the phosphorylation state of the histone H2AX on the Ser-139. To do this, an antibody that only recognises this site was purchased ((γH2AX (cell signalling, catalogue# S139/9718S)). Cells were fixed and immunostained (2.4) at different time points, including its expression in embryonic stem cells. The image analysis was performed using a pipeline in Cell Profiler that allowed us to detect and quantify the integrated intensity of γH2AX antibody per nuclei. PAN-γH2AX nuclei were counted and excluded from intensity analysis by setting specific thresholds for intensity and nuclei coverage.

2.9 Glucose Uptake Assay

In order to asses if there were any differences in the uptake of glucose between the different cell lines, and during the different stages of the differentiation, we decided to do a simple but efficient assay using 6-NBDG (Caymen Chemical, catalogue# CAY13961). 6-NBDG is a fluorescent glucose analogue that can be used to monitor the glucose uptake in living cells without being metabolised.

Cells to be analysed were first put in 1 hour of glucose starvation. This was achieved by refreshing the media with a new one containing DMEM without glucose (ThermoFisher, catalogue# 11966025) as well as adding the signalling molecules corresponding to each stage. Plates were then incubated at 37°C at 5% CO_2 for 1 hour. After this, media was removed and replaced with fresh media, supplemented with 6-NBDG at a final concentration of 100µM. Cells were incubated once more at 37°C at 5% CO_2 for 1 hour. Then cells were then washed once with PBS, harvested (2.2.6) and then cells were analysed in the flow cytometer (BD FACSJazz) using the laser 488 to read the intracellular 6-NBDG.

2.10 Low-Density Analysis

Cells were counted (2.2.7) and plated at a density of 500 cells per cm2 in plates previously coated with Geltrex (2.2.1.1.2.). The media used for plating was Neural Crest then changed to SAP medium the next day. Plates were then incubated at 37°C at 5% CO_2**.** The media was refreshed every 48 hours. Cells were fixed (2.4.2) and stained with Hoechst 33342 (Invitrogen. Cat number H3570) for 5 min. Colonies were detected by imaging using InCell analyser 2200 (GE Healthcare), at a 4X magnification. Images were processed by Cell Profiler.

2.11 Molecular cloning and Transfection

2.11.1 Molecular cloning

PiggyBac Vectors containing the TetON system and the wild type version of *MYCN*(Randolph et al., 2017) were purchased from Addgene: PB-EF1a-TetOn3G (catalogue # 104543)(**Figure 3)** and PB-TRE3G-MYCN (catalogue # 104542)(**Figure 4)**. The plasmids were amplified following transformation into One Shot Top10 Competent Cells (Invitrogen, catalogue# C404010) following the instructions of the manufacturer. Purification of the plasmids was performed using QIAprep Spin MiniPrep kit (Qiagen, catalogue# 27104).

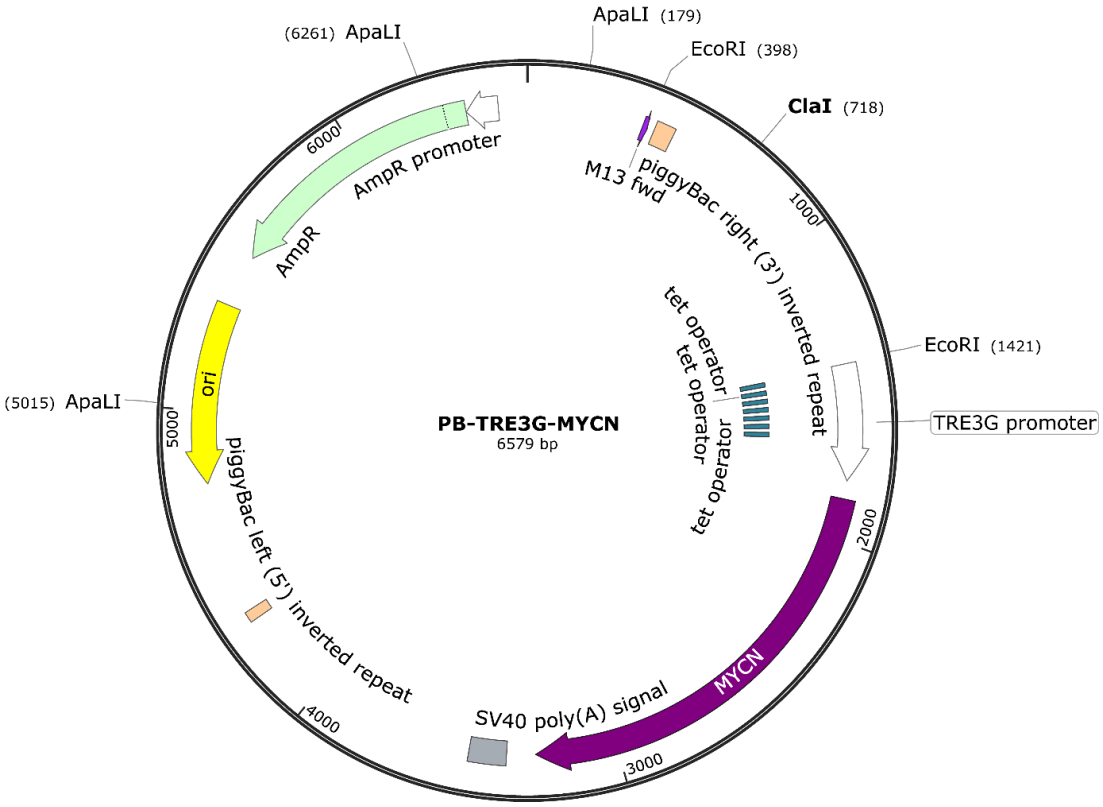

Figure 3 Plasmid map of PiggyBac TRE3G-MYCN

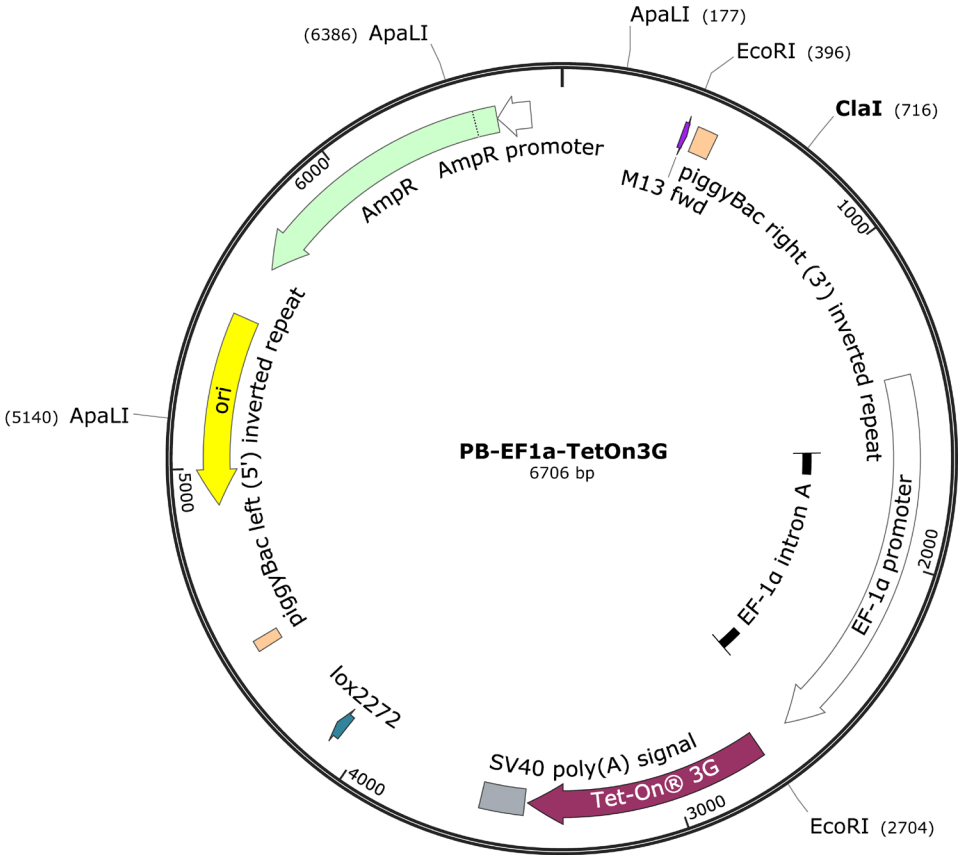

Figure 4 Plasmid map of PiggyBac EF1a-TetOn3G

Plasmids were confirmed first by restriction digest, then gel electrophoresis to visualise bands of the expected size. The enzymes used in both PB-EF1a-TetOn3G and PB-TRE3G-MYCN were ApaLI (ThermoFisher, catalogue# FD0044), EcoRI (ThermoFisher, catalogue# FD0274) and CLAI (ThermoFisher, catalogue# ER0141). Enzyme digest was done following the manufacturer's instructions. The enzyme restriction analysis was performed twice. In the first analysis, the enzymes EcoRI and ClaI were used, being expected three band sizes. For PB-TRE3G-MYCN were EcoRI (5556 bp, 319 bp) and for ClaI (717 bp). The expected three band sizes for PB-EF1a-TetOn3G were EcoRI (4398 bp, 319 bp) and ClaI (1989 bp) (**Figure 5)**. For the second analysis, other three band sizes were expected: for PB-EF1a-TetOn3G were ApaLI (4963 bp, 1246 bp, 497 bp), for PB-TRE3G-MYCN were ApaLI (4836 bp, 1246 bp, 497 bp) **(Figure 6).**

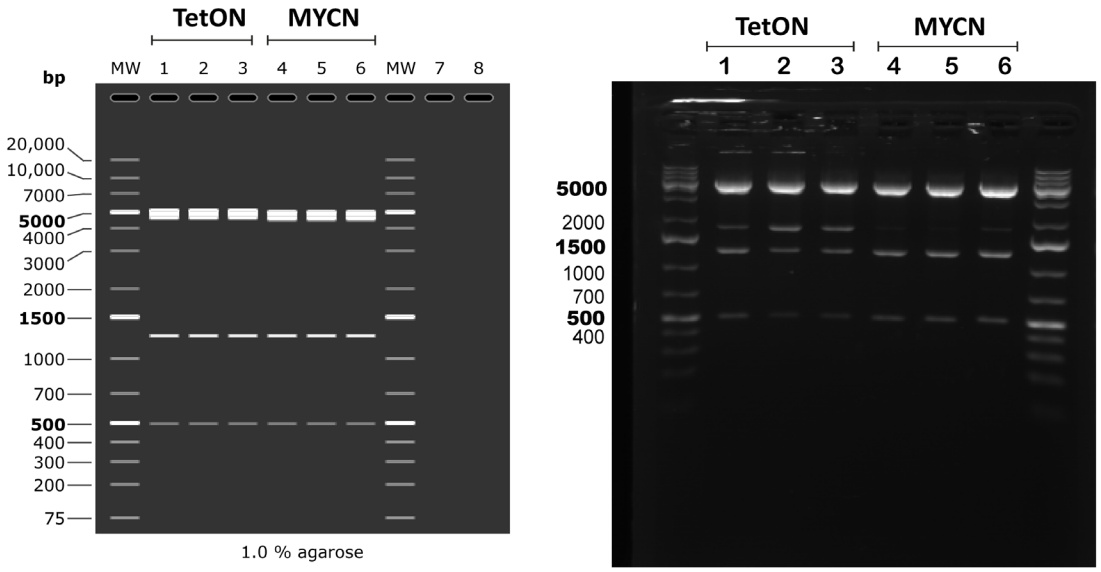

Figure 5 Enzyme restriction of the MYCN and TetOn PiggyBac plasmid using APALI enzyme.

On the left side of the image is a predicted gel after restriction enzyme digest based on the plasmid maps and the APALI enzyme cut sites. On the right side, it is shown the actual gel. 3 clones of each plasmid were digested and run.

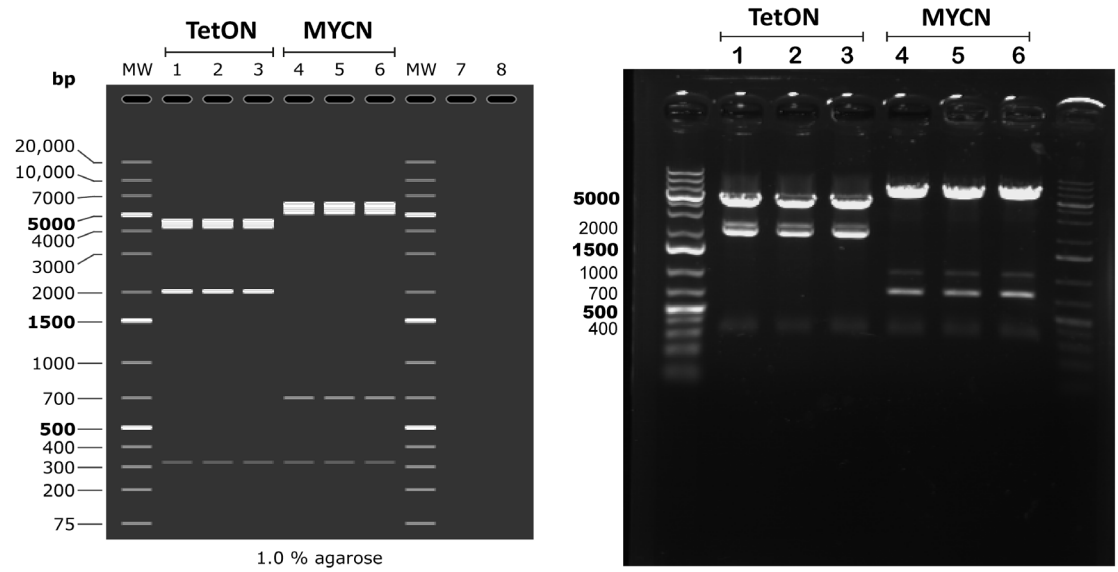

Figure 6 Enzyme restriction of the MYCN and TetOn PiggyBac plasmid using EcoRI and CLAI enzymes.

On the left side of the image is a predicted gel after restriction enzyme digest based on the plasmid maps and the ECORi and CLaI enzyme cut sites. On the right side, it is shown the actual gel. 3 clones of each plasmid were digested and run.

2.11.2 Nucleofection

The nucleofection was performed on a Lonza 4D-Nucleofector System as per the manufacturer's instructions (Amaxa 4D-Nucleofector Basic Protocol for Human Stem Cells). In brief, the 17q hPSC cells were harvested (2.2.6), counted (2.2.7) (800 000 cells in total), and resuspended in the nucleofector solution plus supplement. Cells were then diluted in P3 media. 1µg of each plasmid of interest was added to the solution. The mixture was then transferred into one cuvette, and placed into the Lonza 4D-Nucleofector System. The program we selected was CB-150. Cells were then diluted in pre-warmed media supplemented with Rock Inhibitor (Y-27632) at a concentration of 10µM. Then they were transferred to wells (of a 24 well plate) pre-coated with Geltrex (2.2.1.1.2.). Plates were then incubated at 37°C at 5% CO_2. After four days of growth, cells were harvested for single-cell deposition into 96 well plates by flow cytometry. Clonal lines were established and screened by targeted PCR for the insertion of plasmids.

2.12 Single-cell cloning

Cells of interest were harvested with accutase (2.2.6) and, in order to ensure an aggregate-free suspension, cells were passed through a 70µM filter (Millipore). DAPI (ThermoFisher, #62248) was

added at a ratio of 1:10000 and used to discriminate between live and dead cells. Proper gating was set using the BD software program, and alive cells were sorted as single cells into 96 well plates pre-coated with gelatine and mouse embryonic feeders. The media used was an equal combination of HES medium (KnockOut DMEM (ThermoFisher), 20% KnockOut Serum Replacement (Thermofisher), 1x Non-essential amino acids (ThermoFisher), 1mM L-Glutamine (ThermoFisher), 0.1mM 2-Mercaptoethanol (ThermoFisher) and 4ng/ml FGF2 (Peprotech)) and mTESR medium (Stem Cell Technologies) supplemented with 20µM of Synthechol (Sigma). Media used for plating was also supplemented with Rock Inhibitor (Y-27632). After sorting, cells were centrifuged for 1 min at 1000 rpm, so they could attach more easily to the bottom. 48 hours later, the media was refreshed without Rock Inhibitor. From then on, media was changed every 2 days. Cells were allowed to grow until colonies of reasonable size started to appear. Colonies were then passaged into larger wells (e.g. 48 well plates) by manually scrapping using a p200 tip. These plates were previously coated with Geltrex (2.2.1.1.2.), as we wanted to make the transition to feeder-free culture. Media was also replaced by mTESR medium (STEMCELL Technologies).

2.12.1 PCR

Once single-cell cloning was performed (2.13.), cells were allowed to grow until they formed visible colonies. In order to identify the clones that have successfully integrated the plasmids of interest, genomic DNA was purified using DNeasy Blood and Tissue Kit (Qiagen, #69506). Then, a Polymerase Chain Reaction test was performed. A total of 39 clones were analysed by PCR. Primers were generated using the GenScript tool and the list of the primers and their sequence is showed in **Table 10.**

Table 10. Primers to verify PB-MYCN and PB-TetOn insertion

Gene name	Primer	Length	Tm	%GC	Sequence	Amplicon
PB-MYCN F	Forward	24	58.71	37.5	TAAAAGCAGAGCTCGTTTAGTGAA	506
PB-MYCN R	Reverse	20	61.27	60	TGCAGTCCTGGAGGATGACC	506
PB-TetON F	Forward	20	60.32	50	AGTTGCGTGAGCGGAAAGAT	514
PB-TetON R	Reverse	21	60.13	52.38	TAGACATGGTGAATTCGGGGC	514

The PCR reaction was run with Taq DNA polymerase (M0273) with the following settings

STEP	TEMPERATURE	TIME
Initial Denaturation	95°C	2 MIN
30 cycles	95°C 53°C 68°C	15 SEC 15 SEC 45 SEC
Final Extension	68°C	5 MIN
Hold	4°C	Indefinite period

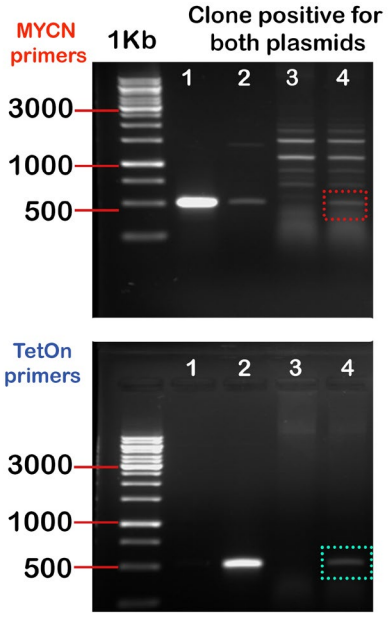

Figure 7 Gel showing the amplification of the region corresponding to MYCN and TetON

Lane 1: MYCN plasmid as a control. **Lane 2**: TetOn plasmid as a control. **Lane 3:** Clonal line negative for both MYCN and TetOn primers. **Lane 4:** Clonal line positive for both MYCN and TetOn primers. A picture of the gel run after the PCR is shown in figure 7

After verification of insert, their response to doxycycline was also confirmed by qPCR and immunofluorescence analysis using MYCN antibody showed in **Table 7**.

2.13 Karyotyping

Karyotyping was performed by Sheffield Children's Hospital Cytogenetics Department by metaphase spread G-banding from live cultures of hPSC.

2.14 Statistical Tests

2.14.1 qPCR and Immunofluorescence

The comparisons of gene expression or percentage positive of protein were split by gene or protein analysed and therefore when the comparison was for two samples I used an Independent Welch t-test. This test is more robust than that of a standard t-test and ANOVA (analysis of variance) as it is less likely to give false positives, it also is reliable for both equal and unequal variance between data sets.

2.14.2 Cell proliferation

Percentage of cells in each stage of the cell cycle were compared for each line/condition obtained by performing the EdU assay (2.7.1). A two-way ANOVA was used as the dataset contained multiple groups with connected comparisons, as in the percentage of cells in S could impact upon the percentage of cells in G1 or G2. Percentage of cells proliferating were compared for each line/condition obtained by performing the Ki-67 staining (2.7.2). An ordinary one-way ANOVA was used as the dataset contained multiple groups with a single variable for comparison. Tests were corrected for multiple comparisons using the Tukey method of correction.

2.14.3 Low-Density cloning

The number of colonies cells were compared for each line/condition obtained by performing the low-density assay (2.10). An ordinary one-way ANOVA was used as the dataset contained multiple groups with a single variable for comparison. Tests were corrected for multiple comparisons using the Tukey method of correction.

2.14.4 DNA Damage

The integrated intensities of γH2AX per cell were compared for each line/condition obtained by performing γH2AX staining (2.8). When only two samples were compared, the Kolmogorov-Smirnov test was used as the data was not normally distributed. The Kolmogorov-Smirnov non-parametric test is better for comparing distributions. When more than two samples were compared, the Kruskal-Wallis test was used instead as this test is equivalent to the One-way ANOVA but for non-parametric distributions. Tests were corrected for multiple comparisons using Dunn's method of correction, this test is more rigorous than Tukey as Dunn's does not tolerate type 1 errors (false positives).

3 Chapter 3: Investigating the effect of chromosome 17q gain on *in vitro* derived neural crest cells and their derivatives

3.1 Introduction

Many biological and genetic factors determine the clinical outcome of neuroblastoma, such as the patient's age, cell ploidy status, histology, and *MYCN* amplification (Cohn et al., 2009, Schleiermacher et al., 2010, Joshi et al., 1992).

Cell ploidy status is, *per se*, an important prognosis indicator of disease progression and response to therapy. Interestingly, the acquisition of hyperdiploidies (additional whole chromosomes) is associated with a better response to therapy and a better prognosis than in those cancers with diploid tumours (Look et al., 1984, Look et al., 1991, Cohn et al., 1990). For example, George et al 2005 discovered that patients with stage 4 of neuroblastoma, and non-amplified *MYCN* status, showed different 4-year EFS (event-free survival) depending on the patient's ploidy status. Infants under 12 months and carrying hyperploidies, showed 83.7% EFS compared to 46.2% of those reporting diploidies. Children between 12 and 18 months showed 92.9% EFS and 37.5% EFS carrying hyperploidies and diploidies respectively. Nonetheless, the influence of ploidy seems to lose reliability after 24 months, when EFS drops below 20% regardless of ploidy or *MYCN* status (George et al., 2005).

Even though tumours presenting hyperploidies are associated with a better prognosis, the rule does not seem to apply to the acquisition of segmental chromosome aberrations. This has been shown using microarray CGH technology (Janoueix-Lerosey et al., 2009, Schleiermacher et al., 2011, Schleiermacher et al., 2007a). Janoueix-Lerosey et al, 2009 showed that when whole chromosome copies are obtained, patients had a superb survival. On the contrary, when segmental aberrations were present, patients showed a very high risk of relapsing. Additionally, when other variables were taken into account in the analysis, such as *MYCN* status, and age, the existence of these chromosomal aberrations was still the strongest predictor marker for relapsing (with or without MYCN presence)(Janoueix-Lerosey et al., 2009).

Deletions in 1p and 11q chromosomes(Attiyeh et al., 2005, Spitz et al., 2003), as well as gains in 1q, 2p and 17q, are the most reported segmental chromosome alterations(Szewczyk et al., 2019) (Diskin et al., 2009, Bown et al., 1999a, Bown et al., 2001) in neuroblastoma. Nonetheless, a gain of 17q and 1q, loss of 1p, and loss of 11q are associated with the unfavourable outcome as they show aggressive relapses and reduced overall survival (Schleiermacher et al., 2012, Janoueix-Lerosey et al., 2009).

As aforementioned, 17q gain has been associated with poor prognosis even in *MYCN non-amplified* tumours (Schleiermacher et al., 2007b) (Bown et al., 1999a, Bown et al., 2001, Theissen et al., 2014).

The 17q-21 quarter is the most recurrent chromosomal aberration, accounting for more than half of all cases of neuroblastoma(Meddeb et al., 1996) (Bown et al., 1999a). The most frequent translocations occur between 17q21-qter and the distal part of 1p or 11q(Meddeb et al., 1996, Van Roy et al., 1995, Lastowska et al., 1997, Savelyeva et al., 1994, McConville et al., 2001, Stark et al., 2003, Stallings et al., 2004), although 17q translocation can take place on a wide range of chromosomes(Lastowska et al., 1997).

Several genes on chromosome 17q have been suggested to be involved in neuroblastoma progression. TBX2 is localised in 17q23.2 and it has been proposed to be a major component in the core regulatory circuits in neuroblastoma tumours and cell lines. Within this regulatory circuit, TBX2 was shown to promote the expression of *MYCN* and other neuroblastoma-related genes. It also showed an effect on cell cycle progression through the indirect inhibition of the DREAM complex, a collection of transcription factors that actively regulate the G2/M transition. When TBX2 was knocked down in neuroblastoma cell lines, the authors saw a decrease in proliferation and an increase in G1 phase arrest (Decaesteker et al., 2019, Decaesteker et al., 2018).

Other genes that are found on chromosome 17q and that could be playing an important role in the development of the disease are genes that participate in WNT signalling, which has a pivotal role in inducing and maintaining the pool of neural crest that, will eventually, differentiate into the sympathoadrenal population. For example, 17q harbours genes for WNT ligands such as WNT3 and WNT9B, the WNT receptor FZD2 and the WNT signalling modulator AXIN2. High expression levels of WNT3 have been related to less favourable outcomes in neuroblastoma patients (Duffy et al., 2016). Whereas downregulation of FZD2 suppressed neuroblastoma outgrowth and vascularisation in mouse(Zins et al., 2016). WNT3 has been shown to impact the differentiation of pluripotent stem cells towards neuroepithelial rosettes (Lee et al., 2015a).

SOX9, an early neural crest marker, has been suggested to have an important role in preventing the differentiation of neuroblastoma cells in high-risk patients, maintaining its expression helped by USP36, a deubiquitinating enzyme, that is also encoded in 17q (Mondal et al., 2018). *The signal transducer and activator of transcription 3* (STAT3) is encoded at the 17q21.2 region, has been reported to contribute to tumorigenesis via conferring resistance to apoptosis by inducing expression of Bcl-xL in myeloma tumour cells(Catlett-Falcone et al., 1999). It has also been related to the development of resistance to chemotherapy in neuroblastoma cell lines (Rebbaa et al., 2001) and a mouse model(Yogev et al., 2019). Finally, it is worth mentioning the presence of the polycomb gene SUZ12 (part of the polycomb repressor complex 2 (PRC2)), which along with EZH2 have been reported to disrupt neuroblastoma differentiation (Li et al., 2018, Chen et al., 2018).

Becker and Wilting 2018 listed some genes contained in chromosomal aberrations that are normally found in neuroblastoma. I have included a modified version of this table to incorporate other genes that could potentially be participating in neuroblastoma progression.

Table 11. Potential driver genes of neuroblastoma located on 17q chromosome. Adapted from Becker and Wilting, 2018.

Pathway	Factor	
WNT pathway	FZD2	Receptor that belongs to the FZD family. Its association with different types of co-receptors allows the activation of both canonical and non-canonical WNT signals. In neuroblastoma, it has been correlated with tumour growth (Zins et al., 2016)
	WNT3	Activator of the canonical WNT pathway, the knock-down of this gene in a *MYCN* amplified neuroblastoma cell line reduced cell viability (Duffy et al., 2016)
	AXIN2 (conductin)	Paralog to AXIN also participates in the stabilisation of the β-catenin destruction complex (Behrens et al., 1998). It has been linked to tumour progression in colorectal cancers (Wu et al., 2012)
Sympathoadrenal development	NGFR	Enhances the interaction of TRK receptors with their ligands (Ho et al., 2011). Demonstrated in a neuroblastoma cell model.
	NOG (codes for the BMP antagonist NOGGIN)	Possible interference in neural crest delamination (Burstyn-Cohen et al., 2004) and sympathoadrenal cell specification (Huber, 2006)
Others	PROHIBITIN	Induction of tumour cell proliferation and de-differentiation (MacArthur et al., 2019)
	Survivin	Prevents activation of the intrinsic apoptotic pathway. Interacts with HBXIP, XIAP, DIABLO. Observed in high-risk neuroblastoma and correlates with bad prognosis (Lamers et al., 2011, Azuhata et al., 2001).
	SOX9	Early neural crest marker. It has been reported its participation in preventing differentiation of high-risk neuroblastoma cell lines (Mondal et al., 2018)
	STAT3	Linked to chemotherapy resistance in a neuroblastoma cell line (Rebbaa et al., 2001) and a mouse model (Yogev et al., 2019)
	BRCA1	Gene involved in DNA damage repair and suppression of tumours (Wu et al., 1996). Deregulation of this protein could compromise the maintenance of genome integrity.
	TBX2	Proposed to be a major component in the core regulatory circuits in neuroblastoma tumours and

		cell lines (Decaesteker et al., 2019, Decaesteker et al., 2018).
	SUZ12	One of the components of the Polycomb repressor complex 2 (PRC2). It has been reported its participation along with EZH2 in differentiation impairment of neuroblastoma (Chen et al., 2018, Li et al., 2018).
	IGF2BP1	The insulin-like growth factor-2 mRNA-binding protein 1 (*IGF2BP1*) gene. Substantial expression is present in around 80% of neuroblastoma tumours, and it has been associated with advanced-stage tumours and bad prognosis. Associated with both amplification and increase transcription of MYCN (Bell et al., 2015)
	TRIM37	High expression is associated with inhibition of the acentrosomal spindle assembly, which leads to mitotic failure and cessation of proliferation (Meitinger et al., 2020).
	JMJD6	It forms protein complexes with MYCN and BRD4. Its knock-down reduces neuroblastoma cell proliferation and survival (Wong et al., 2019)

As has been aforementioned, neuroblastoma is a very complex disease that has been tried to be untangled through different approaches. Whilst the analysis of genes contained within 17q aberration has increased our understanding of their individual contribution to neuroblastoma, the coordinated disruption of the whole of 17q has not been fully investigated.

Moreover, neuroblastoma cell lines are derived from fully-developed tumours, thus understanding the individual contributions of the different chromosomal aberrations is tremendously difficult. The main reason for this difficulty is that neuroblastoma cell lines already harbour many genetic alterations, from not only the original tumour, but also acquired in culture (Kryh et al., 2011). Furthermore, neuroblastoma cell lines normally only allow dissecting a very narrow time frame of the disease, as earlier stages are not accessible with this model.

In order to understand the individual contributions of high-risk chromosomal aberrations in neuroblastoma initiation and progression, we utilised a human pluripotent stem cell line harbouring a similar gain of the long arm of 17 (17q). This tool allows us to investigate the principal effects of a 17q addition alone during differentiation and specification towards the sympathetic lineage.

Additionally, 17q aberration is not exclusive of neuroblastoma as it has also been found in other cancers such as breast cancer, where 17q23 amplification is present in approximately 11% and is linked to both tumorigenesis progression and resistance to therapies (Liu et al., 2018b, Li et al.,

2002). It has also been reported in medulloblastoma to be associated with poor survival (Pfister et al., 2009).

Karyotypic changes are a common phenomenon occurring during *in vitro* culture of hPSC. Recurrent changes often seen in hPSC cultures involve frequent gains of chromosomes 1, 12, 17, 20 and X, with chromosome 17 being the most common at 17% percent of all abnormalities reported (Baker et al., 2016). 17q gain was first reported in hES cell culture in 2004 and it was suggested it might provide a selective advantage (Draper et al., 2004b). Later, this was verified by Enver et al, 2005 when cells showed higher cloning efficiencies. The growth advantage of cells with a gain in 17q has been linked to the expression of WNT3 in hPSC cultures (Lee et al., 2015a).

Because of the high prevalence of 17q in neuroblastoma and the privileged access we have to an hPSC harbouring the 17q aberration, we decided to attempt the very first fully *in vitro* model of neuroblastoma. It must be highlighted that our 17q cell line harbours a gain of the whole long arm (q) of chromosome 17. As it has been aforementioned, the 17q-21 quarter aberration is the most commonly found in neuroblastoma. Nonetheless, different segment size segments from 17q are normally observed in tumours (Lastowska et al., 1998, Van Roy et al., 1997, Brinkschmidt et al., 2001). The smallest addition retained in neuroblastoma is the last 25Mb which corresponds to 17q23.1-17qter (Meddeb et al., 1996), therefore, our cell line contains a plausible aberration. We combined the 17q hPSC line with the protocol developed in our lab for the generation of sympathetic neurons and firstly assessed whether the presence of 17q affected cell fate decisions and lineage specification at key stages of differentiation.

3.2 Results

Graphical abstract summarising the experiments and main findings of chapter 3.

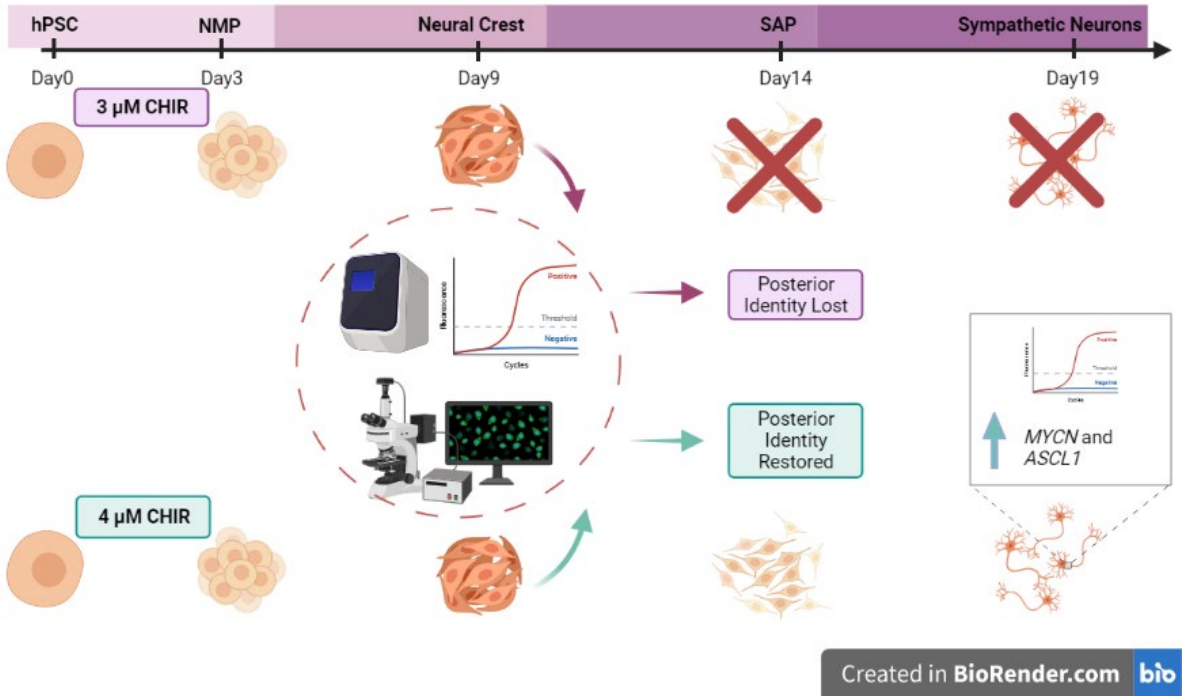

3.2.1 17q chromosome gain interferes with the posterior identity of cells during neural crest specification

In order to examine how chromosome 17q gain influences the specification of trunk neural crest and its derivatives, we employed an hPSC line carrying this genetic aberration as a consequence of culture adaptation (Draper et al., 2004b), together with our published protocol for the in vitro generation of trunk NC cells (Frith and Tsakiridis, 2019). Differentiation of the 17q cells was compared to its wild type counterpart. (**Figure 8**).

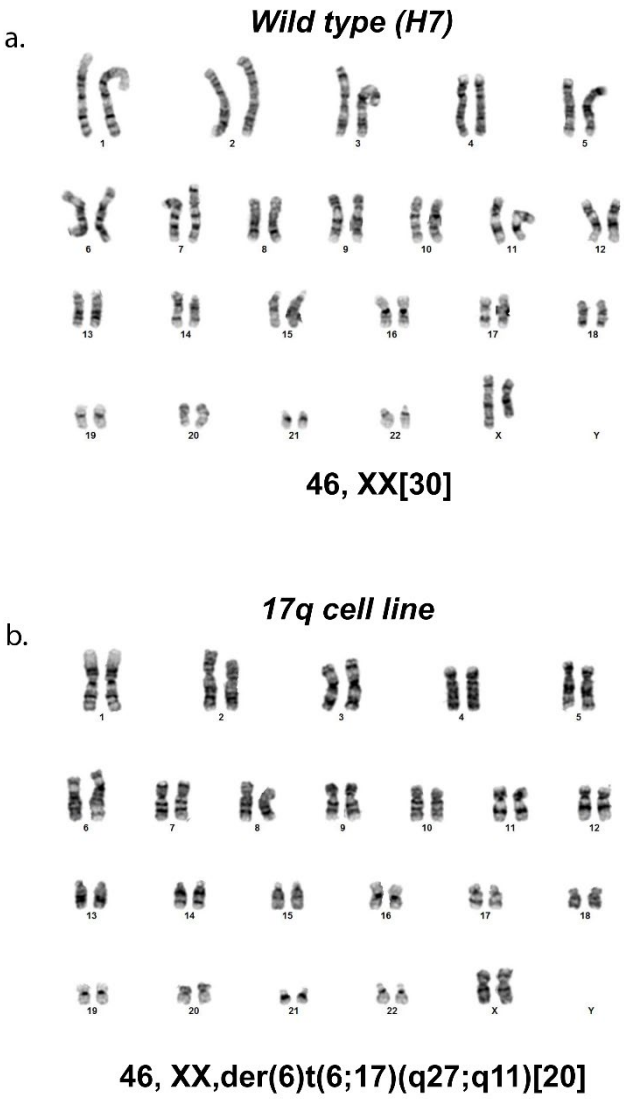

Figure 8. Karyotype of Wild type and 17q cell lines

a. Wild type (H7) cell line karyotype, showing a normal diploid chromosome number (46, XX). In square brackets is shown the number of metaphase spreads analysed. 30 cells examined gives a 95% chance of detecting a 10% population (Baker et al., 2016). **b.** 17q cell line karyotype, showing an abnormal karyotype with a gain of the long (q) arm of chromosome 17 via an unbalanced translocation with chromosome 6 in all cells examined. In square brackets is shown the number of metaphase spreads analysed. 20 cells examined gives a 95% chance of detecting a 14% population (Baker et al., 2016).

We first tested the ability of the isogenic, diploid control hPSC line to differentiate efficiently towards trunk NC and its derivatives. To this end, wild type hPSCs were plated in the presence of WNT and FGF agonists to first generate neuromesodermal progenitors (NMPs) which we have previously shown to subsequently give rise to trunk NC (Frith et al 2018)(**Figure 9-a)**. After three days, wild type cells were harvested and qPCR was performed. A transcript related to the NMP stage (*TBXT*), an early

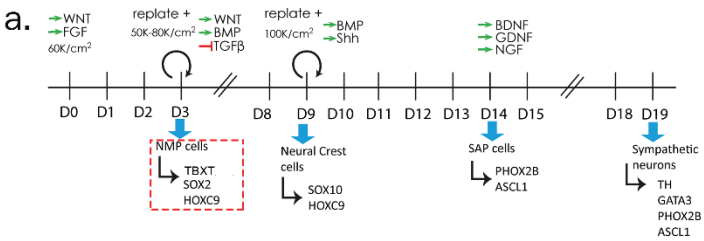
a.
WNT
FGF
60K/cm2
replate +
50K-80K/cm2
WNT
BMP
TGFβ
replate +
100K/cm2
BMP
Shh
BDNF
GDNF
NGF
D0 D1 D2 D3 D8 D9 D10 D11 D12 D13 D14 D15 D18 D19
NMP cells
TBXT
SOX2
HOXC9
Neural Crest cells
SOX10
HOXC9
SAP cells
PHOX2B
ASCL1
Sympathetic neurons
TH
GATA3
PHOX2B
ASCL1

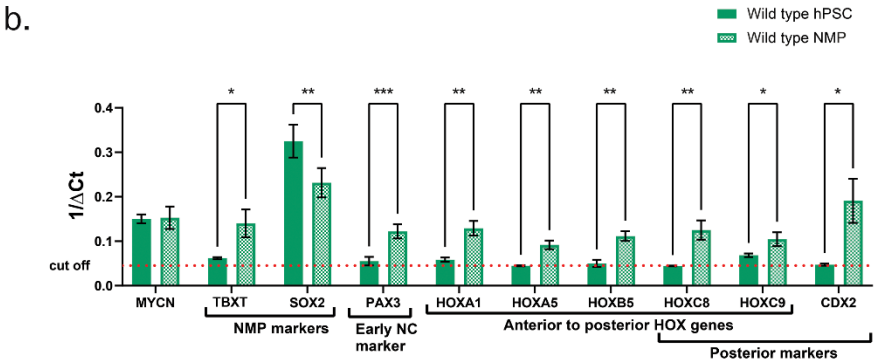
b.
Wild type hPSC
Wild type NMP
1/ΔCt
cut off
MYCN
TBXT
SOX2
PAX3
HOXA1
HOXA5
HOXB5
HOXC8
HOXC9
CDX2
NMP markers
Early NC marker
Anterior to posterior HOX genes
Posterior markers

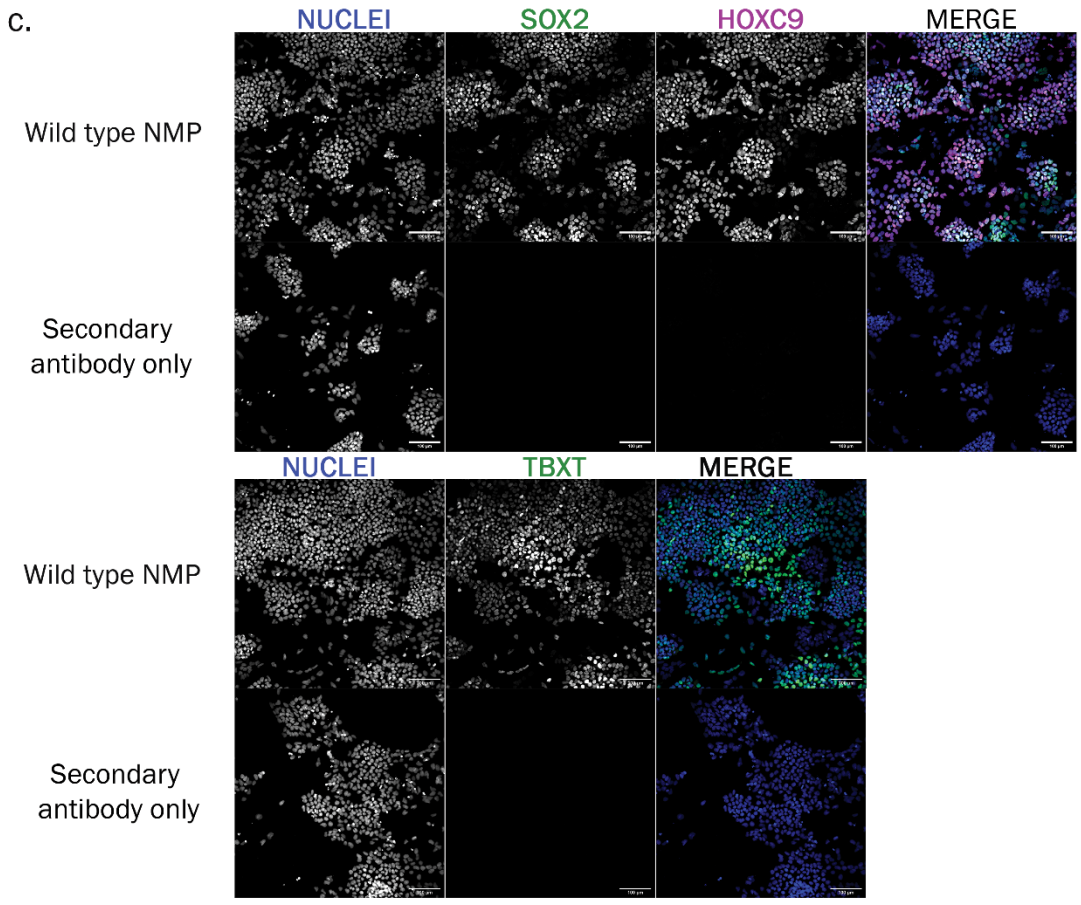
c.
NUCLEI
SOX2
HOXC9
MERGE
Wild type NMP
Secondary antibody only
NUCLEI
TBXT
MERGE
Wild type NMP
Secondary antibody only

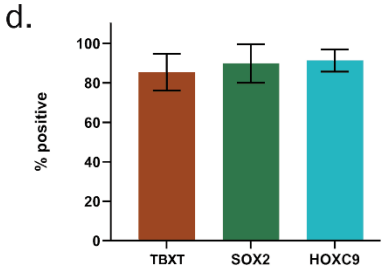
d.
% positive
TBXT
SOX2
HOXC9

Figure 9. Neuromesodermal progenitor differentiation of the wild type cell line

a. Schematic diagram of the directed differentiation of human pluripotent stem cells into Neuromesodermal progenitors (**NMP**), Neural Crest (**NC**), Sympathoadrenal progenitors (**SAP**) and Sympathetic neurons (**SN**). The red rectangle highlights the day cells were harvested, and which markers were used to validate the stage. **b.** Wild type cell line was differentiated into NMP. The bar chart shows the qPCR analysis, gene expression values are plotted as 1/ΔCt for pluripotent stem cells and differentiated NMP (specified in graph legend). A cut off line (dotted red line) has been set at 0.045 as this is the equivalent of 40 cycles on the qPCR machine. Genes related to NMP differentiation show significant upregulation, except for *SOX2* which remains high but is downregulated. (n= 3 biological replicates, error bars= SD, Independent Welch t-tests, $p \leq 0.05$= *, $p \leq 0.01$= **, $p \leq 0.001$= ***, $p \leq 0.0001$= ****). **c.** Immunofluorescence images of the wild type cell line differentiated into NMP. Shown are SOX2, HOXC9 and TBXT staining with its corresponding secondary antibody only test (Merge: Hoechst=blue, SOX2/TBXT=green, HOXC9=magenta). **d.** Percentage of cells expressing SOX2, HOXC9 and TBXT markers in the immunofluorescence analysis (n≥ 3 biological replicates. Error bar= SD).

neural crest marker (*PAX3*) and anterior-posterior identity (*HOXA1, HOXA5, HOXB5, HOXC8, HOXC9, CDX2*) were found to be significantly upregulated when compared to its pluripotent stem cell stage. *SOX2* also remained highly expressed (**Figure 9-b)**. These observations were confirmed at the protein level with immunostaining (**Figure 9-c)**, SOX2, HOXC9 and TBXT were found expressed in around 80% of the population (**Figure 9-d),** highlighting the successful transition to a neuro-mesodermal progenitor state**.** In summary, our wild type control generated NMPs with high efficiency as evidenced by appropriate gene and protein expression.

To know the possible differences between the wild type and 17q cell lines prior to the differentiation, the gene expression of both cell lines was analysed. Markers related to the NMP stage were tested to see if any of the cell lines could have a possible "advantage or disadvantage" before inducing the differentiation. **Figure 10-b** shows the values obtained at day 0 of the differentiation protocol. No differences were found between the cell lines. Afterwards, in order to know the differentiation capacity of the 17q cell line, 17q was differentiated towards the NMP stage. Markers related to the NMP stage, such as *TBXT and SOX2*, were upregulated significantly compared to hPSC, as well as the posterior identity genes *HOXC8* and *CDX2* **(Figure 10-c)**, demonstrating that the 17q cell line can successfully produce NMP cells. To know if chromosome 17q could have caused some differences in the differentiation performance compared to the wild type, qPCR results were analysed between the cell lines **(Figure 10-d)**. The early neural crest marker *PAX3* was significantly downregulated in the 17q cell line compared to wild type, as well as the posterior HOX gene *HOXC8*. *HOXC9* also showed downregulation but this was not significant. This could suggest that 17q gain may have an effect on the establishment of the posterior as well as an early NC identity during differentiation.

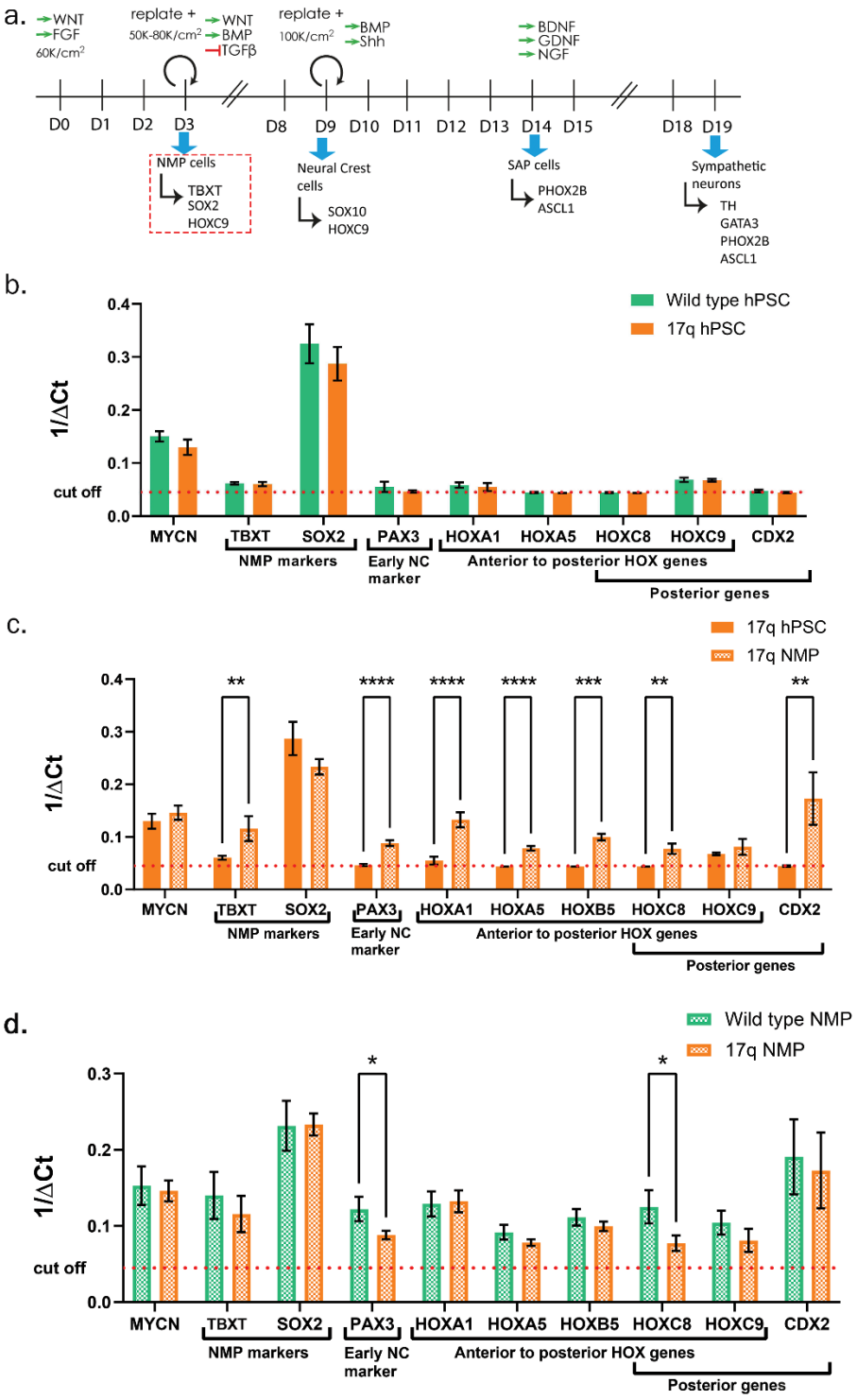

Figure 10. NMP differentiation performance of 17q cell line compared to the wild type.

a. Schematic diagram of the directed differentiation of human pluripotent stem cells into Neuromesodermal progenitors (**NMP**), Neural Crest (**NC**), Sympathoadrenal progenitors (**SAP**) and Sympathetic neurons (**SN**). The red rectangle highlights the day cells were harvested, and which markers were used to validate the stage. **b.** Comparison of wild type and 17q cell line (specified in graph legend) RNA expression at day 0 of differentiation. No significant differences were found. **c.** 17q cell line was differentiated into NMP. Genes related to NMP differentiation show significant upregulation, except for *HOXC9* and *SOX2*. **d.** Comparison of wild type and 17q cell lines

differentiated into NMP stage. *PAX3,* a gene related to an early neural crest marker, shows significant downregulation in 17q compared to wild type, as well as *HOXC8*, a gene related to a posterior identity. **b-d.** Gene expression values are plotted as 1/ΔCt. A cut off line (dotted red line) has been set at 0.045 as this is the equivalent to 40 cycles on the qPCR machine (n= 3 biological replicates, error bars= SD, Independent Welch t-tests, p ≤ 0.05= *, p ≤ 0.01= **, p ≤ 0.001= ***, p ≤ 0.0001= ****).

The expression of key NMP markers was also evaluated by immunofluorescence **(Figure 11-a)**. When 17q NMP was compared to wild type NMP no significant differences were found in the percentage of cells expressing SOX2, HOXC9 and TBXT markers **(Figure 11-b)**.

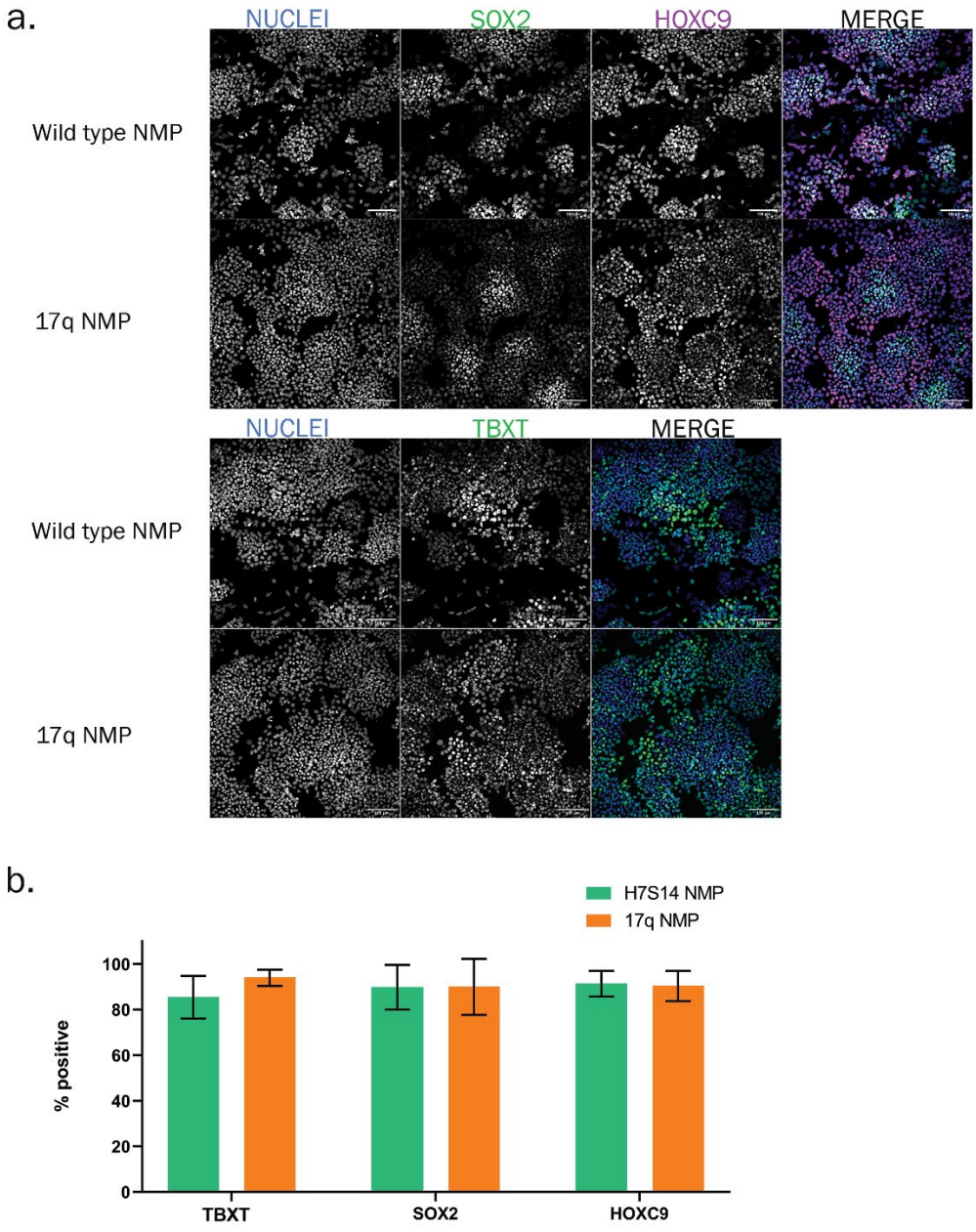

Figure 11. Detection of NMP markers by immunostaining at day 3 in Wild type and 17q cell lines. **a.** Immunofluorescence images of the Wild type and 17q cell lines differentiated into NMP. Shown are SOX2, HOXC9 and TBXT (Merge: Hoechst(blue), SOX2/TBXT(green), HOXC9(magenta)). **b.** Percentage of cells expressing SOX2, HOXC9 and TBXT markers in the immunofluorescence analysis. No significant differences were found (n≥ 3 biological replicates, Independent Welch t-tests, Error bar= SD).

I next tested the behaviour of the two cell lines during their differentiation from NMPs to trunk NC which involves the culture of cells under conditions promoting WNT signalling stimulation, moderate BMP activity while blocking TGFβ signalling, for 6 days. **(Figure 12-a)**. Cells were harvested and analysed by qPCR **(Figure 12-b)**. I found that genes related to the neural crest stage, such as *PAX3* and *SOX10* as well as a posterior identity (posterior *HOXC8, HOXC9, and CDX2*), were significantly upregulated (**Figure 12-b**). The wild type cell line did successfully upregulate these markers when compared against its undifferentiated stage. I also tested for the presence of the early sympathoadrenal marker ASCL1, as it has been reported to be transiently found in the neural crest-derived neural precursors (Lo et al., 1991). *ASCL1* was significantly upregulated in the neural crest-induced wild type cells. These data suggest that the wild type cell line can successfully produce trunk neural crest cells *in vitro.* These observations were verified at the protein level. SOX10 and HOXC9 expression was detected by immunofluorescence **(Figure 12-c).** When images were quantified SOX10/HOXC9 expression represented around 80% of the total population of cells **(Figure 12-d).**

To assess whether 17q aberration could have any significant effect on the specification of neural crest, NMPs of the 17q cell line were differentiated into neural crest cells, following the same protocol used for the wild type **(Figure 13-a)**. In **Figure 13-b** it is shown a comparison of the gene expression profile of the wild type neural crest cell versus the 17q neural crest. It can be observed that the 17q cell line expressed significantly lower levels of the posterior/trunk axial identity markers *HOXA5, HOXC8, and HOXC9*, the latter two are linked to the establishment of the trunk identity in neural crest specification.

Protein expression was assessed by immunofluorescence and representative images of SOX10 and HOXC9 protein expression in both wild type and 17q neural crest are shown **(Figure 13-c)**. HOXC9 expression seems dramatically diminished when compared to the wild type. This observation was confirmed when imaging quantification was done **(Figure 13-d)**. Overall, the percentage of cells expressing HOXC9 were significantly less in the 17q cell line compared to wild type in neural crest conditions. Moreover, when the mean intensity per nuclei of SOX10 and HOXC9 antibodies were measured (**Figure 14-a density plot)**, HOXC9, but not SOX10, showed overall lower expression. This analysis was confirmed in the intensity analysis of three independent biological replicates, showing similar and consistent observations (**Figure 14-b-d**).

In summary, although the wild type cells seem to efficiently generate neural crest cells with a trunk identity, the 17q cell line displayed difficulty in maintaining its posterior identity as evidenced by the lower expression of the trunk-associated markers *HOXC8* and *HOXC9*.

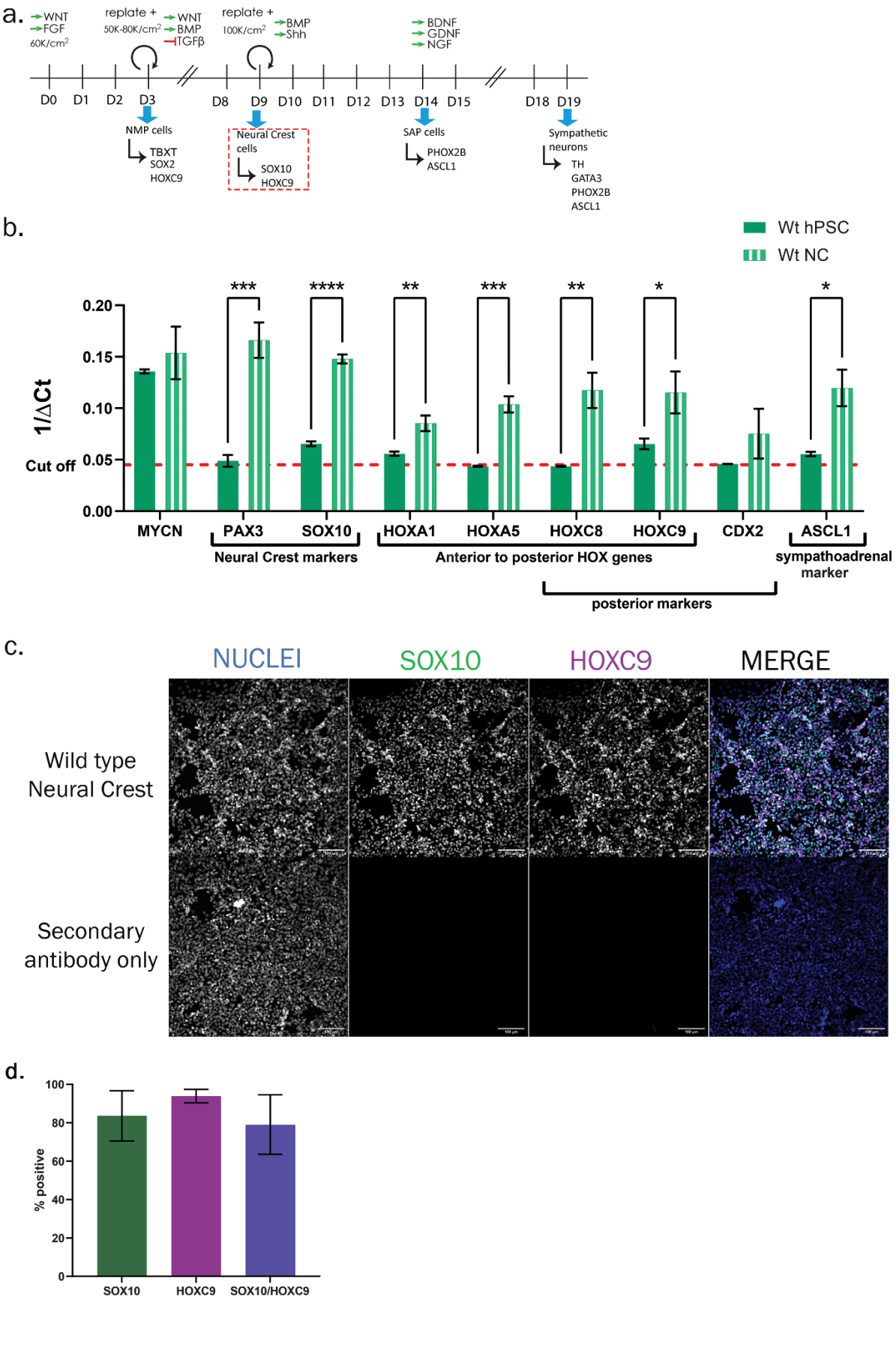
a.
WNT
FGF
60K/cm²
replate +
50K-80K/cm²
WNT
BMP
TGFβ
replate +
100K/cm²
BMP
Shh
BDNF
GDNF
NGF
D0 D1 D2 D3 D8 D9 D10 D11 D12 D13 D14 D15 D18 D19
NMP cells
TBXT
SOX2
HOXC9
Neural Crest cells
SOX10
HOXC9
SAP cells
PHOX2B
ASCL1
Sympathetic neurons
TH
GATA3
PHOX2B
ASCL1
b.
Wt hPSC
Wt NC
1/ΔCt
Cut off
0.20
0.15
0.10
0.05
0.00
***
****
**
***
**
*
*
MYCN
PAX3
SOX10
HOXA1
HOXA5
HOXC8
HOXC9
CDX2
ASCL1
Neural Crest markers
Anterior to posterior HOX genes
sympathoadrenal marker
posterior markers
c.
NUCLEI
SOX10
HOXC9
MERGE
Wild type Neural Crest
Secondary antibody only
d.
% positive
100
80
60
40
20
0
SOX10
HOXC9
SOX10/HOXC9

Figure 12. Neural crest differentiation of the wild type cell line

a. Schematic diagram of the directed differentiation of human pluripotent stem cells into Neuromesodermal progenitors (**NMP**), Neural Crest (**NC**), Sympathoadrenal progenitors (**SAP**) and Sympathetic neurons (**SN**). The red rectangle highlights the day cells were harvested, and which markers were used to validate the stage. **b.** Wild type cell line was differentiated into neural crest (NC). the bar chart shows the qPCR analysis, gene expression values are plotted as 1/ΔCt for pluripotent stem cells and differentiated NMP (specified in graph legend). A cut off line (dotted red line) has been set at 0.045 as this is the equivalent of 40 cycles on the qPCR machine. Genes related to NC differentiation show significant upregulation, except for *CDX2*. (n= 3 biological replicates, error bars= SD, Independent Welch t-tests, $p \leq 0.05$= *, $p \leq 0.01$= **, $p \leq 0.001$= ***, $p \leq 0.0001$= ****). **c.** Immunofluorescence images of the wild type cell line differentiated into NC. Shown are SOX10 and HOXC9 staining with its corresponding secondary antibody only test (Merge: Hoechst=blue, SOX10=green, HOXC9=magenta). **d.** Percentage of cells expressing SOX10, HOXC9 and co-expressing SOX10/HOXC9 markers in the immunofluorescence analysis (n≥ 3 biological replicates. Independent Welch t-tests, error bar= SD).

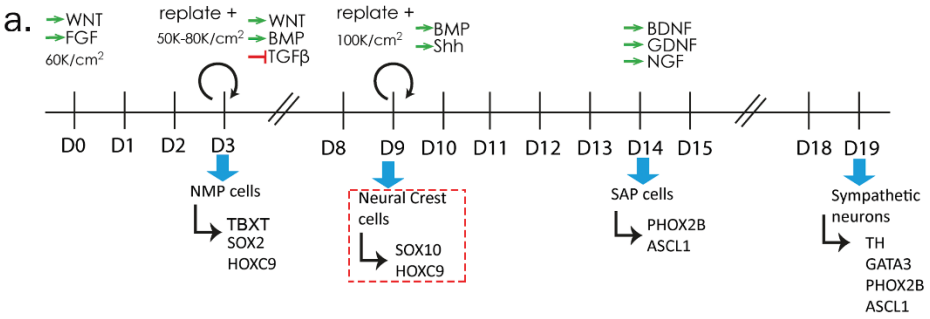
a.
WNT
FGF
60K/cm²
replate +
50K-80K/cm²
WNT
BMP
TGFβ
replate +
100K/cm²
BMP
Shh
BDNF
GDNF
NGF
D0 D1 D2 D3 D8 D9 D10 D11 D12 D13 D14 D15 D18 D19
NMP cells
TBXT
SOX2
HOXC9
Neural Crest cells
SOX10
HOXC9
SAP cells
PHOX2B
ASCL1
Sympathetic neurons
TH
GATA3
PHOX2B
ASCL1

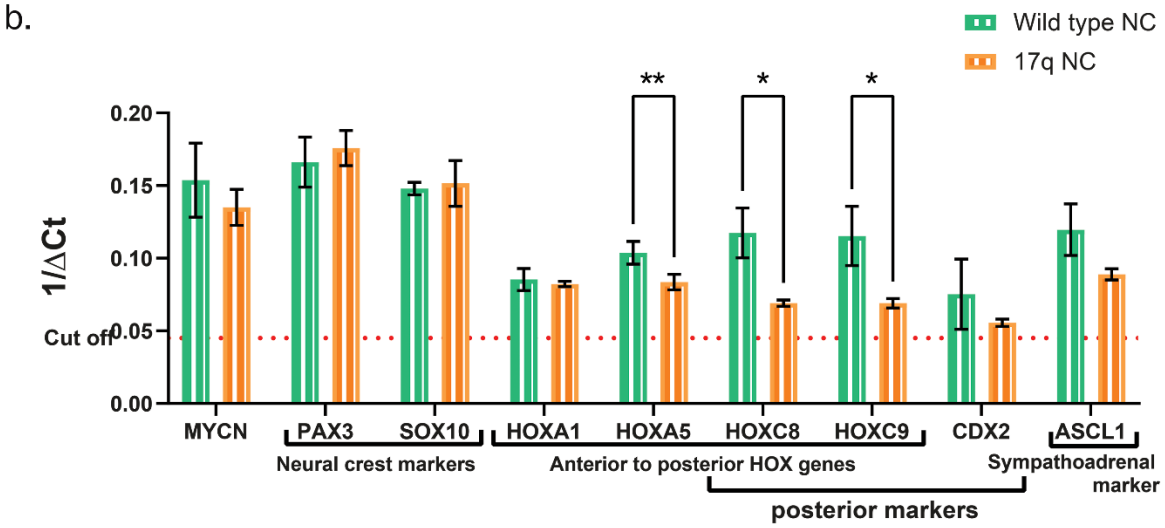
b.
Wild type NC
17q NC
1/ΔCt
Cut off
0.20
0.15
0.10
0.05
0.00
**
*
*
MYCN
PAX3
SOX10
HOXA1
HOXA5
HOXC8
HOXC9
CDX2
ASCL1
Neural crest markers
Anterior to posterior HOX genes
posterior markers
Sympathoadrenal marker

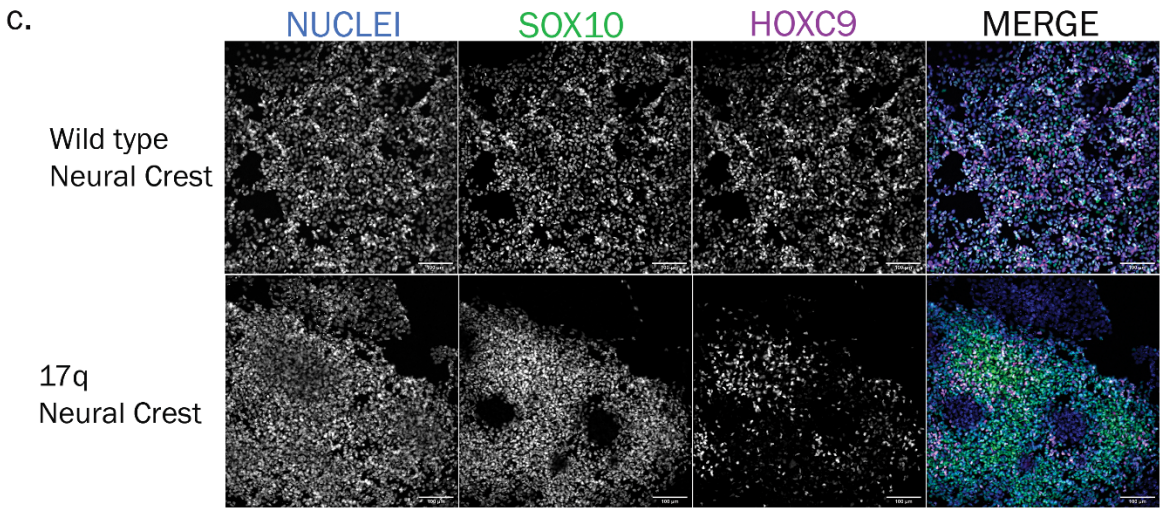
c.
NUCLEI
SOX10
HOXC9
MERGE
Wild type Neural Crest
17q Neural Crest

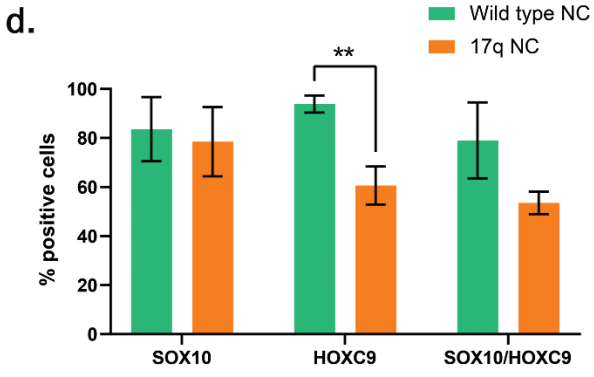
d.
Wild type NC
17q NC
**
% positive cells
100
80
60
40
20
0
SOX10
HOXC9
SOX10/HOXC9

Figure 13. Neural crest differentiation performance of 17q cell line compared to the wild type. **a.**Schematic diagram of the directed differentiation of human pluripotent stem cells into Neuromesodermal progenitors (**NMP**), Neural Crest (**NC**), Sympathoadrenal progenitors (**SAP**) and Sympathetic neurons (**SN**). The red rectangle highlights the day cells were harvested, and which markers were used to validate the stage. **b.** Comparison of wild type and 17q cell lines differentiated into NC stage. A gene linked to central identity (*HOXA5*) showed significant downregulation in 17q compared to wild type as well as two genes related to posterior identity (*HOXC8* and *HOXC9*). **c.** Immunofluorescence images of the wild type and 17q cell lines differentiated into NC. Shown are SOX10 and HOXC9 (Merge: Hoechst(blue), SOX10(green), HOXC9(magenta)). **d.** Percentage of cells expressing SOX10, HOXC9 and co-expressing SOX10/HOXC9 markers in the immunofluorescence analysis. The percentage of cells expressing HOXC9 in 17q was significantly lower in 17q NC compared to wild type (n≥ 3 biological replicates, Independent Welch t-tests, Error bar= SD). Extracted from immunofluorescent imaging and cell profiler analysis. **b, d.** Gene expression values are plotted as 1/ΔCt. A cut off line (dotted red line) has been set at 0.045 as this is the equivalent to 40 cycles on the qPCR machine (n ≥ 3 biological replicates, error bars= SD, Independent Welch t-tests, $p \leq 0.05$= *, $p \leq 0.01$= **, $p \leq 0.001$= ***, $p \leq 0.0001$= ****).

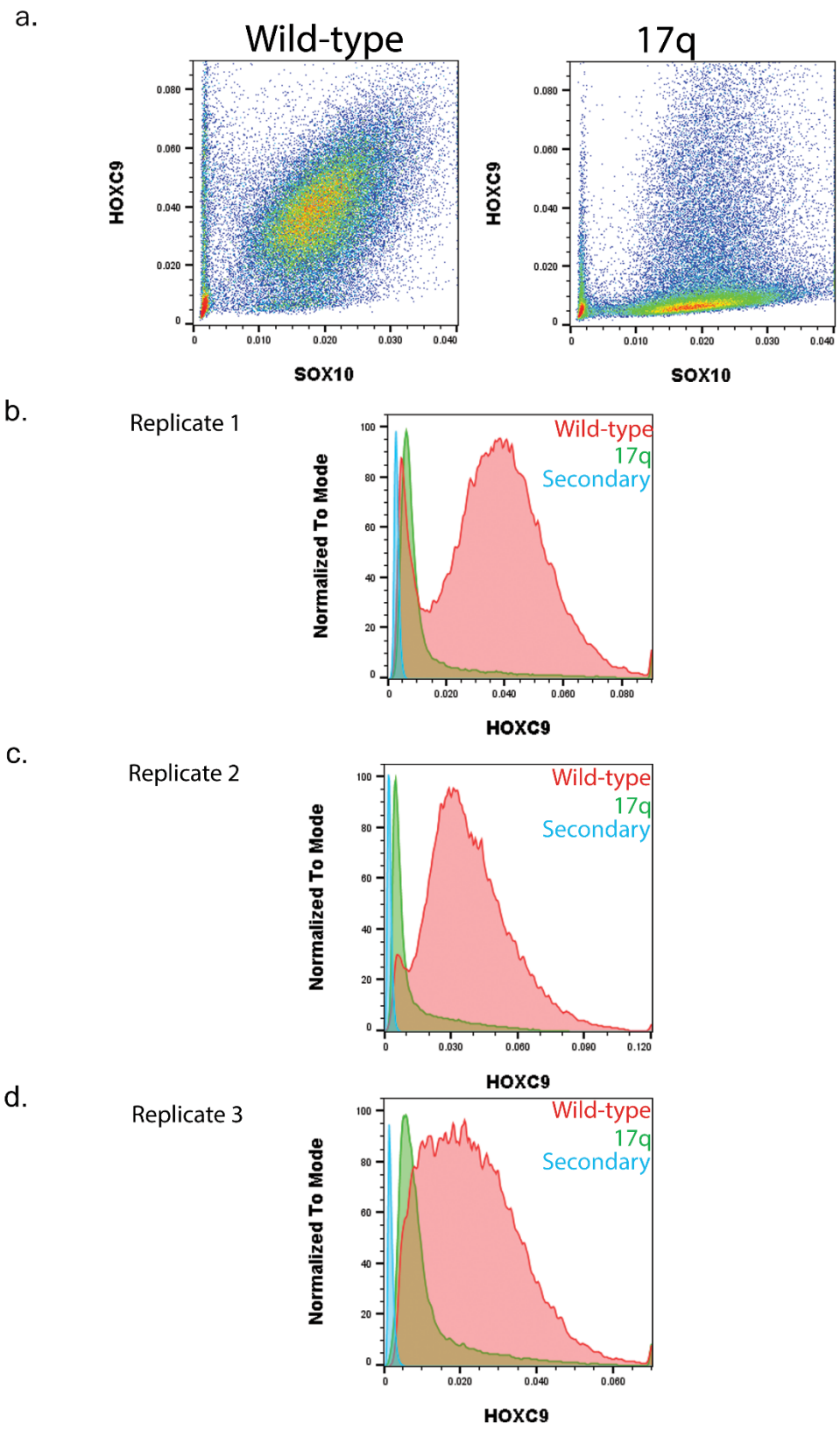

Figure 14. Single-cell immunofluorescence intensity analysis in NC cells
a. Representative density plot of SOX10 vs HOXC9 for wild type and 17q cell lines at NC stage. Extracted from immunofluorescent imaging and cell profiler analysis. Mean florescent intensity plotted per cell. **b-d.** Panels of histograms for HOXC9 in wild type (red), 17q (green) and secondary only (blue). Shown are three pieces of data from three biological replicates.

3.2.2 17q cell line shows underdevelopment during the sympathoadrenal specification when compared to the wild type

I then assessed the next step of the differentiation protocol, which was the generation of sympathoadrenal progenitor cells (**Figure 15-a).** qPCR analysis revealed *SOX10* and *HOXC9* remained highly expressed and the sympathoadrenal markers, *ASCL1 and PHOX2B* showed evident upregulation when compared to the pluripotent stage. Other markers belonging to the sympathoadrenal lineage were also assessed, exhibiting a clear upregulation on *GATA3, GATA2 and DBH* (**Figure 15-b**).

Protein expression assessment of the key sympathoadrenal progenitor markers was also performed by immunofluorescence (**Figure 15-c**). SOX10, ASCL1 and PHOX2B protein expression were found, although, when the percentage of cells expressing the markers was quantified, a low number of cells were positive for ASCL1, contrasting the high efficiencies of both SOX10 and PHOX2B (**Figure 15-d**). All these results together suggest the wild type cell line has the capacity to produce sympathoadrenal progenitors.

Although the 17q line was less efficient in generating trunk neural crest, I decided to take them to the sympathoadrenal stage to evaluate whether the loss of trunk identity would have downstream repercussions. 17q cells at the neural crest stage were induced to generate sympathoadrenal progenitor (SAP) cells (**Figure 16-a**). When 17q gene expression was compared to the wild type at the same stage of the differentiation (**Figure 16-b**). *HOXC9* and the sympathoadrenal lineage markers *ASCL1, PHOX2B and PHOX2A* were expressed at lower levels. This was corroborated at the protein level by immunofluorescence analysis. SOX10, HOXC9, ASCL1 and PHOX2B protein expression was analysed and representative images are shown in **Figure 16-c**. Quantification of the images was performed to assess the percentage of cells expressing the markers. Fewer cells were found to express HOXC9, PHOX2B and ASCL1 (**Figure 16-d**) in 17q SAP in line with the qPCR data. These data suggest that the 17q gain continues to negatively affect the differentiation towards the sympathetic lineage.

Wild type cells growing in SAP medium were induced towards a more mature stage of differentiation by supplementing the medium with NGF, BDNG, and GDNF growing factors (**Figure 17-a**). After 5 days, cells were harvested, and a qPCR analysis was performed to verify the expression of markers corresponding to the sympathetic neuron stage (**Figure 17-b)**. *ASCL1 and PHOX2B* genes are evidently overexpressed (compared with pluripotent stage). *ASCL1* was slightly less expressed than in the previous stage (**Figure 17-b**) but *PHOX2B* expression increased. Although other markers of the sympathoadrenal lineage remained high, such as *GATA3 and GATA2*, no further overexpression was observed in more mature markers such as *TH and DBH*.

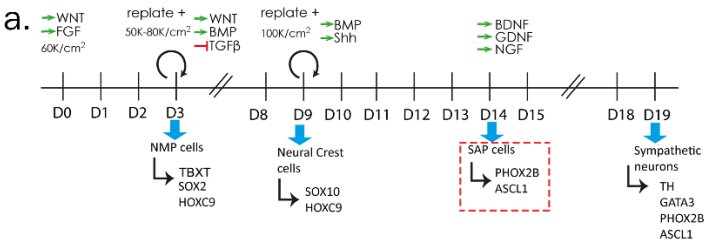
a.
WNT
FGF
60K/cm²
replate +
50K-80K/cm²
WNT
BMP
TGFβ
replate +
100K/cm²
BMP
Shh
BDNF
GDNF
NGF
D0 D1 D2 D3 D8 D9 D10 D11 D12 D13 D14 D15 D18 D19
NMP cells
TBXT
SOX2
HOXC9
Neural Crest cells
SOX10
HOXC9
SAP cells
PHOX2B
ASCL1
Sympathetic neurons
TH
GATA3
PHOX2B
ASCL1

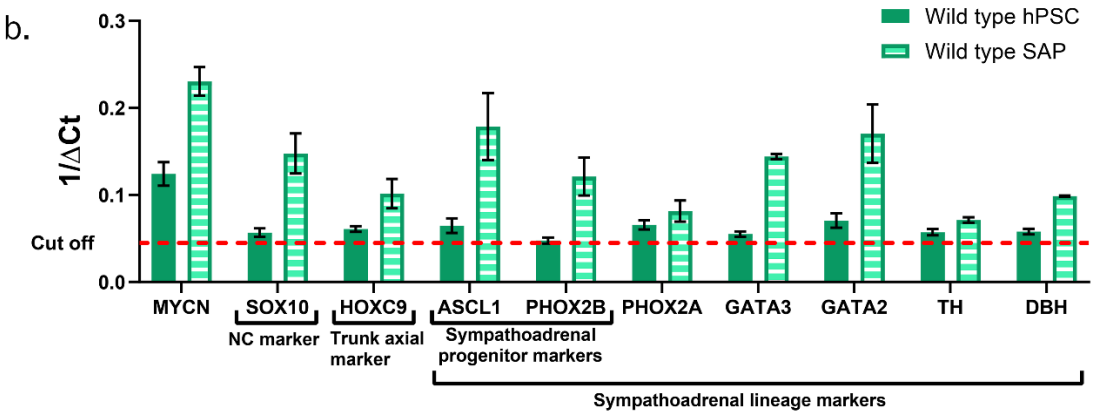
b.
Wild type hPSC
Wild type SAP
1/ΔCt
0.3
0.2
0.1
0.0
Cut off
MYCN
SOX10
HOXC9
ASCL1
PHOX2B
PHOX2A
GATA3
GATA2
TH
DBH
NC marker
Trunk axial marker
Sympathoadrenal progenitor markers
Sympathoadrenal lineage markers

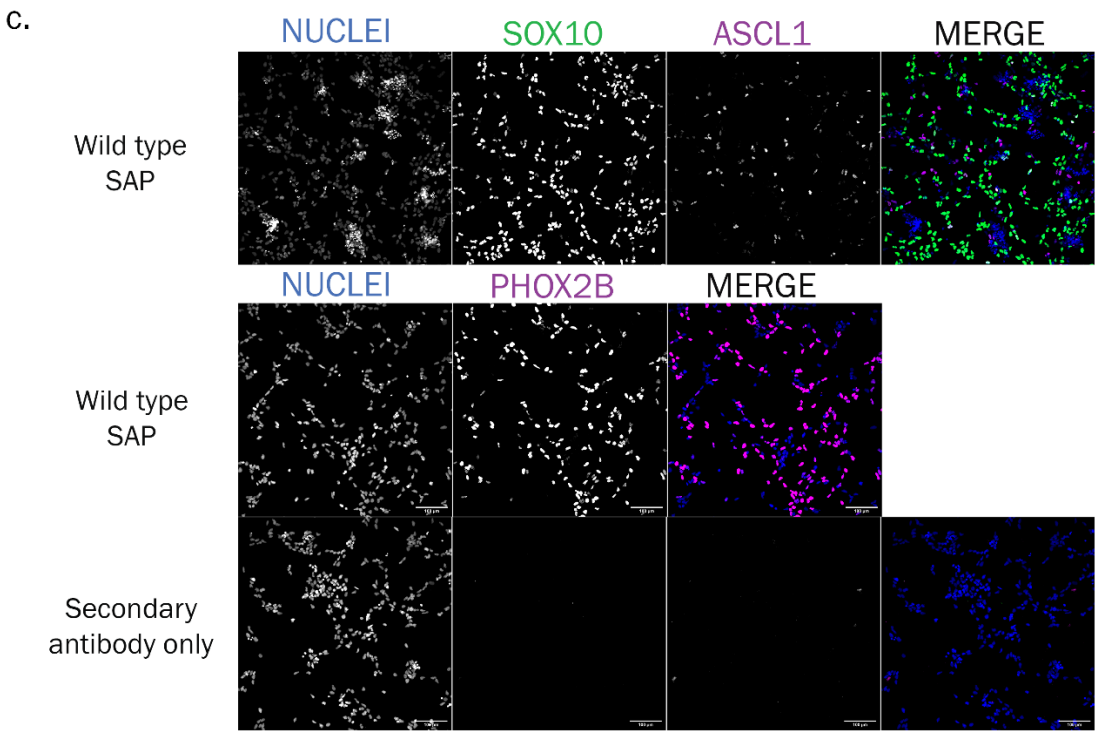
c.
NUCLEI
SOX10
ASCL1
MERGE
Wild type SAP
NUCLEI
PHOX2B
MERGE
Wild type SAP
Secondary antibody only

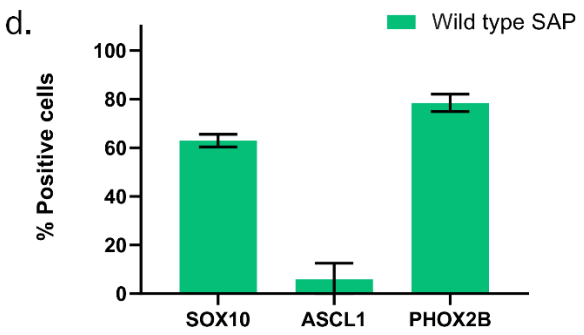
d.
Wild type SAP
% Positive cells
100
80
60
40
20
0
SOX10
ASCL1
PHOX2B

Figure 15. Differentiation of the wild type cell line towards Sympathoadrenal progenitor stage

a. Schematic diagram of the directed differentiation of human pluripotent stem cells into Neuromesodermal progenitors (**NMP**), Neural Crest (**NC**), Sympathoadrenal progenitors (**SAP**) and Sympathetic neurons (**SN**). The red rectangle highlights the day cells were harvested, and which markers were used to validate the stage. **b.** Wild type cell line was differentiated into Sympathoadrenal progenitors (SAP). The bar chart shows the qPCR analysis, gene expression values are plotted as 1/ΔCt for pluripotent stem cells and differentiated SAP (specified in graph legend). A cut off line (dotted red line) has been set at 0.045 as this is the equivalent of 40 cycles on the qPCR machine. Genes related to SAP differentiation show an increase in their expression. (n= 2 biological replicates, error bars= SD, no statistical test was performed) **c.** Immunofluorescence images of the wild type cell line differentiated into SAP. Shown are SOX10, ASCL1 and PHOX2B staining with its corresponding secondary antibody only test (Merge: Hoechst=blue, SOX10=green, ASCL1/PHOX2B=magenta). **d.** Percentage of cells expressing SOX10, ASCL1 and PHOX2B markers in the immunofluorescence analysis (n=2 biological replicates, error bar= SD, no statistical test was performed).

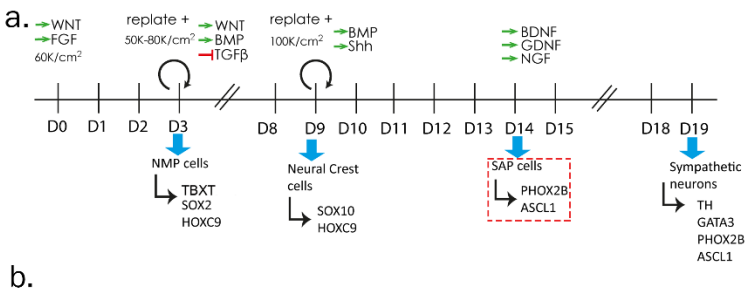
a.
WNT
FGF
60K/cm²
replate +
50K-80K/cm²
WNT
BMP
TGFβ
replate +
100K/cm²
BMP
Shh
BDNF
GDNF
NGF
D0 D1 D2 D3 D8 D9 D10 D11 D12 D13 D14 D15 D18 D19
NMP cells
TBXT
SOX2
HOXC9
Neural Crest cells
SOX10
HOXC9
SAP cells
PHOX2B
ASCL1
Sympathetic neurons
TH
GATA3
PHOX2B
ASCL1

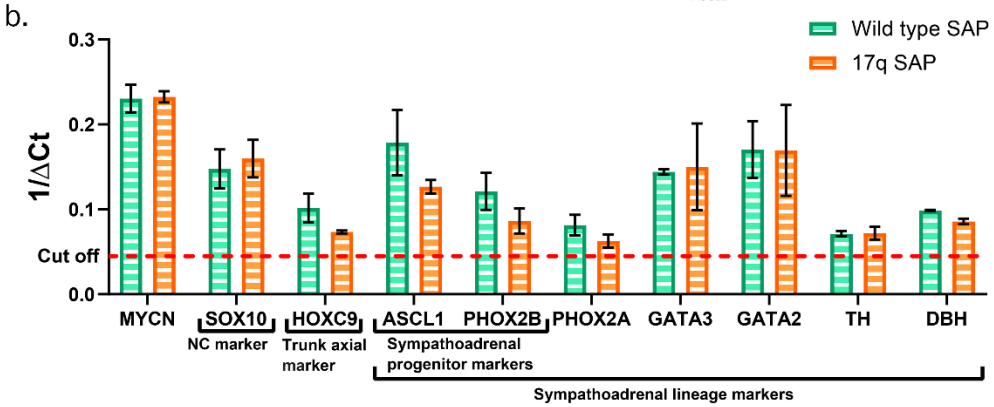
b.
Wild type SAP
17q SAP
1/ΔCt
0.3
0.2
0.1
Cut off
0.0
MYCN
SOX10
NC marker
HOXC9
Trunk axial marker
ASCL1
PHOX2B
Sympathoadrenal progenitor markers
PHOX2A
GATA3
GATA2
TH
DBH
Sympathoadrenal lineage markers

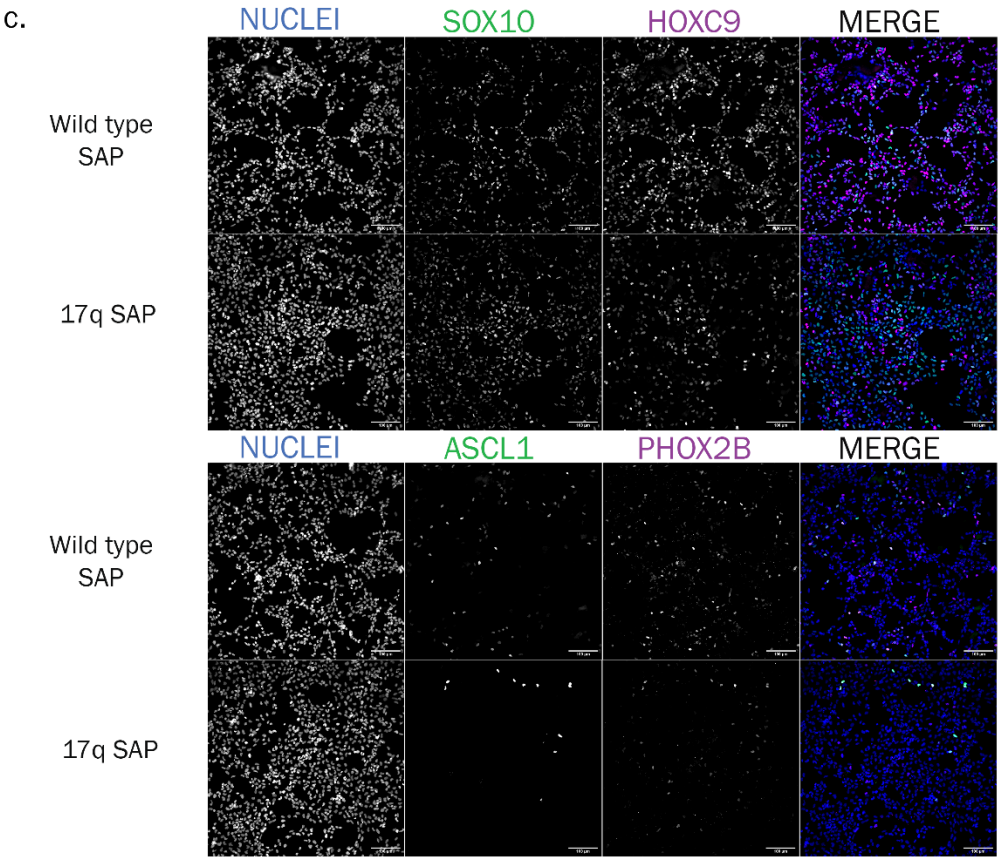
c.
NUCLEI
SOX10
HOXC9
MERGE
Wild type SAP
17q SAP
NUCLEI
ASCL1
PHOX2B
MERGE
Wild type SAP
17q SAP

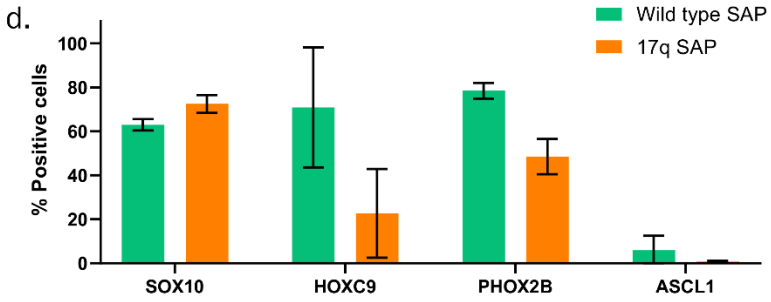
d.
Wild type SAP
17q SAP
% Positive cells
100
80
60
40
20
0
SOX10
HOXC9
PHOX2B
ASCL1

Figure 16. Sympathoadrenal progenitor differentiation performance of 17q cell line compared to the wild type. **a.** Schematic diagram of the directed differentiation of human pluripotent stem cells into Neuromesodermal progenitors (**NMP**), Neural Crest (**NC**), Sympathoadrenal progenitors (**SAP**) and Sympathetic neurons (**SN**). The red rectangle highlights the day cells were harvested, and which markers were used to validate the stage. **b.** Comparison of wild type and 17q cell lines differentiated into SAP stage. *HOXC9, ASCL1 and PHOX2B* expression seem lower in 17q compared to wild type. Gene expression values are plotted as 1/ΔCt. A cut off line (dotted red line) has been set at 0.045 as this is the equivalent of 40 cycles on the qPCR machine (n = 2 biological replicates, error bars= SD) **c.** Immunofluorescence images of the wild type and 17q cell lines differentiated into SAP. Shown are SOX10, HOXC9, ASCL1 and PHOX2B (Merge: Hoechst(blue), SOX10/ASCL1(green), HOXC9/PHOX2B(magenta)). **d.** Percentage of cells expressing SOX10, HOXC9, PHOX2B and ASCL1 markers in the immunofluorescence analysis. The percentage of cells expressing HOXC9 and PHOX2B seem lower in 17q SAP compared to wild type (n=2 biological replicates, no statistical test performed, Error bar= SD). Extracted from immunofluorescent imaging and cell profiler analysis.

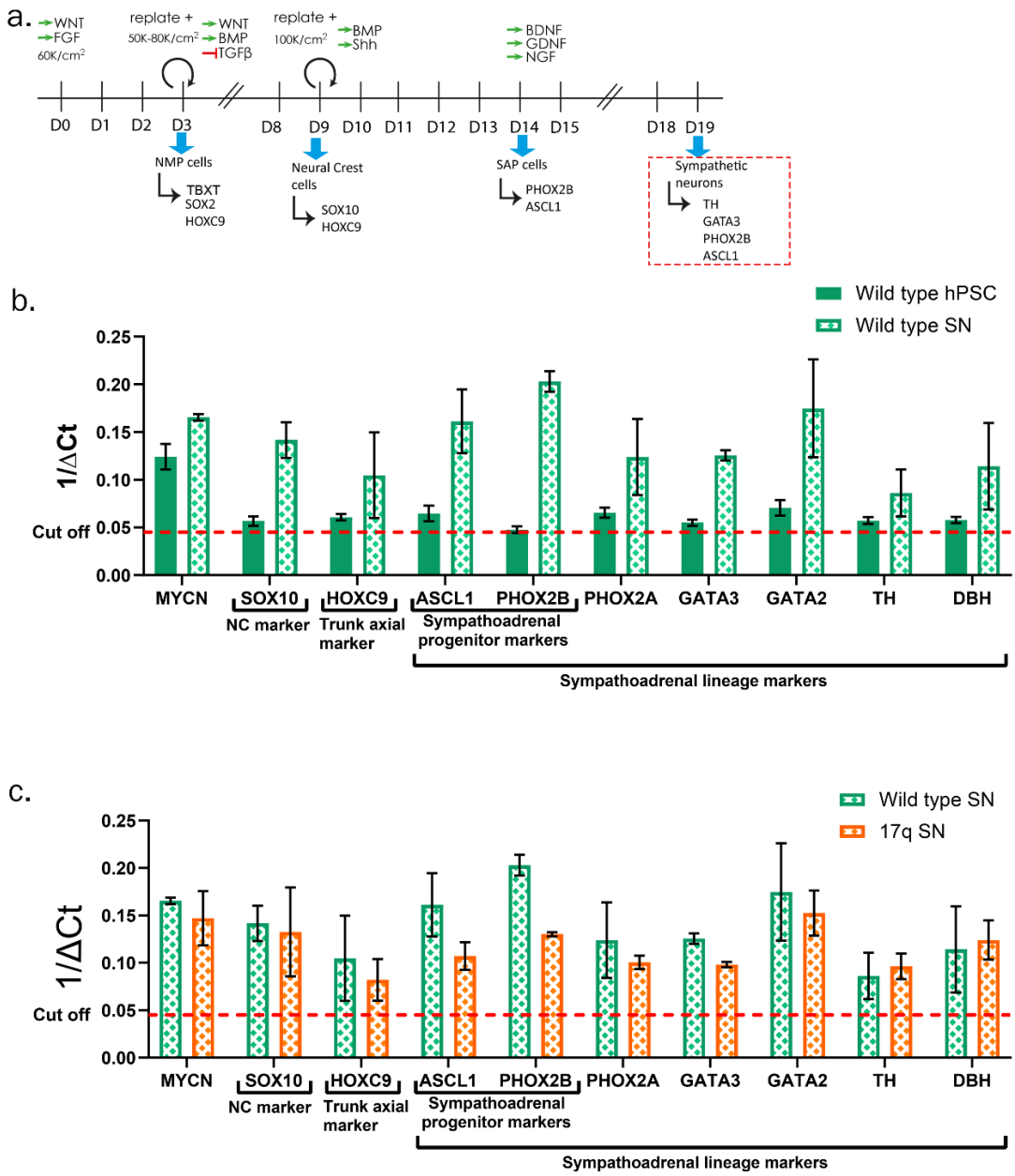

Figure 17. Differentiation of the wild type and 17q cell lines into sympathetic neurons
a. Schematic diagram of the directed differentiation of human pluripotent stem cells into Neuromesodermal progenitors (**NMP**), Neural Crest (**NC**), Sympathoadrenal progenitors (**SAP**) and Sympathetic neurons (**SN**). The red rectangle highlights the day cells were harvested, and which markers were used to validate the stage. **b.** Wild type cell line was differentiated into sympathetic neurons (SN). Genes related to the SN stage showed an increase in their expression. **c.** Comparison of wild type and 17q cell lines differentiated into SN stage. Genes related to the SN stage such as *ASCL1, PHOX2B and GATA3* showed lower expression. **b-c.** Gene expression values are plotted as 1/ΔCt. A cut off line (dotted red line) has been set at 0.045 as this is the equivalent of 40 cycles on the qPCR machine (n= 2 biological replicates, error bars= SD, no statistical test was performed).

17q SAP cells were cultured in the same conditions as the wild type to induce the maturation towards the sympathetic neuron stage (**Figure 17-a**). Then, their gene expression was compared to the SAP wild type. Similar difficulties observed in the previous stage seemed to remain at this stage of the differentiation, as even when *PHOX2B and PHOX2A* expression increased compared to the previous stage, they appear to remain lower in expression when compared to the wild type (**Figure 17-c**). This data suggests that 17q cells fail to induce SAP and/or sympathetic neurons (SN) markers even after further differentiation toward the SN lineage.

3.2.3 WNT elevation improves the ability of 17q hPSCs to generate trunk neural crest and its derivatives.

3.2.3.1 hPSCs to NMPs

Due to the high variability, using the published differentiation protocol, we found that the main effect of the chromosome 17q gain is linked to an inability to efficiently induce posterior axial identity markers. Since these are known to be WNT-dependent (Young et al., 2009, Metzis et al., 2018), we hypothesised that an increase in WNT levels may rectify the effect. The new concentration was first tested in the wild type cell line during NMP induction (**Figure 18-a**). Wild type human pluripotent stem cells (hPSC) were grown in Neuro-mesodermal progenitor medium, consisting in N2B27 medium, supplemented with 20ng/ml of FGF and 4µm of CHIR (**Figure 18-a)**. After three days, wild type cells were harvested and qPCR was performed. The NMP marker *TBXT* was significantly induced, while *SOX2*, although lower in expression compared to the hPSC stage, remained highly expressed. Furthermore, the expression of the trunk markers *HOXC8, HOXC9 and CDX2* were all upregulated (**Figure 18-b**).

To corroborate that at the protein level these markers were also expressed, immunostainings of the wild type after 3 days of treatment were carried out (**Figure 18-c**). These showed widespread presence of SOX2, HOXC9, TBXT and CDX2 in the cultures. Moreover, image analysis and quantification revealed ~70-80% of the cells were positive for all markers analysed (**Figure 18-d**). These data indicate that treatment with 4 µM CHIR is sufficient to drive the induction of NMPs from hPSCs in a wild type background.

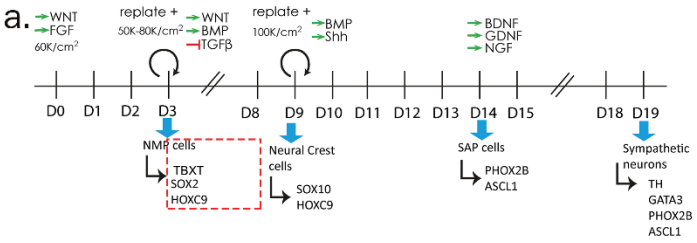
a.
WNT
FGF
60K/cm²
replate +
50K-80K/cm²
WNT
BMP
TGFβ
replate +
100K/cm²
BMP
Shh
BDNF
GDNF
NGF
D0 D1 D2 D3 D8 D9 D10 D11 D12 D13 D14 D15 D18 D19
NMP cells
TBXT
SOX2
HOXC9
Neural Crest cells
SOX10
HOXC9
SAP cells
PHOX2B
ASCL1
Sympathetic neurons
TH
GATA3
PHOX2B
ASCL1

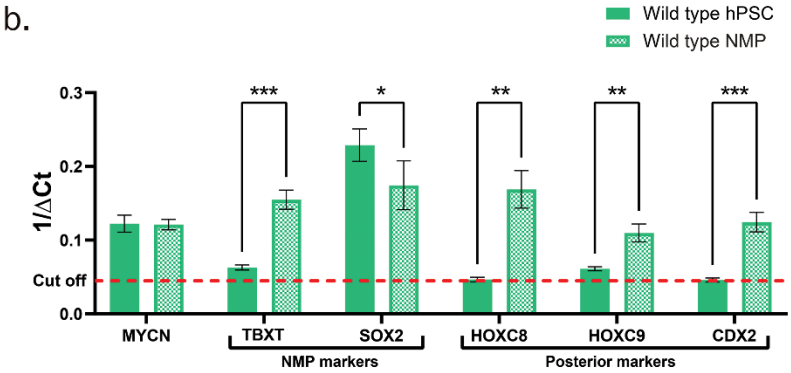
b.
Wild type hPSC
Wild type NMP
1/ΔCt
0.3
0.2
0.1
Cut off
0.0
***
*
**
**
***
MYCN
TBXT
SOX2
HOXC8
HOXC9
CDX2
NMP markers
Posterior markers

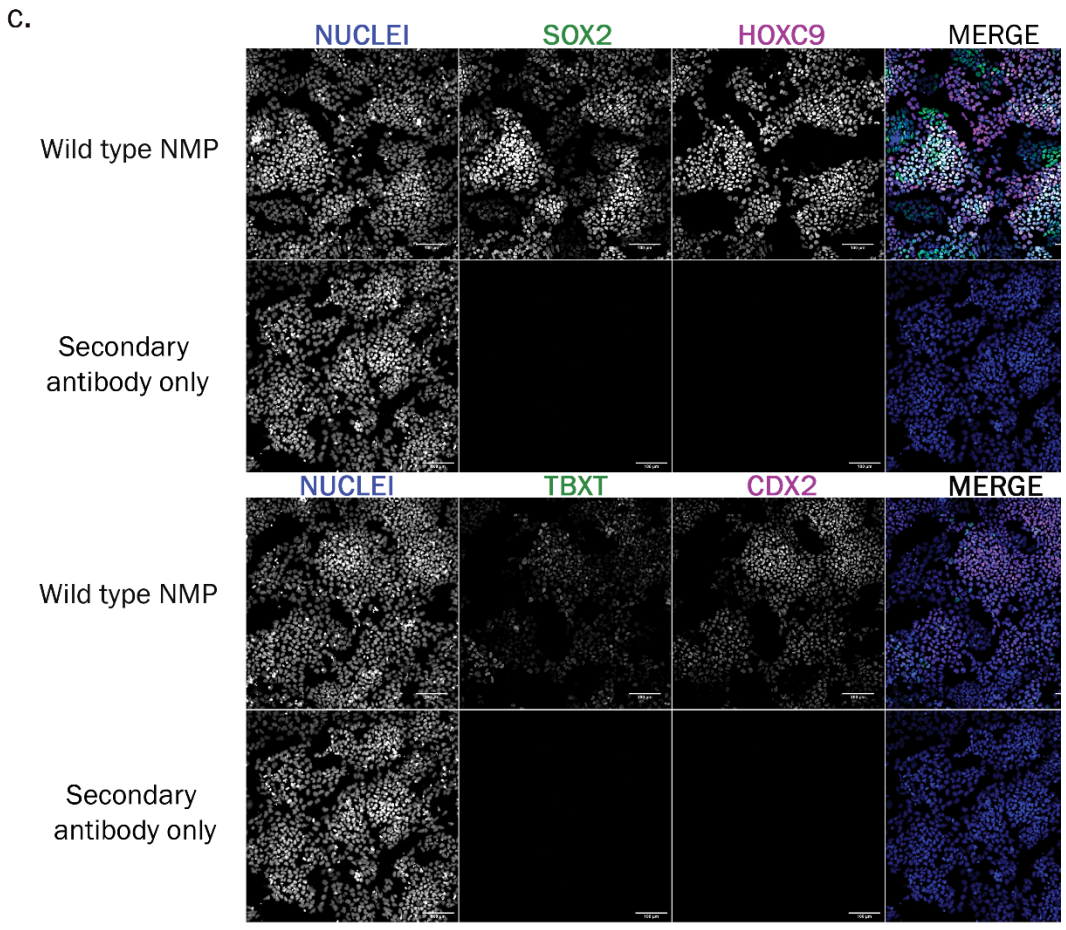
c.
NUCLEI
SOX2
HOXC9
MERGE
Wild type NMP
Secondary antibody only
NUCLEI
TBXT
CDX2
MERGE
Wild type NMP
Secondary antibody only

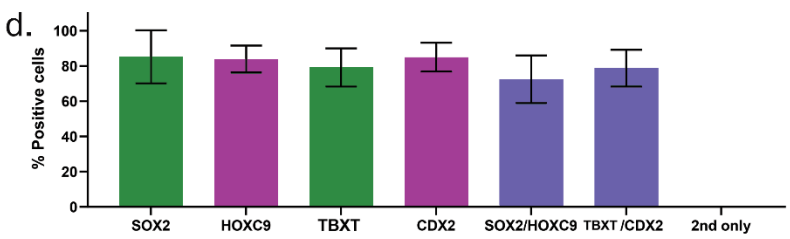
d.
% Positive cells
100
80
60
40
20
0
SOX2
HOXC9
TBXT
CDX2
SOX2/HOXC9
TBXT /CDX2
2nd only

Figure 18. Neuromesodermal progenitor differentiation of the wild type cell line (4μM CHIR)
a. Schematic diagram of the directed differentiation of human pluripotent stem cells into Neuromesodermal progenitors (**NMP**), Neural Crest (**NC**), Sympathoadrenal progenitors (**SAP**) and Sympathetic neurons (**SN**). The red rectangle highlights the day cells were harvested, and which markers were used to validate the stage. **b.** Wild type cell line was differentiated into NMP changing the CHIR concentration from 3μM to 4μM in culture conditions. The bar chart shows the qPCR analysis, gene expression values are plotted as 1/ΔCt for pluripotent stem cells and differentiated NMP (specified in graph legend). A cut off line (dotted red line) has been set at 0.045 as this is the equivalent of 40 cycles on the qPCR machine. Genes related to NMP differentiation show significant upregulation, except for *SOX2* which remains high but is downregulated. (n≥ 3 biological replicates, error bars= SD, Independent Welch t-tests, $p \leq 0.05$= *, $p \leq 0.01$= **, $p \leq 0.001$= ***, $p \leq 0.0001$= ****). **c.** Immunofluorescence images of the wild type cell line differentiated into NMP. Shown are SOX2, HOXC9, TBXT and CDX2 staining with its corresponding secondary antibody only test (Merge: Hoechst=blue, SOX2/TBXT=green, HOXC9/CDX2=magenta). **d.** Percentage of cells expressing SOX2, HOXC9, TBXT and CDX2 markers in the immunofluorescence analysis (n= 4 biological replicates. Error bar= SD).

We next tested the differentiation of 17q hES cells toward NMPs using higher levels of CHIR. 17q cell line was differentiated towards the NMP stage (**Figure 19-a**) using the new CHIR concentration (4μM) used in the wild type cells. NMP induction was corroborated by qPCR. *TBXT and SOX2* NMP markers preserved their high expression when compared to the previous NMP media formulation. When posterior (trunk) genes were analysed, a slight increase in the upregulation of *HOXC8 and HOXC9* was observed (compared to 3μM CHIR). *CDX2* remained significantly expressed as it had been observed before (**Figure 19-b**).

Strikingly, when wild type NMP was compared to 17q NMP cell line, no statistical differences were found (**Figure 19-c**). In previous differentiation when 3μM CHIR concentration was used, *HOXC8* had shown statistically significant differences between the wild type and the 17q cell line.

The qPCR findings were confirmed by immunofluorescence (**Figure 20-a**). SOX2, HOXC9, TBXT and CDX2 proteins were found to be expressed in almost all cells analysed (**Figure 20-b)**. No differences were found in the percentage of positive cells expressing the markers between wild type and 17q NMP cells.

The immunofluorescent intensity of SOX2 and HOXC9 protein expression at the NMP stage mean intensity (per nuclei) was measured in NMP cells grown with 4μM CHIR. **Figure 21-a** shows the correlation between TBXT and HOXC9 intensity for both wild type and 17q NMP from one biological replicate. No significant differences can be perceived in the density plot. Individual histograms of each antibody are shown in **Figure 21-b,c,d** for TBXT, HOXC9 and SOX2 respectively. When the wild type and 17q antibody expression are compared in each of the histograms, no differences are found.

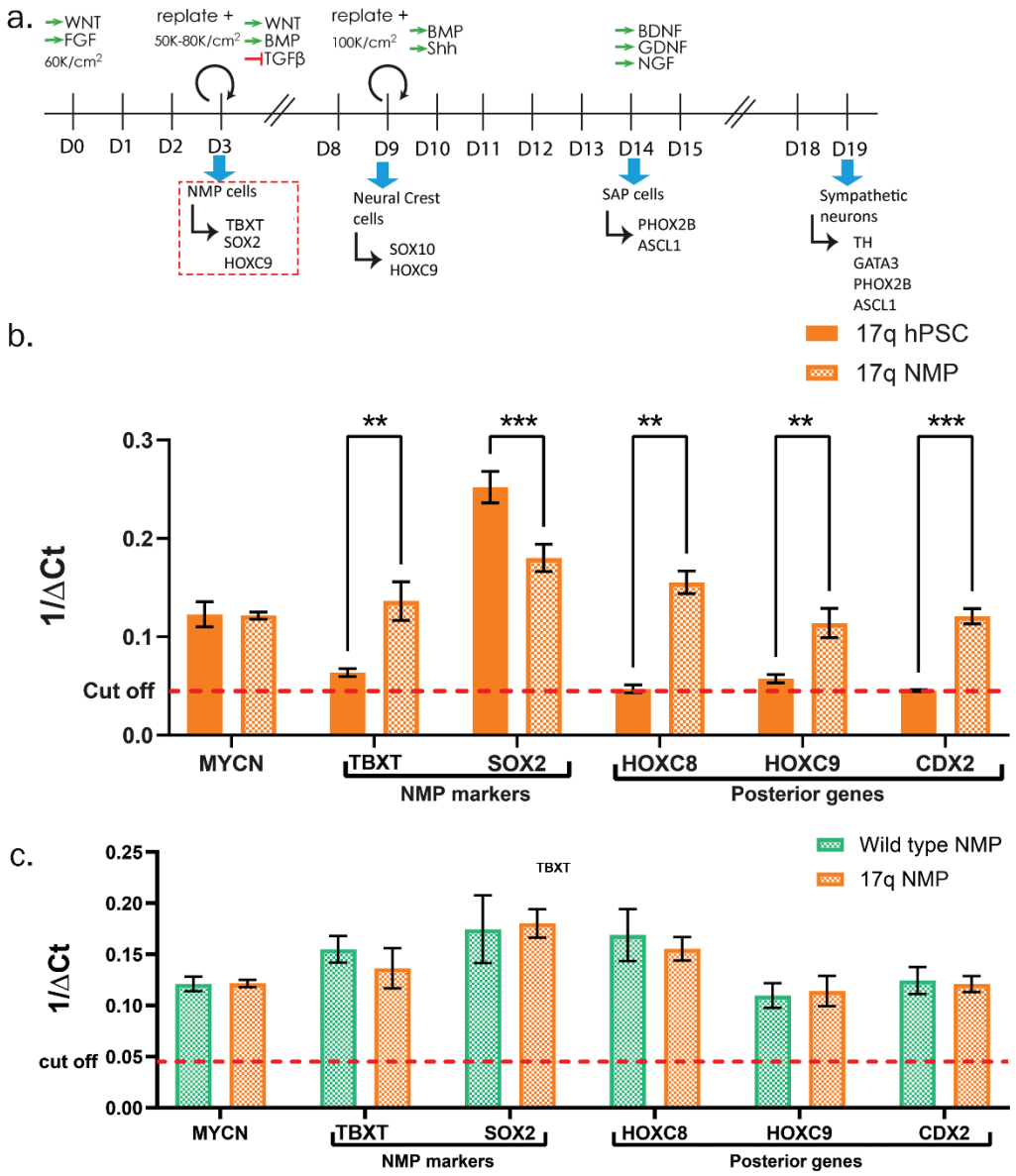

Figure 19. NMP differentiation performance of 17q cell line compared to the wild type (4µM).
a. Schematic diagram of the directed differentiation of human pluripotent stem cells into Neuromesodermal progenitors (**NMP**), Neural Crest (**NC**), Sympathoadrenal progenitors (**SAP**) and Sympathetic neurons (**SN**). The red rectangle highlights the day cells were harvested, and which markers were used to validate the stage. **b.** 17q cell line was differentiated into NMP changing the CHIR concentration from 3µM to 4µM in culture conditions. Genes related to posterior identity and NMP differentiation show significant upregulation, except for SOX2 which remains high but is downregulated. **c.** Comparison of wild type and 17q cell lines differentiated into NMP stage (4µM CHIR). No differences were found in gene expression between the cell lines. **b-c.** Gene expression values are plotted as 1/ΔCt. A cut off line (dotted red line) has been set at 0.045 as this is the equivalent to 40 cycles on the qPCR machine (n≥ 3 biological replicates, error bars= SD, Independent Welch t-tests, $p \leq 0.05$= *, $p \leq 0.01$= **, $p \leq 0.001$= ***, $p \leq 0.0001$= ****).

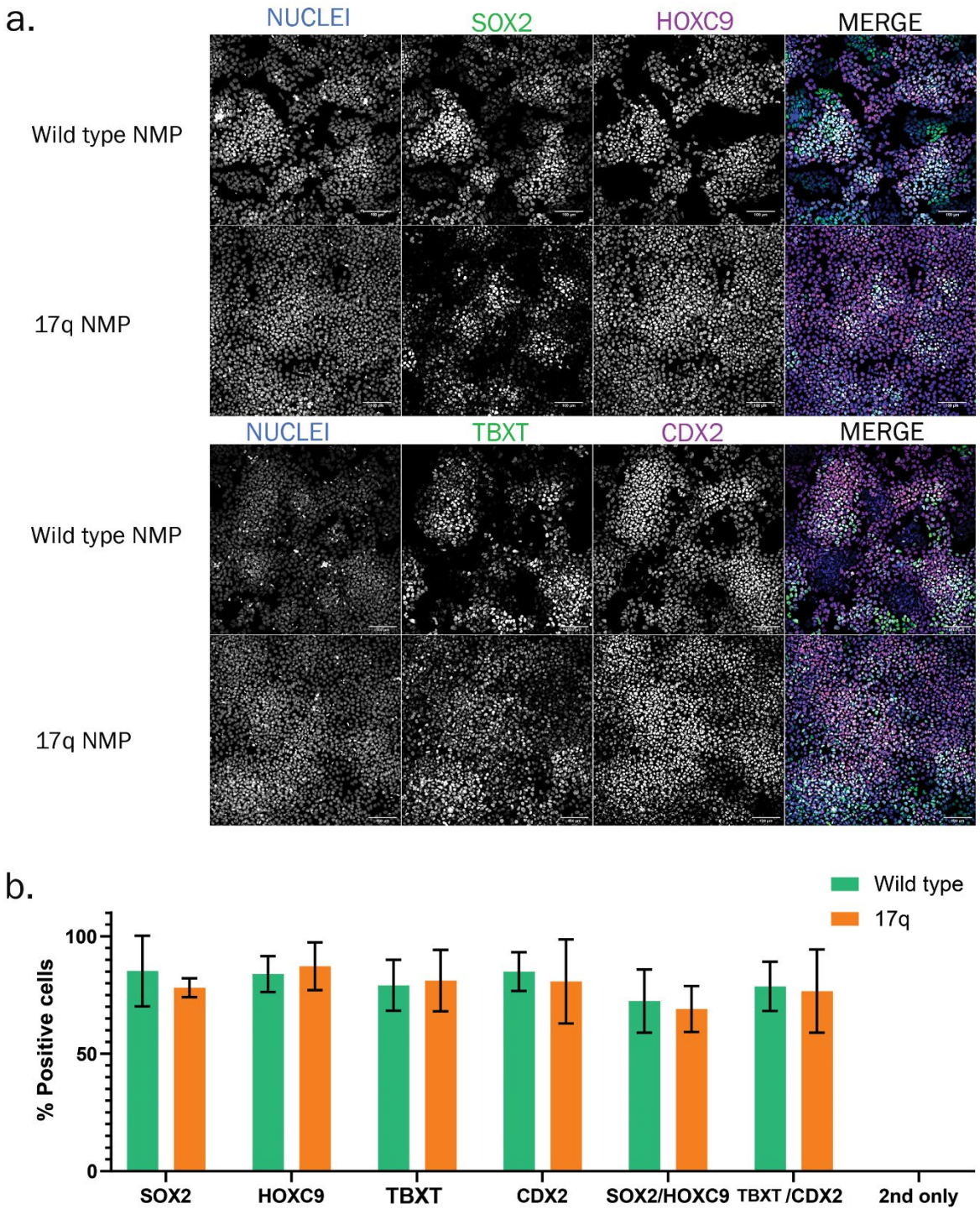

Figure 20. Detection of NMP markers by immunostaining at day 3 in Wild type and 17q cell lines. **a.** Immunofluorescence images of the Wild type and 17q cell lines differentiated into NMP (4µM CHIR). Shown are SOX2, HOXC9, TBXT and CDX2 (Merge: Hoechst(blue), SOX2/TBXT(green), HOXC9/CDX2(magenta)). **b.** Percentage of cells expressing SOX2, HOXC9, TBXT and CDX2 markers alone, as well as cells co-expressing SOX2/HOXC9 and BRA/CDX2 in the immunofluorescence analysis. No significant differences were found (n≥=4 biological replicates, Independent Welch t-tests, Error bar= SD).

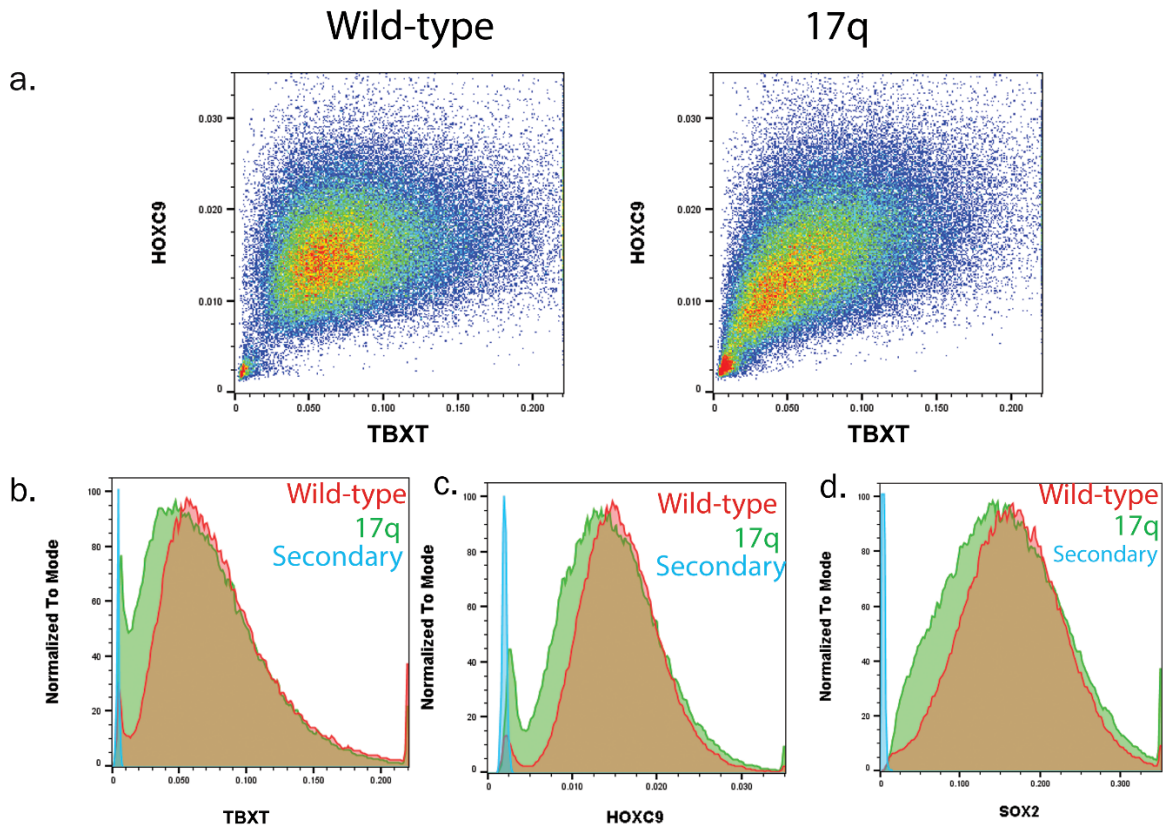

Figure 21. Single-cell immunofluorescence intensity analysis
a. Representative density plot of TBXT vs HOXC9 for wild type and 17q cell lines at NMP stage (4µM CHIR). Extracted from immunofluorescent imaging and cell profiler analysis. Mean florescent intensity plotted per cell. **b-d.** Panels of histograms for HOXC9, TBXT and SOX2 in wild type (red), 17q (green) and secondary only (blue). Shown are data from one representative biological replicate.

These data suggest that by increasing the concentration of CHIR during NMP differentiation, the elevation of WNT signalling corrects for the reduced ability of 17q hPSCs to efficiently acquire a posterior axial identity and 17q can effectively generate neuromesodermal progenitor cells.

3.2.3.2 NMPs to trunk NC

Cell lines grown in the improved NMP 4µM CHIR medium were next taken to the neural crest stage to see if NMP changes could have affected neural crest specification. Wild type neural crest cells were first analysed by qPCR to evaluate the expression of key markers related to the stage (**Figure 22-b)**. The neural crest markers *PAX3* and *SOX10* were significantly upregulated, and all three posterior markers analysed showed increased expression when compared to the pluripotent stage. Furthermore, the sympathoadrenal progenitor marker ASCL1 was also induced at this stage. Similarly, the 17q cell line showed significant upregulation in the neural crest markers, posterior markers and *ASCL1* sympathoadrenal marker (**Figure 22-c**). Surprisingly, when compared with wild type neural crest and 17q side to side, *SOX10* was found to be slightly but significantly upregulated in the 17q neural crest (**Figure 22-d**).

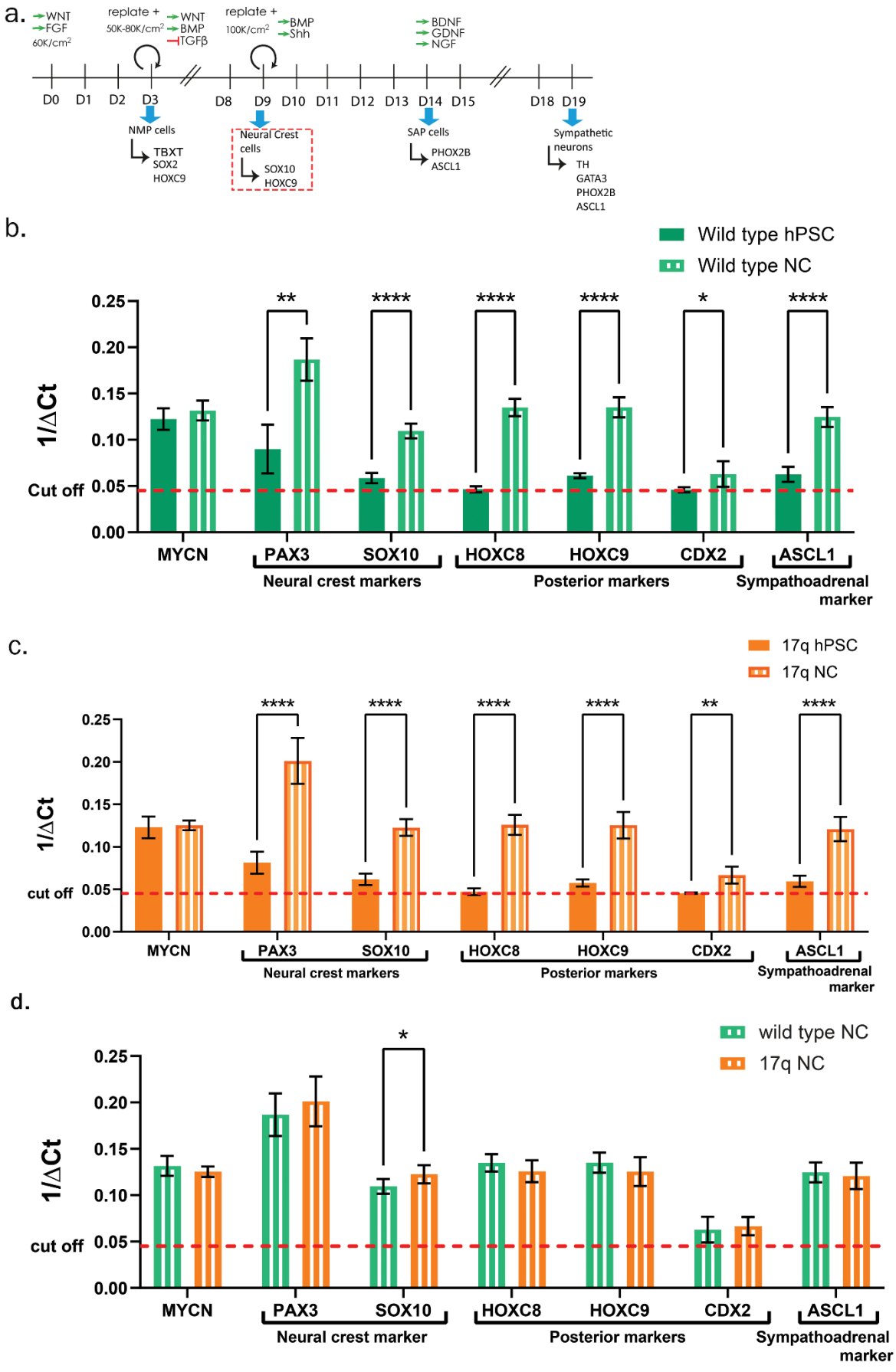
a.
WNT
FGF
60K/cm²
replate +
50K-80K/cm²
WNT
BMP
TGFβ
replate +
100K/cm²
BMP
Shh
BDNF
GDNF
NGF
D0 D1 D2 D3 D8 D9 D10 D11 D12 D13 D14 D15 D18 D19
NMP cells
TBXT
SOX2
HOXC9
Neural Crest cells
SOX10
HOXC9
SAP cells
PHOX2B
ASCL1
Sympathetic neurons
TH
GATA3
PHOX2B
ASCL1
b.
Wild type hPSC
Wild type NC
1/ΔCt
Cut off
0.25
0.20
0.15
0.10
0.05
0.00
**
****
****
****
*
****
MYCN
PAX3
SOX10
HOXC8
HOXC9
CDX2
ASCL1
Neural crest markers
Posterior markers
Sympathoadrenal marker
c.
17q hPSC
17q NC
1/ΔCt
cut off
0.25
0.20
0.15
0.10
0.05
0.00
****
****
****
****
**
****
MYCN
PAX3
SOX10
HOXC8
HOXC9
CDX2
ASCL1
Neural crest markers
Posterior markers
Sympathoadrenal marker
d.
wild type NC
17q NC
1/ΔCt
cut off
0.25
0.20
0.15
0.10
0.05
0.00
*
MYCN
PAX3
SOX10
HOXC8
HOXC9
CDX2
ASCL1
Neural crest marker
Posterior markers
Sympathoadrenal marker

Figure 22. Neural crest differentiation of the wild type and 17q cell lines

a. Schematic diagram of the directed differentiation of human pluripotent stem cells into Neuromesodermal progenitors (**NMP**), Neural Crest (**NC**), Sympathoadrenal progenitors (**SAP**) and Sympathetic neurons (**SN**). The red rectangle highlights the day cells were harvested, and which markers were used to validate the stage. **b.** Wild type cell line was differentiated into neural crest (NC). The bar chart shows the qPCR analysis, all genes related to NC stage and posterior identity were upregulated. **c.** 17q cell line was differentiated into NC cells. All genes related to NC stage and posterior identity showed significant upregulation. **d.** Comparison of wild type and 17q cell lines differentiated into NC stage. Except for *SOX10* which showed significant upregulation in the 17q cell line, no other differences were found in gene expression between the cell lines. **b-d.** Gene expression values are plotted as 1/ΔCt. A cut off line (dotted red line) has been set at 0.045 as this is the equivalent to 40 cycles on the qPCR machine (n≥ 3 biological replicates, error bars= SD, Independent Welch t-tests, $p \leq 0.05$= *, $p \leq 0.01$= **, $p \leq 0.001$= ***, $p \leq 0.0001$= ****).

To verify the qPCR data, immunofluorescence assays were performed. **Figure 23-a** shows representative images of the different antibodies analysed in the immunostaining. HOXC9, ASCL1 and SOX10 antibody staining are observed in both wild type and 17q NC. In appearance, wild type NC cells seem to have more cells expressing the antibody but when images were processed, and the number of cells expressing the antibody was quantified, no significant differences were found (**Figure 23-b)**

Assessment of the neural crest population was also performed by intracellular flow cytometer in the wild type and 17q cell lines (**Figure 24)**. SOX10 and HOXC9 expression were measured simultaneously across three biological replicates. The amount of cells co-expressing the markers varies across the replicates (**Figure 24-b,c,d)**: The wild type cells showed between 71.5% and 90.5% of SOX10/HOXC9 expression, while the percentage of double-positive cells in 17q cells ranged between 94.5% and 96.5%.

Overall, at this stage, both lines exhibited stable HOXC9 expression and high levels of SOX10 but the 17q cell line seemed to differentiate slightly better to trunk NC (based on the apparently higher levels of SOX10).

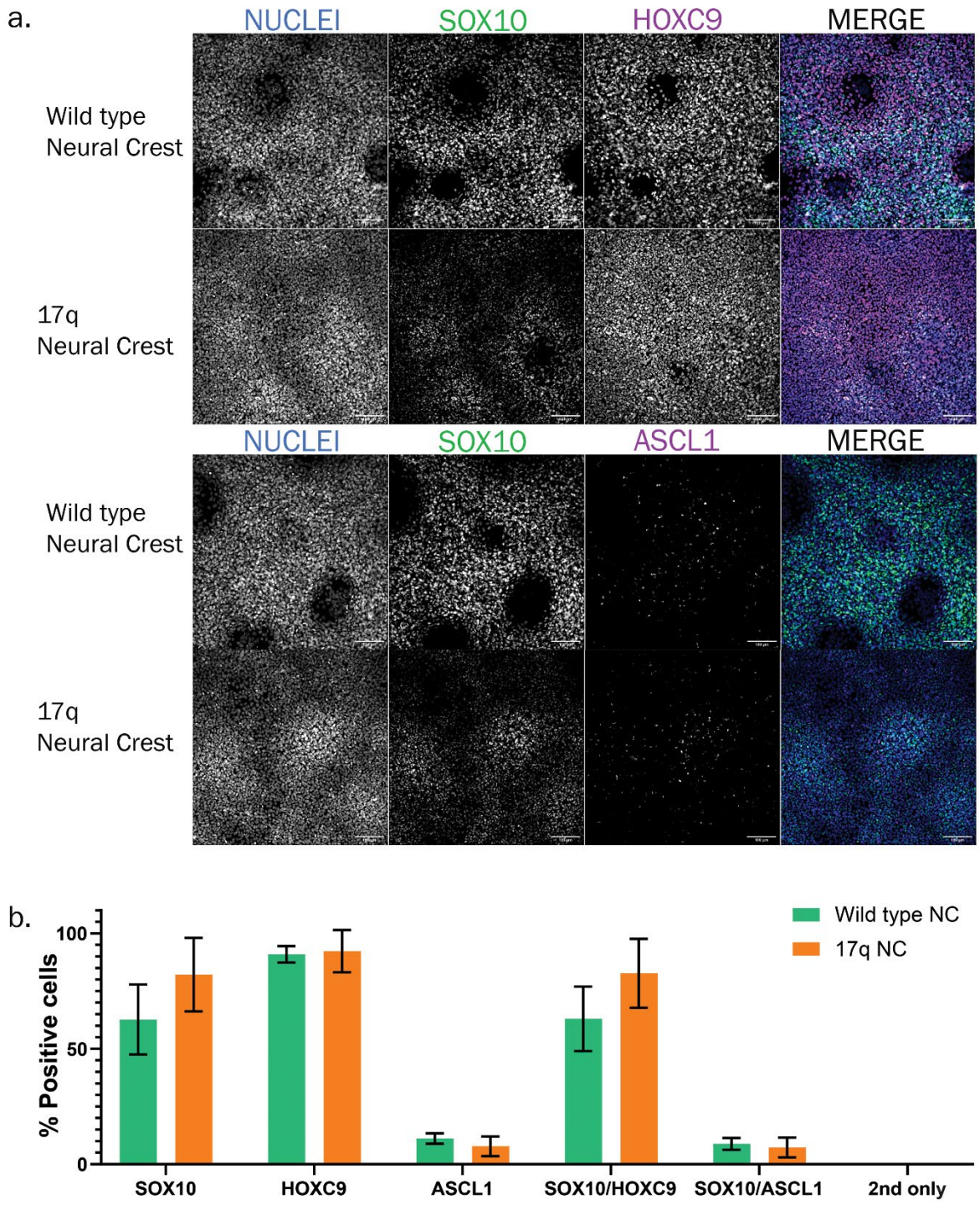

Figure 23. Detection of Neural crest markers by immunostaining in Wild type and 17q cell lines. **a.** Immunofluorescence images of the Wild type and 17q cell lines differentiated into NC. Shown are SOX10, HOXC9 and ASCL1 (Merge: Hoechst(blue), SOX10(green), HOXC9/ASCL1(magenta)). **b.** Percentage of cells expressing SOX10, HOXC9 and ASCL1 markers alone, and co-expression of HOXC9 and ASCL1 with SOX10 in the immunofluorescence analysis. No significant differences were found (n=4 biological replicates, Independent Welch t-tests, Error bar= SD).

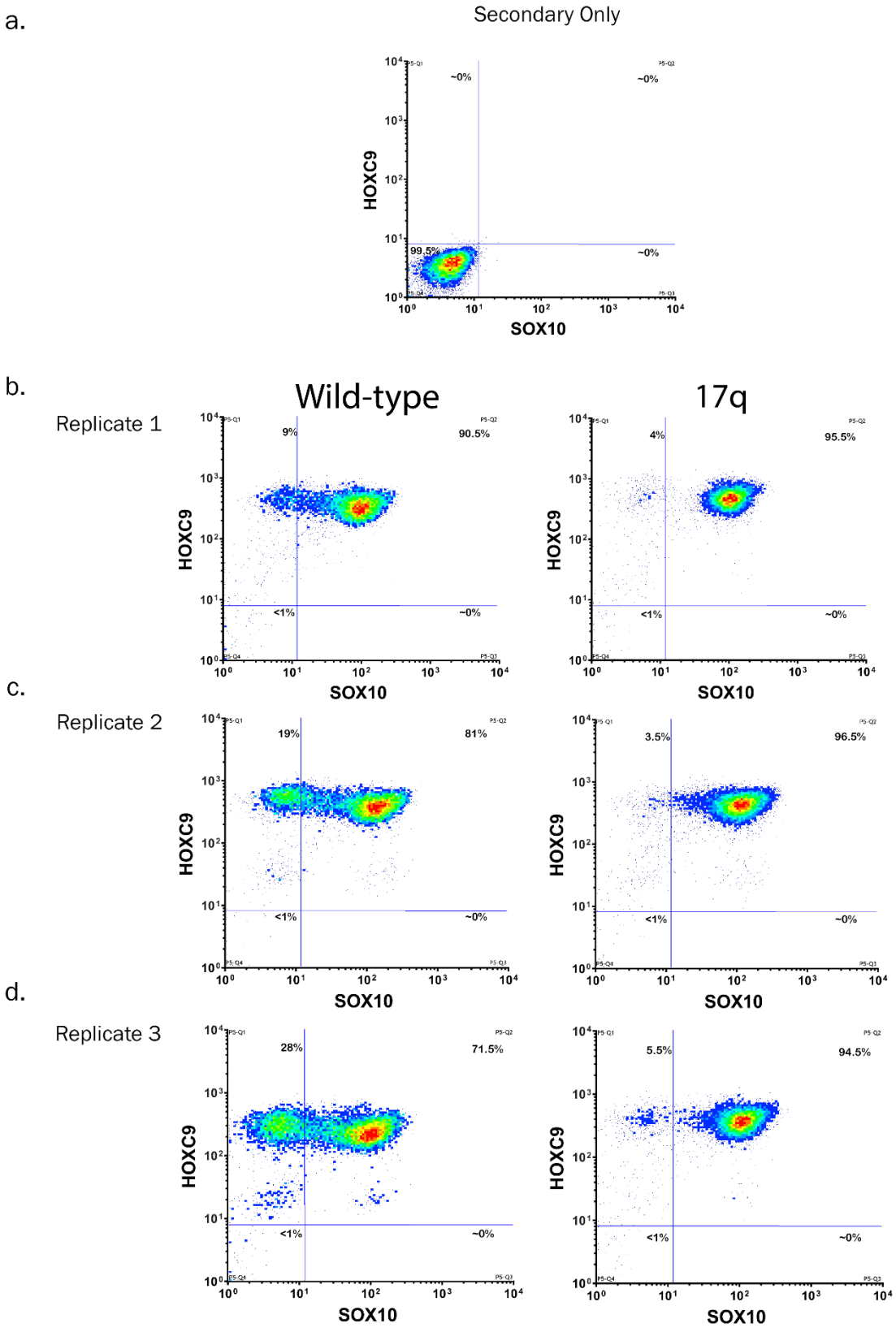

Figure 24. Assessment of trunk neural crest markers SOX10/HOXC9 by intracellular flow cytometer in wild type and 17q cell lines.
a-d. Flow cytometry density plots of SOX10 vs HOXC9 expression in (a) secondary only control, (b-d) Wild type and 17q across three replicates.

3.2.3.3 Trunk NC to sympathoadrenal progenitors

Wild type Neural crest cells were taken to the next step in the protocol: the generation of sympathoadrenal progenitors (**Figure 25-a**). Both wild type and 17q SAP cells were harvested at day 14 of differentiation and analysed by qPCR to verify their identity (**Figure 25-b and 25-c**). Markers such as *HOXC8 and HOXC9* (indicating a posterior identity) were upregulated. Equally, stage-relevant markers like *ASCL1 and PHOX2B* showed significant upregulation in their expression when compared to pluripotent stem cells. Markers related to the next stage were also significantly upregulated (*GATA3, GATA2, TH, DBH*).

When qPCR expression of both wild type and 17q SAP were compared side by side, a few markers showed to be differentially expressed. For example, *SOX10, TH and DBH* were significantly upregulated in 17q SAP, while GATA3 showed higher expression in the wild type (**Figure 25-d**).

To confirm our findings, cells were fixed and immunofluorescences were performed. Markers analysed were SOX10, HOXC9, ASCL1, PHOX2B and the peripheral nervous system marker: PERIPHERIN (**Figure 26-a**). All markers were detected on the wild type and 17q SAP samples. Remarkably, evident differences can be seen in the PERIPHERIN marker between the cell lines as wild type SAP seemed to be more successful in the generation of neurites when compared to 17q SAP. The percentage of cells expressing the markers determined, showing no significant differences between the wild type and 17q SAP (**Figure 26-b**).

In summary, both wild type and 17q cell lines successfully generated sympathoadrenal progenitor cells.

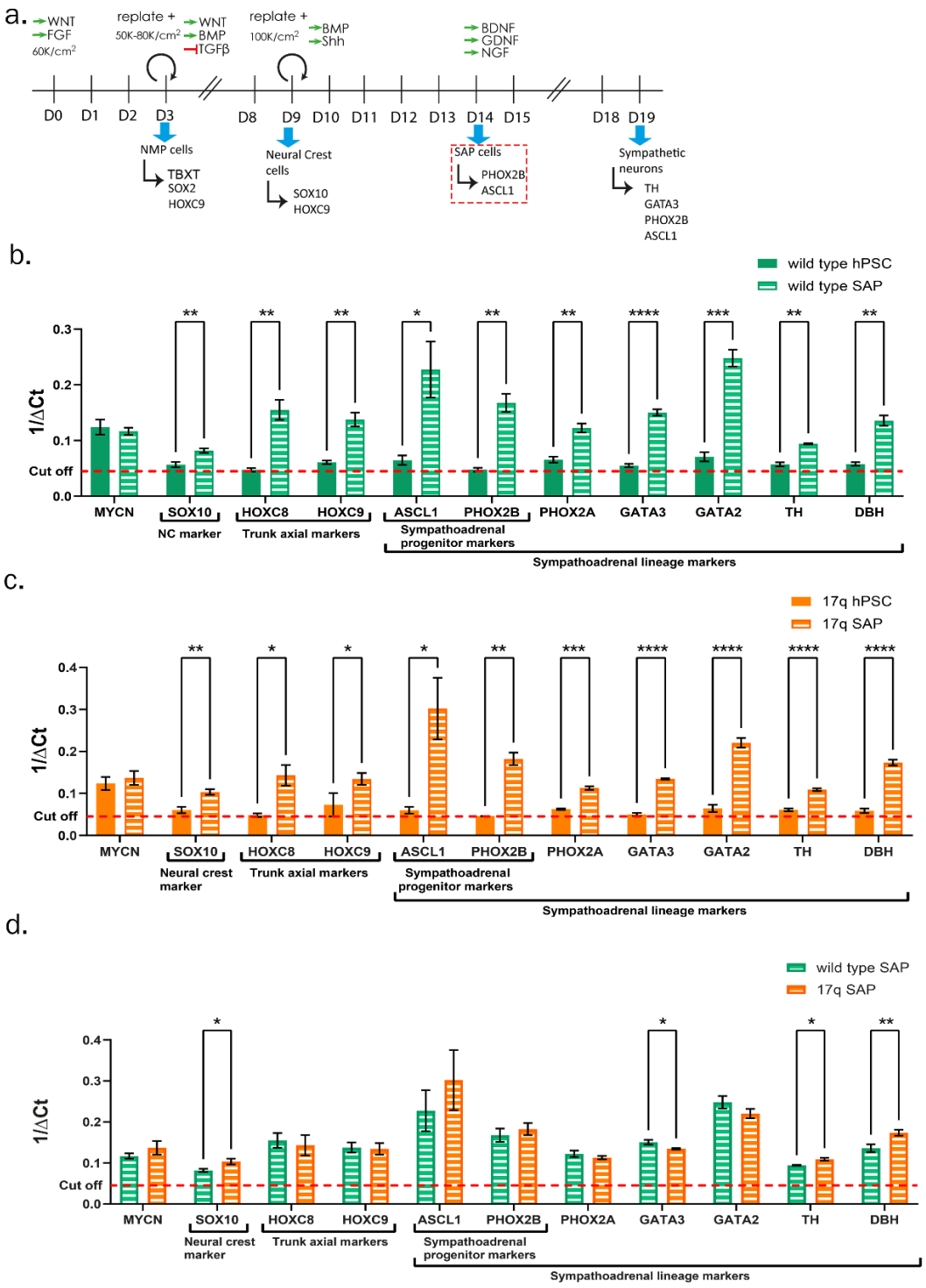

Figure 25. Sympathoadrenal progenitor differentiation of the wild type and 17q cell lines

a. Schematic diagram of the directed differentiation of human pluripotent stem cells into Neuromesodermal progenitors (**NMP**), Neural Crest (**NC**), Sympathoadrenal progenitors (**SAP**) and Sympathetic neurons (**SN**). The red rectangle highlights the day cells were harvested, and which markers were used to validate the stage. **b.** Wild type cell line was differentiated into sympathoadrenal progenitor cells (SAP). The bar chart shows the qPCR analysis, all genes related to SAP stage and posterior identity were significantly upregulated. **c.** 17q cell line was differentiated into SAP cells. All genes related to SAP stage and posterior identity showed significant upregulation. **d.** Comparison of wild type and 17q cell lines differentiated into SAP stage. The neural crest marker, *SOX10*, as well as markers corresponding to the sympathoadrenal lineage GATA3, *TH* and *DBH* showed a significant upregulation in the 17q cell line compared to the wild type. **b-d.** Gene expression values are plotted as 1/ΔCt. A cut off line (dotted red line) has been set at 0.045 as this is the equivalent to 40 cycles on the qPCR machine (n= 3 biological replicates, error bars= SD, Independent Welch t-tests, $p \leq 0.05$= *, $p \leq 0.01$= **, $p \leq 0.001$= ***, $p \leq 0.0001$= ****).

a.

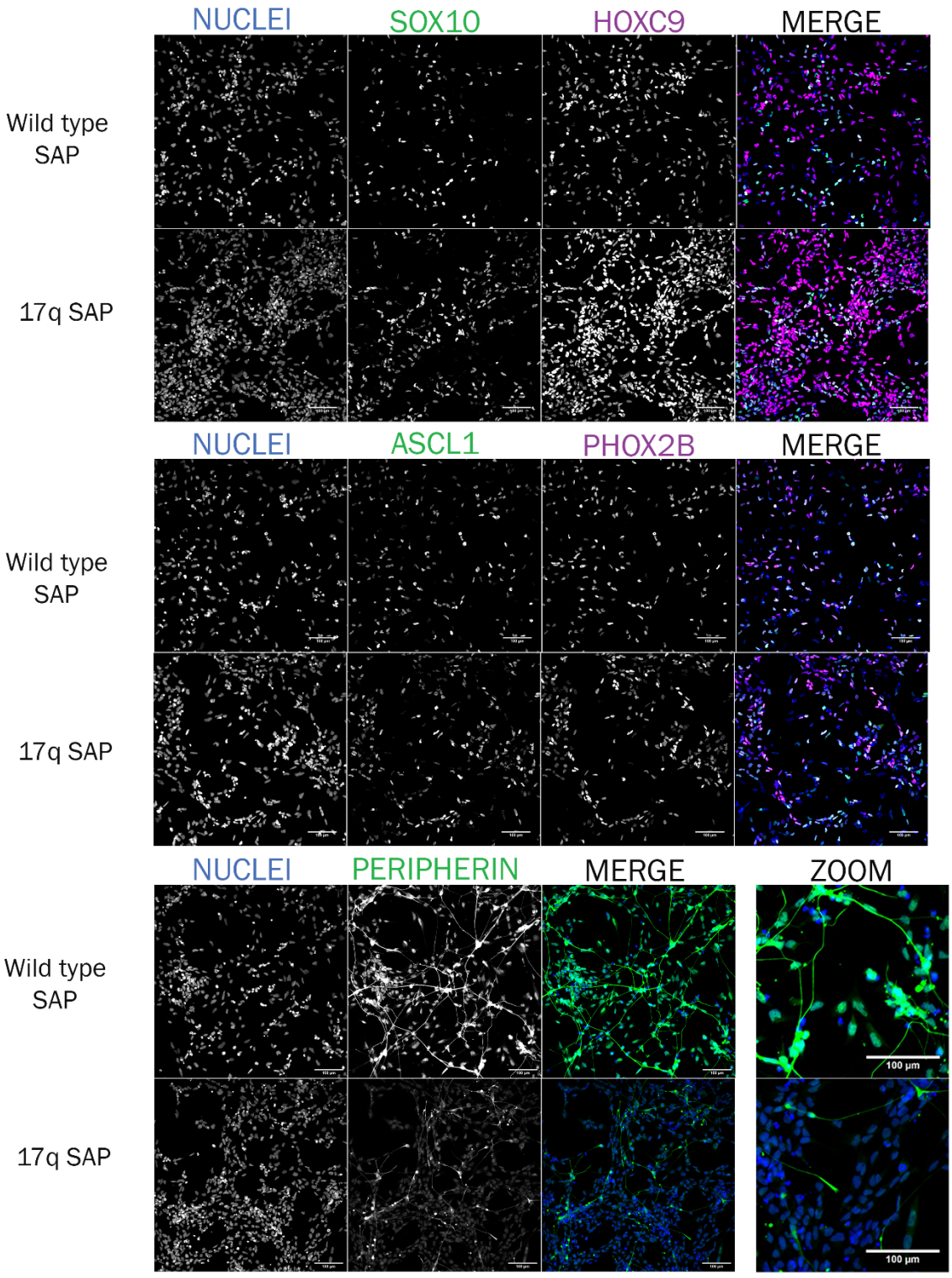
NUCLEI
SOX10
HOXC9
MERGE
Wild type SAP
17q SAP
NUCLEI
ASCL1
PHOX2B
MERGE
Wild type SAP
17q SAP
NUCLEI
PERIPHERIN
MERGE
ZOOM
Wild type SAP
17q SAP
100 µm
100 µm

b.

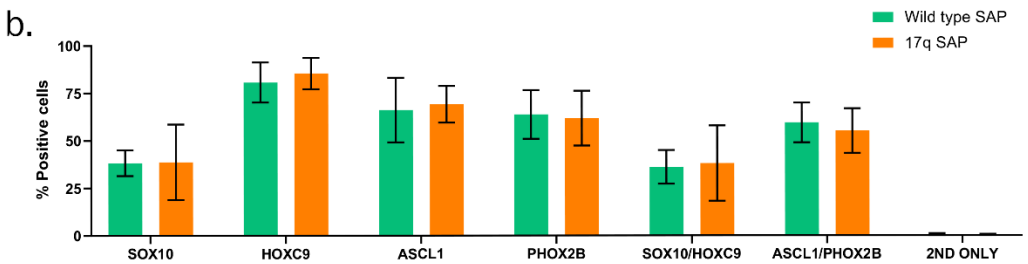
Wild type SAP
17q SAP
% Positive cells
100
75
50
25
0
SOX10
HOXC9
ASCL1
PHOX2B
SOX10/HOXC9
ASCL1/PHOX2B
2ND ONLY

Figure 26. Detection of SAP markers by immunostaining in Wild type and 17q cell lines.
a. Immunofluorescence images of the Wild type and 17q cell lines differentiated into SAP. Shown are SOX10, HOXC9, ASCL1, PHOX2B as well as the peripheral neural marker PERIPHERIN (Merge: Hoechst(blue), SOX10/ASCL1/PERIPHERIN(green), HOXC9/PHOX2B(magenta)). **b.** Percentage of cells expressing SOX10, HOXC9, ASCL1 and PHOX2B markers alone, as well as cells co-expressing SOX10/HOXC9 and ASCL1/PHOX2B in the immunofluorescence analysis. No significant differences were found (n= 3 biological replicates, Independent Welch t-tests, Error bar= SD).

3.2.3.4 Sympathoadrenal progenitor to sympathetic neurons

In order to promote the induction of sympathetic neurons, wild type and 17q sympathetic neuron (SN) cells were grown in a medium containing BDNF, GDNF and NGF factors. They were allowed to grow in these conditions for 5 days (**Figure 27-a**) then, cells were harvested and analysed by qPCR to search for markers appropriate for this stage of differentiation. All markers tested (except for *DBH*) were significantly upregulated in both wild type and 17q SAP cells (**Figure 27 b-c**).

When wild type SN and 17q SN were compared side by side, the expression of *MYCN and ASCL1* was found to be significantly increased in the 17q cell line (**Figure 27-d**).

The presence of these markers at the protein level was confirmed through an immunofluorescence assay (**Figure 28**). ASCL1, PHOX2B and TH were found to be expressed in both wild type and 17q SN at day 19 of differentiation. However, no obvious differences were detected by eye between the two cell lines though further investigation including more biological replicates is required to verify this observation.

In conclusion, the WNT elevated protocol not only improved the 17q line, which had struggled in maintaining its posterior axial identity, but it also improved the wild type differentiation. This improvement was maintained throughout the differentiation, highlighting the importance of properly establishing the axial identity prior to further specification.

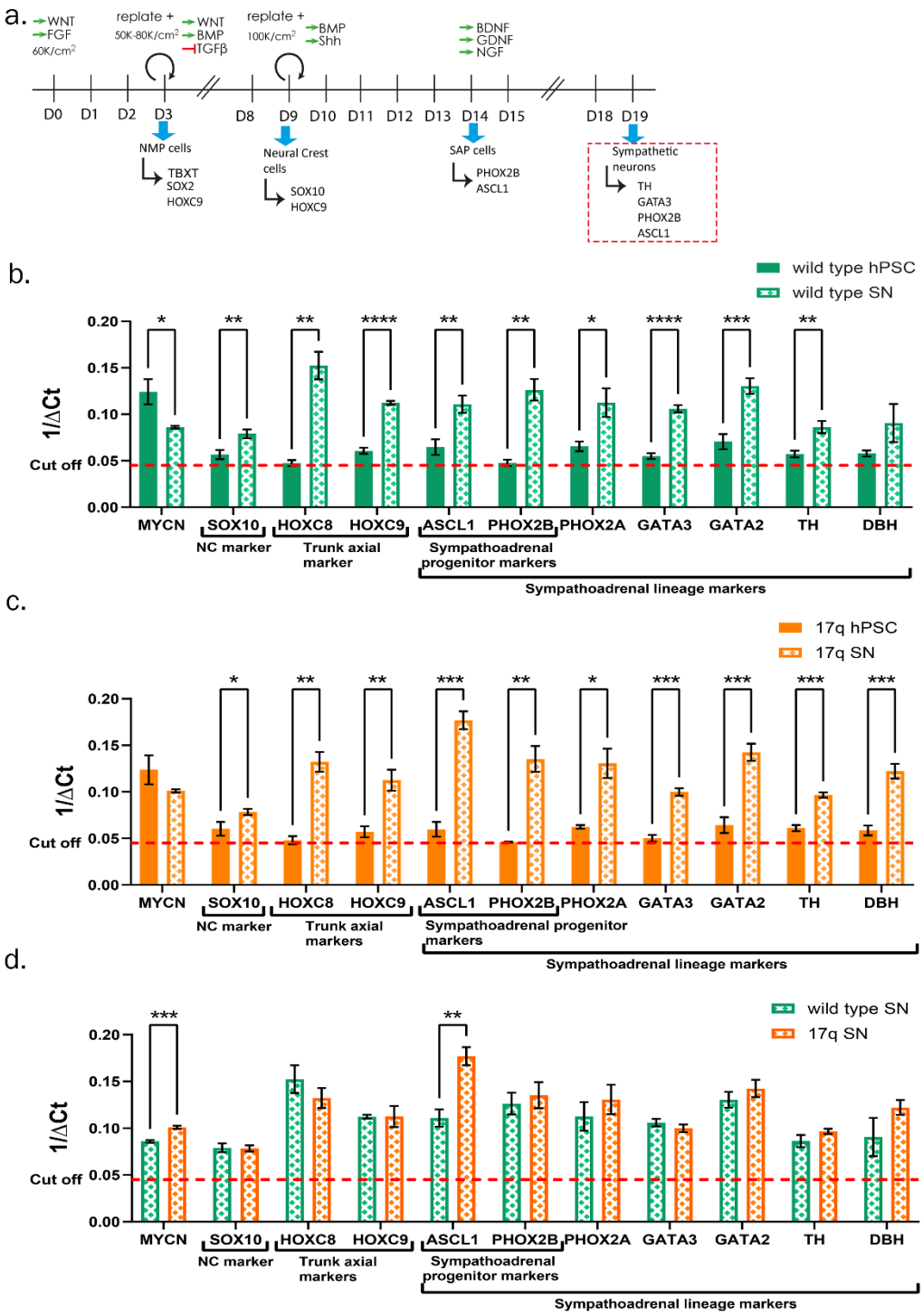

Figure 27. Differentiation of the wild type and 17q cell lines into sympathetic neurons
a. Schematic diagram of the directed differentiation of human pluripotent stem cells into Neuromesodermal progenitors (**NMP**), Neural Crest (**NC**), Sympathoadrenal progenitors (**SAP**) and Sympathetic neurons (**SN**). The red rectangle highlights the day cells were harvested, and which markers were used to validate the stage. **b.** Wild type cell line was differentiated into sympathetic neurons (SN). All genes related to the SN stage (except *DBH*) showed a significant increase in their expression. **c.** 17q cell line was differentiated into Sympathetic neurons (SN). All genes corresponding to sympathoadrenal lineage were significantly upregulated. **d.** Comparison of wild type and 17q cell lines differentiated into SN stage. *MYCN* as well as *ASCL1*, a sympathoadrenal progenitor marker,

showed upregulation that was statistically significant compared to the wild type. **b-d.** Gene expression values are plotted as 1/ΔCt. A cut off line (dotted red line) has been set at 0.045 as this is the equivalent to 40 cycles on the qPCR machine (n= 3 biological replicates, error bars= SD, Independent Welch t-tests, p ≤ 0.05= *, p ≤ 0.01= **, p ≤ 0.001= ***, p ≤ 0.0001= ****).

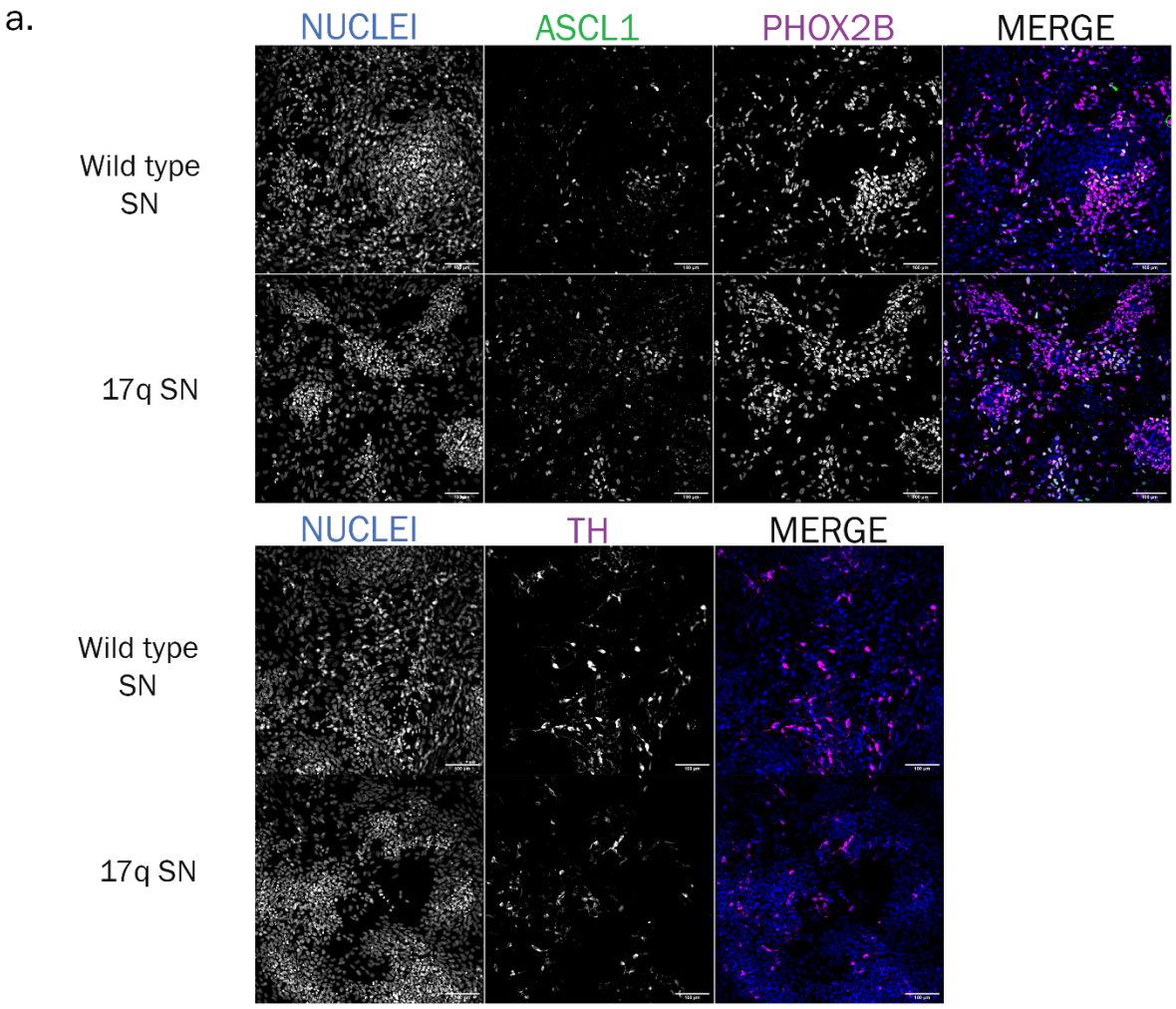

Figure 28. Detection of Sympathetic neuronal markers by immunostaining in Wild type and 17q cell lines.
a. Immunofluorescence images of the Wild type and 17q cell lines differentiated into SN. Shown are ASCL1, PHOX2B and TH (Merge: Hoechst(blue), ASCL1(green), PHOX2B/TH(magenta)). The percentage of cells were not analysed as the images only represent one biological replicate.

3.3 Discussion

In this chapter, I attempted to recapitulate the whole process of normal development towards sympathetic neurons based on a protocol published by Frith et al 2018. This protocol generates sympathetic neurons from human pluripotent stem cells in a step-wise manner, as it allows us to generate all the intermediate cell types involved in the normal process.

Nonetheless, although the published protocol showed a successful generation of the different cell states along the differentiation, their work utilised other cell lines than the ones that my work is based on. It has been reported that different embryonic stem cell lines could render different degrees of response to the same cues (Osafune et al., 2008), therefore, it was crucial to prove that my control (normal) cell line used was able to perform the whole differentiation, accurately generating each stage.

Fortunately, our H7 wild type control was able to differentiate appropriately at the lower level of WNT but also exhibited higher efficiencies when WNT signalling was elevated. From all of our analysis of the wild type and 17q cell lines, the failure of 17q to maintain its posterior identity when induced at 3µM CHIR was the most prominent characteristic. This phenomenon was observed at a low degree during NMP specification but it became clear when the neural crest stage was reached. There are a few hypotheses that can be formulated based on 17q cell line characteristics. One of them is the presence of the AXIN2 gene in the band 17q24.1. AXIN2 is a paralog of AXIN1, and it also participates in the stabilisation of the β-catenin destruction complex (Stamos and Weis, 2013). In contrast to AXIN1, which expression is ubiquitous, AXIN2 shows a more restricted expression pattern. In mouse early development, it is observed in the head folds and posterior neural tube, shortly later it can also be seen along the dorsal neural tube (branchial arches and limb buds as well) (Jho et al., 2002). Interestingly for us, the expression of AXIN2 intersects with areas where intense WNT signalling is taking place, such as the primitive streak and the dorsal neural tube. Also, it has been reported that AXIN2 transcription is triggered when WNT is activated, participating as a negative regulator of the WNT signalling (Jho et al., 2002). Hence, the existence of an extra copy of the AXIN2 gene could be preventing β-catenin to reach its targets in the nuclei impairing the influence of WNT-FGF activity (Frith et al., 2018), CDX2 expression and, ultimately, the acquisition of trunk identity.

Another possibility that could explain HOXC9 downregulation, is its epigenetic state. EZH1 and SUZ12, which are both contained in the 17q chromosome segment, are genes that belong to the Polycomb repressive complex (PRC), which normally mono-di-tri methylate the histone 3-lysine 27 to repress chromatin. Reports have shown that both EZH1 and SUZ12 collaborate, along with the other elements such as EZH2, to not only maintain the stem cell identity (Shen et al., 2008) but also to modulate their

differentiation (Pasini et al., 2007). In literature, analysis of neuroblastoma cell lines resistant to Retinoic Acid-induced differentiation (some of which harboured 17q gains), showed H3K27me3 in the promoter regions of HOXC9, suggesting that epigenetic silencing had occurred(Mao et al., 2011). Nonetheless, in another study of primary tumours, although low levels of HOXC9 also were related to bad prognosis, their analysis did not identify any methylation differences between low and high HOXC9 patients' tumours (Kocak et al., 2013). Therefore, the role of epigenetic control in the suppression of HOXC9 has not been fully uncovered and further investigation is guaranteed. The system we describe here could provide a useful tool to probe this aspect specifically.

A third possibility could be linked to something less complex, as cell density has been shown to influence the culture response to small molecules and other elements in the media. Kempf et al, 2016 demonstrated the impact of cell density on WNT mediated differentiation towards cardiomyocytes (Kempf et al., 2016). Human pluripotent stem cell lines harbouring chromosome 17 gains exhibit an increased single-cell plating survival(Barbaric et al., 2014) and increased growth rates(Lee et al., 2015a). These characteristics could have resulted in a higher cell density in the 17q cell line, becoming sub-optimal for the 3µM CHIR conditions, therefore when the concentration of CHIR was increased, the 17q cell line received the correct amount of signal per cell. It is worth noting that, in real development conditions, it is highly unlikely that the embryo would increase its WNT to cater for a low-responsive population, resulting in poor specification of these cells. In future analysis, more specific markers for trunk neural crest cells such as HES5, HES6, AGPAT4 would be beneficial to characterise in more detail this failure in the specification (Murko et al., 2018).

With the WNT elevated protocol, although 17q aberration did not seem to show high influence during NMP and NC differentiation, further specification towards the sympathoadrenal lineage revealed a possible contribution in the deviation from the normal trajectory. One of the first indications of this deviation was that the 17q line displayed fewer neural projections expressing PERIPHERIN, suggesting some difficulties to progress further in the differentiation properly. A second indicator was observed during the induction of sympathetic neurons as the 17q cell line upregulated significantly the expression of *ASCL1* ($p \leq 0.01$) and *MYCN* ($p \leq 0.001$) when compared to the wild type. In literature, a regulatory loop has been described in neuroblastoma, with ASCL1 and MYCN at its core(Wang et al., 2019). ASCL1 has been found to be upregulated in neuroblastoma and it has been linked to promoting a stem-like stage in glioblastoma, medulloblastoma and neuroblastoma (Rheinbay et al., 2013, Ayrault et al., 2010, Wylie et al., 2015, Kasim et al., 2016). Additionally, ASCL1 phosphorylation status has been shown to be implicated in cell-cycle progression and differentiation status in neuroblastoma (Ali et al., 2020). This data seems to provide an early indication of the potential critical juncture where 17q could play a role in neuroblastoma initiation

Overall, what has become evident is how pivotal a role in the establishment of a robust posterior identity plays in the efficient generation of cells from the sympathetic lineage. It is not just whether the cells express or not the marker at the NMP stage, but also whether enough cells are capable to sustain the correct expression level throughout the stages.

4 Chapter 4: Investigating the combined effects of MYCN overexpression and chromosome 17q gain on *in vitro* derived neural crest cells and their derivatives

4.1 Introduction

The causes of neuroblastoma are still a subject matter of debate and investigation. Although neuroblastoma was first described in 1864 by the physician Rudolf Virchow, it was not until the early 1980s when a "commonly amplified gene" started to attract attention as a potential contributor to neuroblastoma tumorigenesis(Schwab et al., 1983, Kohl et al., 1983). This sequence which was described as "to have homology to the v-myc oncogene but distinct from the classical c-myc" was finally named simply N-myc(Kohl et al., 1983) (or MYCN). Further association analysis showed that an increased number of copies of *MYCN* in the tumours was directly related to the aggressiveness and progression of the disease(Seeger et al., 1985).

Shortly afterwards, in the late '80s, the oncogenic capacity of N-myc was demonstrated in experiments utilising rat fibroblast transfected with MYCN-overexpressing vectors. Transfected cells showed abnormal culture growth, morphological transformation and other tumorigenic hallmarks (Small et al., 1987, Schwab and Bishop, 1988). These findings would propel further research to try to understand the participation of MYCN in the initiation and progression of neuroblastoma.

The cancerous power of MYCN has been demonstrated in many tumour types apart from neuroblastoma such as medulloblastoma, retinoblastoma, Wilm's tumour, hematologic malignancies, small-cell lung cancer, pancreatic cancer, prostate cancer and rhabdomyosarcoma (reviewed in (Rickman et al., 2018)). *MYCN* amplification is found in neuroblastoma in around 20% (Cohn et al., 2009, Brodeur, 2003) of the cases and its presence is linked to a poor prognosis as less than 50% of the patients harbouring *MYCN* amplification survive. This is independent of the age of diagnosis or the stage of the disease (Cohn et al., 2009, Brodeur et al., 1984, Seeger et al., 1985). Therefore, it has become critical to understand the mechanisms by which MYCN influences neuroblastoma progression to find better treatments that could improve the overall survival of the patients.

Studies in established neuroblastoma cell lines have also provided some answers in both developmental questions as well as mechanisms involved in neuroblastoma phenotype/maintenance. For example, MYCN has been associated with blocking differentiation pathways, enhancing proliferation, inhibiting apoptosis, and maintaining pluripotency (Kang et al., 2006, Nara et al., 2007, Cotterman and Knoepfler, 2009).

Investigations using neuroblastoma cell lines have been found that MYCN increases the expression of stem cell-related factors in neuroblastoma, including KLF2, KLF4, and LIN28B. Such factors are normally found in tumours and stem cells. The control that MYCN enforces over these genes suggests an aberrant re-activation of a pluripotency program, which may contribute to the onset of neuroblastoma (Cotterman and Knoepfler, 2009). These observations correlate with what has been initially reported by Cartwright et al 2005 as the sustained expression of MYC in feeder-free media mouse pluripotent stem cells (mPSC) could mitigate the absence of LIF. The latter was required to maintain the pluripotent stem cell stage. The same conclusions can be obtained when either MYCN or MYC are repressed in mPSC culture, one can compensate for the loss of the other and maintain pluripotency and self-renewal. In the same way, when MYCN and MYC are simultaneously repressed these cells undergo spontaneous differentiation towards primitive endoderm and mesoderm lineages. Additionally, the role of MYCN in enhancing proliferation and maintaining pluripotency may be intertwined, as the loss of MYCN and its paralogue cMYC result in the inability to progress through the S phase and the G2/M checkpoint (Smith et al., 2010).

In terms of apoptosis, in neuroblastoma p53 does not normally present any driver mutations, therefore, other mechanisms of cell control must be implicated in the anti-apoptotic phenotype of neuroblastoma. It has been suggested that MYCN cooperates with other factors involved in p53 suppression, such as MDM2, H-Twist and BMI1, among others (Valsesia-Wittmann et al., 2004, Slack et al., 2005, Huang et al., 2011). Essentially, it has been proposed that a regulatory circuit exists between MYCN, MDM2 and P53, where MYCN promotes the expression of MDM2 which is an ubiquitin ligase responsible for the degradation of p53 (review in Huang et al, 2013). Table 12 displays a collection of factors that MYCN has been implicated in the control of neuroblastoma.

A hallmark of *MYCN*-amplified neuroblastomas is their ability to drive cells cycle progression even in times of cellular stress leading to enhanced proliferation. MYCN's action is focused on preventing cell cycle arrest, possibly by regulating the expression levels of Cycline-dependant Kinase 4 (CDK4) and the S-phase kinase-associated protein 2 (SKP2). High levels of both CDK4 and SKP2 can lead to activation of CDK2, further driving cell cycle progression (Muth et al., 2010, Evans et al., 2015). MYCN also sustains WNT/β-catenin signalling activity by downregulating one of its natural antagonists DKK1 (Koppen et al., 2007a).

Table 12: Factors regulated by MYCN in Neuroblastoma

Characteristic	Gene / Protein	MYCN Effect	Interaction	Reference
Apoptosis	P53	Promote	Direct transcriptional target of MYCN. Overexpressed in Neuroblastoma	(Chesler et al., 2008, Chen et al., 2010)
Anti-Apoptosis	BCL2	Promote	Increased expression in neuroblastoma tumours and correlated with a poor prognosis	(Castle et al., 1993, Lamers et al., 2012, Lestini et al., 2009, Jasty et al., 2001)
Cell Cycle arrest	DKK1	Suppress	MYCN suppresses its expression	(Koppen et al., 2007a)
	TP53INP1	Suppress	MYCN suppresses its expression	(Bell et al., 2007)
Proliferation	CDK4	Promote	Elevated in MYCN Neuroblastoma	(Gogolin et al., 2013)
	CHK1	Promote	Elevated and increased phosphorylation in MYCN Tumours	(Cole et al., 2011)
	ID2	Promote	Direct transcriptional target of MYCN. Overexpressed in Neuroblastoma	(Lasorella et al., 2000, Lasorella et al., 2002)
	MCM	Promote	Direct transcriptional target of MYCN. Overexpressed in Neuroblastoma	(Koppen et al., 2007b)
	MYBL2	Promote	Direct transcriptional target of MYCN. Overexpressed in Neuroblastoma	(Gualdrini et al., 2010)
	SKP2	Promote	Direct transcriptional target of MYCN. Overexpressed in Neuroblastoma	(Evans et al., 2015)
Immune Surveillance	MCP-1/CCL2	Suppress	Represses expression of this natural killer T cell chemoattractant	(Song et al., 2007)
Pluripotency	KLF2	Promote		(Cotterman and Knoepfler, 2009)
	KLF4	Promote		

	LIN-28b	Promote	Upregulation of Pluripotency Factors	
Self-Renewal	BMI1	Promote	Direct transcriptional target of MYCN. Overexpressed in Neuroblastoma	(Huang et al., 2011, Ochiai et al., 2010)
	DLL3	Promote	Regulates expression of this Notch Ligand linked to stem cell fate	(Zhao et al., 2009)
Differentiation	CDKL5	Suppress	Direct transcriptional repression	(Valli et al., 2012)
Angiogenesis	Angiogen	Promote	Upregulation correlated with MYCN expression	(Dungwa et al., 2012)
	VEGF	Promote	Upregulation via activation of the mTOR pathway	(Kang et al., 2008)
Anti-Angiogenesis	Activin A	Suppress	Direct transcriptional repression	(Hatzi et al., 2000)
	IL-6	Suppress	Down Regulation when MYCN is overexpressed	(Hatzi et al., 2002)
Migration/Metastasis	FAK	Promote	Direct transcriptional target of MYCN. Overexpressed in Neuroblastoma	(Beierle et al., 2007)
Anti-Migration/Metastasis	E-Cadherin	Suppress	Suppresses expression through upregulation of miR-9	(Dunwoodie, 2009)
Survival	H-Twist	Promote	Overexpressed in MYCN amplified tumours	(Valsesia-Wittmann et al., 2004)
	TRKB	Promote	Expression correlates with MYCN tumours	(Nakagawara et al., 1994)
	MDM2	Promote	Direct transcriptional target of MYCN. Overexpressed in Neuroblastoma	(Slack et al., 2005)

Beyond MYCN's ability to influence the direct expression of genes that affect cell cycle progression, apoptosis and differentiation, it can also influence the status of chromatin and by doing this, influence the transcription profile of the cell. It has been reported that when MYCN is repressed in neuronal progenitors, the global level of acetylation decreases while methylation increases, leading to a widespread condensation of the chromatin (Knoepfler et al., 2006). One of the approaches that MYCN uses to exert control over chromatin arrangements is through EZH2, a member of the polycomb repressor complex 2 (corvette et al 2013), by methylating the Histone 3 K27 (a silencing hallmark)(Liu and Zhu, 2017, Au et al., 2012). It has been reported that in a mouse model of prostate cancer, MYCN cooperates with EZH2 to initiate the neuroendocrine phenotype tumours(Dardenne et al., 2016). And *in vitro*, the sole inhibition of PRC2 in a MYCN-overexpressed neuroblastoma model suppressed the growth of cell culture (Tsubota et al., 2017).

MYCN belongs to the MYC family of oncogenes along with two other members: C-MYC and L-MYC(DePinho et al., 1991). Structurally, MYCN and CMYC are very similar as they present high homology within their coding regions and the sizes of their gene products (~50 kDa) (Kohl et al., 1986, Stanton et al., 1986)and both proteins possess regions that allow DNA-protein and protein-protein interactions(Meyer and Penn, 2008). Also, both MYCN and CMYC dimerise with MAX (MYC interacting protein X) to form a complex that normally binds E-box sequences (Enhancer-box), these are usually located close to genes that are regulated by either CMYC or MYCN (Kretzner et al., 1992, Ferrucci et al., 2018). Additionally, the induction of MYCN and CMYC has shown the ability to induce neoplastic transformation in rat embryonic cells and to trigger DNA replication in fibroblasts (Schwab et al., 1983, Cavalieri and Goldfarb, 1988).

Regardless of their similarities, CMYC and MYCN have been reported to be expressed dissimilarly, as CMYC appears to have a more generalised expression while MYCN seems to be in a more stage-tissue specific manner during mouse development mainly expressed in new-born forebrain, hindbrain, kidney and intestine (Zimmerman et al., 1996, Sawai et al., 1993). Moreover, mouse embryos that were homozygous for a non-functional MYCN allele died in the first 12 days of gestation, showing underdevelopment in tissues and organs where MYCN is normally expressed (Charron et al., 1992). These experiments demonstrated the importance of MYCN during early development.

Higher-resolution analysis, at the single-cell level, of the developing chick embryo, has demonstrated that the expression of MYCN is highly regulated during differentiation. During neural tube closure, c-myc is expressed in the dorsal neural tube area (neural crest cell region), whereas N-myc expression is restricted to the remaining parts of the neural tube that will be part of the CNS. Nonetheless, N-myc expression has been found, although in low levels, in migrating neural crest (Khudyakov and Bronner-

Fraser, 2009b, Wakamatsu et al., 1997, Kerosuo et al., 2018). During sympathetic differentiation, MYCN was absent from the peripheral ganglia during the early stages of embryogenesis (Kerosuo et al., 2018). This restricts the time- frame for N-myc expression in sympathoadrenal development being somewhere between the migration of neural crest and establishment of the sympathetic ganglion.

Several approaches have been generated to understand the role that MYCN expression has in Neuroblastoma initiation and progression. Moreover, even when evidence existed about its oncogenic potential(Small et al., 1987, Schwab and Bishop, 1988), it was not until Weiss et al 1997 engineered a murine model able to develop neuroblastoma that MYCN's contribution in tumorigenesis was proved. In this model, a tyrosine hydroxylase (TH) promoter was employed to drive MYCN transgene expression, therefore, restricting MYCN expression to lineages that express TH such as the sympathetic nervous system. The transgenic mice in the study developed tumours and when these cells were cytogenetically analysed the researchers observed gains and losses in chromosomal regions syntenic to those observed in human neuroblastomas. A similar approach was done by *Althoff et al* 2015 that generated transgenic mice where the expression of MYCN was restricted to dopamine β-hydroxylase (*DBH*) expressing cells. They reported an even higher incidence of neuroblastic tumours (>75%) than those observed by Weiss et al 1997.

MYCN's tumorigenic power had been demonstrated, but exactly where and when it wields its power remains elusive. In an attempt to refine to what extent MYCN could influence sympathoadrenal development, sympathoadrenal progenitors cells from the adrenal gland of a postnatal mouse were isolated and transfected with lentivirus expressing MYCN. Although differentiation and proliferation increased in transfected cells, MYCN was not sufficient to form tumours when cells were engrafted in immune-compromised mice (Mobley et al., 2015). It can be implied that MYCN on its own is unable to exert tumorigenesis, and perhaps requires additional mutations/aberrations. A noticeable caveat in the study is that the MYCN overexpressing cells were injected subcutaneously, instead of the regions where tumours normally appear. This raises the possibility that MYCN overexpressing cells might require further environmental signals to eventually trigger tumour formation.

A couple of years later, another group established another system based on the transformation of trunk neural crest explants isolated from a mouse embryo. Cells were p53-compromised and then transfected with a retrovirus to overexpress MYCN. Transformed neural crest cells were then injected subcutaneously into immune-compromised or wild type mice. All mice developed tumours at different times (Olsen et al., 2017). This could be seen as finally having the correct cell of origin, but the fact that the authors used a p53-knock downs/outs cannot be ignored when studying tumorigenic potential, as this could be enhancing unauthentic cancer-like characteristics.

Apart from the sole amplification of MYCN some high-risk neuroblastomas concomitantly present a mutation in the ALK receptor(Wang et al., 2013b). Berry et al 2012, generated a mouse model containing both MYCN and ALK mutation (*ALK*^{F1174L}), proving the existence of a functional interaction between them. They also showed that ALK increases oncogenesis driven by MYCN *in vivo,* as mice developed masses similar to those observed in humans showing therapy resistance (Berry et al., 2012). In another study using chick sympathetic neuroblasts, individual contributions of ALK^{F1174L} and MYCN were assessed. They found that the sole overexpression of MYCN increased proliferation but did not enhanced cell survival, whilst ALK^{F1174L} promoted differentiation and increased survival of postmitotic neurons. Nonetheless, when both were present it was observed an increase in cell survival and long-term proliferation (Kramer et al., 2016).

In a more recent study, Cohen et al 2020 developed a mouse-human chimaera model that was able to recapitulate not only the tumour formation but also the immune response normally observed in neuroblastoma patients. This model first relied on the *in vitro* generation of neural crest cells derived from hPSC, these cells contained a doxycycline-inducible system that allowed them to overexpress the neuroblastoma oncogenes MYCN and an ALK mutation *ALK*^{F1174L}. Then, cells were transplanted in mouse during *in utero* development, where cells successfully developed along with their host (Cohen et al., 2020).

Even though MYCN amplification has been shown to be co-existing with other mutations, like ALK aforementioned, an underinvestigated relationship with segmental chromosomal aberrations has a much higher prevalence. High-risk neuroblastoma without MYCN amplification shows a high level of chromosomal instability related to the presence of varied chromosomal aberrations such as 17q gain, 11q loss, 1p loss, 3p loss, and 1q gain. Although, MYCN amplified tumours show less segmental chromosomal changes, the gain of 17q and the loss of 1p remain highly prevalent within this group, present in 82% and 77% respectively (Stigliani et al., 2012).

Given that the concurrent gain of 17q and amplification of MYCN are highly prevalent within neuroblastoma, and considering that to date, no model has been developed to understand the specific dynamics of this association in neuroblastoma, we decided to overexpress MYCN on a 17q background in our system. Furthermore, because 17q aberration alone showed little effect on neural crest specification, we also wanted to test whether the combination of MYCN overexpression would lead to a greater response.

4.2 Results

Graphical abstract summarising the experiments and main findings of chapter 4.

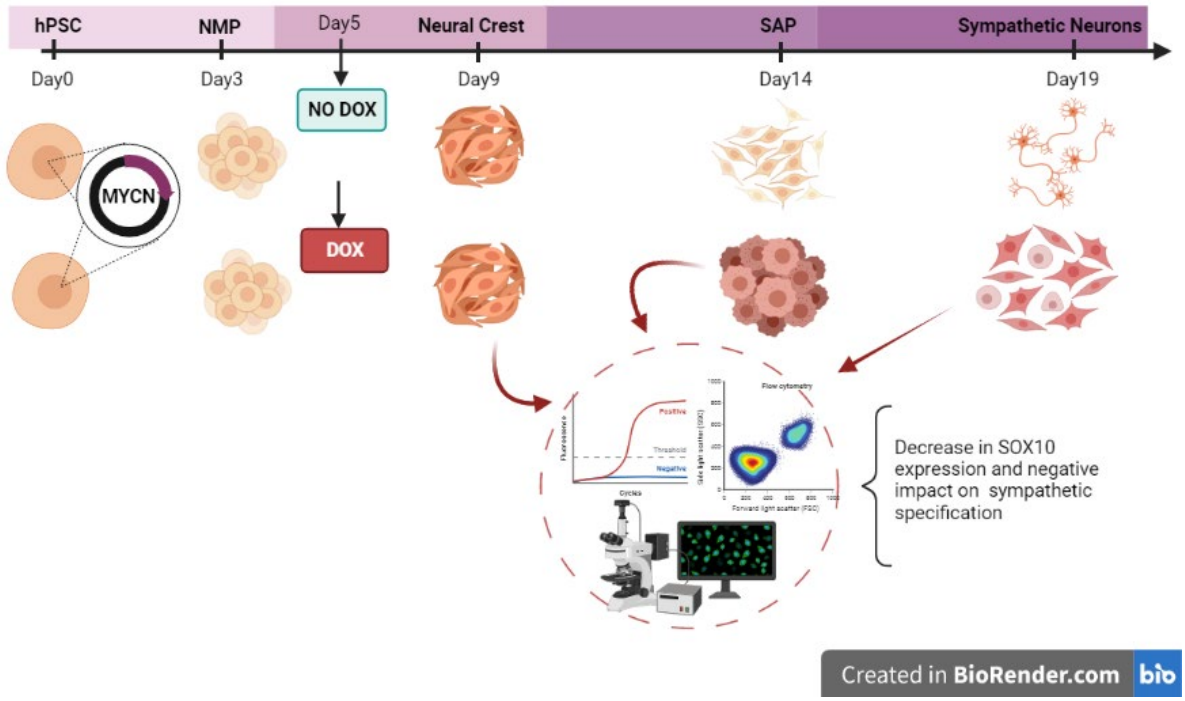

4.2.1 Minimal impact on NMP specification from additional 1q gain and MYCN overexpression.

In order to understand how MYCN overexpression on a 17q background could influence the onset of neuroblastoma, we engineered a human pluripotent stem cell (hPSC) line carrying a 17q aberration (See chapter 2), briefly to overexpress MYCN, we employed a PiggyBac plasmid with a TetOn doxycycline-inducible system driving the expression of MYCN. Interestingly we observed a gain in the chromosomal region 1q21 that was acquired post-transfection **(Figure 29-a)**, an aberration that has also been frequently reported in neuroblastoma (Diskin et al., 2009, Hirai et al., 1999)**.** This newly generated line was then differentiated into neural crest cells and subsequently to their sympathoadrenal derivatives whilst inducing MYCN expression at different time points.

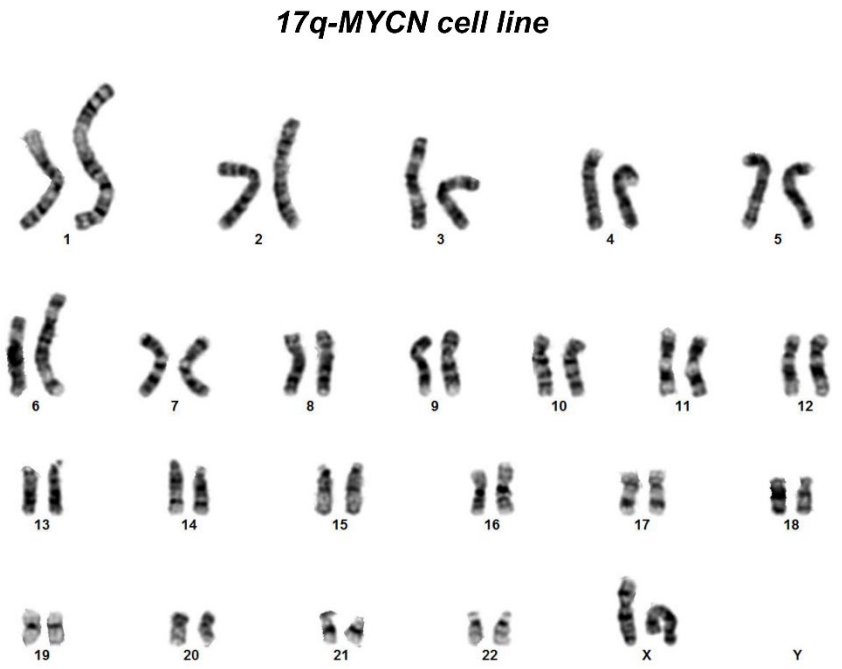

Figure 29. Karyotype of 17q-MYCN cell line. 17q-MYCN cell line karyotype, showing an abnormal karyotype with a gain of the long (q) arm of chromosome 17 via an unbalanced translocation with chromosome 6 and a duplication of the long arm of chromosome 1 via an unbalanced translocation with the second chromosome 1. The region gained is from 1q21 to 1q terminal and includes 1q32 possible minimal 1q amplicon in all cells examined. In square brackets is shown the number of metaphase spreads analysed. 20 cells examined gives a 95% chance of detecting a 14% population.

The 17q-MYCN cell line was tested alongside the control 17q only cell line for its NMP differentiation efficiency. The first sets of differentiations were done using CHIR at a 3µM concentration (during the NMP stage). 17q, 17q-MYCN (without doxycycline) and a 17q cell line supplemented with doxycycline (as control) were grown in the NMP media consisting in N2B27 medium, supplemented with FGF and CHIR (**Figure 30-a).** qPCR analysis of NMP markers *TBXT* and *SOX2* showed no differences between cell lines, neither the early neural crest marker *PAX3* nor any of the anterior to posterior genes tested (**Figure 30-b)**.

Images of the antibody staining of SOX2, HOXC9, TBXT and MYCN are shown (**Figure 30-c**). At a glance, all cell lines/conditions seem to express all the markers in a similar fashion, but when further immunofluorescence quantification was done (**Figure 30-d**), differences in the percentage of cells expressing MYCN were found. 17q NMP showed a fewer number of cells expressing MYCN compared

to 17q(+DOX) and 17q-MYCN(-DOX). There was a wide degree of variation of MYCN expression in the 17q cell line, this difference was not observed in the qPCR analysis.

The 17q-MYCN(-DOX) did not show differences in the expression of NMP markers when compared to the 17q cell line, this implies that the addition of chromosome 1q gain had little impact on the differentiation. Therefore, I decided to test the effects that MYCN overexpression could cause in NMP specification. The overexpression of MYCN in previous studies has been shown to have a significant impact on cellular behaviour. MYCN overexpression has been related to morphological transformation, blockage of differentiation pathways, enhancing of proliferation, inhibition of apoptosis, etc (Schwab and Bishop, 1988, Small et al., 1987, Kang et al., 2006, Nara et al., 2007). Based on this, I hypothesised that overexpression this early would severely hamper the differentiation process.

17q-MYCN(-DOX) and 17q-MYCN(+DOX) (induction from day 0) were grown in NMP media (**Figure 31-a**). After three days, cell lines were harvested and analysed by qPCR. MYCN induction was verified by comparing MYCN expression in 17q-MYCN(-DOX) and 17q-MYCN(+DOX)(**Figure 31-b**). Cells treated with doxycycline showed an increase of around 100 times in MYCN compared to those untreated. Markers related to the NMP stage showed small but statistically significant differences. *TBXT* showed downregulation when MYCN was overexpressed, while *SOX2* increased its expression.

To verify our findings, an immunofluorescence assay testing for SOX2, HOXC9, TBXT and MYCN was done (**Figure 31-c**). In appearance, no differences can be seen in the number of cells expressing the markers between conditions. Quantifications of the immunofluorescences shown no statistically significant differences between 17q-MYCN(-DOX) and 17q-MYCN(+DOX)(**Figure 31-d**).

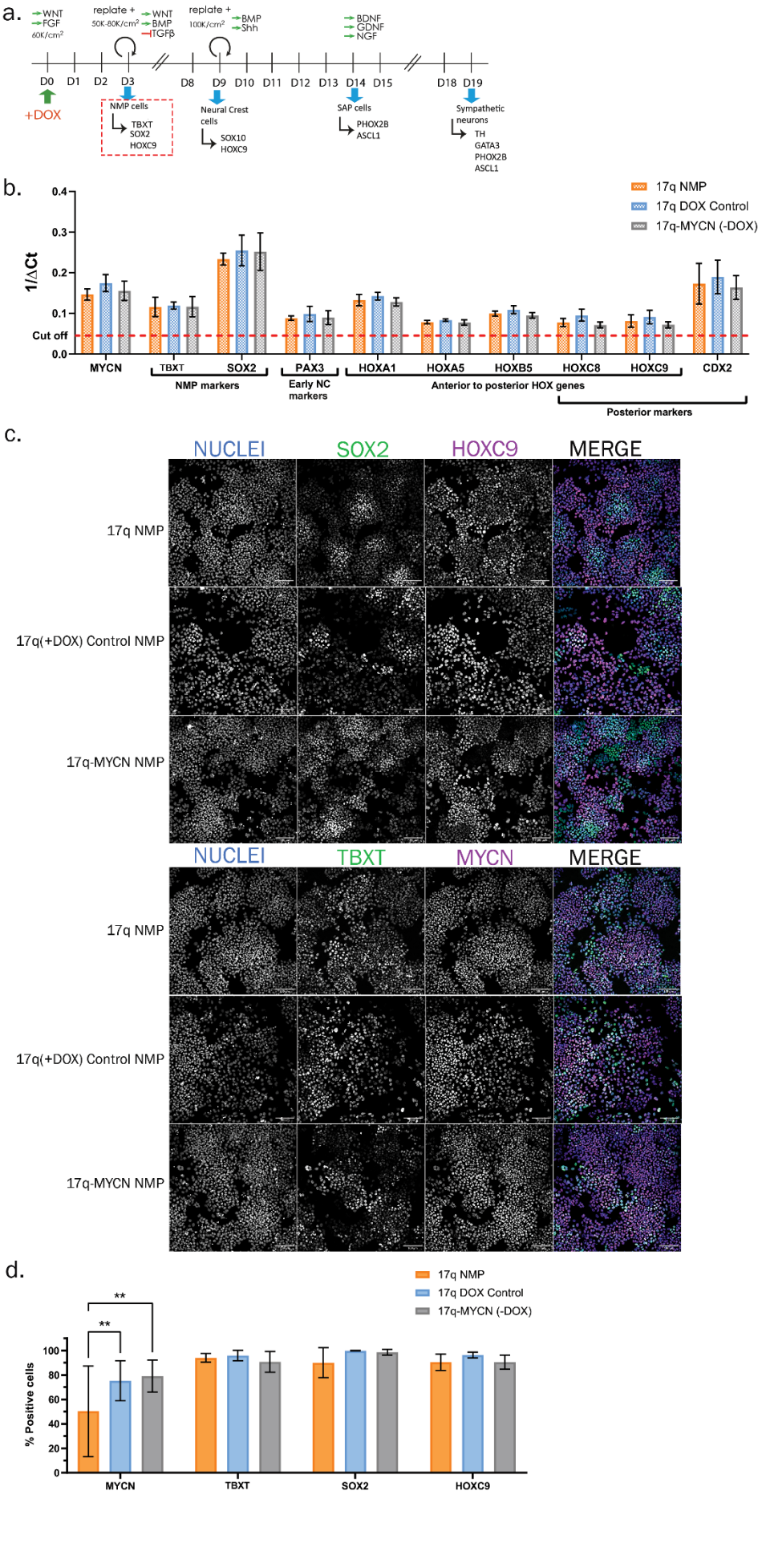
a.
WNT
FGF
60K/cm²
replate +
50K-80K/cm²
WNT
BMP
TGFβ
replate +
100K/cm²
BMP
Shh
BDNF
GDNF
NGF
D0 D1 D2 D3 D8 D9 D10 D11 D12 D13 D14 D15 D18 D19
+DOX
NMP cells
TBXT
SOX2
HOXC9
Neural Crest cells
SOX10
HOXC9
SAP cells
PHOX2B
ASCL1
Sympathetic neurons
TH
GATA3
PHOX2B
ASCL1
b.
17q NMP
17q DOX Control
17q-MYCN (-DOX)
1/ΔCt
0.4
0.3
0.2
0.1
Cut off
0.0
MYCN
TBXT
SOX2
PAX3
HOXA1
HOXA5
HOXB5
HOXC8
HOXC9
CDX2
NMP markers
Early NC markers
Anterior to posterior HOX genes
Posterior markers
c.
NUCLEI
SOX2
HOXC9
MERGE
17q NMP
17q(+DOX) Control NMP
17q-MYCN NMP
NUCLEI
TBXT
MYCN
MERGE
17q NMP
17q(+DOX) Control NMP
17q-MYCN NMP
d.
17q NMP
17q DOX Control
17q-MYCN (-DOX)
**
**
% Positive cells
100
80
60
40
20
0
MYCN
TBXT
SOX2
HOXC9

Figure 30. Assessment of NMP specification in control lines and control conditions

a. Schematic diagram of the directed differentiation of human pluripotent stem cells into Neuromesodermal progenitors (**NMP**), Neural Crest (**NC**), Sympathoadrenal progenitors (**SAP**) and Sympathetic neurons (**SN**). The red rectangle highlights the day cells were harvested, and which markers were used to validate the stage. **b.** Comparison of RNA expression at NMP stage between 17q cell line, 17q with Doxycycline (as a doxycycline control) and 17q-MYCN without Doxycycline treatment. The bar chart shows the qPCR analysis, gene expression values are plotted as $1/\Delta Ct$ (specified in graph legend). a cut off line (dotted red line) has been set at 0.045 as this is the equivalent of 40 cycles on the qPCR machine. No genes related to NMP differentiation showed significant differences. **c.** Immunofluorescence images of the 17q, 17q(+DOX) Control and 17q-MYCN(-DOX) cell line differentiated into NMP. Shown are SOX2, HOXC9, TBXT and MYCN staining (Merge: Hoechst(blue), SOX2/TBXT(green), HOXC9/MYCN(magenta)). **d.** Percentage of cells expressing MYCN, TBXT, SOX2 and HOXC9 markers in the immunofluorescence analysis. Protein expression related to NMP did not show significant differences, nonetheless, MYCN expression was significantly different in 17q versus 17q(+DOX)control and 17q-MYCN(-DOX). **b-d.** ($n \geq 3$ biological replicates, , error bars= SD, Independent Welch t-tests, $p \leq 0.05$= *, $p \leq 0.01$= **, $p \leq 0.001$= ***, $p \leq 0.0001$= ****).

a.

b.

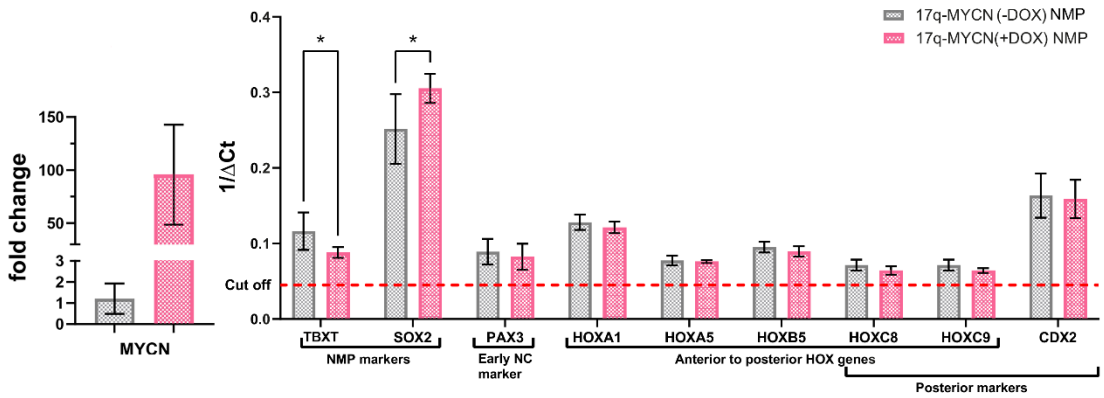
17q-MYCN (-DOX) NMP
17q-MYCN(+DOX) NMP
fold change
MYCN
1/ΔCt
Cut off
TBXT
SOX2
PAX3
HOXA1
HOXA5
HOXB5
HOXC8
HOXC9
CDX2
NMP markers
Early NC marker
Anterior to posterior HOX genes
Posterior markers

c.

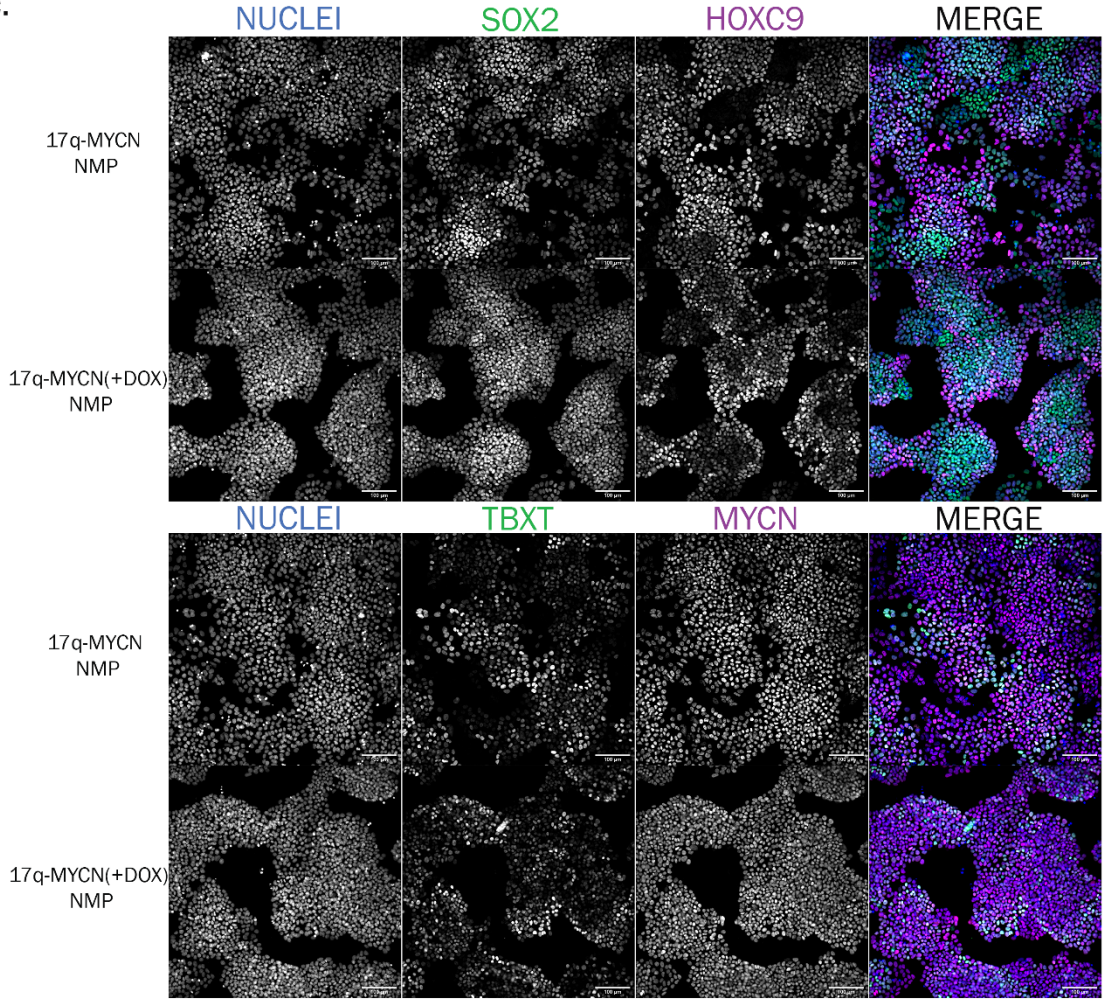
NUCLEI
SOX2
HOXC9
MERGE
17q-MYCN NMP
17q-MYCN(+DOX) NMP
NUCLEI
TBXT
MYCN
MERGE
17q-MYCN NMP
17q-MYCN(+DOX) NMP

d.

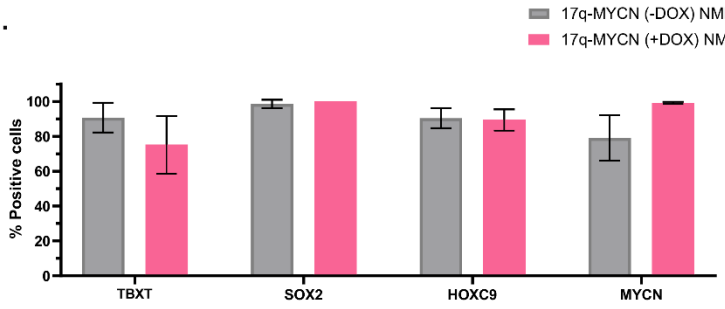
17q-MYCN (-DOX) NMP
17q-MYCN (+DOX) NMP
% Positive cells
TBXT
SOX2
HOXC9
MYCN

Figure 31. Assessment of NMP specification in the MYCN-inducible 17q cell line in the presence and absence of doxycycline

a. Analysis in the fold change of MYCN expression between 17q-MYCN(-DOX) versus 17q-MYCN(+DOX). Up to 100 times fold increase can be observed in 17q-MYCN in presence of DOX. **b.** Comparison of RNA expression at NMP stage between 17q-MYCN(-DOX) and 17q-MYCN(+DOX). Both genes analysed as NMP markers showed differences between the conditions: *TBXT* expression was lower in 17q-MYCN(+DOX), whereas *SOX2* showed an increase in its expression in the same condition. **c.** Immunofluorescence images of the 17q-MYCN(-DOX) and 17q-MYCN(+DOX) cell line differentiated into NMP. Shown are SOX2, HOXC9, TBXT and MYCN staining (Merge: Hoechst(blue), SOX2/TBXT(green), HOXC9/MYCN(magenta)). **d.** Percentage of cells expressing TBXT, SOX2, HOXC9 and MYCN markers in the immunofluorescence analysis. Protein expression related to NMP did not show statistically significant differences, nonetheless, TBXT expression seems slightly lower in 17q-MYCN(+DOX) images. **b,d.** Gene expression values are plotted as $1/\Delta Ct$. A cut off line (dotted red line) has been set at 0.045 as this is the equivalent of 40 cycles on the qPCR machine. Percentage of positive cells was quantified using immunofluorescent imaging and cell profiler analysis ($n \geq 3$ biological replicates, error bars= SD, Independent Welch t-tests, $p \leq 0.05$= *, $p \leq 0.01$= **, $p \leq 0.001$= ***, $p \leq 0.0001$= ****).

Further analysis was done by measuring the mean intensity (per nuclei) of each antibody tested (**Figure 32**). These clearly showed a significant increase in the mean intensity of MYCN protein expression in 17q-MYCN(+DOX) NMPs confirming efficient transgene induction **(Figure 32b).** Density plots of TBXT against HOXC9 show some fluctuations in TBXT expression when Dox is added from Day 0, this is apparent in the TBXT histograms (**Figure 32-c**). Nevertheless, only minor differences in the intensity of the antibodies can be seen between the conditions. HOXC9 (**Figure 32-d**) and SOX2 (**Figure 32-e**). These data suggest cells did acquire an NMP identity with minimal differences compared to the control line.

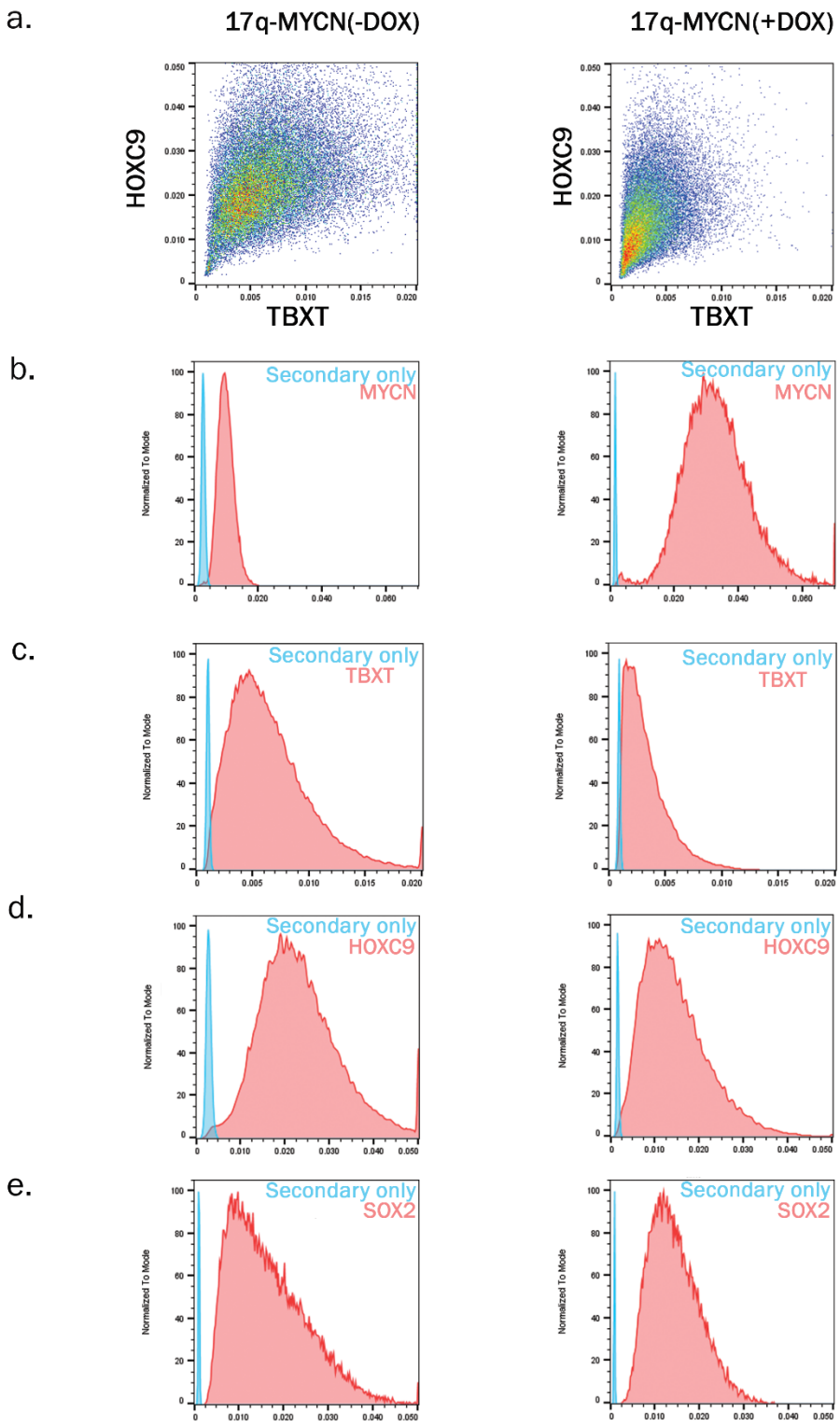

Figure 32. Single-cell immunofluorescence intensity analysis
a. Representative density plot of TBXT vs HOXC9 for 17q-MYCN(-DOX) and 17q-MYCN(+DOX) cell lines at NMP stage. Extracted from immunofluorescent imaging and cell profiler analysis. Mean florescent intensity plotted per cell. **b-e.** Panels of histograms for MYCN, TBXT, HOXC9 and SOX2 in 17q-MYCN(-DOX) (left panel), 17q-MYCN(+DOX)(right panel). Secondary only is depicted in each image (blue). Shown are data from one representative biological replicate.

4.2.2 MYCN over expression from day 0 of differentiation impairs neural crest acquisition.

After generating NMPs using the new line, even in the presence of doxycycline, I next examined the ability of the line to generate trunk neural crest (**Figure 33**). qPCR analysis for markers related to neural crest stage, posterior identity and an early neural sympathoadrenal marker revealed no statistical differences, except for MYCN that was slightly reduced in 17q-MYCN(-DOX) compared to 17q(+DOX) (**Figure 33-a**).

Immunofluorescences analysis was performed. At first sight, no differences can be perceived between the conditions (**Figure 33-b**), but when quantification was done, fewer cells are positive for MYCN in 17q(+DOX) control (**Figure 33-c**). There seems to be a disparity between qPCR quantification of MYCN *versus* its protein levels.

After showing that there is no difference between 17q and 17q-MYCN cells in their ability to produce trunk NC cells, I next tested the effect of MYCN overexpression. 17q-MYCN(-DOX) and 17q-MYCN(+DOX) NMP cells were replated and grown in NC media for 5 days. Doxycycline was added to the media from day 0 of the differentiation protocol (day 0 in NMP stage). Cells treated with doxycycline showed an increase of around 150 times in MYCN expression compared to those untreated (**Figure 34-a**). Both of the Neural crest markers analysed (*PAX3* and *SOX10*) showed a significant downregulation when MYCN was induced, especially *SOX10* whose expression was almost abolished (**Figure 34-b**). Another gene that seemed to be affected was the early sympathoadrenal marker ASCL1, which showed significant downregulation in the presence of doxycycline. None of the HOX genes nor CDX2 showed any differences between the conditions compared.

To verify these findings, immunofluorescence analysis was performed. Specific antibodies against SOX10, MYCN and HOXC9 were used and similar results to those observed in the qPCR analysis were detected by immunofluorescence (**Figure 34-c**). At first glance, SOX10 protein expression seems almost depleted in 17q-MYCN(+DOX) condition. When images were quantified, not only the number of cells expressing SOX10 but also HOXC9 were significantly lower in the cells when MYCN was induced (**Figure 34-d**). To further understand the link between MYCN overexpression in SOX10 behaviour at the single-cell level, the mean intensity (per nuclei) of each antibody was measured. When MYCN is overexpressed, SOX10 was practically depleted (**Figure 34-e**). Therefore, the induction of MYCN from day 0 completely impairs the specification of migratory neural crest, as evidenced by the lack of SOX10 expression.

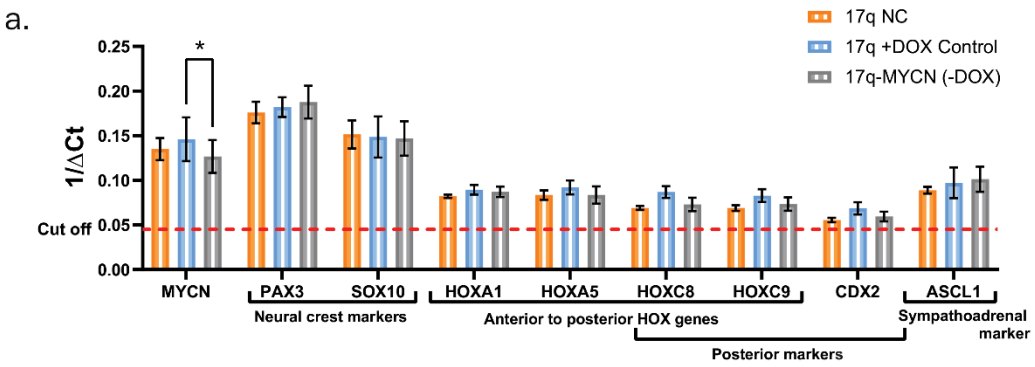
a.
17q NC
17q +DOX Control
17q-MYCN (-DOX)
1/ΔCt
0.25
0.20
0.15
0.10
Cut off 0.05
0.00
*
MYCN
PAX3
SOX10
Neural crest markers
HOXA1
HOXA5
HOXC8
HOXC9
Anterior to posterior HOX genes
CDX2
ASCL1
Sympathoadrenal marker
Posterior markers

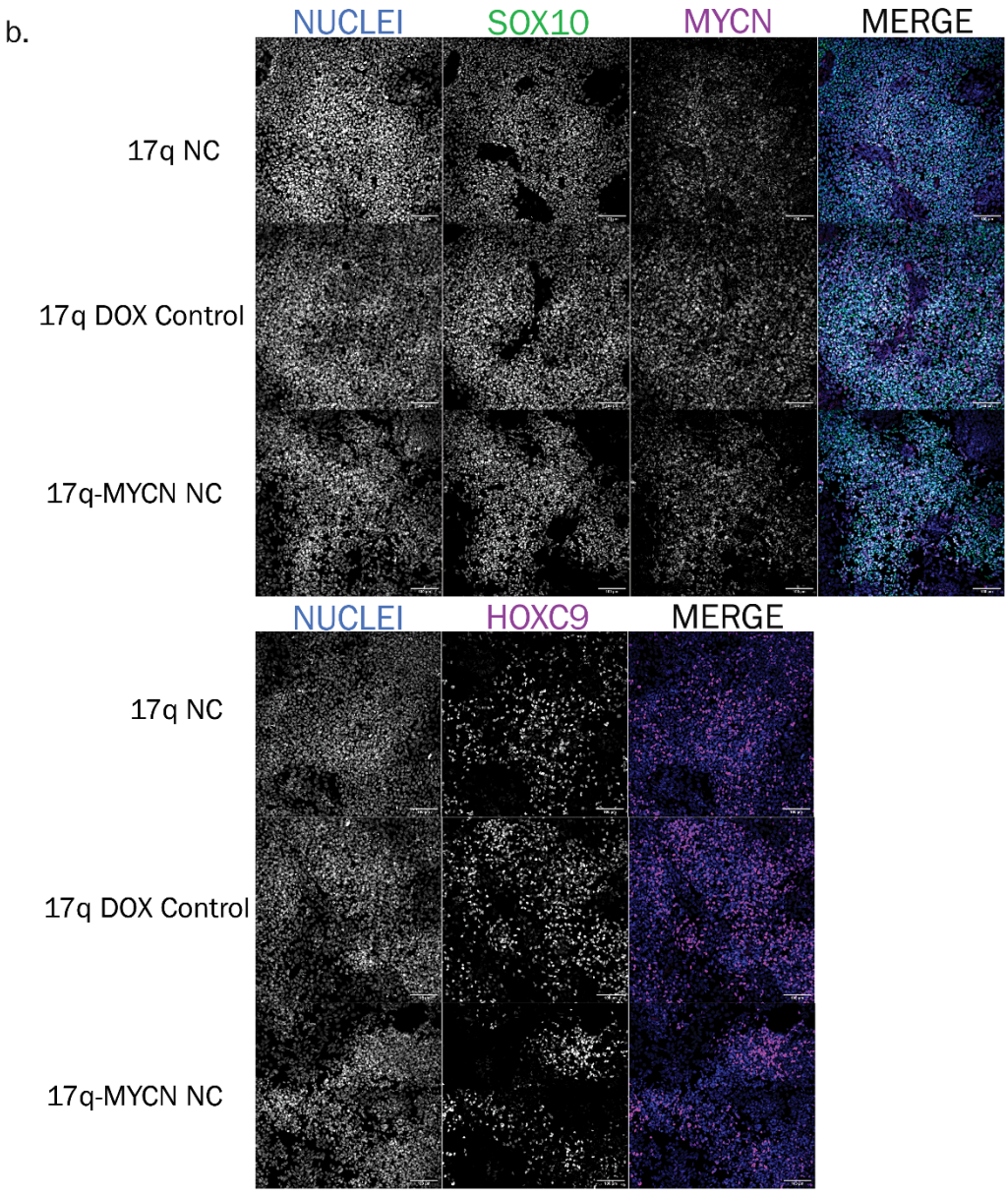
b.
NUCLEI
SOX10
MYCN
MERGE
17q NC
17q DOX Control
17q-MYCN NC
NUCLEI
HOXC9
MERGE
17q NC
17q DOX Control
17q-MYCN NC

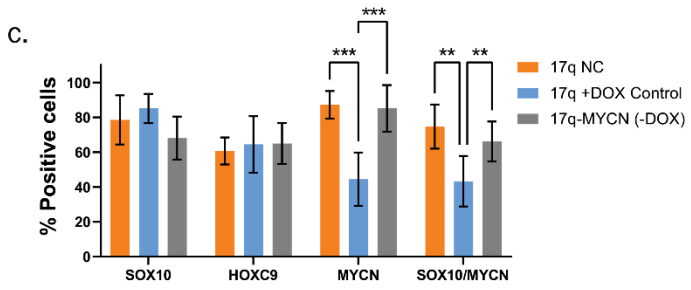
c.
% Positive cells
100
80
60
40
20
0
***
***
**
**
SOX10
HOXC9
MYCN
SOX10/MYCN
17q NC
17q +DOX Control
17q-MYCN (-DOX)

Figure 33. Assessment of NC specification in control lines and control conditions

a. Comparison of RNA expression at NC stage between 17q cell line, 17q with Doxycycline (as a doxycycline control) and 17q-MYCN without Doxycycline treatment. The bar chart shows the qPCR analysis, gene expression values are plotted as 1/ΔCt (specified in graph legend). A cut off line (dotted red line) has been set at 0.045 as this is the equivalent of 40 cycles on the qPCR machine. No genes related to NMP differentiation showed significant differences though *MYCN* showed lower expression in 17q-MYCN(-DOX) compared to 17q(+DOX) control. **b.** Immunofluorescence images of the 17q, 17q(+DOX) Control and 17q-MYCN(-DOX) cell line differentiated into NC. Shown are SOX10, MYCN and HOXC9 staining (Merge: Hoechst(blue), SOX10(green), MYCN/HOXC9(magenta)). **c.** Percentage of cells expressing SOX10, MYCN and HOXC9 markers in the immunofluorescence analysis. Protein expression related to NC did not show significant differences, although MYCN expression was significantly varied among the different lines and conditions. **a,c.** Gene expression values are plotted as 1/ΔCt. A cut off line (dotted red line) has been set at 0.045 as this is the equivalent of 40 cycles on the qPCR machine. Percentage of positive cells was quantified using immunofluorescent imaging and Cell Profiler analysis (n≥ 3 biological replicates, error bars= SD, Independent Welch t-tests, $p \leq 0.05$= *, $p \leq 0.01$= **, $p \leq 0.001$= ***, $p \leq 0.0001$= ****).

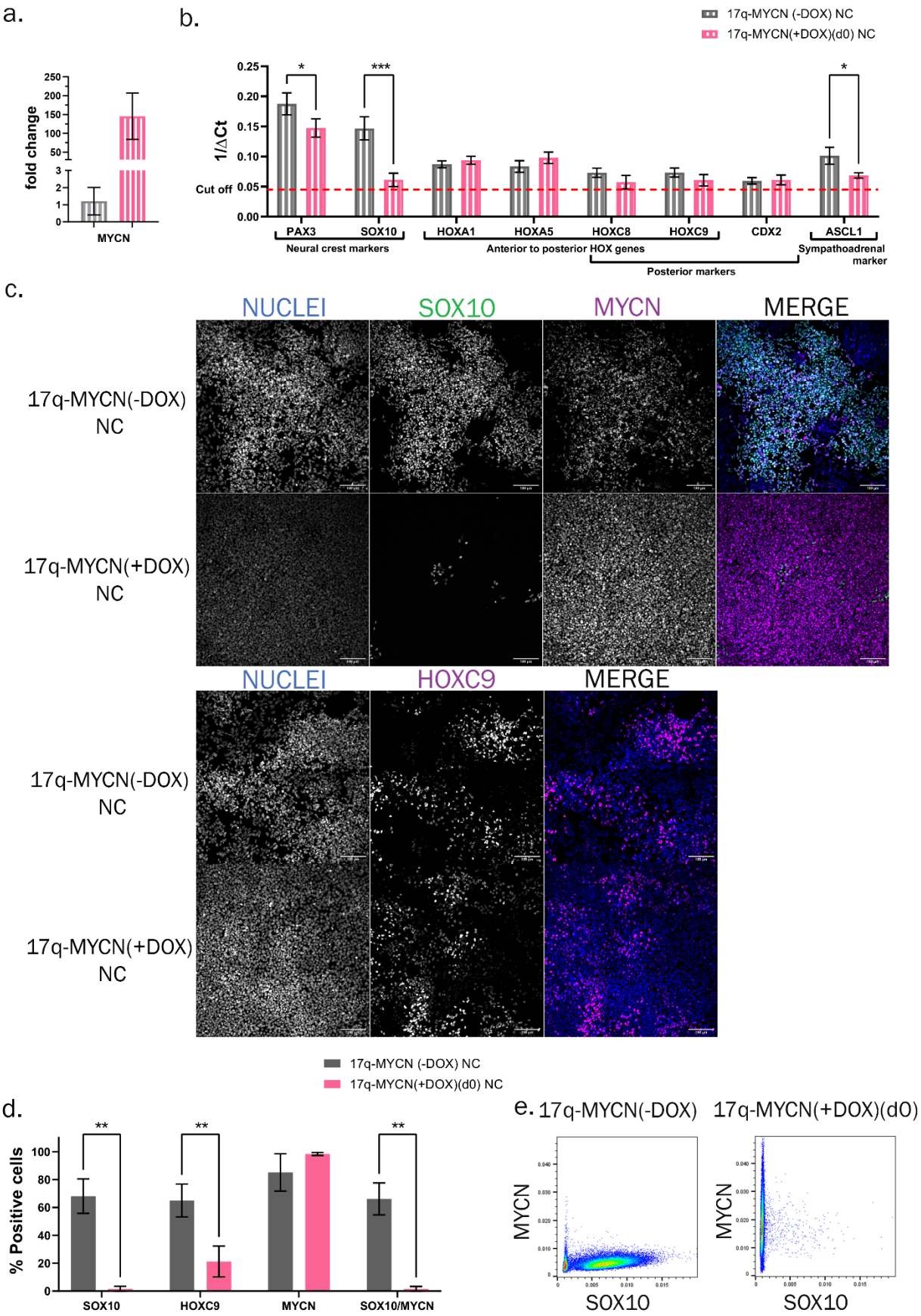
a.
fold change
MYCN
b.
17q-MYCN (-DOX) NC
17q-MYCN(+DOX)(d0) NC
1/ΔCt
Cut off
PAX3
SOX10
HOXA1
HOXA5
HOXC8
HOXC9
CDX2
ASCL1
Neural crest markers
Anterior to posterior HOX genes
Posterior markers
Sympathoadrenal marker
c.
NUCLEI
SOX10
MYCN
MERGE
17q-MYCN(-DOX) NC
17q-MYCN(+DOX) NC
NUCLEI
HOXC9
MERGE
17q-MYCN(-DOX) NC
17q-MYCN(+DOX) NC
17q-MYCN (-DOX) NC
17q-MYCN(+DOX)(d0) NC
d.
% Positive cells
SOX10
HOXC9
MYCN
SOX10/MYCN
e.
17q-MYCN(-DOX)
17q-MYCN(+DOX)(d0)
MYCN
SOX10

Figure 34. Assessment of NC specification in the MYCN-inducible 17q cell line in the presence and absence of doxycycline from day 0 of differentiation
a. Fold change of *MYCN* expression between 17q-MYCN(-DOX) versus 17q-MYCN(+DOX) in NC stage. Up to 150 times fold increase of *MYCN* mRNA can be observed in 17q-MYCN in presence of Doxycycline treatment started at day 0. **b.** Comparison of RNA expression at NC stage between 17q-MYCN(-DOX) and 17q-MYCN(+DOX). Both genes used as NC markers showed differences between the conditions: both *PAX3* and *SOX10* showed a statistically significant decrease in gene expression in 17q-MYCN(+DOX)(d0) compared to the control 17q-MYCN(-DOX), as well as the early sympathoadrenal marker *ASCL1*. **c.** Immunofluorescence images of the 17q-MYCN(-DOX) and 17q-MYCN(+DOX) cell line differentiated into NC. Shown is staining for SOX10, MYCN and HOXC9 (Merge: Hoechst(blue), SOX10(green), MYCN/HOXC9(magenta)). **d.** Percentage of cells expressing SOX10, HOXC9, MYCN and cells co-expressing SOX10/MYCN markers in the immunofluorescence analysis. Protein expression related to NC show statistically significant differences, as both SOX10 and HOXC9, were much less expressed when MYCN expression was induced in the presence of doxycycline, nonetheless MYCN overall expression, although higher, was not significantly different between conditions at the single-cell protein level. **b,d.** Gene expression values are plotted as 1/ΔCt. A cut off line (dotted red line) has been set at 0.045 as this is the equivalent of 40 cycles on the qPCR machine. Percentage of positive cells was quantified using immunofluorescent imaging and cell profiler analysis (n≥ 3 biological replicates, error bars= SD, Independent Welch t-tests, $p \leq 0.05$= *, $p \leq 0.01$= **, $p \leq 0.001$= ***, $p \leq 0.0001$= ****). **e.** Representative density plot of SOX10 and MYCN for 17q-MYCN(-DOX) and 17q-MYCN(+DOX from day 0) cell lines at NC stage. Analysed from immunofluorescent images and Cell Profiler analysis. Mean florescent intensity plotted per cell.

4.2.3 Later MYCN induction during neural crest differentiation partially decreases SOX10 expression and impacts further sympathetic specification.

Due to the impaired neural crest differentiation when MYCN was induced from day 0, media containing doxycycline was given from day 5 of the differentiation protocol instead (2 days after the Neural crest protocol started). The latter based on the hypothesis that cells at day 5 could be more committed to a neural crest differentiation trajectory. Kerosuo et al 2018, found that pre-migratory neural crest cells are still susceptible to MYCN influence, having their cellular fate affected. Therefore, as day 5 represents an intermediate stage between pre and post migratory neural crest, overexpression of MYCN at this stage might circumvent the impaired neural crest differentiation seen when MYCN was induced from day 0.

At the end of the Neural crest protocol (day 9), cells were harvested and analysed by qPCR. *MYCN* was induced around 80 times when cells were treated with doxycycline (**Figure 35-a**). Neural crest markers *PAX3* and *SOX10* were significantly downregulated when compared to the control (**Figure 35-b**). *ASCL1* expression was also downregulated in cells treated with doxycycline.

SOX10, MYCN and HOXC9 immunofluorescence images show that 17q-MYCN(+DOX)(from day 5) had fewer cells expressing SOX10 when compared to the control (**Figure 35-c**). These findings were corroborated by quantifying the staining, which showed that the number of cells expressing SOX10

and HOXC9 seemed less than the control, although no statistical significances were found (**Figure 35-d**). To understand the effect that MYCN overexpression had on SOX10, the mean intensity of SOX10 and MYCN antibodies was analysed. This showed that when MYCN is not induced, high levels of SOX10 are expressed. In contrast, when MYCN is induced, different levels of SOX10 intensity are found in the culture (**Figure 35-e**). i.e. we see an inverse correlation between SOX10 and MYCN expression levels.

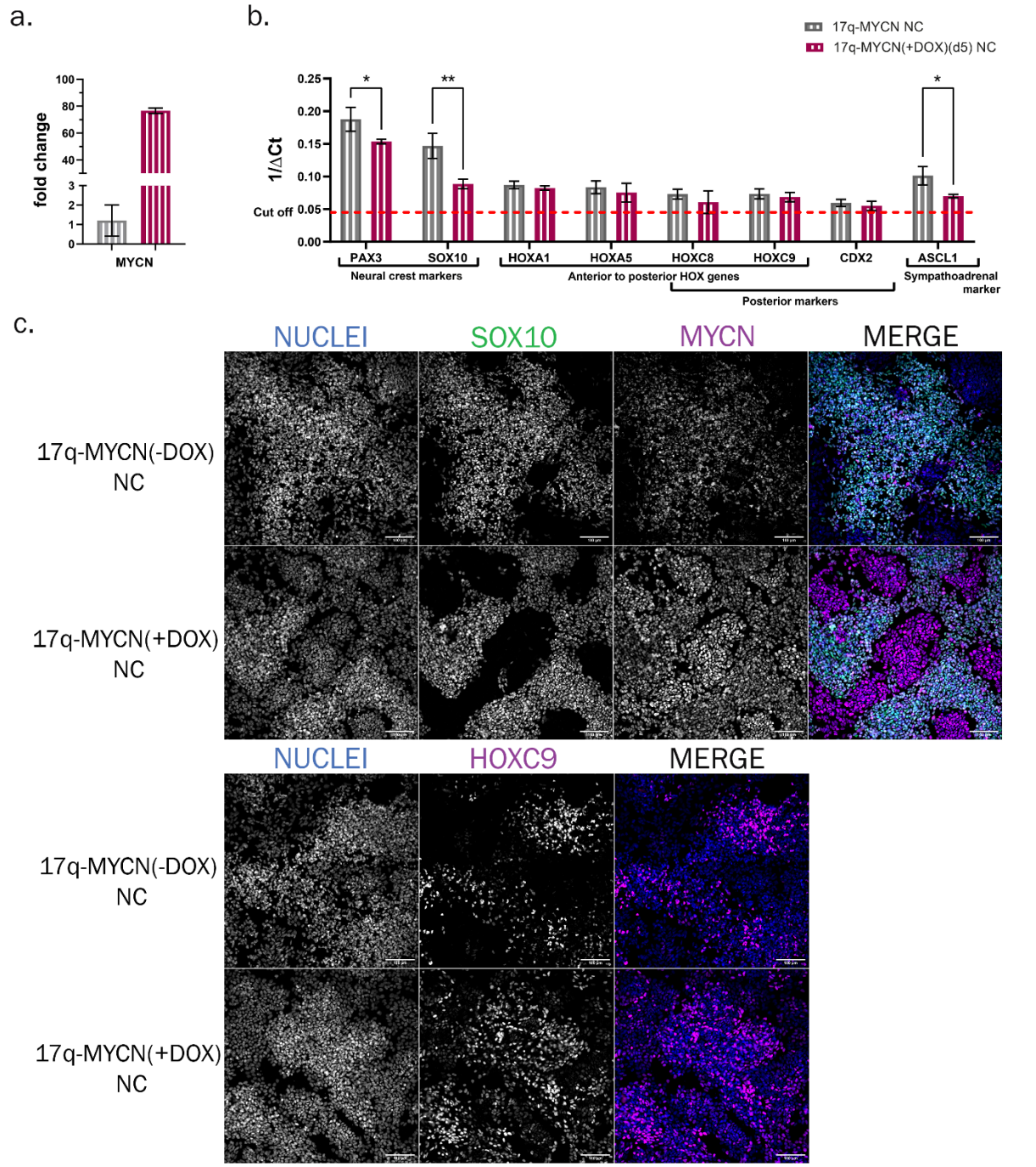
a.
b.
17q-MYCN NC
17q-MYCN(+DOX)(d5) NC
fold change
MYCN
1/ΔCt
Cut off
PAX3
SOX10
HOXA1
HOXA5
HOXC8
HOXC9
CDX2
ASCL1
Neural crest markers
Anterior to posterior HOX genes
Posterior markers
Sympathoadrenal marker
c.
NUCLEI
SOX10
MYCN
MERGE
17q-MYCN(-DOX) NC
17q-MYCN(+DOX) NC
NUCLEI
HOXC9
MERGE
17q-MYCN(-DOX) NC
17q-MYCN(+DOX) NC
d.
17q-MYCN NC
17q-MYCN(+DOX)(d5) NC
% Positive cells
SOX10
HOXC9
MYCN
SOX10/MYCN
e.
17q-MYCN(-DOX)
17q-MYCN(+DOX)(d5)
MYCN
SOX10
MYCN
SOX10

Figure 35. Assessment of NC specification in the MYCN-inducible 17q cell line in the presence and absence of doxycycline from day 5 of differentiation
a. Schematic diagram of the directed differentiation of human pluripotent stem cells into Neuromesodermal progenitors (**NMP**), Neural Crest (**NC**), Sympathoadrenal progenitors (**SAP**) and Sympathetic neurons (**SN**). The red rectangle highlights the day cells were harvested, and which markers were used to validate the stage. It is also indicated with a green arrow when was started the treatment with doxycycline **b.** Analysis in the fold change of *MYCN* expression between 17q-MYCN(-DOX) versus 17q-MYCN(+DOX) in the NC stage. Up to ~ 80 times fold increase of *MYCN* mRNA can be observed in 17q-MYCN in presence of Doxycycline treatment started at day 5. **c.** Comparison of RNA expression at NC stage between 17q-MYCN(-DOX) and 17q-MYCN(+DOX)(day5). Both genes used as NC markers showed differences between the conditions: both *PAX3* and *SOX10* showed a statistically significant decrease in gene expression in 17q-MYCN(+DOX)(d5) compared to the control 17q-MYCN(-DOX), as well as the early sympathoadrenal marker *ASCL1*. **d.** Immunofluorescence images of the 17q-MYCN(-DOX) and 17q-MYCN(+DOX) cell line differentiated into NC. Shown are SOX10, MYCN and HOXC9 staining (Merge: Hoechst(blue), SOX10(green), MYCN/HOXC9(magenta)). **e.** Percentage of cells expressing SOX10, HOXC9, MYCN and cells co-expressing SOX10/MYCN markers in the immunofluorescence analysis. No statistically differences were found, although protein presence of SOX10 and HOXC9 seemed lower in 17q-MYCN(+DOX)(day5) cell line. **b-c,e.** Gene expression values are plotted as $1/\Delta Ct$. A cut off line (dotted red line) has been set at 0.045 as this is the equivalent of 40 cycles on the qPCR machine. Percentage of positive cells was quantified using immunofluorescent imaging and cell profiler analysis ($n \geq 3$ biological replicates, error bars= SD, Independent Welch t-tests, $p \leq 0.05$= *, $p \leq 0.01$= **, $p \leq 0.001$= ***, $p \leq 0.0001$= ****). **f.** Representative density plot of SOX10 and MYCN for 17q-MYCN(-DOX) and 17q-MYCN(+DOX from day 5) cell lines at NC stage. Extracted from immunofluorescent imaging and cell profiler analysis. Mean florescent intensity plotted per cell.

As MYCN induction from day 5 did diminish but did not completely prevent neural crest specification, I decided to take these cells to the sympathoadrenal progenitors (SAP) stage (**Figure 36-a**). Hence, no remarkable differences were observed between the control 17q SAP population against 17-MYCN(-DOX) SAP (**Figure 36-b**). However, when *MYCN* was induced, 25 times higher in cells treated with doxycycline (**Figure 36-c**), *SOX10*, *PHOX2B and DBH* seem to be downregulated in the cells treated with doxycycline when compared to the untreated ones. No other evident differences were observed at the transcript level.

In order to promote the development of sympathoadrenal progenitors into a more mature state, 17q-MYCN(-DOX) SAP and 17q-MYCN(+DOX) were grown in medium containing BDNF, GDNF, and NGF factors. Cells were allowed to grow in these conditions for 5 days (**Figure 37-a**) before they were harvested and analysed by qPCR. *PHOX2B, PHOX2A, GATA3* and *DBH* showed downregulation in the 17q-MYCN cell line when compared to 17q (**Figure 37-b**), highlighting the first signs of a possible impact of the 1q gain upon the differentiation.

Once the control cell lines were analysed, the influence of MYCN on the differentiation was determined. In 17q-MYCN supplemented with doxycycline, the expression of *MYCN* was up to 100 times higher than the untreated cell line (**Figure 37-c**). Other markers showed differences as well. The

most evident were *PHOX2B, PHOX2A, GATA3 and GATA2*, all of which appeared to be downregulated when compared to the control cell line.

The induction of MYCN at the later stage permitted the expression of SOX10 in some cells and further differentiation towards the sympathetic lineage. Nevertheless, diminished SOX10 expression remained the standout feature and further differentiation seemed to be impeded.

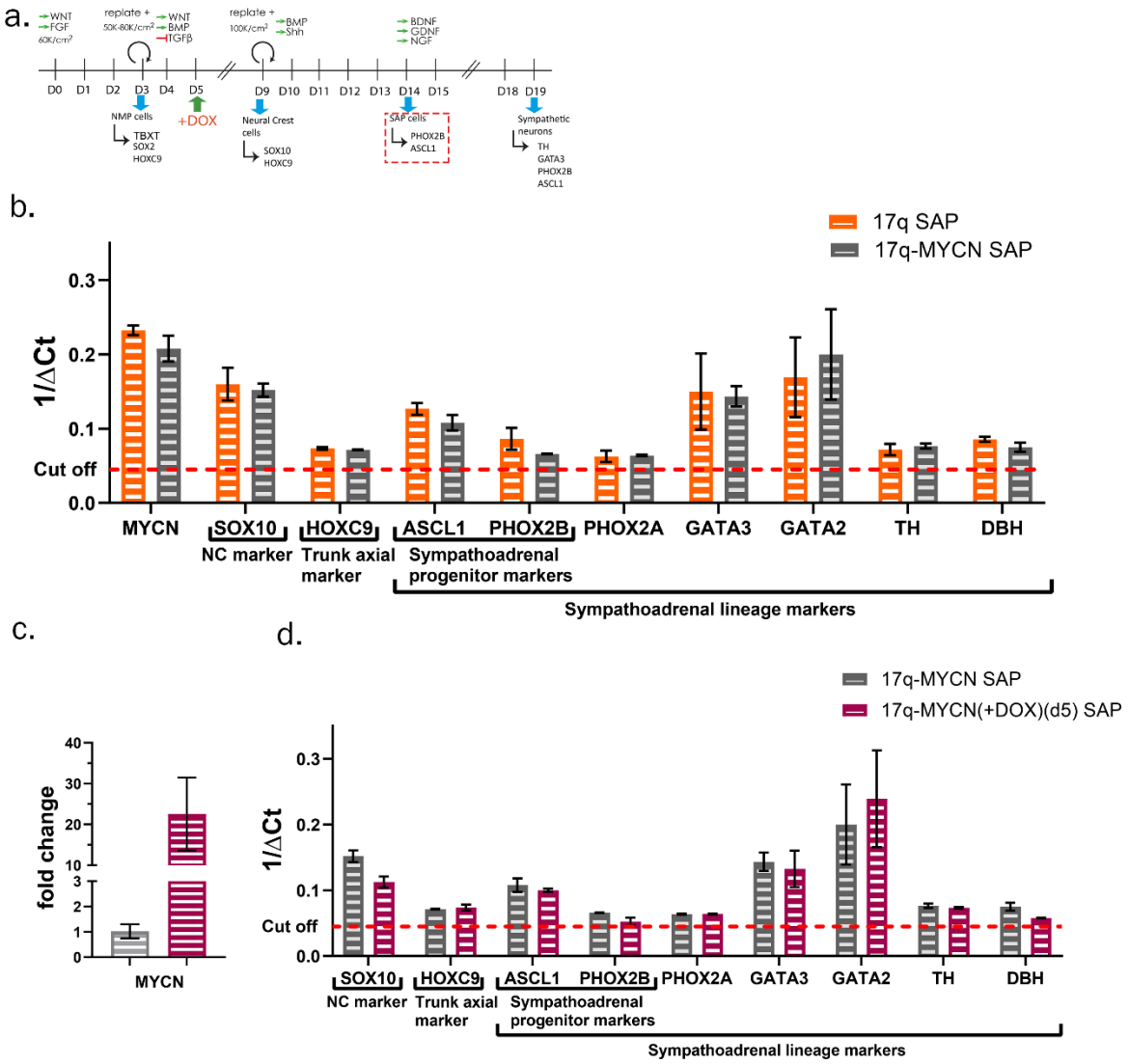

Figure 36. Assessment of SAP specification in the MYCN-inducible 17q cell line in the presence and absence of doxycycline from day 5 of differentiation

a. Schematic diagram of the directed differentiation of human pluripotent stem cells into Neuromesodermal progenitors (**NMP**), Neural Crest (**NC**), Sympathoadrenal progenitors (**SAP**) and Sympathetic neurons (**SN**). The red rectangle highlights the day cells were harvested, and which markers were used to validate the stage. It is also indicated with a green arrow when was started the treatment with doxycycline **b.** Comparison of RNA expression at SAP stage between 17q cell line and 17q-MYCN without Doxycycline treatment. **c.** Analysis in the fold change of *MYCN* expression between 17q-MYCN(-DOX) versus 17q-MYCN(+DOX) in the SAP stage. Up to ~ 20 times fold increase of *MYCN* mRNA can be observed in 17q-MYCN in presence of Doxycycline treatment started at day 5. **d.** Comparison of RNA expression at SAP stage between 17q-MYCN(-DOX) and 17q-MYCN(+DOX)(day5).

Differences in *SOX10* and *DBH* expression can be presumed. **b,d.** Gene expression values are plotted as 1/ΔCt. A cut off line (dotted red line) has been set at 0.045 as this is the equivalent of 40 cycles on the qPCR machine (n= 2 biological replicates, error bars= SD, no statistical test was performed).

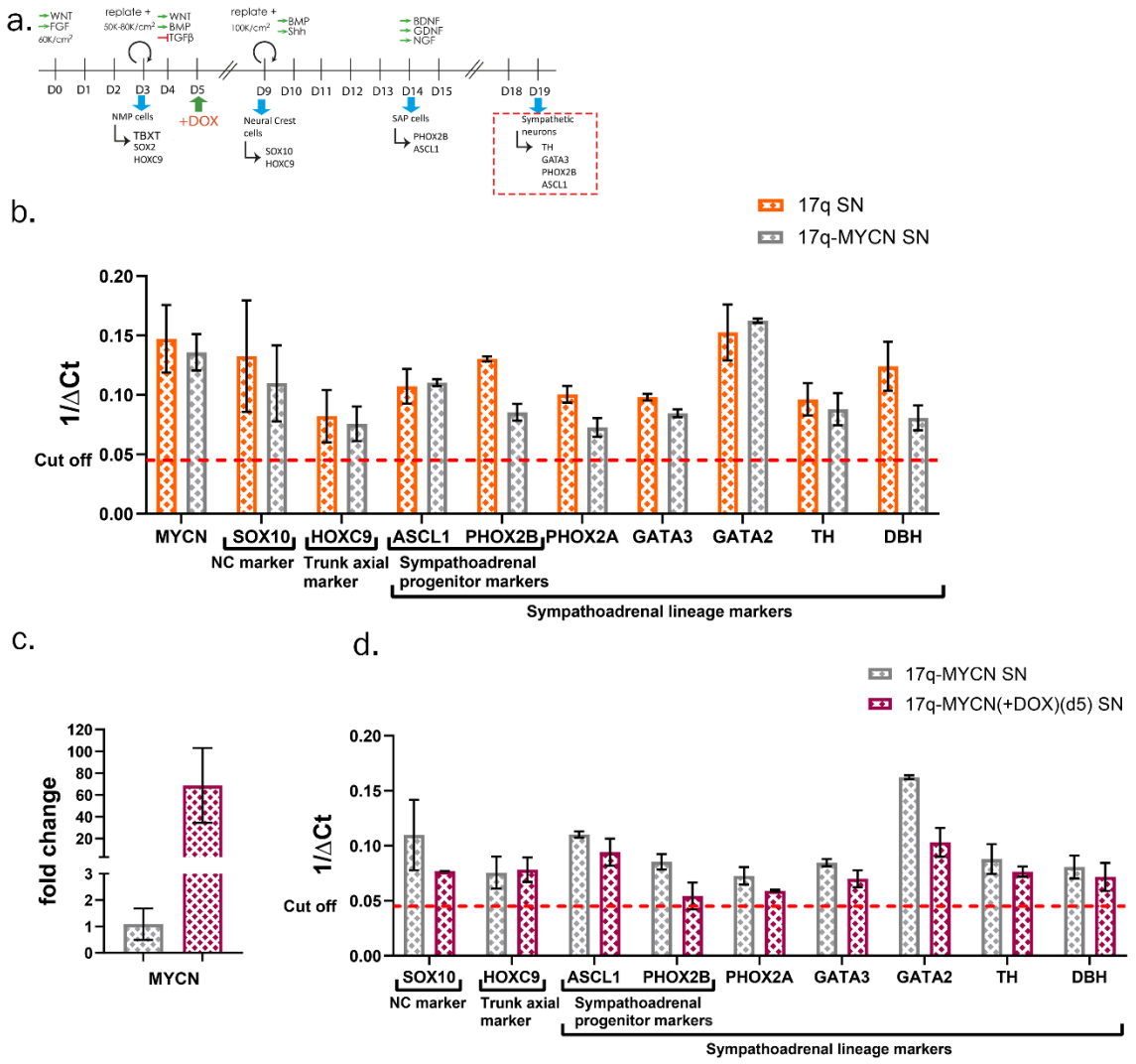

Figure 37. Assessment of SN specification in the MYCN-inducible 17q cell line in the presence and absence of doxycycline from day 5 of differentiation

a. Schematic diagram of the directed differentiation of human pluripotent stem cells into Neuromesodermal progenitors (**NMP**), Neural Crest (**NC**), Sympathoadrenal progenitors (**SAP**) and Sympathetic neurons (**SN**). The red rectangle highlights the day cells were harvested, and which markers were used to validate the stage. It is also indicated with a green arrow when was started the treatment with doxycycline **b.** Comparison of RNA expression at SN stage between 17q cell line and 17q-MYCN without Doxycycline treatment. **c.** Analysis in the fold change of *MYCN* expression between 17q-MYCN(-DOX) versus 17q-MYCN(+DOX) in the SAP stage. Up to ~ 70 times fold increase of *MYCN* mRNA can be observed in 17q-MYCN in presence of Doxycycline treatment started at day 5. **d.** Comparison of RNA expression at SAP stage between 17q-MYCN(-DOX) and 17q-MYCN(+DOX)(day5). Differences in the expression of sympathoadrenal markers can be presumed. **b,d.** Gene expression values are plotted as 1/ΔCt. A cut off line (dotted red line) has been set at 0.045 as this is the equivalent of 40 cycles on the qPCR machine (n= 2 biological replicates, error bars= SD, no statistical test was performed).

4.2.4 Mycn Overexpression In The WNT Elevated Differentiation

4.2.4.1 Normal neural crest profile is altered when MYCN is overexpressed from day 5 of differentiation.

Previously, I demonstrated that the 17q cell line differentiated better with elevated WNT signalling. Therefore, I assessed the cell lines in the elevated WNT protocol. 17q and 17q-MYCN(-DOX) pluripotent stem cells were grown in Neuro-mesodermal progenitor medium, consisting of N2B27 medium, supplemented with 20ng/ml of FGF and 4μm of CHIR (**Figure 38, a)**. After three days, cells were harvested and qPCR was performed. The only gene that showed a significant difference between the cell lines was *SOX2*, which was slightly but significantly upregulated in 17q-MYCN(-DOX) (**Figure 38-b**). Immunofluorescence analysis of SOX2, HOXC9, TBXT, CDX2 and MYCN exhibited minimal differences (**Figure 38-c**). Quantification of the antibody staining revealed similar results to those observed in the qPCR analysis, as more cells expressed SOX2 in 17q-MYCN(-DOX) NMP cells (**Figure 39-a**). Deeper analysis at a single cell nuclear intensity level, revealed only a small downregulation in HOXC9 in 17q-MYCN(-DOX) NMP when compared to 17q NMP(**Figure 39-b**).

qPCR analysis at the neural crest stage showed no significant differences between 17q and 17q-MYCN(-DOX) (**Figure 40-b**). At the protein level, the immunofluorescence analysis of SOX10, HOXC9 and MYCN did not show any differences in the images (**Figure 40-c**) nor when quantification analysis was performed (**Figure 40-d**).

In summary, both lines, 17q and 17q-MYCN, behave similarly in their capacity to generate trunk NC and thus the 1q gain does not seem to influence differentiation to trunk NC.

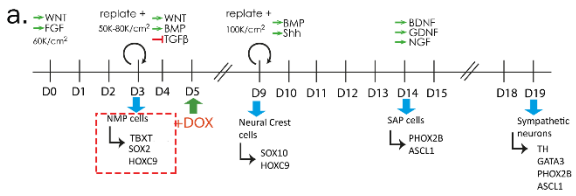
a.
WNT
FGF
60K/cm²
replate +
50K-80K/cm²
WNT
BMP
TGFβ
replate +
100K/cm²
BMP
Shh
BDNF
GDNF
NGF
D0 D1 D2 D3 D4 D5 D9 D10 D11 D12 D13 D14 D15 D18 D19
NMP cells
TBXT
SOX2
HOXC9
+DOX
Neural Crest cells
SOX10
HOXC9
SAP cells
PHOX2B
ASCL1
Sympathetic neurons
TH
GATA3
PHOX2B
ASCL1

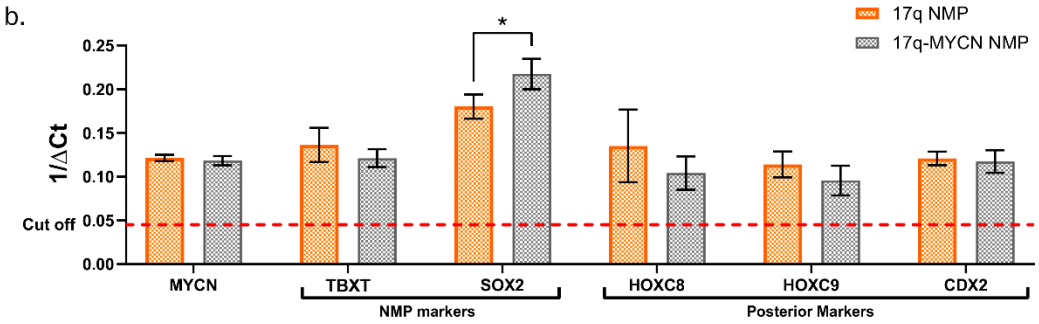
b.
17q NMP
17q-MYCN NMP
1/ΔCt
0.25
0.20
0.15
0.10
Cut off 0.05
0.00
*
MYCN
TBXT
SOX2
HOXC8
HOXC9
CDX2
NMP markers
Posterior Markers

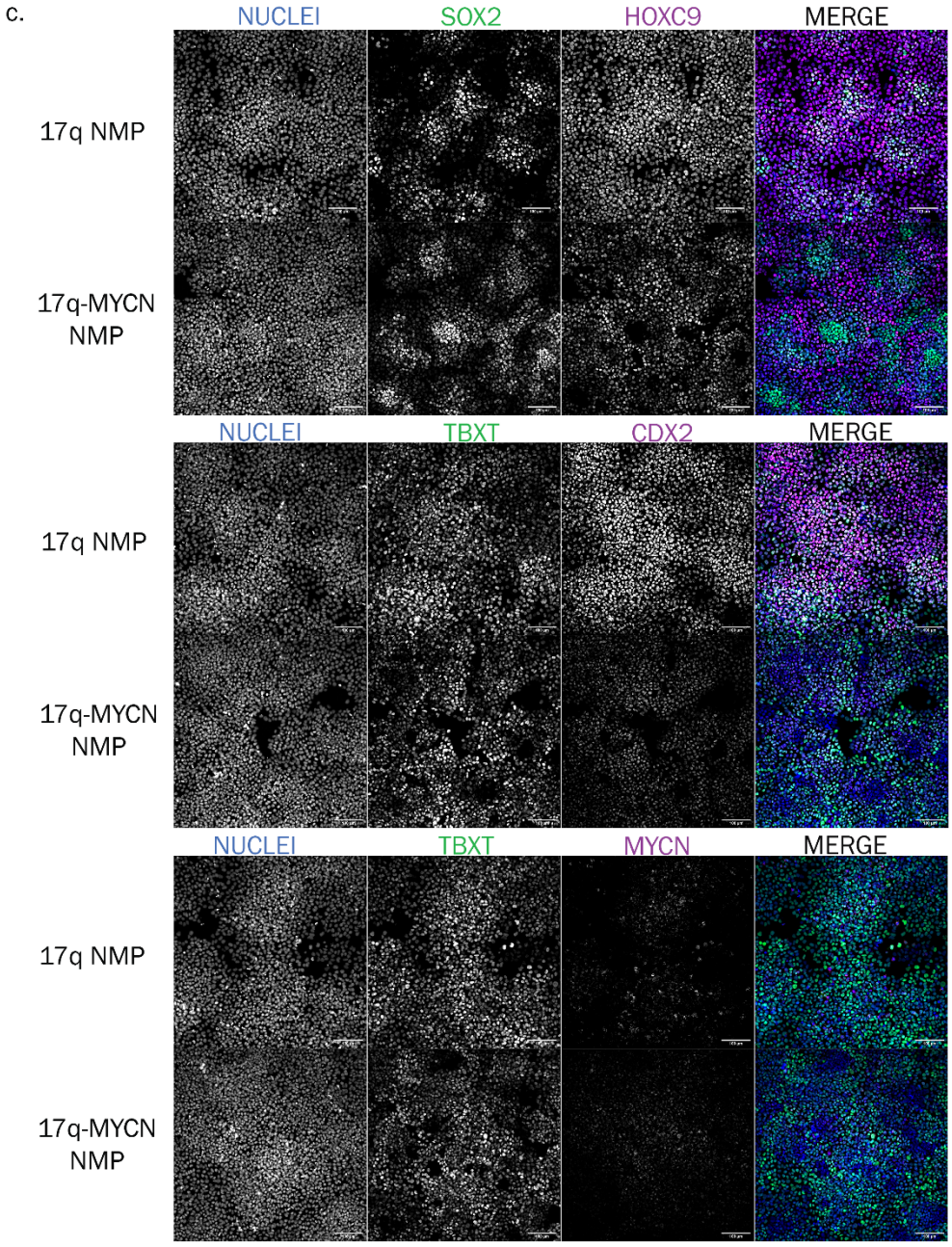
c.
NUCLEI
SOX2
HOXC9
MERGE
17q NMP
17q-MYCN NMP
NUCLEI
TBXT
CDX2
MERGE
17q NMP
17q-MYCN NMP
NUCLEI
TBXT
MYCN
MERGE
17q NMP
17q-MYCN NMP

Figure 38. Assessment of NMP specification in control lines and control conditions

a. Schematic diagram of the directed differentiation of human pluripotent stem cells into Neuromesodermal progenitors (**NMP**), Neural Crest (**NC**), Sympathoadrenal progenitors (**SAP**) and Sympathetic neurons (**SN**). The red rectangle highlights the day cells were harvested, and which markers were used to validate the stage. **b.** Comparison of RNA expression at NMP stage between 17q cell line and 17q-MYCN without Doxycycline treatment, 17q cell line was differentiated into NMP changing the CHIR concentration from 3µM to 4µM in culture conditions. *SOX2* showed a significant difference in 17-MYCN(-DOX) compared to 17q. The bar chart shows the qPCR analysis, gene expression values are plotted as 1/ΔCt (specified in graph legend). A cut off line (dotted red line) has been set at 0.045 as this is the equivalent to 40 cycles on the qPCR machine(n≥ 3 biological replicates, , error bars= SD, Independent Welch t-tests, $p \leq 0.05$= *, $p \leq 0.01$= **, $p \leq 0.001$= ***, $p \leq 0.0001$= ****). **c.** Immunofluorescence images of the 17q and 17q-MYCN(-DOX) cell line differentiated into NMP (4µM CHIR). Shown are SOX2, HOXC9, TBXT, CDX2 and MYCN staining (Merge: Hoechst(blue), SOX2/TBXT(green), HOXC9/CDX2/MYCN(magenta)).

a.

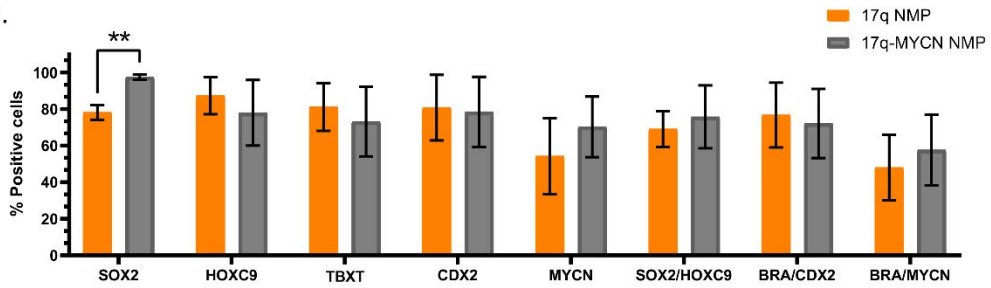
17q NMP
17q-MYCN NMP
**
% Positive cells
100
80
60
40
20
0
SOX2
HOXC9
TBXT
CDX2
MYCN
SOX2/HOXC9
BRA/CDX2
BRA/MYCN

b.

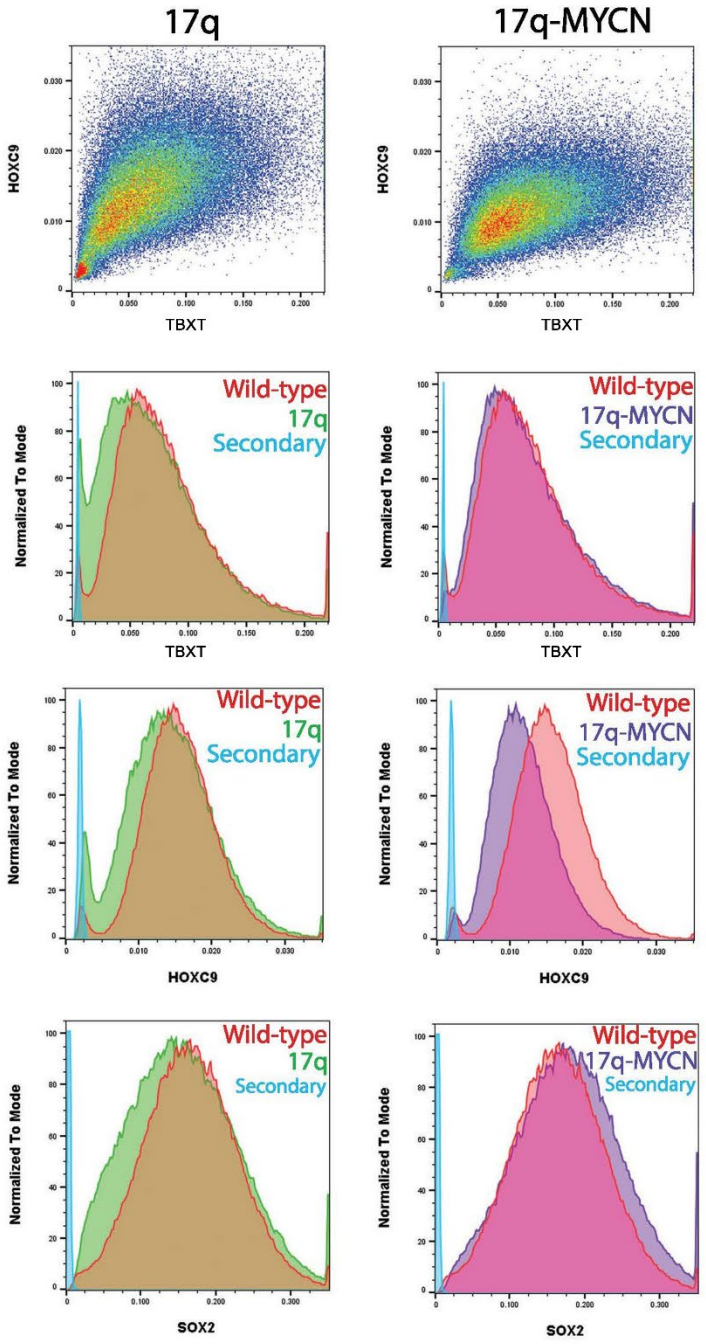
17q
17q-MYCN
HOXC9
TBXT
Wild-type
17q
Secondary
17q-MYCN
Normalized To Mode
HOXC9
SOX2

Figure 39. Single-cell immunofluorescence intensity analysis in NMP specification

a. Percentage of cells expressing SOX2, HOXC9, TBXT, CDX2, MYCN and cells co-expressing SOX2/HOXC9, TBXT/CDX2 and BRACHUYRY/MYCN markers in the immunofluorescence analysis. Protein expression related to NMP only showed downregulation in SOX2 expression in 17-MYCN(-DOX) compared to 17q NMP. **b.** Representative density plot of TBXT vs HOXC9 for 17q and 17q-MYCN(-DOX) cell lines at NMP stage. Extracted from immunofluorescent imaging and cell profiler analysis. Mean florescent intensity plotted per cell. **c-e.** Panels of histograms for TBXT, HOXC9 and SOX2 in 17q (left panel), 17q-MYCN(-DOX)(right panel). Secondary only is depicted in each image (blue). Shown are data from one representative biological replicate.

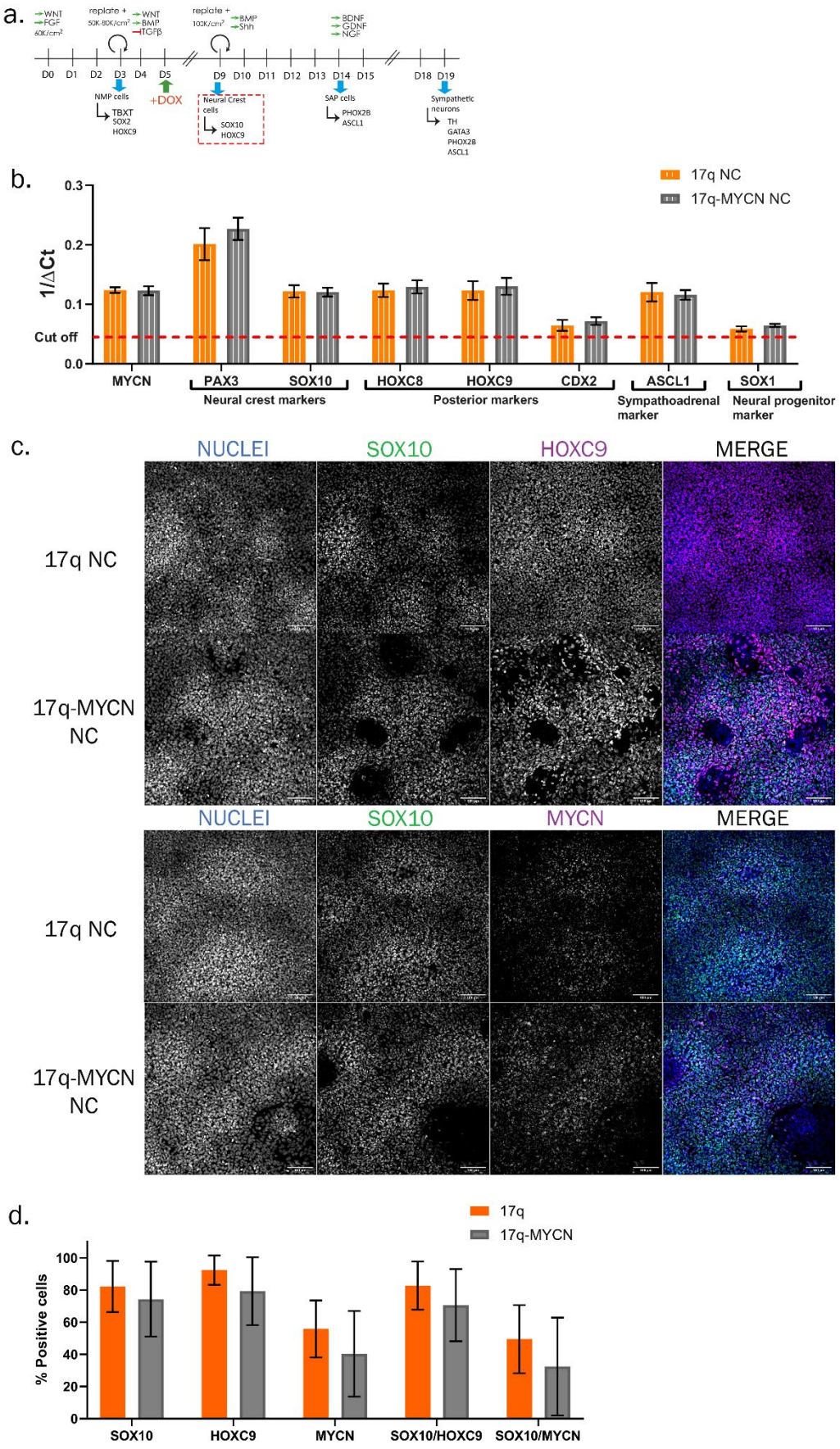
a.
WNT
FGF
60K/cm²
replate +
50K-80K/cm²
WNT
BMP
TGFβ
replate +
100K/cm²
BMP
Shh
BDNF
GDNF
NGF
D0 D1 D2 D3 D4 D5 D9 D10 D11 D12 D13 D14 D15 D18 D19
NMP cells
TBXT
SOX2
HOXC9
+DOX
Neural Crest cells
SOX10
HOXC9
SAP cells
PHOX2B
ASCL1
Sympathetic neurons
TH
GATA3
PHOX2B
ASCL1
b.
17q NC
17q-MYCN NC
1/ΔCt
0.3
0.2
0.1
Cut off
0.0
MYCN
PAX3
SOX10
HOXC8
HOXC9
CDX2
ASCL1
SOX1
Neural crest markers
Posterior markers
Sympathoadrenal marker
Neural progenitor marker
c.
NUCLEI
SOX10
HOXC9
MERGE
17q NC
17q-MYCN NC
NUCLEI
SOX10
MYCN
MERGE
17q NC
17q-MYCN NC
d.
17q
17q-MYCN
% Positive cells
100
80
60
40
20
0
SOX10
HOXC9
MYCN
SOX10/HOXC9
SOX10/MYCN

Figure 40. Assessment of NC specification in control lines and control conditions
a. Schematic diagram of the directed differentiation of human pluripotent stem cells into Neuromesodermal progenitors (**NMP**), Neural Crest (**NC**), Sympathoadrenal progenitors (**SAP**) and Sympathetic neurons (**SN**). The red rectangle highlights the day cells were harvested, and which markers were used to validate the stage. **b.** Comparison of RNA expression at NC stage between 17q cell line and 17q-MYCN without Doxycycline treatment. The bar chart shows the qPCR analysis. No genes related to NC differentiation showed significant differences. **c.** Immunofluorescence images of the 17q and 17q-MYCN(-DOX) cell line differentiated into NC. Shown are SOX10, HOXC9 and MYCN staining (Merge: Hoechst(blue), SOX10(green), HOXC9/MYCN(magenta)). **d.** Percentage of cells expressing SOX10, HOXC9 and MYCN as well as cells co-expressing SOX10/HOXC9 and SOX10/MYCN markers in the immunofluorescence analysis. No significant changes were observed. **b,d.** Gene expression values are plotted as 1/ΔCt. A cut off line (dotted red line) has been set at 0.045 as this is the equivalent of 40 cycles on the qPCR machine. Percentage of positive cells was quantified using immunofluorescent imaging and cell profiler analysis (n≥ 3 biological replicates, error bars= SD, Independent Welch t-tests, $p \leq 0.05$= *, $p \leq 0.01$= **, $p \leq 0.001$= ***, $p \leq 0.0001$= ****).

To assess MYCN overexpression effects on neural crest 17q-MYCN(-DOX) and 17q-MYCN(+DOX)(from day 5) were grown in neural crest media and harvested at day 9 (NMP+NC differentiation). qPCR analysis revealed that *MYCN* was overexpressed up to 80 times when compared to the untreated cell line (**Figure 41-a)**. The neural crest markers, *PAX3* and *SOX10* both showed a significant downregulation when grown in presence of doxycycline. The early sympathoadrenal marker, *ASCL1* exhibited lower expression of the transcript (**Figure 41-b**). I also tested for a neural progenitor marker (*SOX1*), in order to explore additional routes of differentiation that our cell line could be following. A small but significant upregulation was found in 17q-MYCN(+DOX) when compared to the control.

Protein expression of SOX10, HOXC9 and MYCN markers was done by immunofluorescence (**Figure 41-c**). Although SOX10 was considerably downregulated at the transcript level, no statistically significant differences were found when images were examined (**Figure 41-d**). Nonetheless, a high level of variation was found in the percentage of positive cells expressing SOX10 between the conditions.

Moreover, 17q-MYCN(-DOX) and 17q-MYCN(+DOX) were assessed by intracellular flow cytometry. The markers tested were SOX10 and HOXC9 across three biological replicates (**Figure 42-a,b,c**). Although HOXC9 expression seemed consistent between the replicates/conditions, SOX10 showed different patterns between 17q-MYCN with and without doxycycline. When MYCN was not induced, the percentages of cells expressing SOX10 ranged between 70-91% but, when MYCN was overexpressed, SOX10 expression varied between 9.5% and 59%. As before, the most dramatic effect of MYCN overexpression remains the downregulation of the migratory marker SOX10.

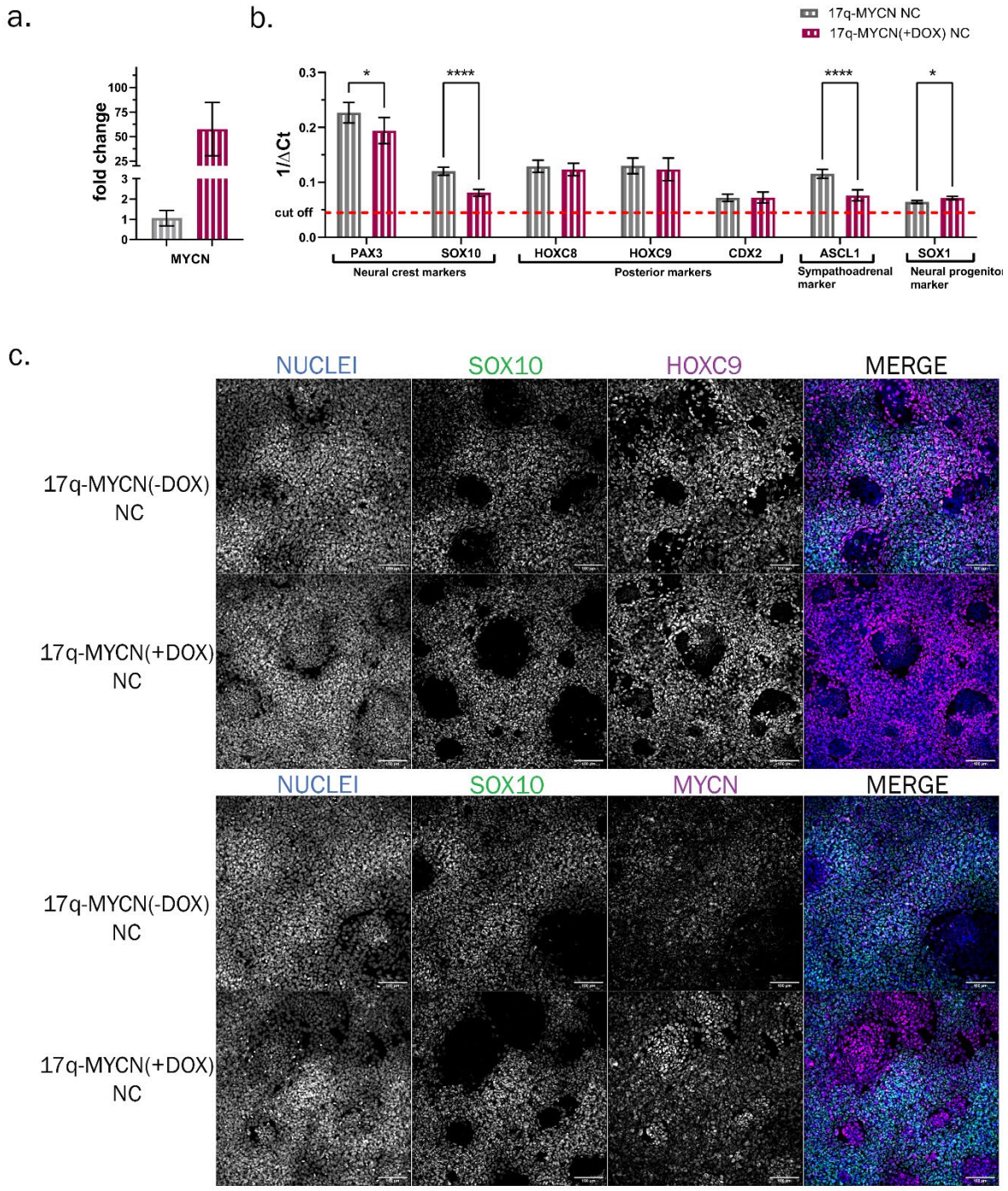
a.
b.
17q-MYCN NC
17q-MYCN(+DOX) NC
fold change
MYCN
1/ΔCt
cut off
PAX3
SOX10
HOXC8
HOXC9
CDX2
ASCL1
SOX1
Neural crest markers
Posterior markers
Sympathoadrenal marker
Neural progenitor marker
c.
NUCLEI
SOX10
HOXC9
MERGE
17q-MYCN(-DOX) NC
17q-MYCN(+DOX) NC
NUCLEI
SOX10
MYCN
MERGE
17q-MYCN(-DOX) NC
17q-MYCN(+DOX) NC
d.
17q-MYCN
17q-MYCN(+DOX)
% Positive cells
SOX10
HOXC9
MYCN
SOX10/HOXC9
SOX10/MYCN

Figure 41. Assessment of NC specification in the MYCN-inducible 17q cell line in the presence and absence of doxycycline from day 5 of differentiation

a. Analysis in the fold change of *MYCN* expression between 17q-MYCN(-DOX) versus 17q-MYCN(+DOX) in NC stage. Around ~ 60 times fold increase of *MYCN* mRNA can be observed in 17q-MYCN in presence of Doxycycline treatment started at day 5. **b.** Comparison of RNA expression at NC stage between 17q-MYCN(-DOX) and 17q-MYCN(+DOX)(day5). Both genes used as NC markers showed differences between the conditions: both *PAX3* and *SOX10* showed a statistically significant decrease in gene expression in 17q-MYCN(+DOX)(d5) compared to the control 17q-MYCN(-DOX), as well as the early sympathoadrenal marker *ASCL1*. On the other hand, *SOX1*, a neural progenitor marker, showed a small but statistically significant increase in 17q-MYCN(+DOX). **c.** Immunofluorescence images of the 17q-MYCN(-DOX) and 17q-MYCN(+DOX) cell line differentiated into NC. Shown are SOX10, HOXC9 and MYCN staining (Merge: Hoechst(blue), SOX10(green), HOXC9/MYCN(magenta)). **d.** Percentage of cells expressing SOX10, HOXC9, MYCN and cells co-expressing SOX10/HOXC9 and SOX10/MYCN markers in the immunofluorescence analysis. No statistically differences were found, although protein presence of SOX10 seemed lower in 17q-MYCN(+DOX)(day5) cell line. **a,b,d.** Gene expression values are plotted as 1/ΔCt. A cut off line (dotted red line) has been set at 0.045 as this is the equivalent of 40 cycles on the qPCR machine. Percentage of positive cells was quantified using immunofluorescent imaging and cell profiler analysis (n≥ 3 biological replicates, error bars= SD, Independent Welch t-tests, $p \leq 0.05$= *, $p \leq 0.01$= **, $p \leq 0.001$= ***, $p \leq 0.0001$= ****).

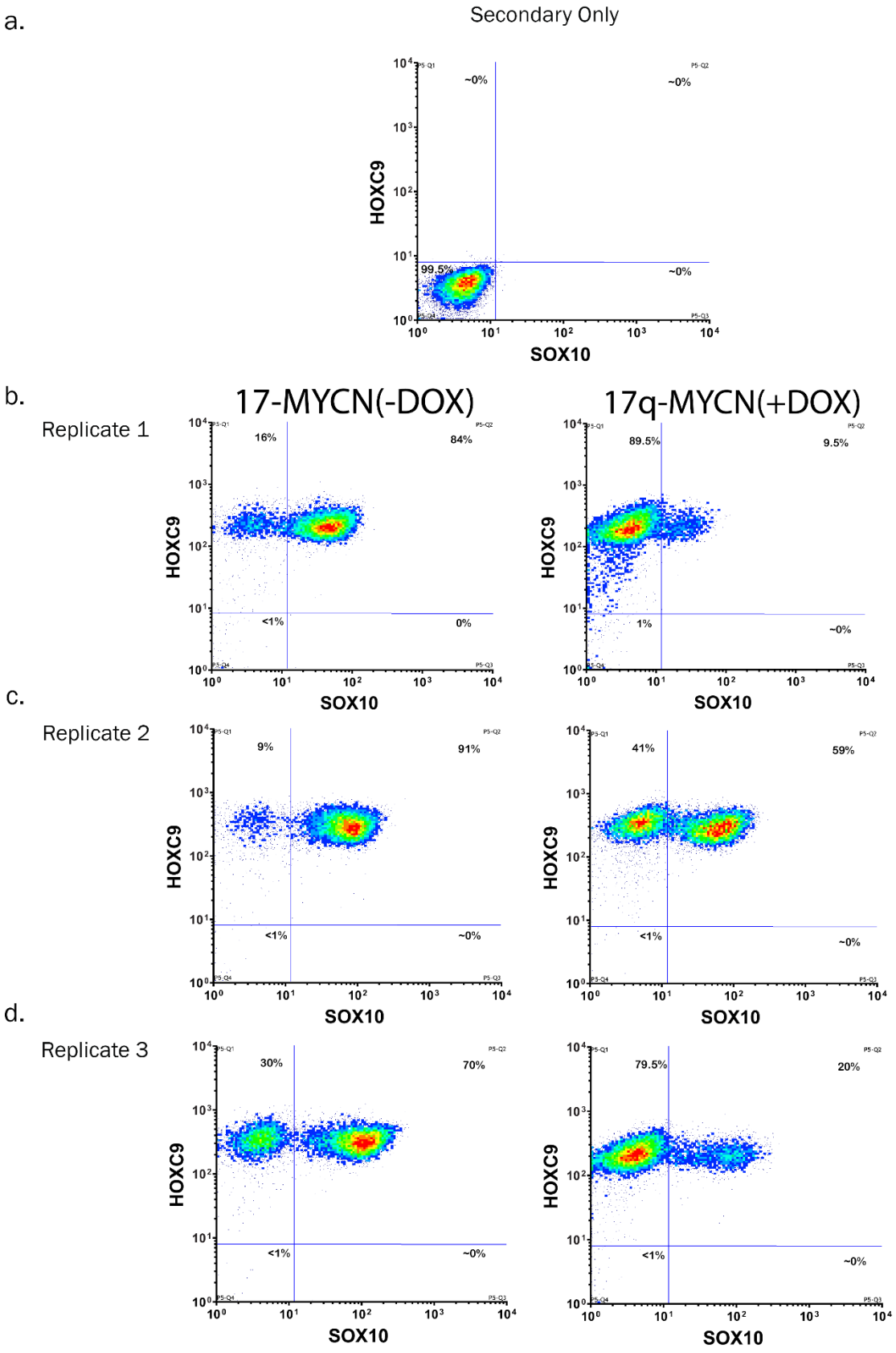

Figure 42. Assessment of trunk neural crest markers SOX10/HOXC9 by intracellular flow cytometer in 17q-MYCN cell line with and without Doxycycline.

a-d. Flow cytometry density plots of SOX10 vs HOXC9 expression in (a) secondary only control, (b-d) 17q-MYCN(-DOX) and 17q-MYCN(+DOX) across three replicates.

4.2.4.2 MYCN overexpression hinders sympathetic lineage specification

17q and 17q-MYCN(-DOX) Neural Crest control cell lines were plated and grown in sympathoadrenal progenitor media for 5 days. Then cells were harvested and analysed by qPCR to verify the expression of markers related to the SAP stage, such as *PHOX2B and ASCL1* (**Figure 43-a**). When data was analysed, two markers (*PHOX2B* and *GATA2*) showed significant downregulation in 17q-MYCN(-DOX) versus the 17q control line.

Representative images of the immunofluorescence analysis of 17q and 17q-MYCN(-DOX) at the SAP stage are shown in **Figure 43-b**. No evident differences can be distinguished between the conditions. Although, the PERIPHERIN marker shows that 17q-MYCN(-DOX) was much more efficient in developing neurites when compared to 17q control. Quantification of the number of cells expressing the antibody was assessed, confirming first sight observations (**Figure 43-c**). This was an interesting observation that might be indicating the presence of 1q aiding neural projection.

We next examined the effect of elevated MYCN activity on SAP specification. 17q-MYCN(-DOX) and 17q-MYCN(+DOX) Neural crest cells were plated and grown in sympathoadrenal progenitor media for 5 days. Cells were then harvested and analysed to verify if MYCN induction had been successful. **Figure 44-a** shows that the over expression of *MYCN* has an approximately 15-fold increase over the control. Significant downregulation was observed in the expression *SOX10*, *HOXC8*, *PHOX2B* and *GATA3* in the cells induced with doxycycline. There was also a downregulation in *ASCL1*, but this one was not significant **(Figure 44-b)**.

Immunofluorescence analysis shows the expression of SOX10, HOXC9, ASCL1, PHOX2B and PERIPHERIN (**Figure 44-c**). With respects to SOX10 and HOXC9, the overexpression of MYCN appears to have a greater effect on the expression of SOX10 with relatively small changes on the expression of HOXC9. The sympathetic progenitor markers ASCL1 and PHOX2B show lower expression levels when MYCN was over expressed. In the final panel of the images, the expression of PERIPHERIN was assessed and, although the cells over expressing MYCN stained positive for this marker, it can be appreciated that these cells have not formed neuronal-like structures like the control. Indeed, when viewing all of the immunofluorescent images, the addition of doxycycline cause distinct changes in the morphology of the cells, resulting in tight-compacted colonies forming as opposed to the intricate neural networks forming in the controls. It is worth mentioning that, during this stage of differentiation, cell death was visually higher in the cells over expressing MYCN, reaching its highest peak at the fourth day growing in SAP media.

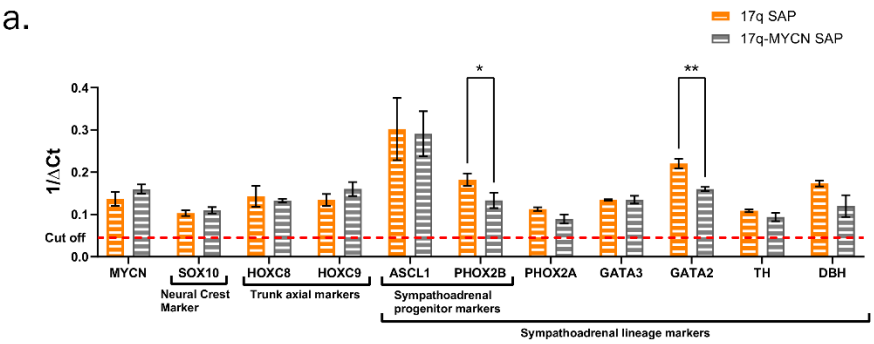
a.
17q SAP
17q-MYCN SAP
1/ΔCt
0.4
0.3
0.2
0.1
Cut off
0.0
*
**
MYCN
SOX10
HOXC8
HOXC9
ASCL1
PHOX2B
PHOX2A
GATA3
GATA2
TH
DBH
Neural Crest Marker
Trunk axial markers
Sympathoadrenal progenitor markers
Sympathoadrenal lineage markers

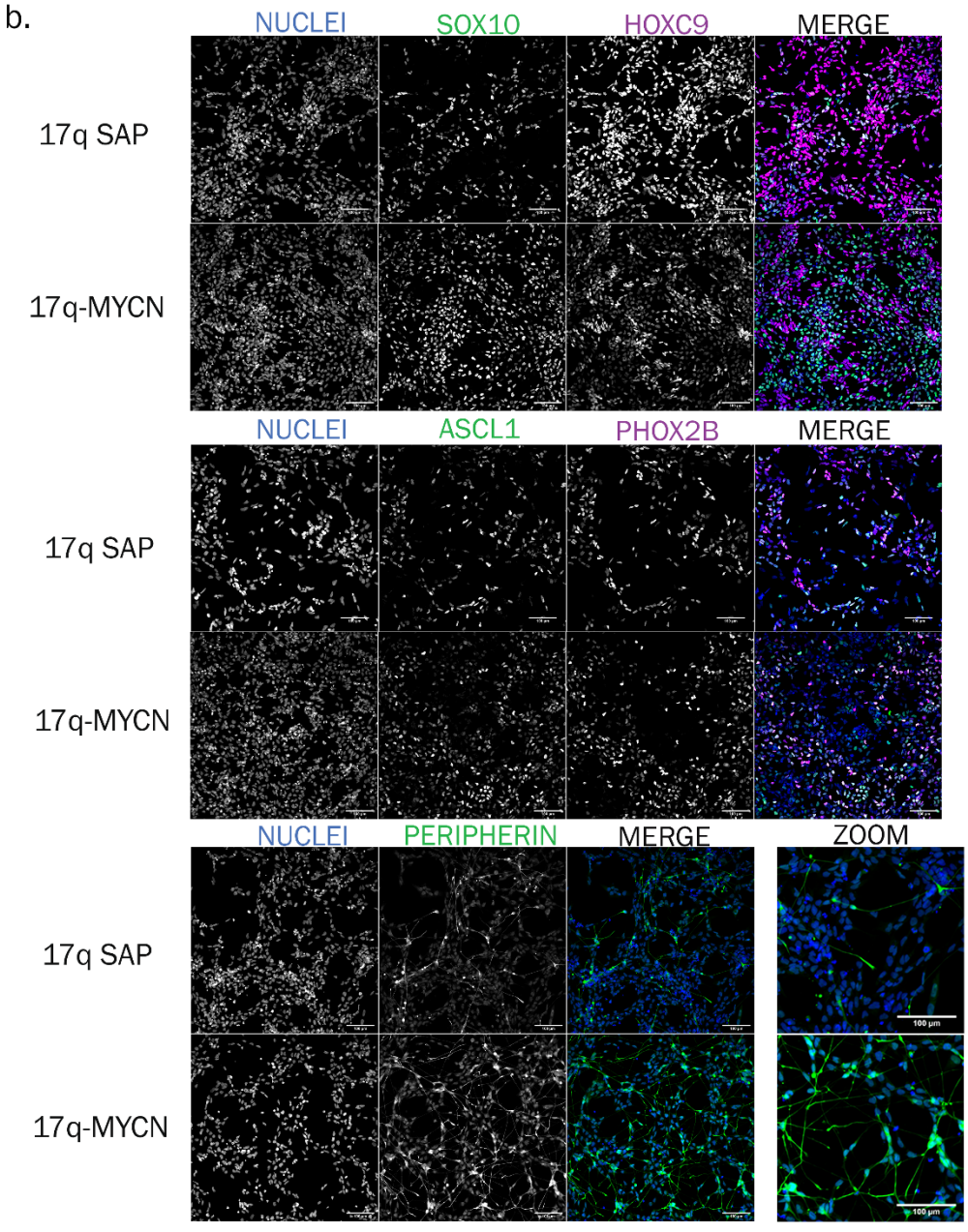
b.
NUCLEI
SOX10
HOXC9
MERGE
17q SAP
17q-MYCN
NUCLEI
ASCL1
PHOX2B
MERGE
17q SAP
17q-MYCN
NUCLEI
PERIPHERIN
MERGE
ZOOM
17q SAP
17q-MYCN
100 µm
100 µm

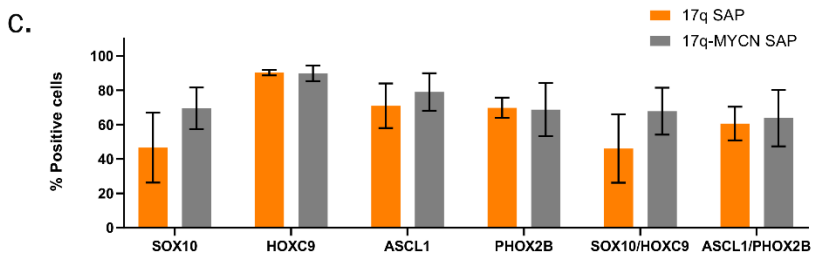
c.
17q SAP
17q-MYCN SAP
% Positive cells
100
80
60
40
20
0
SOX10
HOXC9
ASCL1
PHOX2B
SOX10/HOXC9
ASCL1/PHOX2B

Figure 43. Assessing SAP specification in the control cell lines.

a. Comparison of RNA expression at SAP stage between 17q and 17q-MYCN(-DOX). Significant differences are observed in PHOX2B and *GATA2* expression. Gene expression values are plotted as 1/ΔCt. A cut off line (dotted red line) has been set at 0.045 as this is the equivalent to 40 cycles on the qPCR machine (n= 3 biological replicates, error bars= SD, Independent Welch t-tests, $p \leq 0.05$= *, $p \leq 0.01$= **, $p \leq 0.001$= ***, $p \leq 0.0001$= ****). **b.** Immunofluorescence images of the 17q and 17q-MYCN(-DOX) cell line differentiated into SAP. Shown are SOX10, HOXC9, ASCL1, PHOX2B and PERIPHERIN staining (Merge: Hoechst(blue), SOX10/ASCL1/PERIPHERIN(green), HOXC9/PHOX2B(magenta)). **c.** Percentage of cells expressing SOX10, HOXC9, ASCL1 and PHOX2B as well as cells co-expressing SOX10/HOXC9 and ASCL1/PHOX2B markers in the immunofluorescence analysis. No statistical analysis was performed as n= 2 biological replicates.

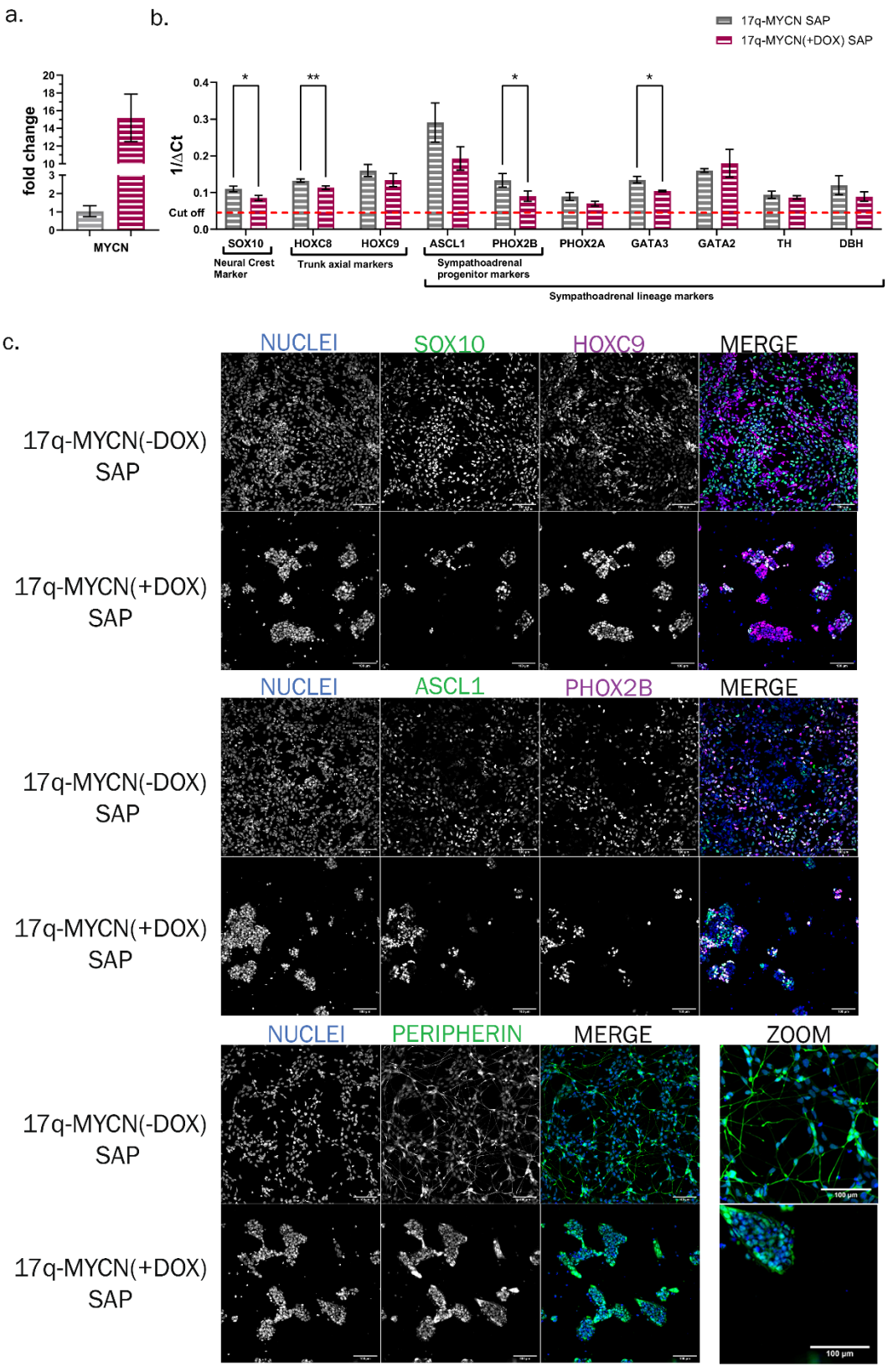
a.
b.
17q-MYCN SAP
17q-MYCN(+DOX) SAP
fold change
MYCN
1/ΔCt
Cut off
SOX10
HOXC8
HOXC9
ASCL1
PHOX2B
PHOX2A
GATA3
GATA2
TH
DBH
Neural Crest Marker
Trunk axial markers
Sympathoadrenal progenitor markers
Sympathoadrenal lineage markers
c.
NUCLEI
SOX10
HOXC9
MERGE
17q-MYCN(-DOX) SAP
17q-MYCN(+DOX) SAP
NUCLEI
ASCL1
PHOX2B
MERGE
17q-MYCN(-DOX) SAP
17q-MYCN(+DOX) SAP
NUCLEI
PERIPHERIN
MERGE
ZOOM
17q-MYCN(-DOX) SAP
17q-MYCN(+DOX) SAP
100 µm
100 µm
d.
17q-MYCN
17q-MYCN(+DOX)
% Positive cells
SOX10
HOXC9
ASCL1
PHOX2B
SOX10/HOXC9
ASCL1/PHOX2B

Figure 44. SAP specification in the MYCN-inducible 17q cell line in the presence and absence of doxycycline from day 5 of differentiation

a. Analysis in the fold change of *MYCN* expression between 17q-MYCN(-DOX) versus 17q-MYCN(+DOX) in SAP stage. Up to ~ 20 times fold increase of *MYCN* mRNA can be observed in 17q-MYCN in presence of Doxycycline treatment started at day 5. **b.** Comparison of RNA expression at SAP stage between 17q-MYCN(-DOX) and 17q-MYCN(+DOX)(day5). Significant differences were observed in *SOX10*, *HOXC8*, *PHOX2B and GATA3* expression. Gene expression values are plotted as 1/ΔCt. A cut off line (dotted red line) has been set at 0.045 as this is the equivalent to 40 cycles on the qPCR machine (n= 3 biological replicates, error bars= SD, Independent Welch t-tests, $p \leq 0.05$= *, $p \leq 0.01$= **, $p \leq 0.001$= ***, $p \leq 0.0001$= ****). **c**. Immunofluorescence images of the 17q-MYCN(-DOX) and 17q-MYCN(+DOX)(day5) cell line differentiated into SAP. Shown are SOX10, HOXC9, ASCL1, PHOX2B and PERIPHERIN staining (Merge: Hoechst(blue), SOX10/ASCL1/PERIPHERIN(green), HOXC9/PHOX2B(magenta)). **d.** Percentage of cells expressing SOX10, HOXC9, ASCL1 and PHOX2B as well as cells co-expressing SOX10/HOXC9 and ASCL1/PHOX2B markers in the immunofluorescence analysis. No statistical analysis was performed as n= 2 biological replicates.

With the cells that did remain, quantification was performed of the immunofluorescence revealing around 50% reduction in SOX10 expressing cells and, a large reduction in cells expressing ASCL1 and PHOX2B, but HOXC9 was not as poorly affected (**Figure 44-d**).

17q and 17q-MYCN(-DOX) SAP cells were matured further in NB27 media supplemented with BDNF, NGF and GDNF to stimulate the maturation of the cells towards sympathetic neurons (**Figure 45-a**).

Cells were harvested at day 19 of differentiation, then analysed by qPCR to verify the presence of markers related to the sympathetic neuron profile. Only two genes showed significant differences between the cell lines: *MYCN*, which was slightly upregulated in 17q-MYCN(-DOX) and SOX10 marker (also upregulated in 17q-MYCN). Compared to what has been observed in the SAP stage, it seems that the 17q-MYCN cell line become level with 17q at this stage of the differentiation, as no sympathoadrenal lineage marker showed any differences with respect to 17q control (**Figure 45-b**).

Immunofluorescence analysis shows the expression of ASCL1, PHOX2B and TH. It must be said that although images were taken, no statistical analysis was performed due to technical problems during the fixing of the samples, nonetheless, images are still shown as they work as proof of the existence of protein expression (**Figure 45-c**).

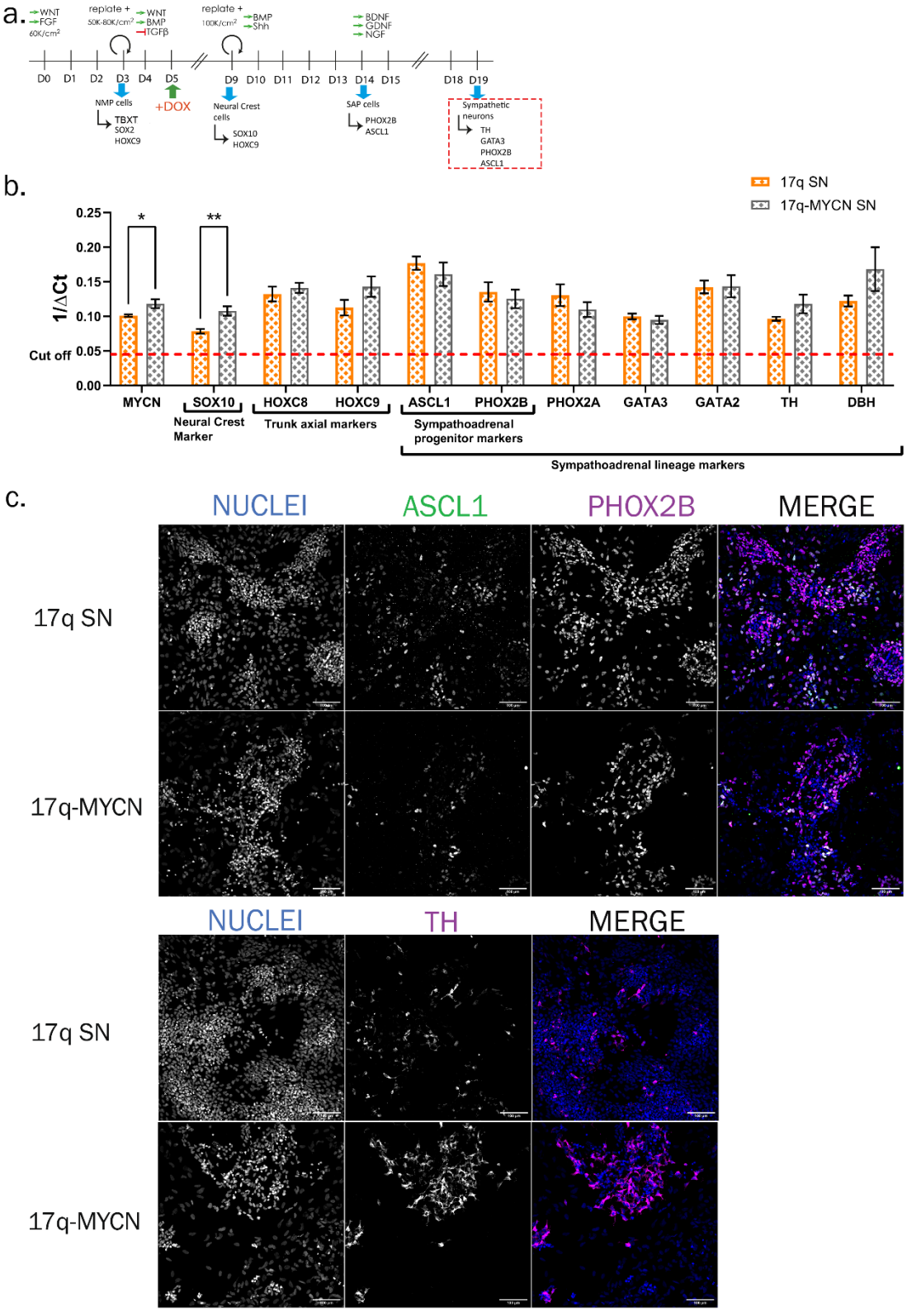
a.
WNT
FGF
60K/cm²
replate +
50K-80K/cm²
WNT
BMP
TGFβ
replate +
100K/cm²
BMP
Shh
BDNF
GDNF
NGF
D0 D1 D2 D3 D4 D5 D9 D10 D11 D12 D13 D14 D15 D18 D19
NMP cells
TBXT
SOX2
HOXC9
+DOX
Neural Crest cells
SOX10
HOXC9
SAP cells
PHOX2B
ASCL1
Sympathetic neurons
TH
GATA3
PHOX2B
ASCL1
b.
17q SN
17q-MYCN SN
1/ΔCt
Cut off
0.25
0.20
0.15
0.10
0.05
0.00
*
**
MYCN
SOX10
HOXC8
HOXC9
ASCL1
PHOX2B
PHOX2A
GATA3
GATA2
TH
DBH
Neural Crest Marker
Trunk axial markers
Sympathoadrenal progenitor markers
Sympathoadrenal lineage markers
c.
NUCLEI
ASCL1
PHOX2B
MERGE
17q SN
17q-MYCN
NUCLEI
TH
MERGE
17q SN
17q-MYCN

Figure 45. Assessing Sympathetic neuron specification in the control cell lines.
a. Schematic diagram of the directed differentiation of human pluripotent stem cells into Neuromesodermal progenitors (**NMP**), Neural Crest (**NC**), Sympathoadrenal progenitors (**SAP**) and Sympathetic neurons (**SN**). The red rectangle highlights the day cells were harvested, and which markers were used to validate the stage. It is also indicated with a green arrow when was started the treatment with doxycycline **b.** Comparison of RNA expression at SN stage between 17q and 17q-MYCN(-DOX). Significant differences are observed in *MYCN* and *SOX10* expression. Gene expression values are plotted as 1/ΔCt. A cut off line (dotted red line) has been set at 0.045 as this is the equivalent to 40 cycles on the qPCR machine (n= 3 biological replicates, error bars= SD, Independent Welch t-tests, $p \leq 0.05$= *, $p \leq 0.01$= **, $p \leq 0.001$= ***, $p \leq 0.0001$= ****). **c.** Immunofluorescence images of the 17q and 17q-MYCN(-DOX) cell line differentiated into SN. Shown are ASCL1, PHOX2B and TH staining (Merge: Hoechst(blue), ASCL1(green), PHOX2B/TH (magenta)). **d.** Immunofluorescence images of the 17q and 17-MYCN(-DOX) differentiated into SN. Shown are ASCL1, PHOX2B and TH (Merge: Hoechst(blue), ASCL1(green), PHOX2B/TH(magenta)). The percentage of cells were not analysed as the images only represent one biological replicate.

17q-MYCN(-DOX) and 17q-MYCN(+DOX) was grown in N2B27 media supplemented with BDNF, NGF and GDNF to further stimulate maturation towards the development of sympathetic neurons (**Figure 46-a**).

Cells were harvested at day 19 of differentiation and the presence of markers was assessed by qPCR. The fold change analysis of *MYCN* expression in cells treated with doxycycline revealed a fold change of 35 times compared to the control line (**Figure 46-b**). The effects of MYCN over expression can be observed in the markers *SOX10* and *HOXC8*, but also in markers specific to the sympathoadrenal lineage such as *PHOX2B, GATA3 and DBH*. All the aforementioned markers were significantly downregulated in 17q-MYCN(+DOX). Other genes were also close to significance such as *ASCL1* and *TH* (**Figure 46-c**). The panel of genes analysed suggests that MYCN has affected negatively the specification into sympathetic neurons of these cells.

Immunofluorescence analysis shows the expression of ASCL1, PHOX2B and TH markers. No statistical analysis was performed due to technical problems during the sample processing. Nonetheless, images are still proof of the existence of the proteins (**Figure 46-d).**

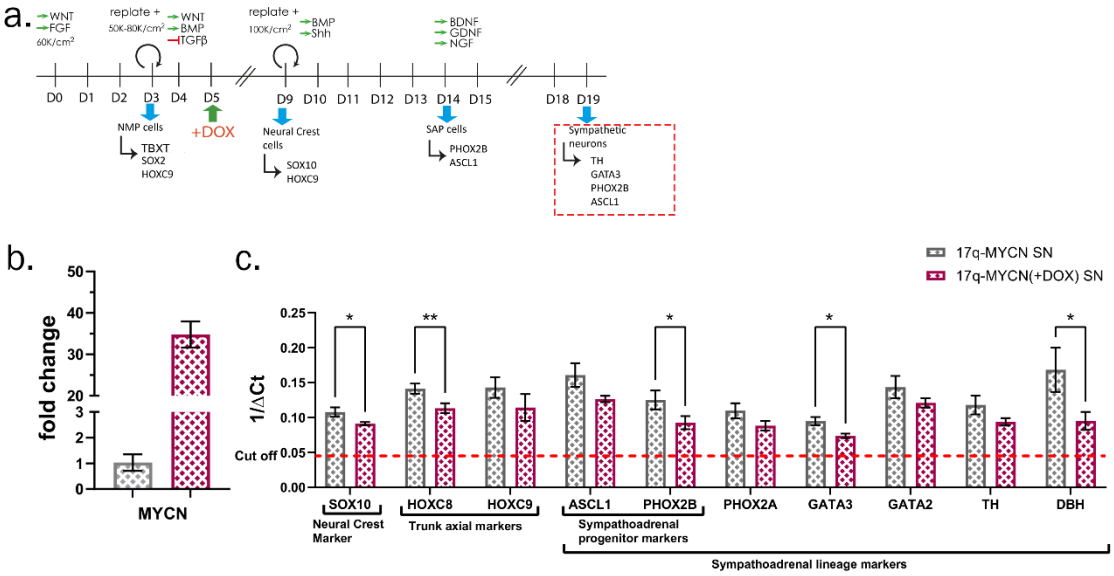
a.
WNT
FGF
60K/cm²
replate +
50K-80K/cm²
WNT
BMP
TGFβ
replate +
100K/cm²
BMP
Shh
BDNF
GDNF
NGF
D0 D1 D2 D3 D4 D5 D9 D10 D11 D12 D13 D14 D15 D18 D19
NMP cells
TBXT
SOX2
HOXC9
+DOX
Neural Crest cells
SOX10
HOXC9
SAP cells
PHOX2B
ASCL1
Sympathetic neurons
TH
GATA3
PHOX2B
ASCL1

b.
fold change
MYCN
c.
17q-MYCN SN
17q-MYCN(+DOX) SN
1/ΔCt
Cut off
SOX10
HOXC8
HOXC9
ASCL1
PHOX2B
PHOX2A
GATA3
GATA2
TH
DBH
Neural Crest Marker
Trunk axial markers
Sympathoadrenal progenitor markers
Sympathoadrenal lineage markers

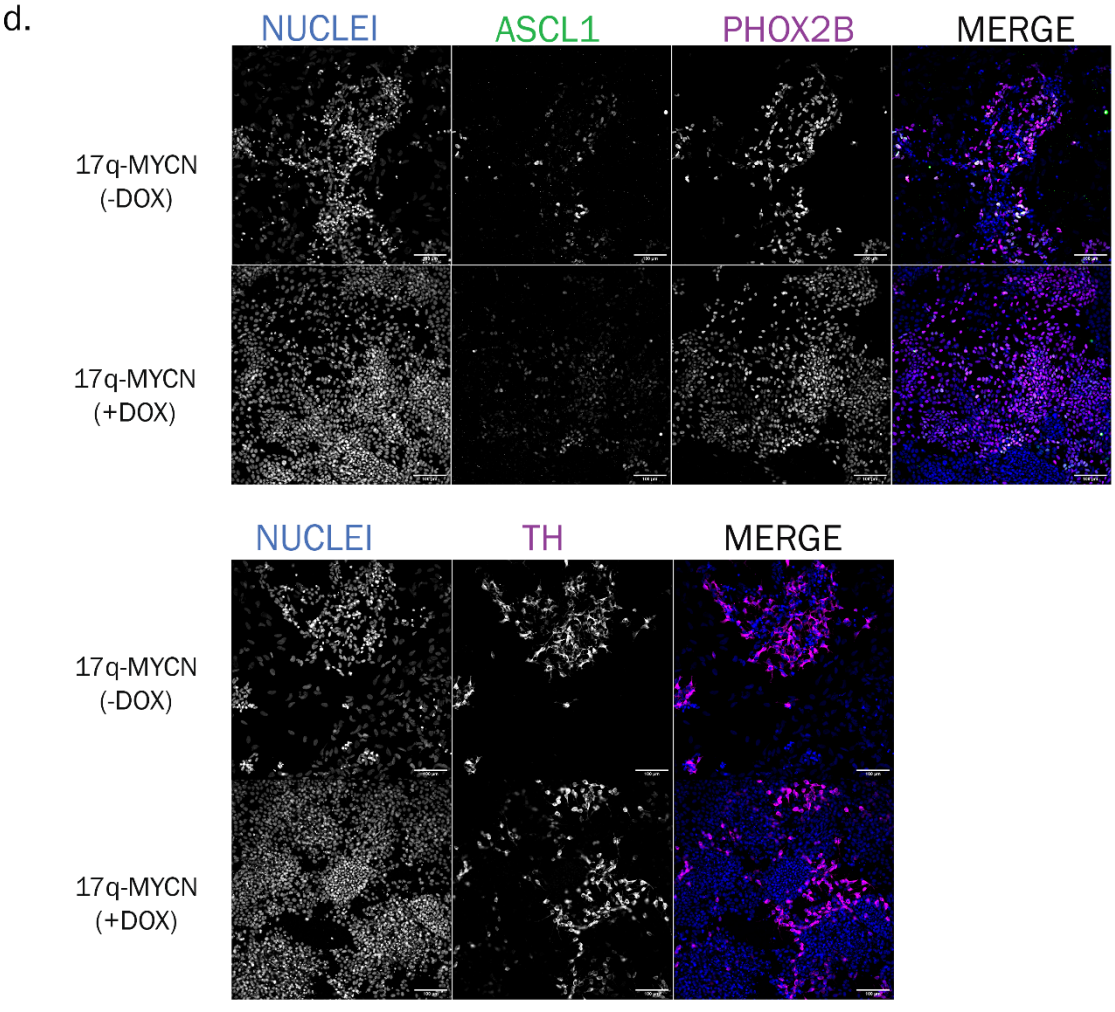
d.
NUCLEI
ASCL1
PHOX2B
MERGE
17q-MYCN (-DOX)
17q-MYCN (+DOX)
NUCLEI
TH
MERGE
17q-MYCN (-DOX)
17q-MYCN (+DOX)

Figure 46 Detection of Sympathetic neuronal markers in 17q-MYCN and 17q-MYCN(+DOX) cell lines. **a.** Schematic diagram of the directed differentiation of human pluripotent stem cells into Neuromesodermal progenitors (**NMP**), Neural Crest (**NC**), Sympathoadrenal progenitors (**SAP**) and Sympathetic neurons (**SN**). The red rectangle highlights the day cells were harvested, and which markers were used to validate the stage. It is also indicated with a green arrow when was started the treatment with doxycycline **b.** Analysis in the fold change of *MYCN* expression between 17q-MYCN(-DOX) versus 17q-MYCN(+DOX) in the SN stage. Around ~ 35 times fold increase of *MYCN* mRNA can be observed in 17q-MYCN in presence of Doxycycline treatment started at day 5. **c.** Comparison of RNA expression at SN stage between 17q-MYCN(-DOX) and 17q-MYCN(+DOX)(day5). *SOX10* neural crest marker, as well as the trunk axial marker HOXC8, are significantly downregulated also, the sympathoadrenal markers *PHOX2B, GATA3 and DBH* showed lower expression in 17q-MYCN(+DOX) compared to 17-MYCN(-DOX). Gene expression values are plotted as 1/ΔCt. A cut off line (dotted red line) has been set at 0.045 as this is the equivalent to 40 cycles on the qPCR machine (n= 3 biological replicates, error bars= SD, Independent Welch t-tests, $p \leq 0.05$= *, $p \leq 0.01$= **, $p \leq 0.001$= ***, $p \leq 0.0001$= ****). **d.** Immunofluorescence images of the 17q-MYCN(-DOX) and 17-MYCN(+DOX) differentiated into SN. Shown are ASCL1, PHOX2B and TH (Merge: Hoechst(blue), ASCL1(green), PHOX2B/TH(magenta)). The percentage of cells were not analysed as the images only represent one biological replicate.

As we have observed before, the time when MYCN is induced can affect the differentiation efficiency. Therefore, later induction times were included in the analysis, inducing MYCN overexpression from day 9 and day 14 of differentiation (**Figure 47-a**). Day 9 and day 14 were chosen as they represent the time-points of fully mature migratory neural crest/sympathoadrenal progenitors, marked by widespread SOX10 and PHOX2B expression respectively. Therefore, I hypothesised that fully mature neural crest/sympathoadrenal cells would be less susceptible to MYCN influence in their differentiation trajectory, as Mobley et al 2015 did not observe a tumourigenic behaviour but an increase in differentiation and proliferation in sympathoadrenal cells overexpressing MYCN.

Cells were harvested at day 14 (SAP stage) and analysed by qPCR (**Figure 47-b**). When SAP cells induced at day 9 are compared to non-induced ones, the only gene that appears to be significantly different is *GATA3*, although, *ASCL1* also showed some reduction.

a.

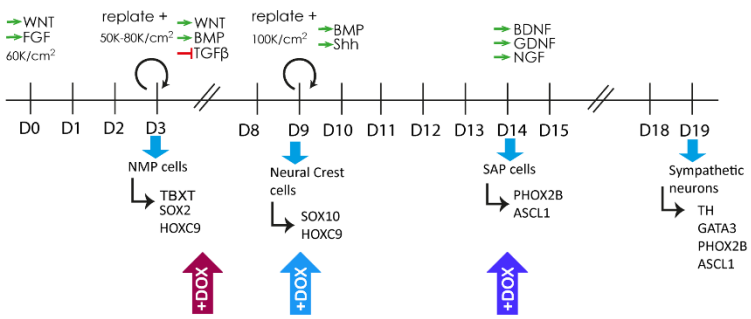
WNT
FGF
60K/cm²
replate +
50K-80K/cm²
WNT
BMP
TGFβ
replate +
100K/cm²
BMP
Shh
BDNF
GDNF
NGF
D0 D1 D2 D3 D8 D9 D10 D11 D12 D13 D14 D15 D18 D19
NMP cells
TBXT
SOX2
HOXC9
Neural Crest cells
SOX10
HOXC9
SAP cells
PHOX2B
ASCL1
Sympathetic neurons
TH
GATA3
PHOX2B
ASCL1
+DOX
+DOX
+DOX

b.

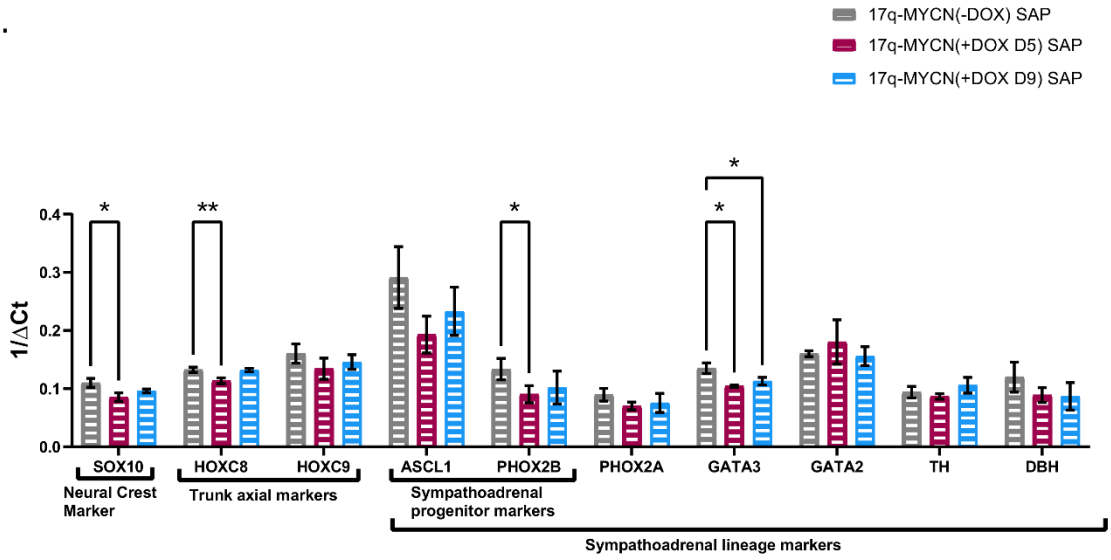
17q-MYCN(-DOX) SAP
17q-MYCN(+DOX D5) SAP
17q-MYCN(+DOX D9) SAP
1/ΔCt
0.0
0.1
0.2
0.3
0.4
SOX10
HOXC8
HOXC9
ASCL1
PHOX2B
PHOX2A
GATA3
GATA2
TH
DBH
Neural Crest Marker
Trunk axial markers
Sympathoadrenal progenitor markers
Sympathoadrenal lineage markers

c.

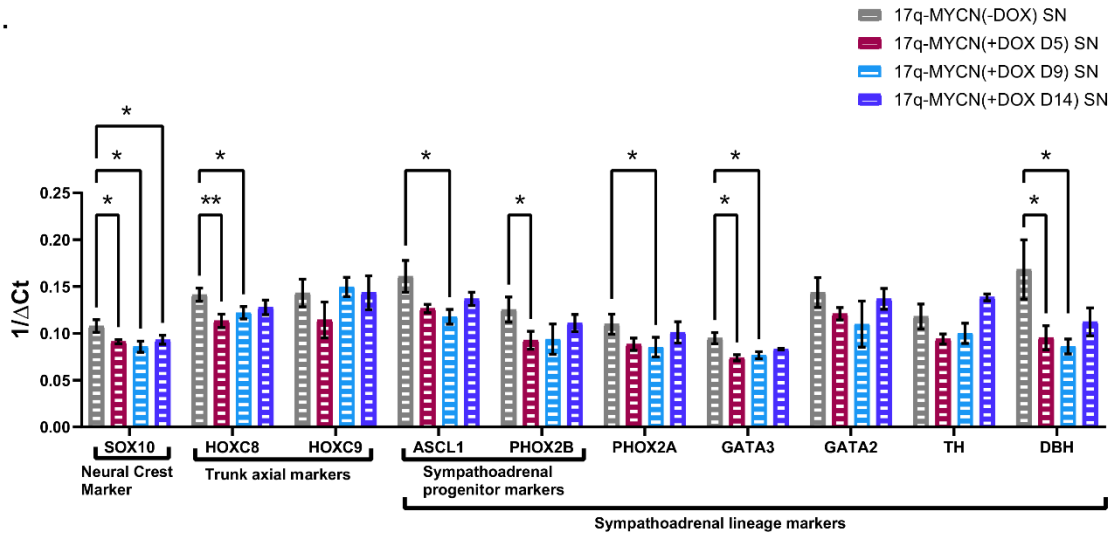
17q-MYCN(-DOX) SN
17q-MYCN(+DOX D5) SN
17q-MYCN(+DOX D9) SN
17q-MYCN(+DOX D14) SN
1/ΔCt
0.00
0.05
0.10
0.15
0.20
0.25
SOX10
HOXC8
HOXC9
ASCL1
PHOX2B
PHOX2A
GATA3
GATA2
TH
DBH
Neural Crest Marker
Trunk axial markers
Sympathoadrenal progenitor markers
Sympathoadrenal lineage markers

Figure 47: Detection of Sympathoadrenal progenitors and Sympathetic neuronal markers by qPCR in 17q-MYCN and 17q-MYCN(+DOX) cell lines induced at different time points.

a. Schematic diagram of the directed differentiation of human pluripotent stem cells into Neuromesodermal progenitors (**NMP**), Neural Crest (**NC**), Sympathoadrenal progenitors (**SAP**) and Sympathetic neurons (**SN**). It is indicated with coloured arrows when was started the treatment with doxycycline (doxycycline from day 5, day9 and day14). **b.** Comparison of RNA expression at SAP stage between **17q-MYCN(-DOX)** and **17q-MYCN(+DOX)(day5)**: *SOX10* neural crest marker, as well as the trunk axial marker HOXC8, are significantly downregulated also, the sympathoadrenal markers *PHOX2B, GATA3.* Comparison between **17q-MYCN(-DOX)** and **17q-MYCN(+DOX)(day9)**: only *GATA3* marker showed a significant difference with the control. **c.** Comparison of RNA expression at SN stage between **17q-MYCN(-DOX)** and **17q-MYCN(+DOX)(day5)**: *SOX10* neural crest marker was significantly regulated as well as *HOXC8* and the sympathoadrenal lineage markers *PHOX2B, GATA3 and DBH.* Comparison between **17q-MYCN(-DOX)** and **17q-MYCN(+DOX)(day9)**: *SOX10*, *HOXC8* as well as the sympathoadrenal markers *ASCL1*, *PHOX2A*, GATA3 and *DBH*. Comparison between **17q-MYCN(-DOX)** and **17q-MYCN(+DOX)(day14)**: only *SOX10* marker showed significant downregulation when compared to the control. **b- c.** Gene expression values are plotted as 1/ΔCt. A cut off line (dotted red line) has been set at 0.045 as this is the equivalent to 40 cycles on the qPCR machine (n= 3 biological replicates, error bars= SD, Independent Welch t-tests, $p \leq 0.05$= *, $p \leq 0.01$= **, $p \leq 0.001$= ***, $p \leq 0.0001$= ****).

qPCR analysis of sympathetic neurons showed that when *MYCN* was induced at day 9, several genes were affected: *SOX10* was one of them and showed a similar degree of downregulation than when MYCN was induced at day 5. *HOXC8* was also downregulated (but oddly *HOXC9* did not show the same trend). *ASCL1* was significantly downregulated and seem to follow the same behaviour as 17q-MYCN(+DOX from day5). Other genes that showed downregulation were *PHOX2A*, *GATA3 and DBH*. All these genes aforementioned were the same ones affected when doxycycline was added at day 5, which implies that sympathetic neuron differentiation is still affected even when MYCN expression is induced later at the end of Neural crest specification. When doxycycline was added at day 14, the only gene that showed significant downregulation was *SOX10*, *DBH* showed strong, however non-significant downregulation.

Overall, MYCN overexpression consistently downregulated *SOX10* in every stage regardless of the time point of induction. That impairment could potentially have influenced the expression of further genes related to the sympathetic lineage.

4.3 Discussion

Despite the diverse multitude of cellular and animal models that have been developed to understand the contribution of MYCN in the onset and progression of neuroblastoma, to our knowledge none have been able to examine MYCN's role in a defined and temporally controlled manner. The problem with previous approaches is that MYCN upregulation is governed by the expression of markers at particular cell stages, precluding analysis of increased MYCN expression outside this window. Existing models that use inducible expression systems have a focus on genetic abnormalities present in neuroblastoma that, although possess high penetrance, their presence in neuroblastoma tumours are particularly rare. Simultaneous MYCN amplification and ALK F1174 are present in less than 1.5% of neuroblastoma tumours (De Brouwer et al., 2010).

Here I used a DOX-inducible MYCN human pluripotent stem cell line harbouring a gain in 17q, one of the most common chromosomal aberrations found in neuroblastoma. In MYCN amplified tumours, 85% also carry 17q gain, these accounts for approximately 17% of all neuroblastoma tumours (Bown et al., 1999a).

A MYCN-inducible system allows us to assess how the sympathoadrenal differentiation profile can be affected when MYCN is overexpressed at different time points during the differentiation *in vitro.* Potentially enabling us to generate tumours similar to those found in neuroblastoma. Unfortunately, during the transfection process, 1q chromosome aberration was acquired. However, this aberration has also been reported in neuroblastoma cell lines and ultimately, it did not seem to affect significantly the expression of the specific markers along the differentiation.

Due to the vast majority of neuroblastoma analysis having been done in either tumours derived from mouse models or neuroblastoma cell lines, the scope of analysis is restricted to the late stages of the disease, becoming unfeasible to dissect the initial mechanisms behind neuroblastoma onset. I have taken advantage of the protocol developed in our lab, as it allows for the generation of neuro-mesodermal progenitors, trunk neural crest, sympathoadrenal progenitors and sympathetic neurons in a controlled step-wise manner (Frith et al., 2018, Frith and Tsakiridis, 2019). This strategy along with the DOX-inducible MYCN human pluripotent stem cell line allows us to over-express MYCN at potential key stages of development that range from pre-migratory, migratory and sympathoadrenal stage, and evaluate its impact in posterior sympathetic identity.

MYCN overexpression from day 0 caused an increase in the expression of SOX2 marker at the Neuro-mesodermal progenitors (NMP) when compared to the control cell line (**Figures 30-34**). Interestingly, Kerosuo et al, 2018 observed an increase in the expression of SOX2 throughout the neural tube when MYCN was ectopically induced. They also reported a negative correlation between MYCN

overexpression and PAX7(Kerosuo et al., 2018). Similar results are observed in our model at the neural crest stage, albeit with *PAX3*, a marker of human in pre-migratory neural crest cells(Betters et al., 2010) rather than PAX7, also showed lower expression during NC specification (**Figure 34**). They also reported that the cells were able to undergo EMT, however, they showed a delay in their migration profile(Kerosuo et al., 2018). Our analysis showed a highly significant reduction of SOX10, a marker of migrating neural crest cells when MYCN was overexpressed. SOX10 expression not only showed a clear negative correlation with the level of MYCN at the single-cell level (**Figure 34**) but also with the time point when MYCN was induced, as higher levels of SOX10 were observed when MYCN overexpression was delayed (**Figures 35 and 42**). On the other hand, the levels of TBXT and HOXC9 were equally affected in NMP and NC cells when MYCN was induced from day 0. Overall, cells induced for MYCN from day 0 did not show a satisfactory trunk neural crest gene expression profile, therefore the overexpression of MYCN at such an early developmental time point is unlikely to correlate to clinical outcomes, but further analysis of markers of other lineages, especially neural, might be needed to confirm this.

Taking this into account, I elected to induce MYCN at a later time point. Day 5 was chosen as a time point between the pre-migratory neural crest and the onset of SOX10, the migratory marker, at day 7(Frith et al., 2018). In the first instance, when WNT signalling was elevated in the protocol, we observed that MYCN was not responsible for the disruption in axial identity (**Figures 35 and 42**) demonstrated by the maintenance of HOXC9 beyond the NMP stage. Additionally, although MYCN overexpression was delayed up to day 5, SOX10 downregulation remains the strongest effect observed. When compared to day 0 induction where SOX10 was practically abolished, day 5 induction exhibited SOX10 percentages between 10-60%.

In the WNT elevated protocol, when cells were differentiated into Sympathoadrenal progenitors (SAP) and Sympathetic Neurons (SN), the effect of MYCN overexpression from day 5 caused a generalised downregulation (although not depletion) of sympathoadrenal lineage markers such as ASCL1 and PHOX2B in SAP, and GATA3 and DBH in SN. A remarkable observation is although the marker PERIPHERIN was detected in sympathoadrenal cells with and without MYCN overexpression, only those with normal MYCN profile developed neurites (**Figure 44**).

One thing worth mentioning is that each analysis has its limitations. For example, the qPCR technique is an analysis of the gene expression from the bulk population, therefore, discrete changes within the population are masked. Another caveat comes from the analysis of the percentage of positive cells in the immunofluorescence images. If we are looking for changes in the protein expression of a gene that is always present to some degree, changes in the percentage of protein expression will not be as

noticeable. One example of this was observed in **Figure 34** where no statistical differences were found in the percentage of MYCN positive cells even when MYCN expression was elevated after doxycycline treatment. This problem was easily circumvented by measuring the protein intensity at the single-cell level, which demonstrated clear upregulation of MYCN (**Figure 34e**). Likewise, a single cell approach could be applied to the qPCR technique to give us a better resolution of the gene expression within the population.

Overall, the data indicate that cells overexpressing MYCN are presenting a delay in the specification, possible through mediating the expression of SOX10, along the different stages of differentiation. MYCN induction at day 9 and day 14 suggests that MYCN influence decreases when cells are close to their maturation stage. Finally, cells at the sympathetic neuron stage (SN), which had MYCN expression induced at earlier times of the protocol, showed a general reduction in the expression of SN markers (**Figure 47**), suggesting that either the cells are trapped at the SAP stage, or the cells are only delayed in their differentiation. To clarify this, cells should be matured further to corroborate the findings.

5 Chapter 5: Tracking initiation of tumourigenesis using hPSC-based models of neuroblastoma

5.1 Introduction

Cancer is a broad term to describe a group of diseases that are inherently diverse and complex. Normal cells progress through a highly dysregulated proliferative state whilst acquiring further attributes, these could eventually facilitate their transition towards the development of a malignant phenotype. These attributes are often shared by different types of cancer, regardless of the cell of origin or site of tumour formation(Hanahan and Weinberg, 2000).

Hanahan and Weinberg first conceptualised six different traits, which they deemed as the "hallmarks of cancer" in the year 2000, to subsequently incorporate four more in their 2011. These hallmarks are: sustaining proliferative signalling, evading growth suppressors, avoiding immune destruction, enabling replicative immortality, tumour-promoting inflammation, activating invasion and metastasis, inducing angiogenesis, genome instability and mutation, resisting cell death and deregulating cellular energetics.

Fortunately, many techniques have been developed to assess these traits in cell culture (reviewed in Menyhart et al, 2016). A collection of these hallmarks is easier to assess *in vitro* without requiring advanced machinery and/or specialised expertise. Changes in cell morphology such as cell size reduction, condensation of the nuclei, bleb formation, among others can be symptoms that might indicate divergence from normal cellular function. Live-cell time-lapse imaging can be used as a powerful tool to follow in detail these changes (Artymovich and Appledorn, 2015). Also, Flow cytometry analysis can provide rapid information of relative cell size (Darzynkiewicz et al., 1997).

Uncontrolled cell proliferation due to deregulation of growth signals and their internal cell cycle dynamics enable cells to change tissue organisation and promote tumour formation(Hanahan and Weinberg, 2011). Assays are based on normal events that occur during cell division such as metabolic activity, DNA synthesis, membrane integrity status, protein content, etc(Menyhárt et al., 2016). Radiolabeled thymidine analogue precursors can be incorporated during DNA synthesis *in vivo* to be subsequently analysed by flow cytometry or immunohistochemistry. EdU is another method, which allows the incorporation of a thymidine analogue, where a terminal alkyne group has been replaced, into the nuclear DNA during the S phase. It does not require DNA denaturation and its signal is easily detected through a reaction with fluorescent azides, making this, one of the most reliable methods to measure the proliferation profile of a cell population (Salic and Mitchison, 2008). An alternative method is the use of an antibody against Ki-67. The Ki-67 antigen has been observed in every phase of the cell cycle, although it is not expressed in cells in the G0 phase (reviewed in Jurikova, 2016).

These characteristics make Ki-67 protein a convenient marker to determine if cells are proliferating in a given population. Its biological function is still not well understood, nonetheless, it is believed that Ki-67 has a role in cell division as cell proliferation arrests when Ki-67 is blocked (Starborg et al., 1996). Also, it has been shown its participation in the stabilisation and maintenance of the mitotic spindle in mitosis (Vanneste et al., 2009).

Another indication of modification in normal cell behaviour is the abnormal increase in cell survival. To assess this, different approaches have been developed. Among these is the soft agar assay which can determine the ability of non-adhered cells to proliferate. An alternative test is the clonogenic assay, which measures the capacity of a single cell to overcome stress signals and undergo successfully proliferation to form a colony (Woolston and Martin, 2011, Franken et al., 2006).

The glucose metabolism of cancer cells is different from that of normal cells, favouring glycolysis over oxidative phosphorylation, a phenomenon known as "the Warburg effect". As glycolysis produces a lower yield of ATP, more glucose supply is needed to drive their enhanced proliferation (Muñoz-Pinedo et al., 2012). Indeed, in neuroblastoma cells, the fluorescently labelled glucose analogue FDG (^{18}F-Fluorodeoxyglucose) can be used to label and target neuroblastoma tumours *in vivo* due to their enhanced uptake. The level of FDG uptake was shown to correlate with poor prognosis and tumours that harboured MYCN amplification and gains in 17q (Shin et al., 2020).

Finally, genetic instability is a shared characteristic among cancers. The origin of this is still a source of great debate. There are different types of genomic instabilities. One of the most prominent in cancer is chromosomal instability (CIN), which comprises changes in the number and/or arrangement of chromosomes over time(Negrini et al., 2010). It has been theorised that activation of oncogenes driving cellular proliferation stimulate DNA replication stress and ultimately triggers genomic instability(Halazonetis et al., 2008). Aberrant oncogene activation can interfere with the normal replication process of DNA, therefore increasing the chances of getting double-strand breaks (DSBs). These would normally lead to cell death, however, the chance of bypassing this mechanism increases when further mutations are accrued (Halazonetis et al., 2008). A prompt response of the cell to DSBs is the phosphorylation on the Ser-139 of the histone H2AX. This phosphorylation and its link to DNA damage and repair have been well characterised (Sedelnikova et al., 2002, Karagiannis and El-Osta, 2004b). Therefore, the use of an antibody that recognises this phosphorylated version of H2AX (yH2AX) can provide an accurate readout of the level of DSBs within cell culture.

Like many cancers, neuroblastoma presents these aforementioned hallmarks, which facilitate its aggressiveness in patients and models *in vivo* (Weiss et al., 1997, Cohen et al., 2020). Therefore, as both 17q and 17q-MYCN(+DOX) cells have shown some differences during certain developmental

stages when compared to wild type, such as a block/delay in differentiation, I wanted to know if these observations were correspondent to the acquisition of tumourigenic hallmarks. Moreover, if these might be indicating the existence of a stage-specific cell context triggering tumorigenesis. Shedding light to the cell-of-origin in neuroblastoma cases marked by 17q/MYCN amplification. **Figure 48** depicts the current hallmarks of cancer as well as some *in vitro* assays I used to investigate these particular hallmarks.

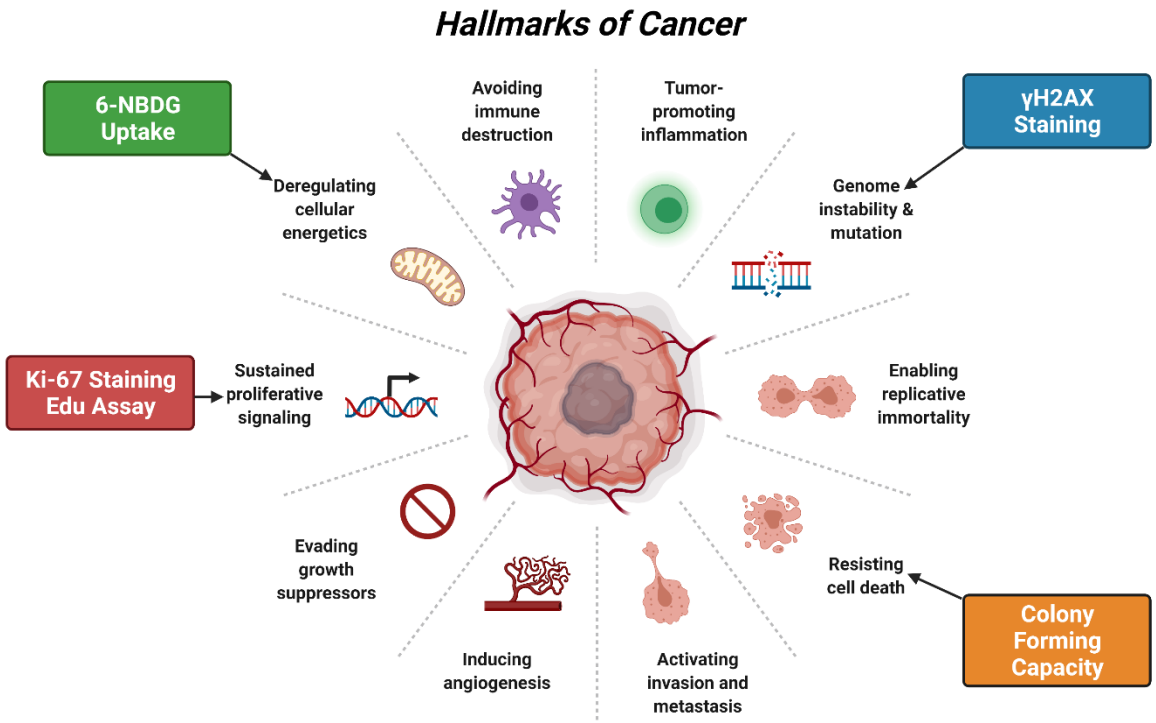

Figure 48. Current Hallmarks of cancer
Illustration adapted from Hanahan and Weinberg, 2011. Shown are the different capabilities that allow tumours to proliferate and disseminate successfully. Boxes around the outside indicate the assays used in this work to test particular hallmarks.

5.2 Results

Graphical abstract summarising the experiments and main findings of chapter 5.

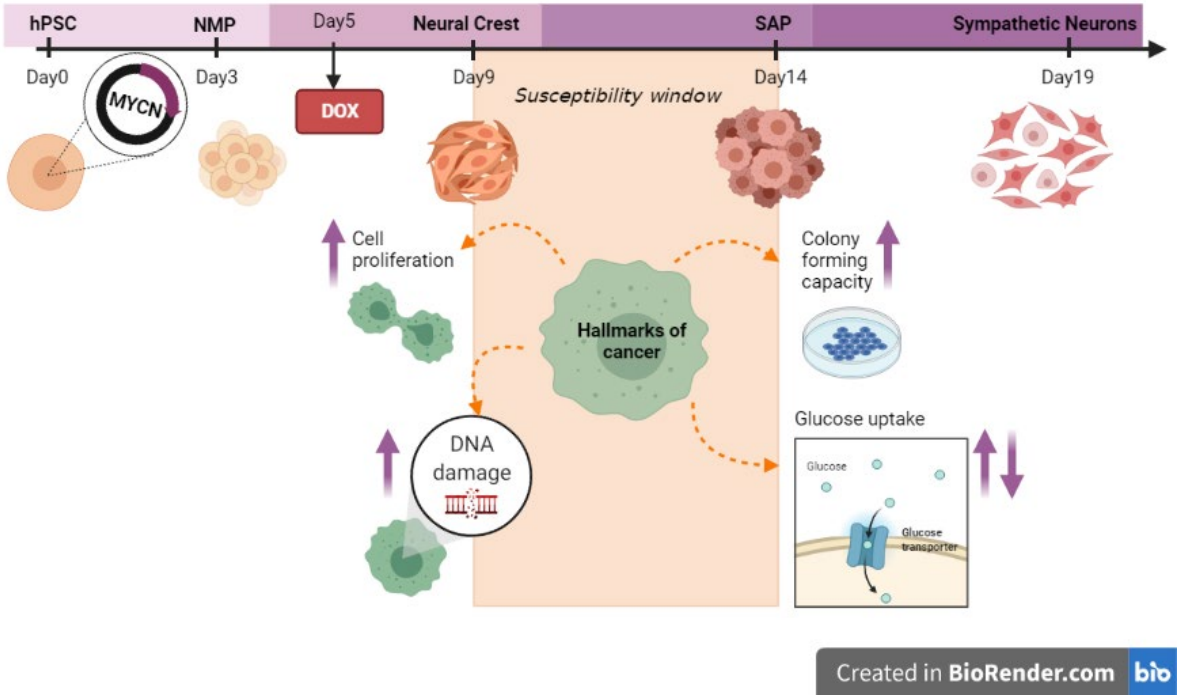

5.2.1 Morphological characteristics

5.2.1.1 Wild type and 17q cell lines are morphologically similar at the different stages of the differentiation process.

Bright-field images of the wild type and 17q cell line were captured at different stages of the differentiation process **(Figure 49-50)**. No evident morphological changes were observed between wild type and 17q cell line during the differentiation process. Images of the 17q-MYCN cell line along the differentiation process were also taken (**Figure 51-53)**. During neural crest differentiation, 17q-MYCN was assessed in two different conditions: with and without doxycycline. A representative image of 17q-MYCN without doxycycline treatment is shown in **Figure 51-c**. Cells have formed a monolayer with similar morphologic characteristics to control cell lines. 17q-MYCN cell line treated with doxycycline from day 5 of the differentiation protocol can be observed in **Figure 51-d**. Cells form a monolayer, similar to that one in 17q-MYCN(-DOX), but more cell death can be noticed.

When 17q-MYCN(-DOX) neural crest cells were plated in the presence of SAP media for 24 hours, cells display a similar morphology to that one observed in the 17q cell line. Cells show a "neuron-like" morphology but no long neurites are observed (**Figure 52-a, left panel**). On the other hand, 17q-MYCN(+DOX) cells have a spiky-like structure, similar to the one without doxycycline, however, they seemed to be shinier and more compacted in their morphology (**Figure 52-a, right panel**). As the differentiation treatment continued, cells treated with doxycycline changed dramatically their morphology, resulting in tight dome-like colonies (**Figure 52-b, right panel**). These structures were not seen in the control line, which showed a behaviour more similar to 17q. Neuron-like cells with the presence of neurites (**Figure 52-b, left panel**).

Images of day 19 of the differentiation are shown in **Figure 52-c**. On the left-hand panel, we observed that 17q-MYCN(-DOX) has grown throughout the days, showing longer neurites and also forming "neural conglomerates". In **Figure 52-c, right panel**, 17q-MYCN cell line treated with doxycycline has duplicated very quickly. Overall, cells do not look like neurons, although some projections can be found occasionally.

To investigate whether changes in morphology and hence, differentiation defects are linked to a specific differentiation stage/cell population being more sensitive to MYCN overexpression, doxycycline was supplemented at later stages: day 9 and day 14 of the protocol. When doxycycline was administrated on day 9, no significant morphological differences were found 24 hours later (day 10) (**Figure 53-a**). However, on day 14 cells adopted the "tight dome-like" colonies shape previously seen (**Figure 53-b**). By the end of the differentiation (day 19), cells supplied with doxycycline from day 9 have proliferated highly and did not show neuron-like characteristics, although some projections could be seen occasionally. On the other hand, cells grown with doxycycline from day 14 did not either develop neurons, even when the treatment was provided in the latter stage of the differentiation protocol (**Figure 53-c**).

Morphology analysis of the different cell lines/conditions showed that the presence of MYCN overexpression during the differentiation protocol seemed to greatly influence cellular morphology, specifically during sympathoadrenal specification, regardless of the starting day of doxycycline treatment.

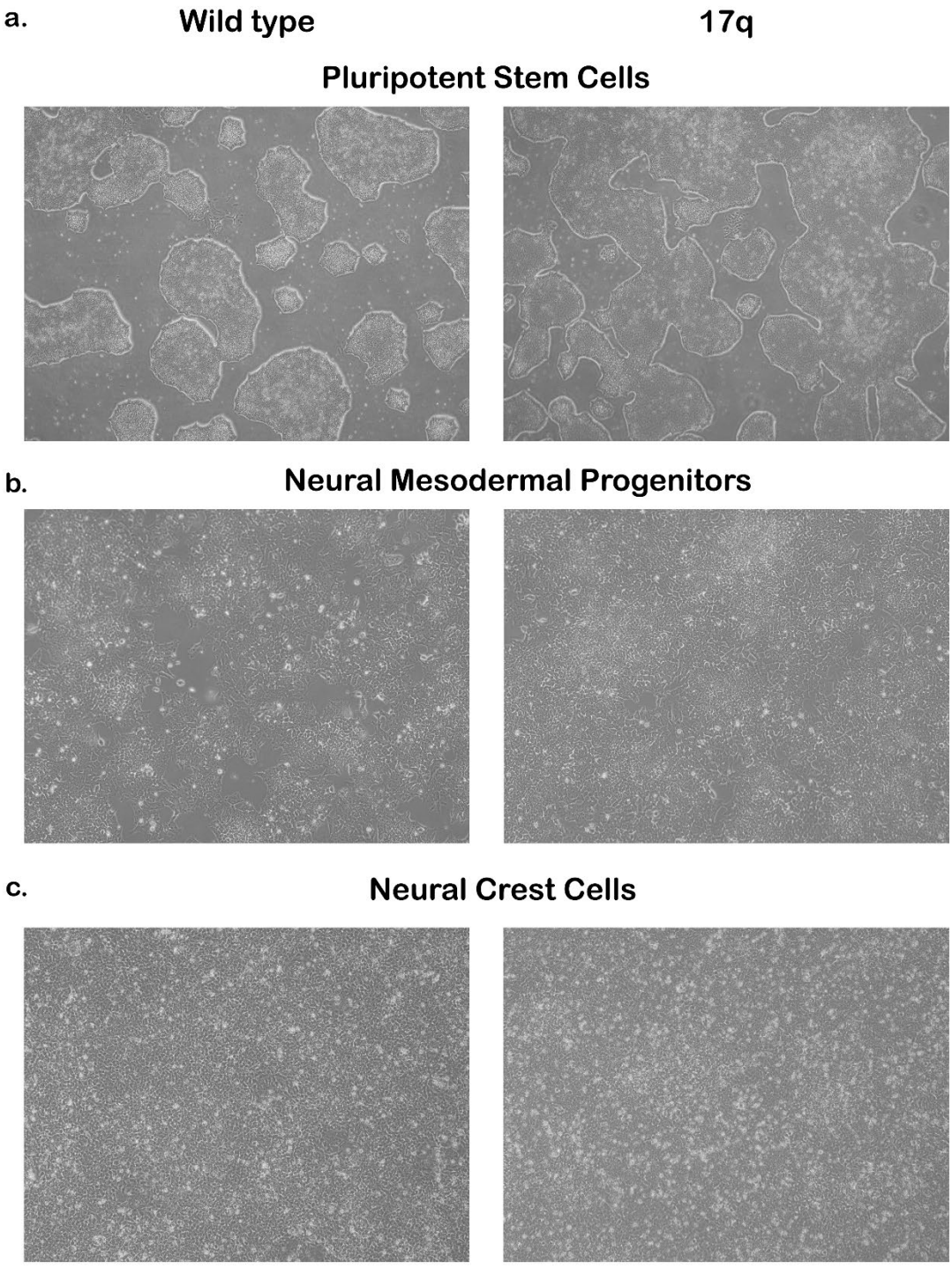

Figure 49. Bright-field images of the wild type and 17q cell lines at stem cell, NMP and NC stages. A-C. Comparative bright-field images at, **a.** Pluripotent stage (4X magnification), **b.** Neuromesodermal progenitor stage (10x magnification) and **c.** Neural crest stage (10x magnification) of wild type and 17q cell lines.

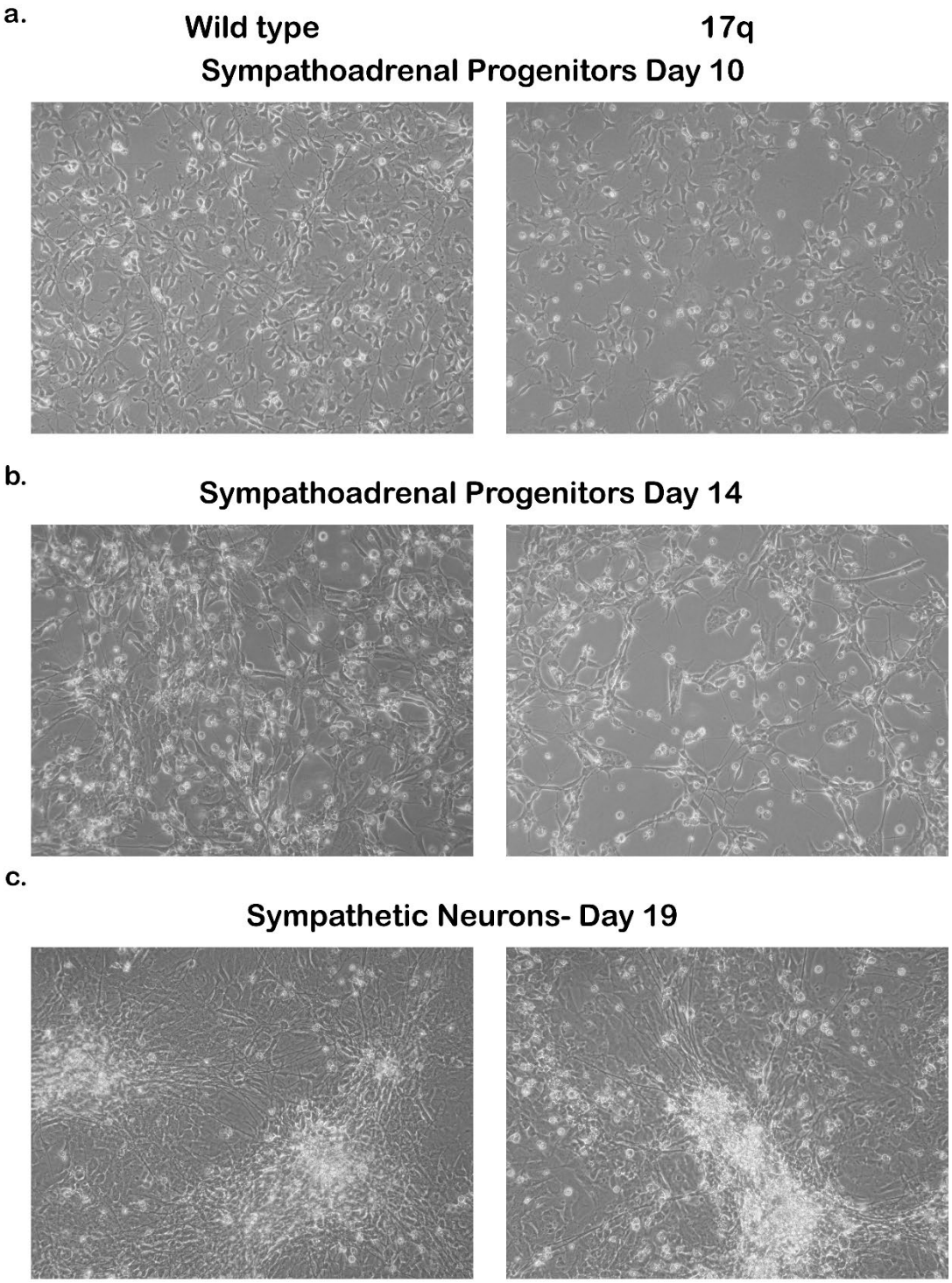

Figure 50. Bright-field images of the wild type and 17q cell lines at different points of the sympathoadrenal specification.
a. Comparative bright-field images at 20x magnification of the wild type and 17q cell lines at day 10 (SAP stage), **b.** Day 14 (SAP) and **c.** Day 19 (SN) of the differentiation protocol.

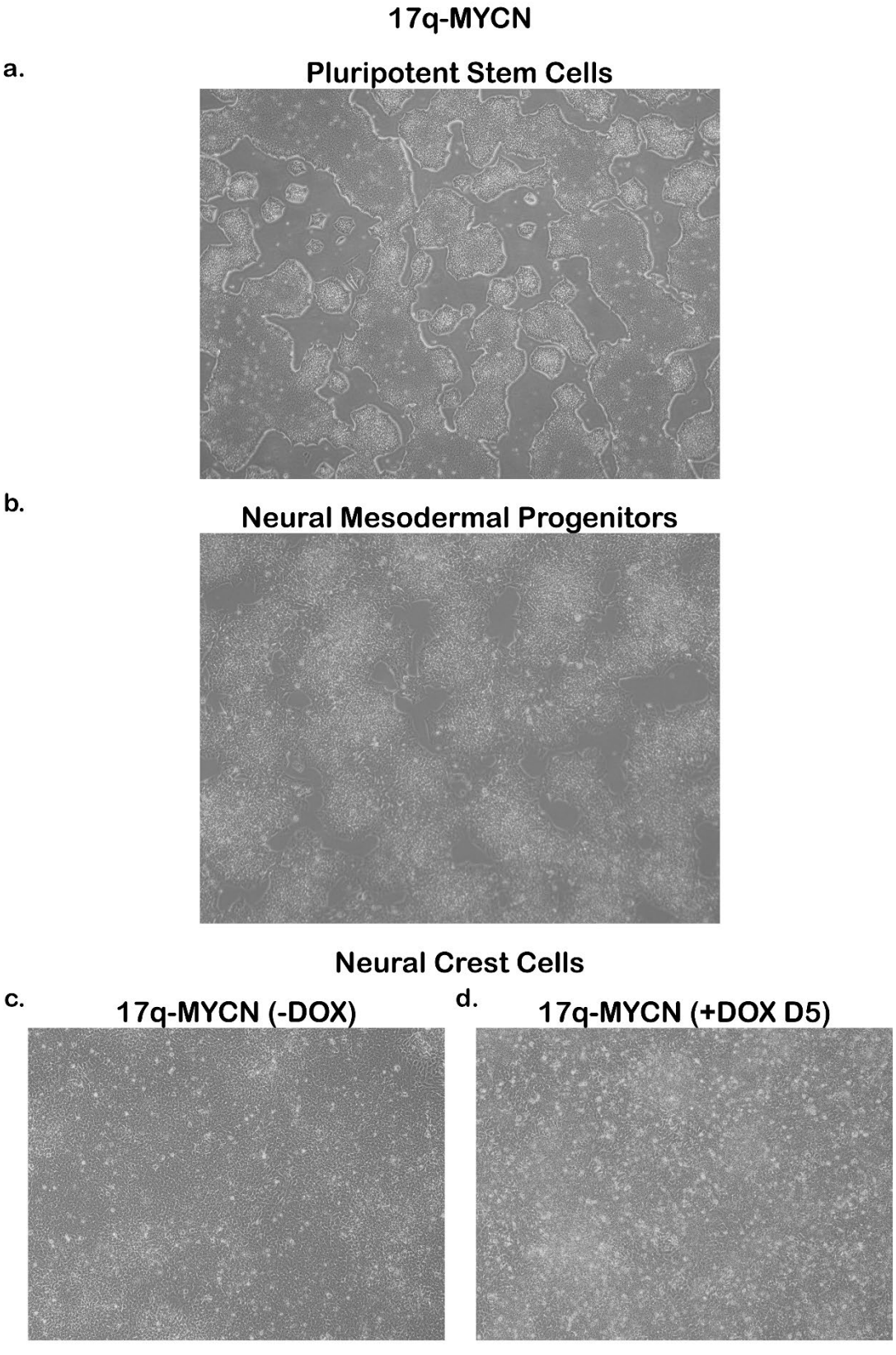

Figure 51. Bright-field images of the 17q-MYCN(-/+DOX) cell line at the stem cell, NMP and NC stages.

a. Comparative bright-field images at different magnification of the 17q-MYCN(-DOX) cell line at pluripotent stage (4X magnification) and **b.** Neuromesodermal progenitor stage (10X magnification).

In **c.** and **d.** are shown representative images of 17q-MYCN(-DOX) and 17q-MYCN(+DOX from day 5) respectively, at the neural crest stage (10X magnification).

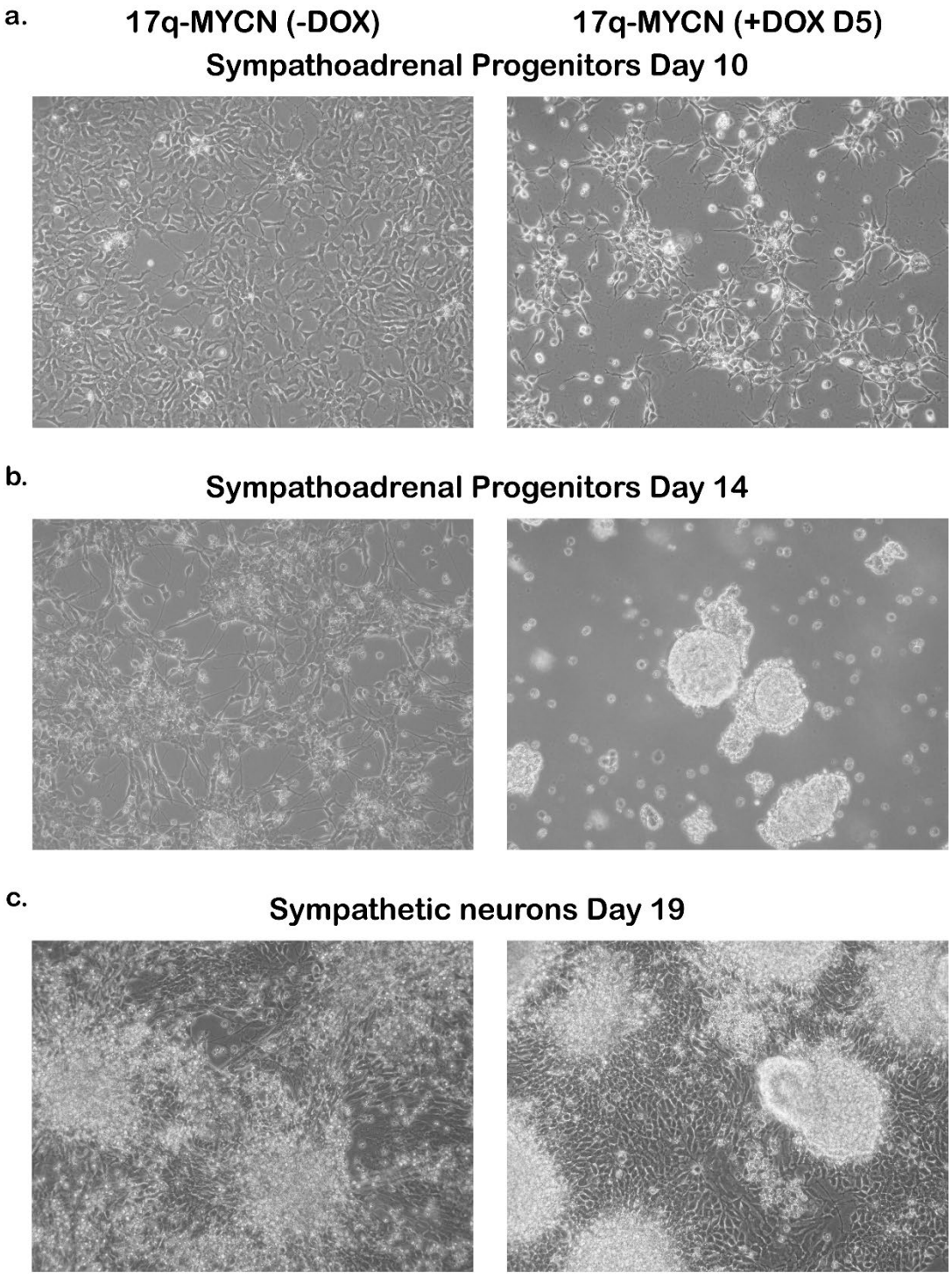

Figure 52. Bright-field images of 17q-MYCN(-DOX) and 17q-MYCN(+DOX) cell lines at different points of the sympathoadrenal specification.
a. Comparative bright-field images at 20x magnification of 17q-MYCN(-DOX) and 17q-MYCN(+DOX) cell lines at day 10 (SAP stage), **b.** day 14 (SAP) and **c.** day 19 (SN) of the differentiation protocol.

17q-MYCN (+DOX D9) 17q-MYCN (+DOX D14)

Sympathoadrenal Progenitors- Day 10

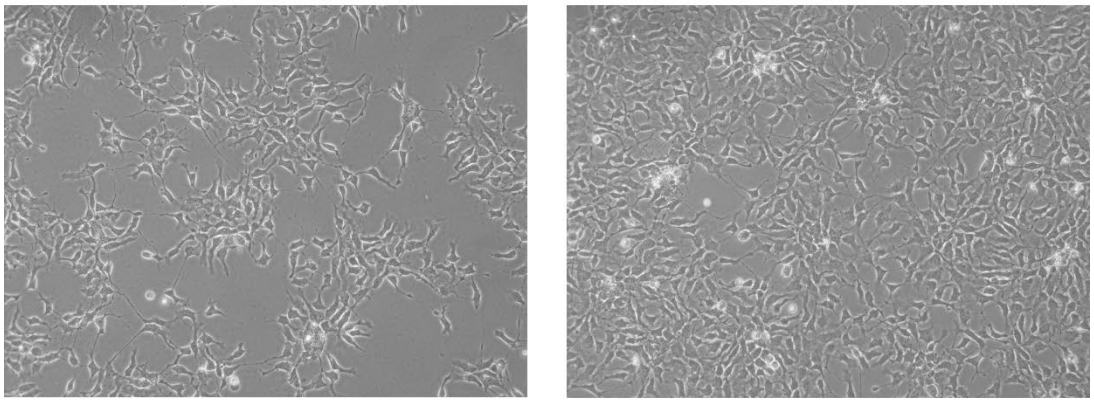

Sympathoadrenal Progenitors- Day 14

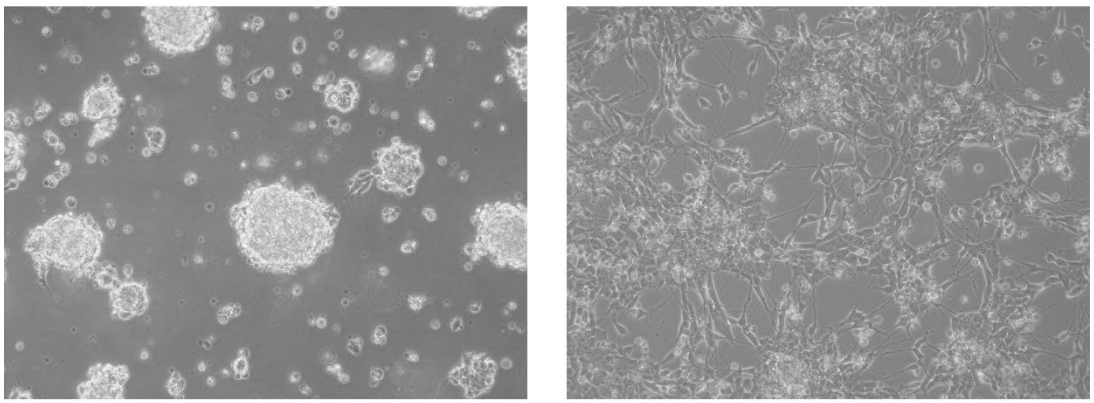

Sympathoadrenal Neurons- Day 19

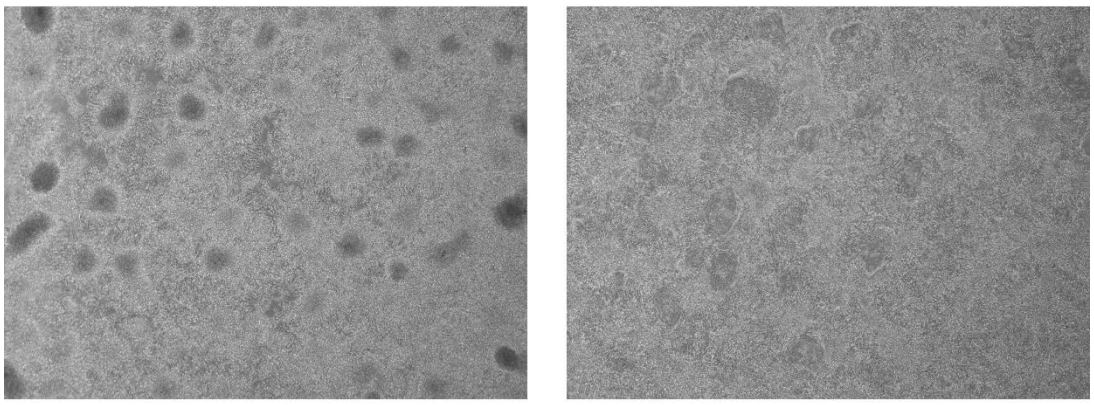

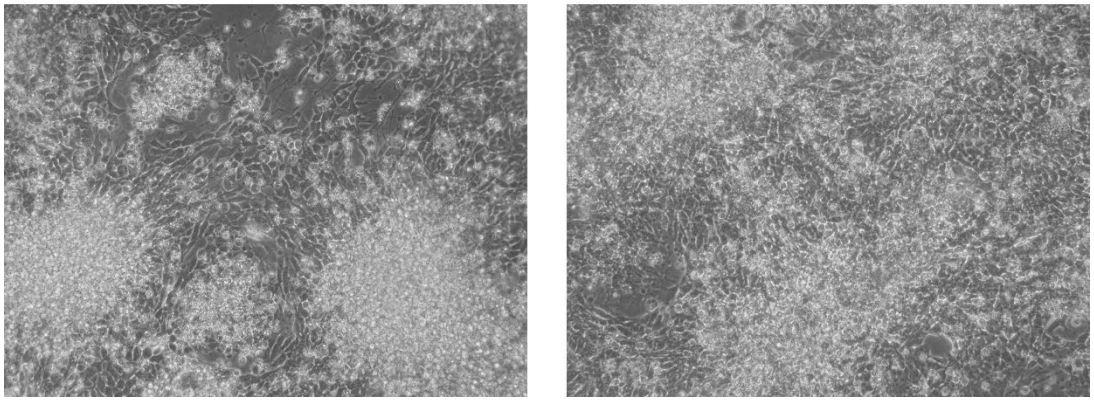

Figure 53. Bright-field images of 17q-MYCN(+DOX) cell lines at different points of the sympathoadrenal specification.
a. Comparative bright-field images at 20x magnification of 17q-MYCN(+DOX D9) and 17q-MYCN(+DOX D14) cell lines at day 10 (SAP stage), **b.** day 14 (SAP) and **c.** day 19 at 4x magnification (SN) and **d.** day 19 at 20x magnification (SN) of the differentiation protocol.

5.2.2 Sustaining proliferation

5.2.2.1 MYCN overexpression increases the number of cells in the S phase during the differentiation process.

As an increase in cell proliferation is one of the main hallmarks of cancer, I decided to perform the EdU Flow Cytometry Assay analysis (Salic and Mitchison, 2008)(described in materials and methods (2.7.1)). This method only allows the incorporation of the labelled thymidine analogue into the DNA during the S phase, this, along with DAPI staining, becomes a powerful tool to accurately determine the cell cycle profile of a population of interest.

I first examined the cell cycle profile of NMPs derived from hPSCs of different genetic backgrounds (Wild type, 17q, 17q-MYCN(-DOX) and 17q-MYCN(+DOX)(induction from day 0). **Figure 54-a** are shown representative flow cytometer EdU plots of the different cell lines analysed at day 3 (NMP stage) of differentiation. Some subtle differences were observed between the different genotypes. For example, wild type NMPs were marked by lower numbers of cells in G1 and higher in the S phase when compared to cells marked by chromosome 17q gain. Similarly, induction of MYCN in a 17q gain background leads to a reduction in the number of cells present in G1 and an increase in the cell fraction in the S phase compared to the un-induced control (**Figure 54-b**). A similar effect was also observed in the neural crest and SAP stages of differentiation (**Figure 56-57**). No differences in the percentage of cells in G2 was observed.

As cell density can affect the number of cycling cells(Wu et al., 2015), I decided to test the cells on day 5 of the differentiation protocol (second day of neural crest differentiation). However, no differences were found between cell lines (**Figure 55**).

Overall, the cell cycle profile did not seem to be affected by the gain of the 17q chromosome when compared to the wild-type, nonetheless, the overexpression of MYCN oncogene on top of 17q has a significant impact on cell cycle dynamics.

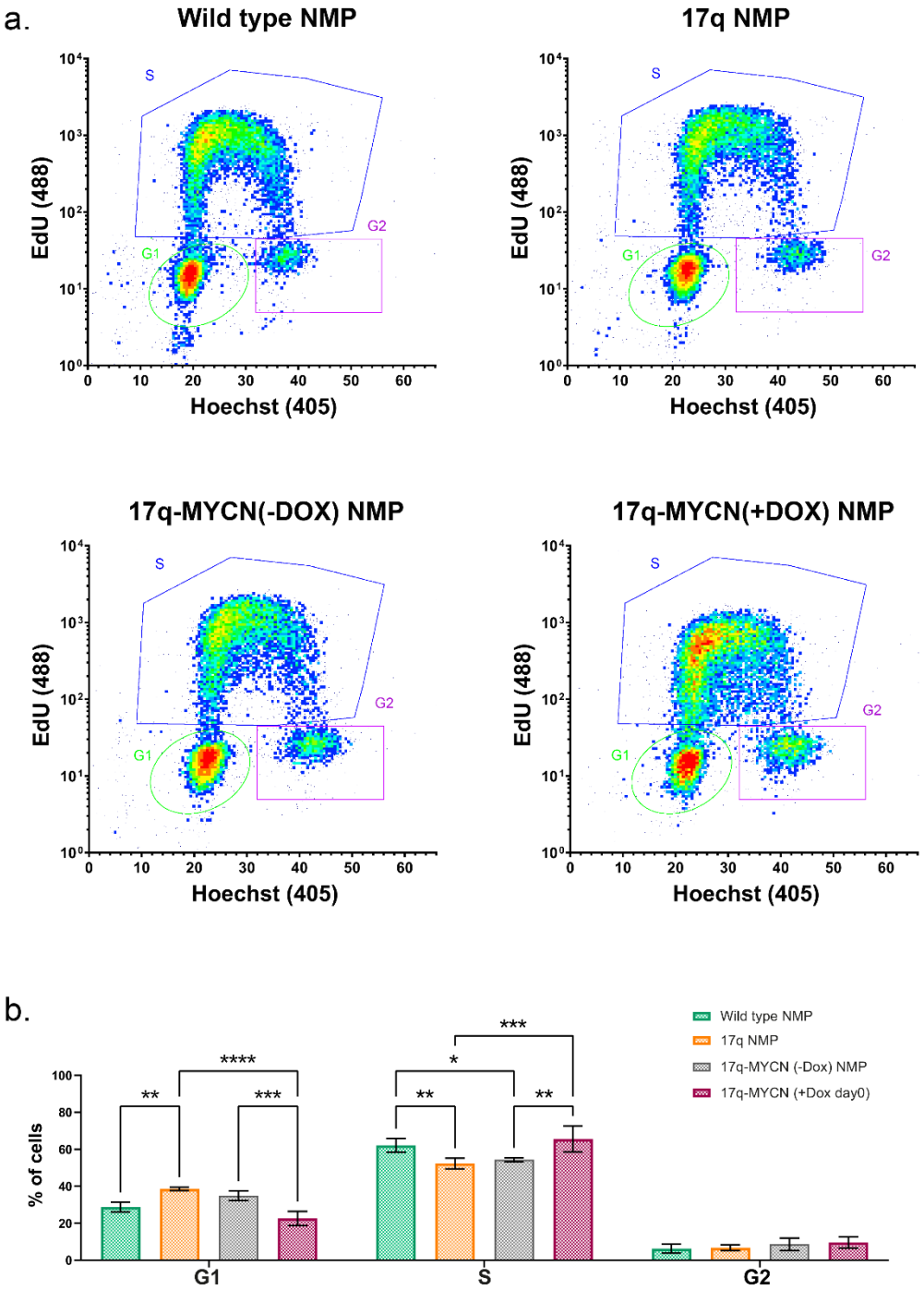

Figure 54. Cell cycle profile of the different cell lines at the NMP stage of differentiation.
a. Representative flow cytometer Edu plots of each of the different cell lines/conditions analysed at the NMP stage of differentiation (Day 3). The area in the blue gate corresponds to the S phase of the cell cycle, in green (G1 phase) and magenta (G2 phase). **b.** Comparison of the results obtained from the EdU analysis on the different cell lines at the NMP stage (Day 3). It is shown the percentage of cells found in each of the different stages of the cell cycle (G1, S, G2). Statistically significant differences were found in G1 and S stages between the different cell lines, except 17q vs 17q-MYCN(-DOX) show no significance. (n= 3 biological replicates, error bars= SD, Two-way ANOVA test, $p \leq 0.05$= *, $p \leq 0.01$= **, $p \leq 0.001$= ***, $p \leq 0.0001$= ****)

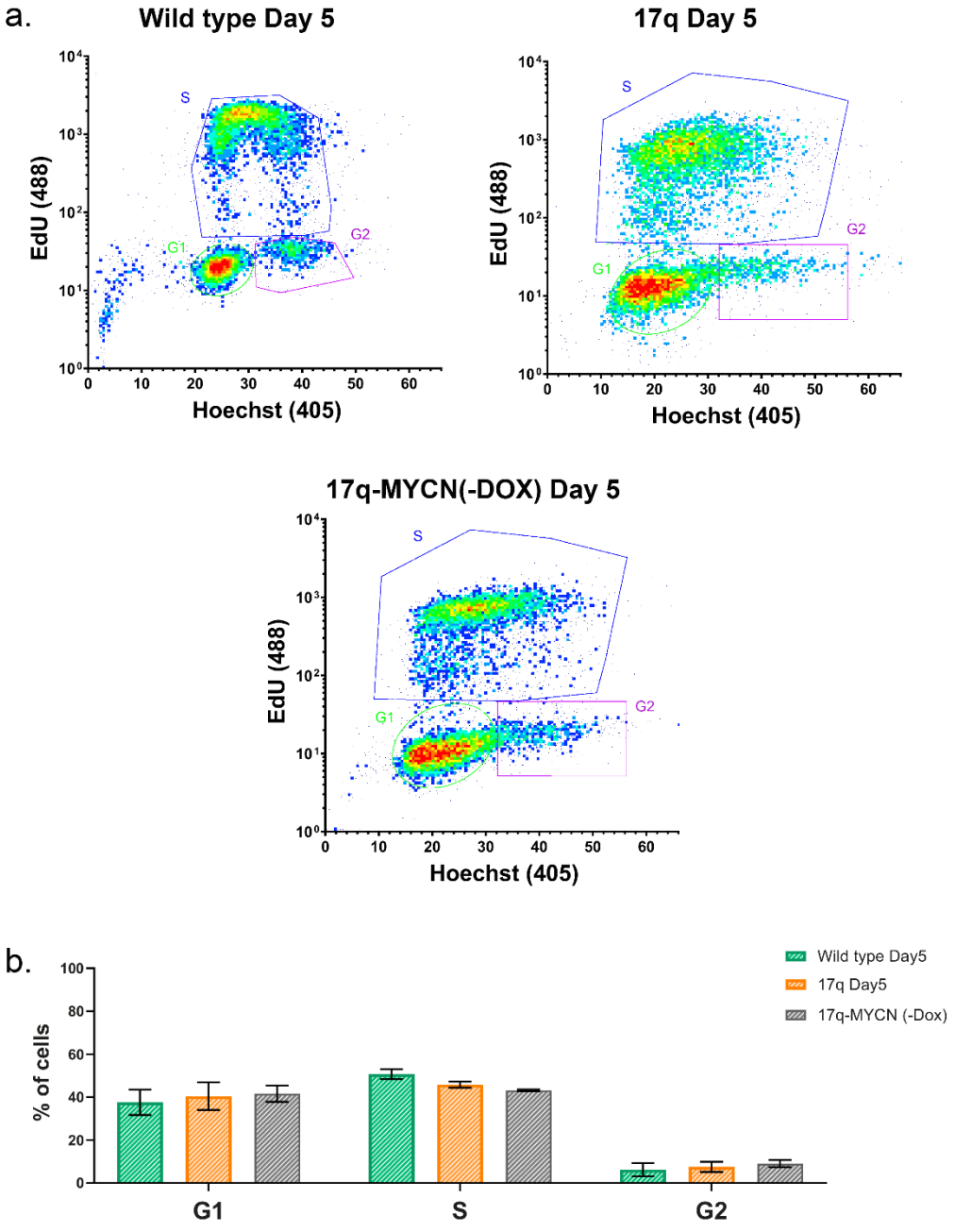

Figure 55. Cell cycle profile of the different cell lines at day 5 of the differentiation protocol.
a. Representative flow cytometer Edu plots of each of the different cell lines/conditions analysed at day 5 of differentiation. The area inside the blue gate corresponds to the S phase of the cell cycle, in green (G1 phase) and magenta (G2 phase). **b.** Comparison of the results obtained from the EdU analysis on the different cell lines at day 5 of the differentiation protocol. In the graph, it is shown the percentage of cells found in each of the different stages of the cell cycle (G1, S, G2). No statistically significant differences were found (n= 3 biological replicates, error bars= SD, Two-way ANOVA test, $p \leq 0.05$= *, $p \leq 0.01$= **, $p \leq 0.001$= ***, $p \leq 0.0001$= ****)

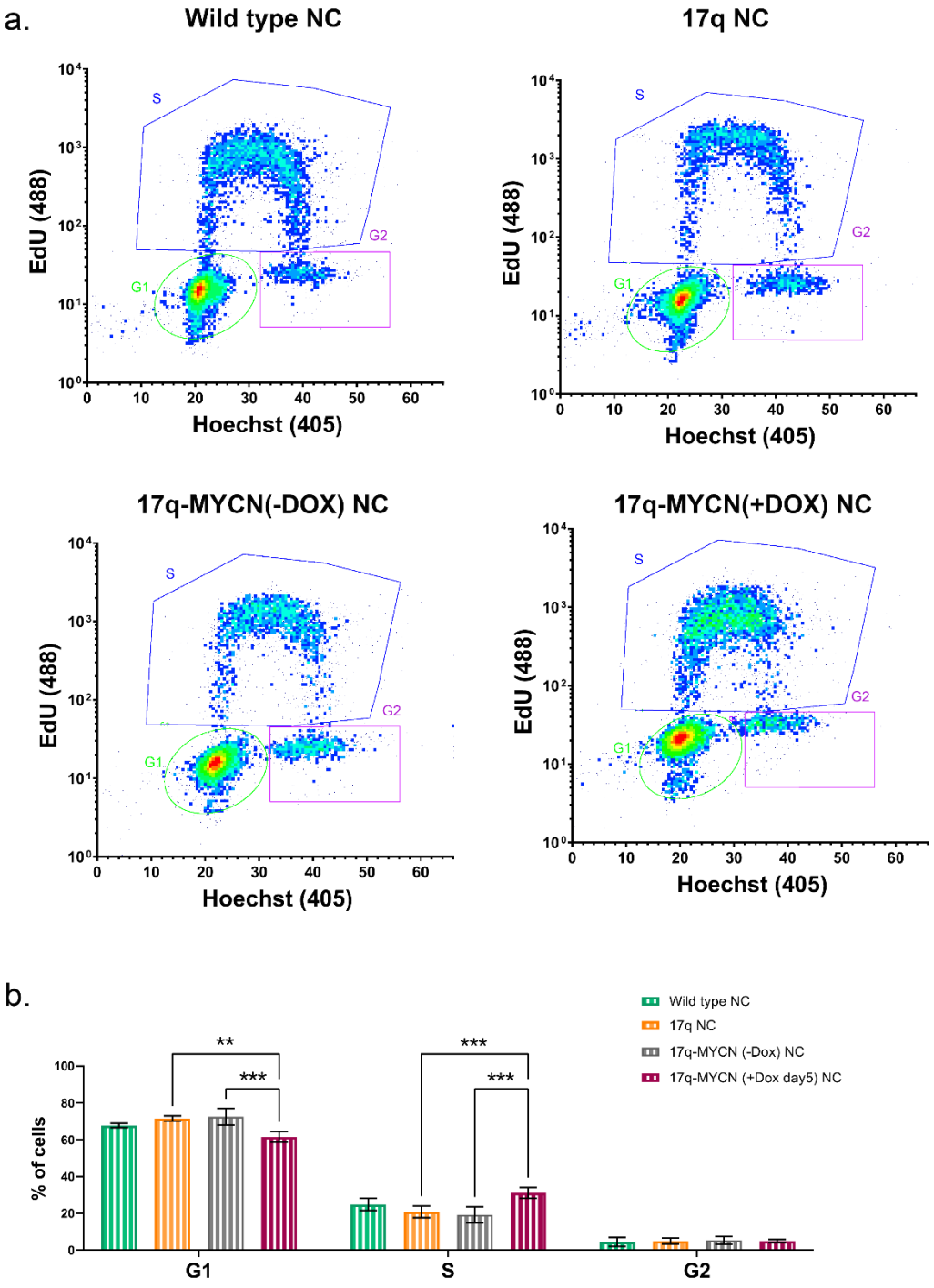

Figure 56. Cell cycle profile of the different cell lines at the end of the NC stage.
a. Representative flow cytometer Edu plots of each of the different cell lines/conditions analysed at day 9, corresponding to the NC stage of the protocol. The area inside the blue gate corresponds to the S phase of the cell cycle, in green (G1 phase) and magenta (G2 phase). **b.** Comparison of the results obtained from the EdU analysis on the different cell lines. In the graph, it is shown the percentage of cells found in each of the different stages of the cell cycle (G1, S, G2). Statistically significant differences were found between 17q-MYCN(+DOX) against both 17q and 17q-MYCN(-DOX) at G1 and S stages of the cell cycle (n= 3 biological replicates, error bars= SD, Two-way ANOVA test, $p \leq 0.05$= *, $p \leq 0.01$= **, $p \leq 0.001$= ***, $p \leq 0.0001$= ****)

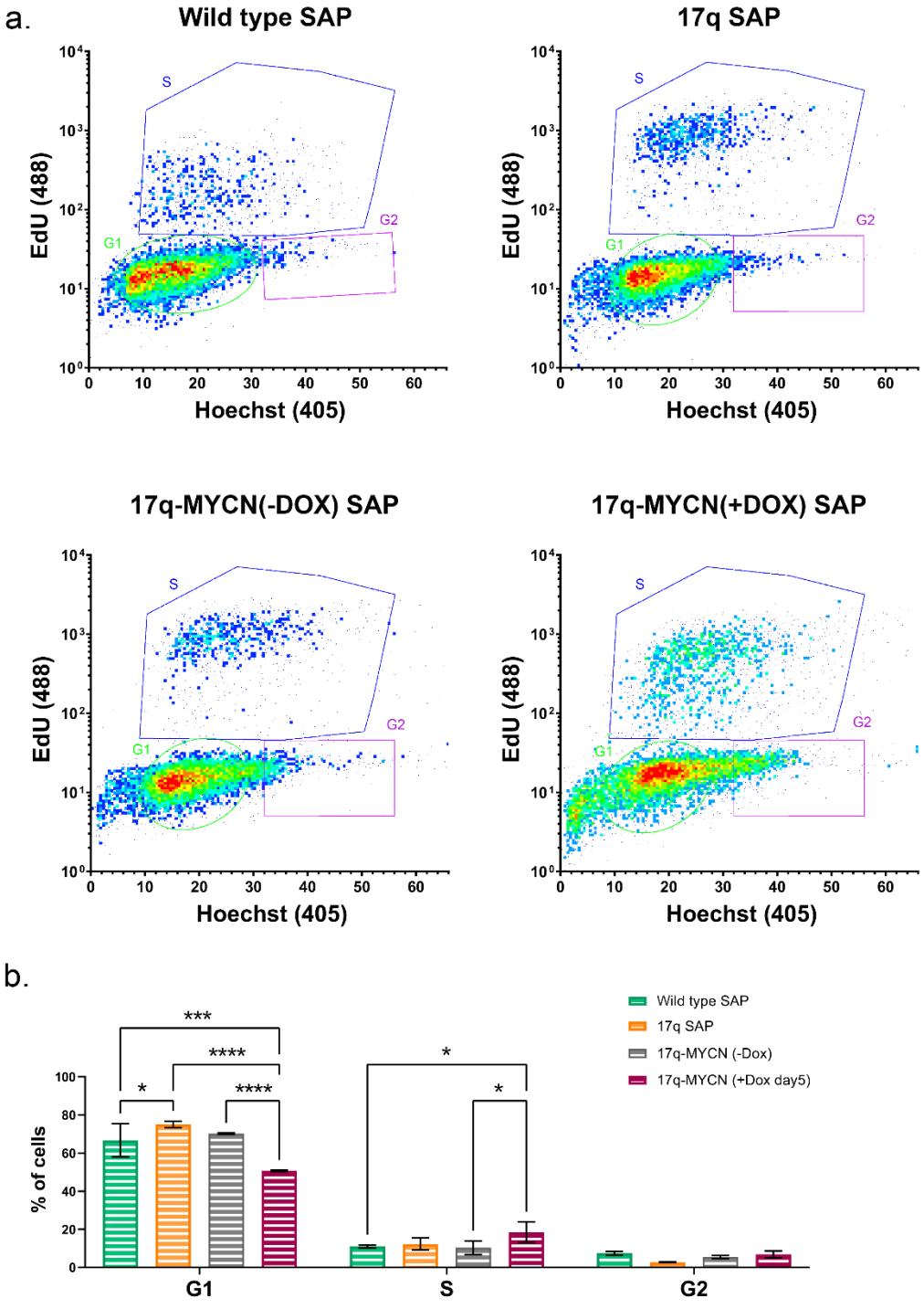

Figure 57. Cell cycle profile of the different cell lines at the Sympathoadrenal progenitor stage. **a.** Representative flow cytometer Edu plots of each of the different cell lines/conditions analysed during the SAP stage. The area inside the blue gate corresponds to the S phase of the cell cycle, in green (G1 phase) and magenta (G2 phase). **b.** Comparison of the results obtained from the EdU analysis on the different cell lines. In the graph, it is shown the percentage of cells found in each of the different stages of the cell cycle (G1, S, G2). Statistically significant differences were found at G1 and S stages of the cell cycle (n= 3 biological replicates, error bars= SD, Two-way ANOVA test, $p \leq 0.05$= *, $p \leq 0.01$= **, $p \leq 0.001$= ***, $p \leq 0.0001$= ****)

5.2.2.2 Proliferative profile varies along the differentiation process and depends on MYCN status

In a second approach to analyse cell proliferation status, I decided to use an antibody against Ki-67. Ki-67 has been reported to be present in every phase of the cell cycle except for cells in G0 (Juríková et al., 2016). These characteristics make this protein a good tool to determine if cells are proliferating in a certain population.

I analysed the presence of the protein throughout the different stages of the differentiation protocol following immunostaining and images analysis: pluripotent stem cells, neuromesodermal progenitors, neural crest, sympathoadrenal progenitors and sympathetic neurons. The cell lines used were: wild type, 17q, 17q-MYCN with and without the presence of doxycycline. MYCN induction was carried out only from day 5 of the differentiation protocol.

Cells at the pluripotent stage were highly proliferative as almost 100% showed expression of the Ki-67 marker (**Figure 58-a**). Similar findings were observed at the NMP stage as they also showed a high percentage of cells proliferating (**Figure 58-b**).

At the NC stage of the protocol, several differences were observed between the cell lines: First of all, 17q-MYCN(+DOX) cell line increased significantly its proliferation rate when compared to the untreated control. On the other hand, the wild type cell line showed higher proliferation rates when compared to 17q (**Figure 58-c**). Cells at the sympathoadrenal progenitor stage showed similar behaviour to that observed at the NC stage. However, the margin of difference between 17q-MYCN(-DOX) and 17q-MYCN(+DOX) was greater (**Figure 58-e**). These observations correlate with the representative images taken from the immunofluorescence assays against the Ki-67 protein at the SAP stage (**Figure 58-f**).

Finally, cells were differentiated into sympathetic neurons, which is the last stage of the protocol. Unfortunately, only two biological replicates were analysed at this point. However, 17q-MYCN(+DOX) remained highly proliferative when compared to the other cell lines/conditions. It is worth mentioning that the wild type cels did not decrease their proliferation rate, suggesting that cells did not reach the post-mitotic stage of their differentiation on this day (**Figure 58-g**). In agreement with the cell cycle proliferation (EdU) results, MYCN overexpression on top of 17q gain increased the amount of proliferating cells, particularly during the neural crest and sympathoadrenal progenitor stages.

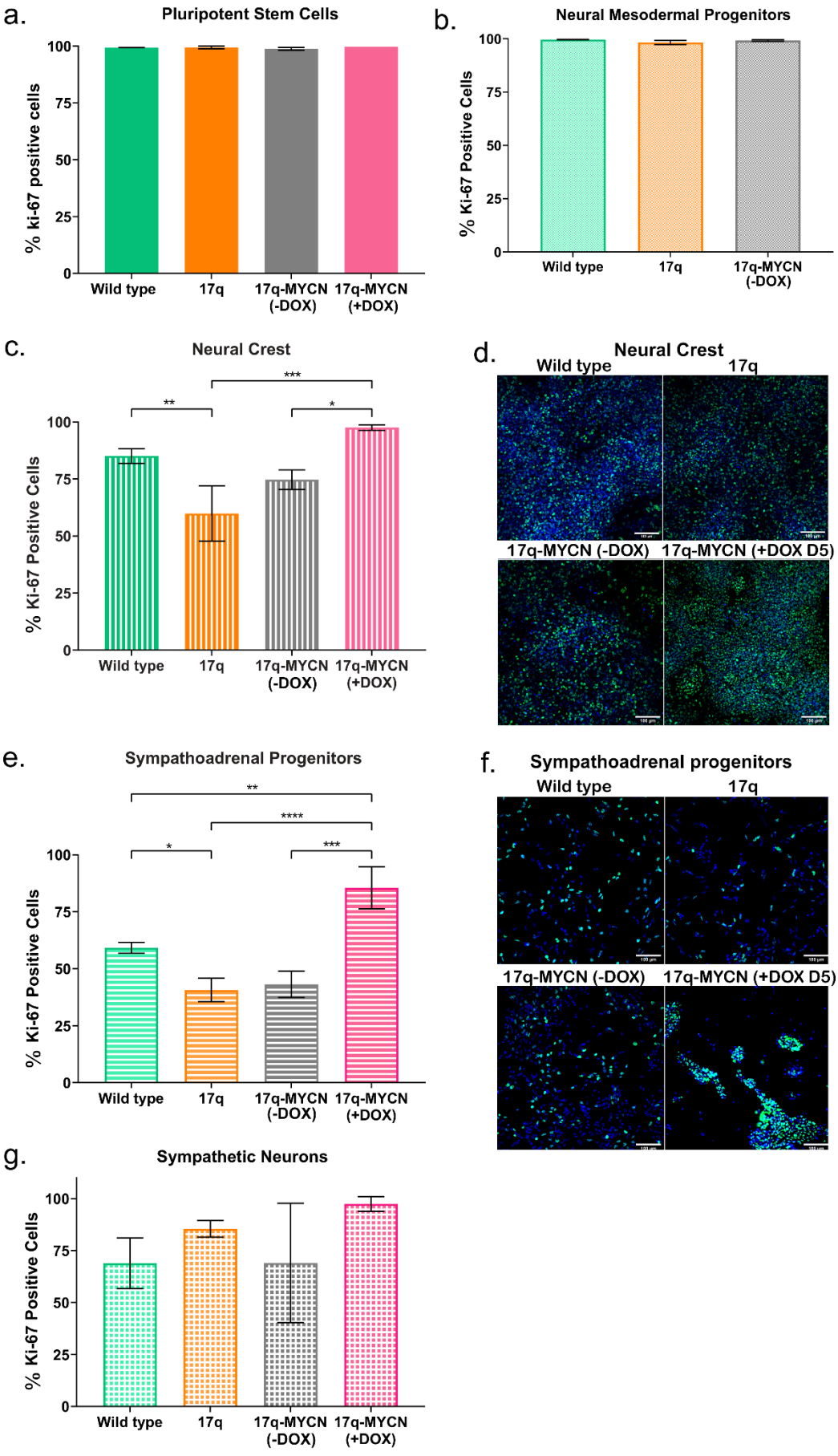
a.
Pluripotent Stem Cells
% ki-67 positive cells
100
75
50
25
0
Wild type
17q
17q-MYCN (-DOX)
17q-MYCN (+DOX)
b.
Neural Mesodermal Progenitors
% Ki-67 Positive Cells
100
75
50
25
0
Wild type
17q
17q-MYCN (-DOX)
c.
Neural Crest
% Ki-67 Positive Cells
***
**
*
100
75
50
25
0
Wild type
17q
17q-MYCN (-DOX)
17q-MYCN (+DOX)
d.
Neural Crest
Wild type
17q
17q-MYCN (-DOX)
17q-MYCN (+DOX D5)
e.
Sympathoadrenal Progenitors
% Ki-67 Positive Cells
**
****
*
***
100
75
50
25
0
Wild type
17q
17q-MYCN (-DOX)
17q-MYCN (+DOX)
f.
Sympathoadrenal progenitors
Wild type
17q
17q-MYCN (-DOX)
17q-MYCN (+DOX D5)
g.
Sympathetic Neurons
% Ki-67 Positive Cells
100
75
50
25
0
Wild type
17q
17q-MYCN (-DOX)
17q-MYCN (+DOX)

Figure 58.Proliferation profile of the different cell lines at stem cell, NMP, NC, SAP and SN stages. **a.** Comparison of the percentage of cells expressing the proliferative marker (Ki-67) at the pluripotent stage, **b.** NMP stage, **c.** Neural crest stage, **e.** SAP stage and **g.** Sympathetic neuron stage. Ubiquitous expression of Ki-67 was observed in all conditions at pluripotent (a) and NMP (b) stages. Statistic analysis was not performed as these figures only represent two biological replicates. **c.** At the Neural crest stage (day 9), statistically significant differences were found in the expression of Ki-67 among the different cell lines and conditions, being 17q cell line the least proliferative and 17q-MYCN(+DOX) the most proliferative at this stage of differentiation. **d.** Representative images of the immunofluorescences used for the data analysis of figure **c.**. (Merge: Hoechst(blue), KI-67(green)). **e.** At the SAP stage (Day 14) there were statistically significant differences found in the expression of Ki-67 among the different cell lines and conditions, being 17q and 17q-MYCN(-DOX) cell lines the least proliferative and 17q-MYCN(+DOX) the most proliferative at this stage of differentiation. **f.** Representative images of the immunofluorescences used for the data analysis of figure **e.**. (Merge: Hoechst(blue), KI-67(green)). **g.** At the SN stage (Day 19) statistic analysis was not performed as this figure only represents two biological replicates. Nonetheless, 17q-MYCN(+DOX) showed the highest proliferation levels near to 100% in both replicates. **a- e.** Cell lines and conditions are depicted as follows: wild type (green), 17q (orange), 17q-MYCN(-DOX) (grey) and 17q-MYCN(+DOX)(pink). **a, b, g.** (n= 2 biological replicates, error bars= SD). **c,e.** (n= 3 biological replicates, error bars= SD, Ordinary One-way ANOVA test with Tukey correction, $p \leq 0.05$= *, $p \leq 0.01$= **, $p \leq 0.001$= ***, $p \leq 0.0001$= ****)

5.2.3 Resisting cell death

5.2.3.1 MYCN overexpression in Sympathoadrenal progenitors cells increases their colony formation capacity.

Given the fact that one of the indicators of tumourigenesis is the abnormal increase in cell survival, I decided to test their clonogenic capacity, as this evaluates the ability of a single cell to defeat several stress signals to successfully proliferate and give rise to a colony (Woolston and Martin, 2011, Franken et al., 2006). To assess if the presence of 17q and/or MYCN overexpression on 17q background could provide a survival advantage, cells were plated at low density (500 cells/cm2) and the resulting colonies were counted after five days. The stage assessed was the transition between neural crest and sympathetic progenitors because at these stages significant differences in Ki-67 expression were detected.

Representative pictures of the assay are in **Figure 59-a**. In wild type and 17q cell line, although mainly isolated cells were detected, some colonies were also found, whilst 17q-MYCN(-DOX) condition showed rather spread cells forming colonies-like structures. On the other hand, 17q-MYCN in the presence of doxycycline formed compacted but highly dense colonies (**last panel, Figure 59-a**).

Image quantification showed that all cell lines/conditions were able to form colonies. Nonetheless, only 17q-MYCN(+DOX) significantly generated a higher amount of colonies when compared to all the other conditions (**Figure 59-b**)

Time-lapse analysis of the 17q-MYCN line with and without doxycycline revealed differences in cellular morphology, survival and proliferation. 17q-MYCN(-DOX) showed some survival although with fairly

low proliferation rates as they tended to form motile neuron-like cells (**Figure 60-a)**. On the other hand, 17q-MYCN in presence of doxycycline generated small-compacted cells that seemed to be proliferating at higher rates (**Figure 60-b**).

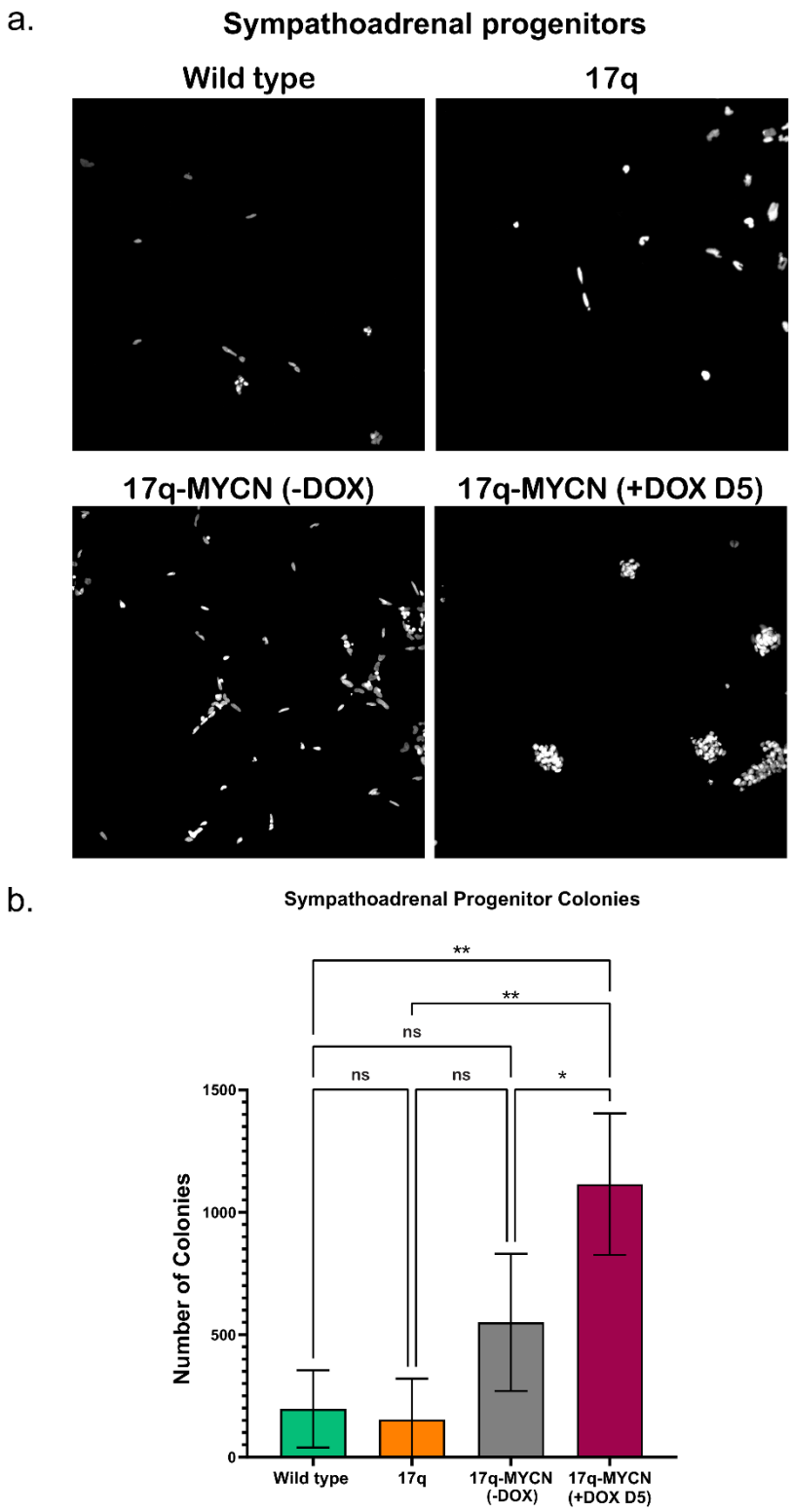

Figure 59. Colony-forming capacity of the different cell lines in SAP conditions.
a. Representative images that were used to calculate the number of colonies formed when plated at day 9 of differentiation at low density (500 cells/cm^2), and being let to grow for 5 days in SAP media. Cells were fixed and stained with Hoechst. **b.** Comparison of the number of colonies formed by the different cell lines plated at low density. 17q-MYCN(+DOX) condition was statistically the most successful to grow colonies compared to the other conditions. (n= 3 biological replicates, error bars= SD, Ordinary One-way ANOVA test with Tukey correction, $p \leq 0.05$= *, $p \leq 0.01$= **, $p \leq 0.001$= ***, $p \leq 0.0001$= ****)

Low Density - Sympathoadrenal Progenitors

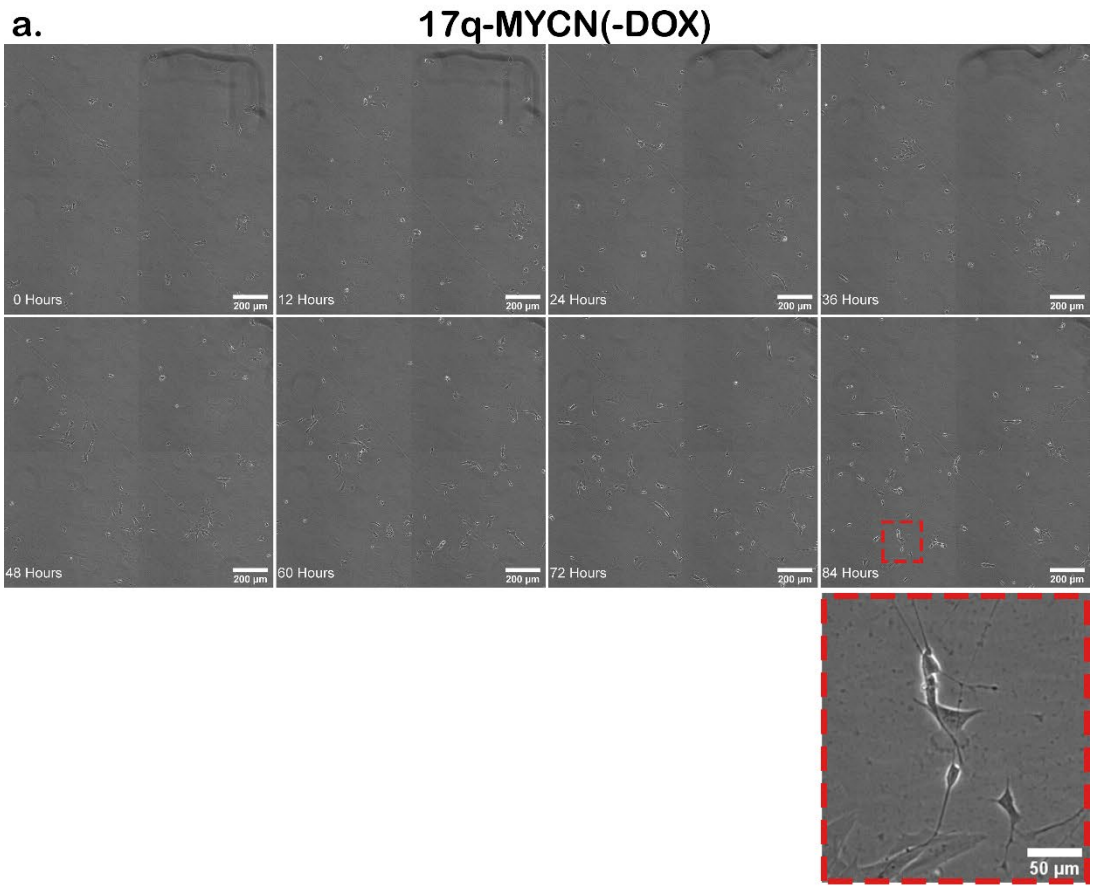

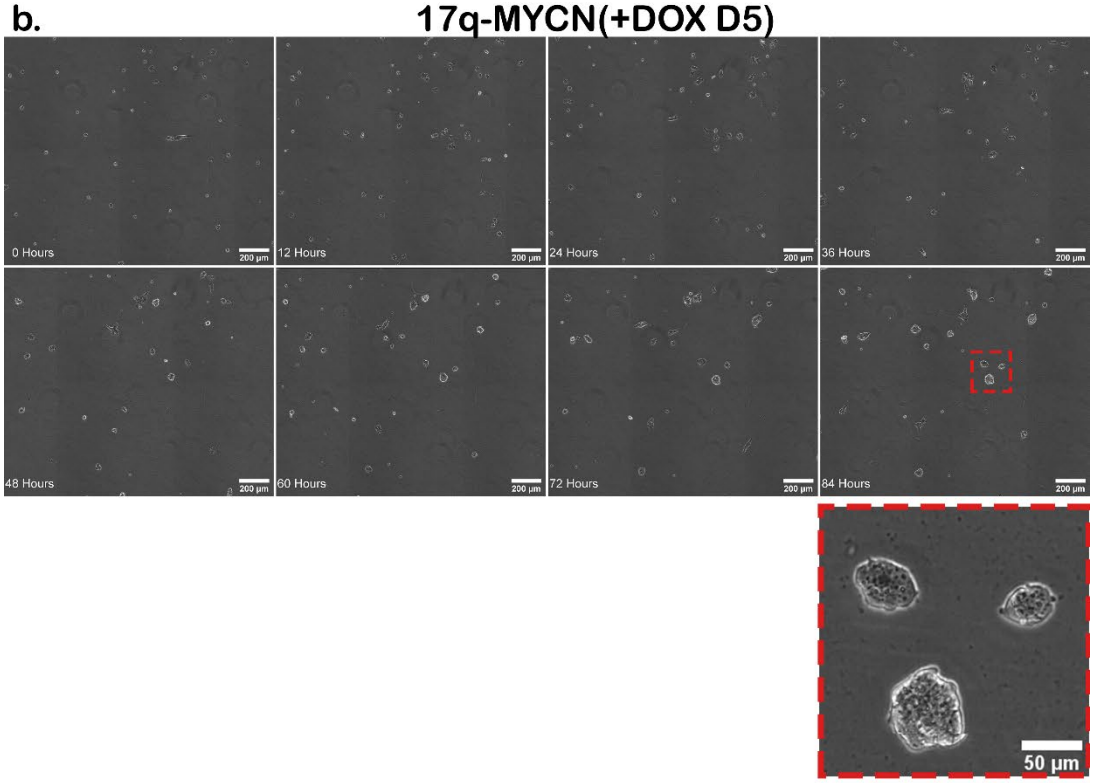

Figure 60. Time-lapse images of the colony formation of 17q-MYCN(-DOX) and 17q-MYCN(+DOX D5) Time-lapse images of 17q-MYCN(-DOX) taken every 12 hours, from 0 to 84 hours. Imaging started 24 hours after plating and after media was switched from NC to SAP. The red box displays the magnified image of a typical cell/colony morphology. **a.** Is 17q-MYCN(-DOX). Less colony formation is observed, cells showed a neuron-like spikey morphology. **b.** is 17q-MYCN(+DOX)(from day 5). Cells formed tight rounded colonies. Almost no single cells were found at 84 hours.

5.2.4 Cellular energetics

5.2.4.1 MYCN-induced cell line showed a distinctive glucose uptake profile

To assess if there were any differences in the uptake of glucose between the different cell lines, and during the different stages of the differentiation, I carried out a glucose uptake assay using 6-NBDG. 6-NBDG is a fluorescent glucose analogue that can be used to monitor the glucose uptake in living cells without being metabolised(Speizer et al., 1985, Barros et al., 2009)

The first stage to be analysed was the NMP stage. The cell lines that were analysed were wild type, 17q and 17q-MYCN without doxycycline induction. No apparent differences in the amount of glucose uptake were detected (**Figure 61-a)**. Thereafter, the glucose intake profile was analysed at the end of the neural crest stage, the cell lines/conditions analysed were wild type, 17q, 17q-MYCN(-DOX), 17q-MYCN(+DOX)(from day 5). Similar findings to those observed in NMP differentiation were observed as no remarkable differences were found between conditions (**Figure 61-b**).

The next stage analysed was the sympathoadrenal progenitor stage. Conditions analysed were wild type, 17q (**Figure 62-a)**, 17q-MYCN(-DOX) and 17q-MYCN plus doxycycline from day 5 and day 9 of the differentiation protocol (**Figure 63-a)**. Doxycycline induction on day 9 was performed to evaluate if MYCN overexpression during early sympathoadrenal specification could influence metabolic changes.

Although no differences were found between the wild type and 17q cell lines (**Figure 62-a**), clear differences in the glucose uptake profile can now be distinguished between 17q-MYCN(-DOX) and 17q-MYCN(+DOX)(day 5 and day 9) (**Figure 63-a**). Overall, it seems that two populations have appeared as two main peaks can be observed in the cells treated with doxycycline. One of the populations appears to be taking less glucose when compared to 17q-MYCN(-DOX), whilst the other population showed an increase in glucose uptake.

The glucose uptake profile was then assessed during the sympathetic neuron stage. Cell lines/conditions analysed were wild type vs 17q (**64-a**) and 17q-MYCN(-DOX) vs 17q-MYCN plus doxycycline given at different days of the differentiation protocol (day 5, day9, day14) (**Figure 64**-**b**). Induction with doxycycline from day 14 was included as cells at this day represent a more mature sympathetic neuron, and I wanted to test if MYCN overexpression could also modify the normal intake

profile in this stage. Once more, no differences were found between the wild type and 17q, whilst changes were still observed on samples that received the doxycycline treatment, except for 17q-MYCN(+DOX)(from day 14) as this sample did not show significant differences when compared to 17q-MYCN(-DOX).

Overall, no apparent differences were observed in the glucose uptake profile between the 17q and wild type cell line. On the other hand, the overexpression of MYCN on the 17q background showed interesting results as no differences were found between 17q-MYCN(+DOX) and the control during neural crest specification. Nonetheless, when cells reach the sympathoadrenal lineage, changes in their glucose uptake profile were observed in both 17q-MYCN(+DOX D5) and 17q-MYCN(+DOX D9), but no significant differences were observed when doxycycline was induced at day 14.

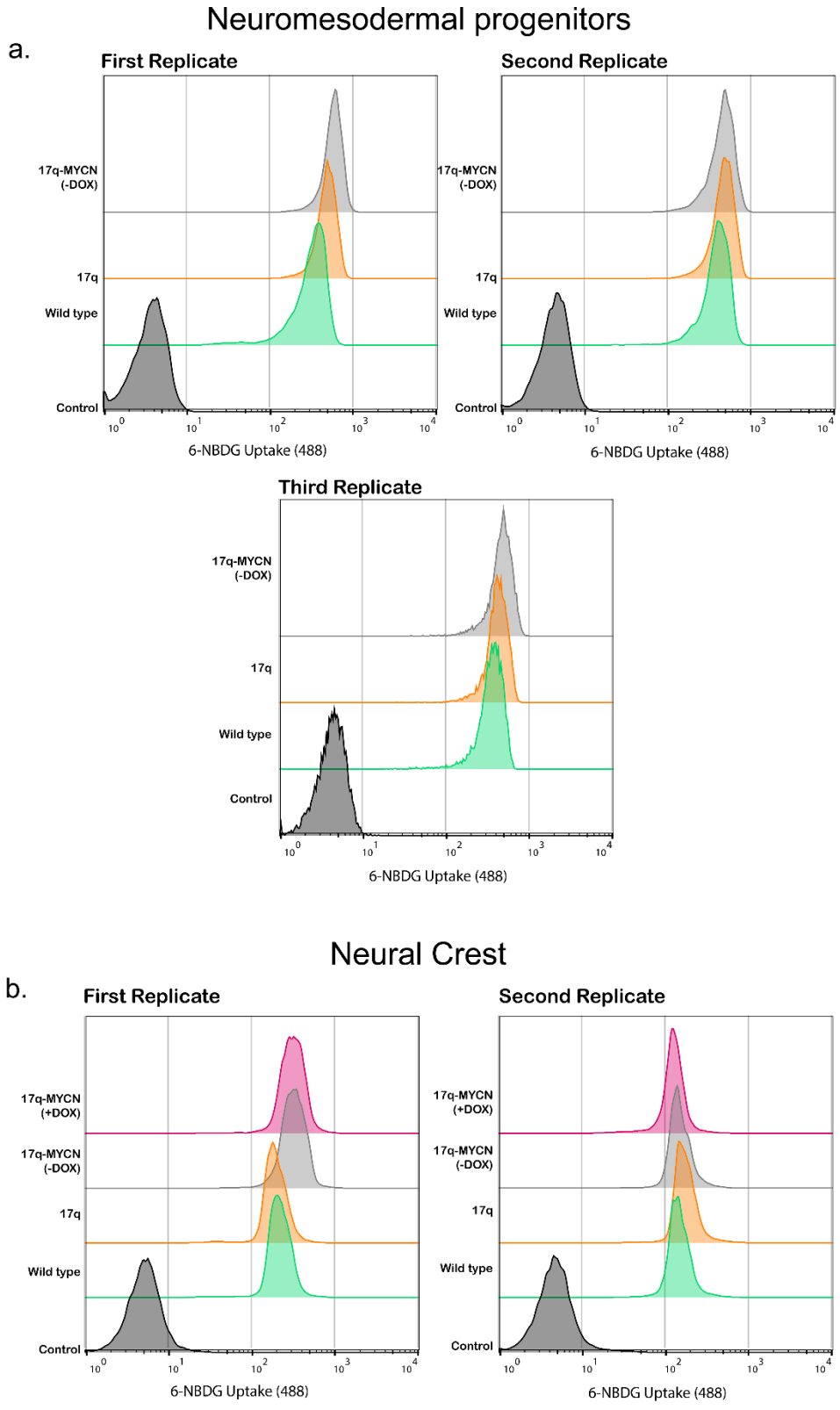

Figure 61. Glucose uptake profile of the wild type, 17q and 17q-MYCN(-DOX) cells during NMP and NC differentiation. Flow cytometry histograms for 6-NBDG uptake. Glucose uptake assay, with Wild type (green), 17q (orange), 17q-MYCN(-DOX) (grey), 17q-MYCN(+DOX) (magenta) and the control untreated sample (black). **a.** NMP glucose intake profile. Three biological replicates. **b.** NC glucose intake profile. Two biological replicates.

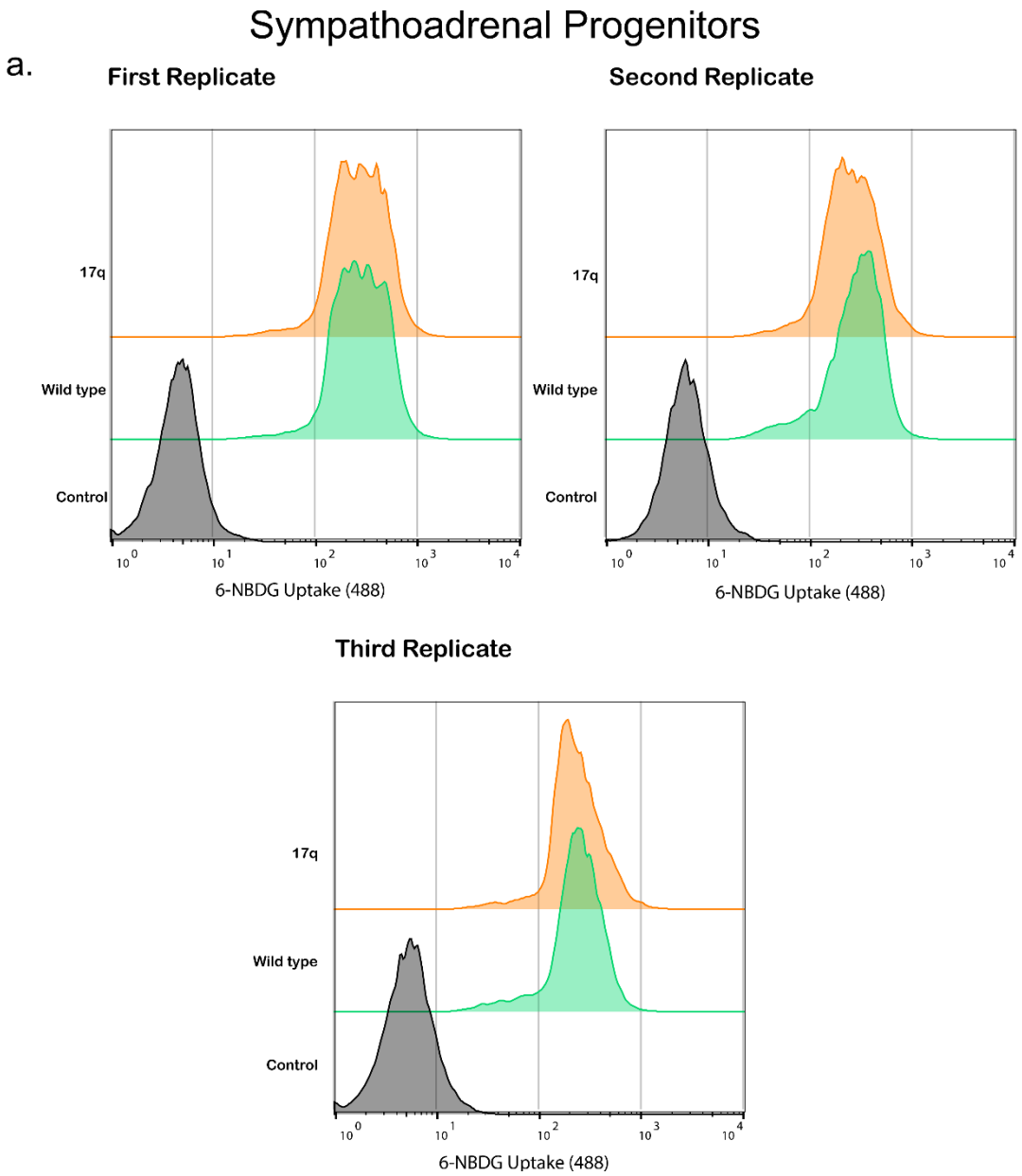

Figure 62. Glucose uptake profile of the wild type and 17q cells during SAP differentiation. **a.** Flow cytometry histograms for 6-NBDG uptake. Shown are three biological replicates of glucose uptake assay at SAP stage, with Wild type (green), 17q (orange), 17q-MYCN(-DOX) (grey) and the control untreated sample (black).

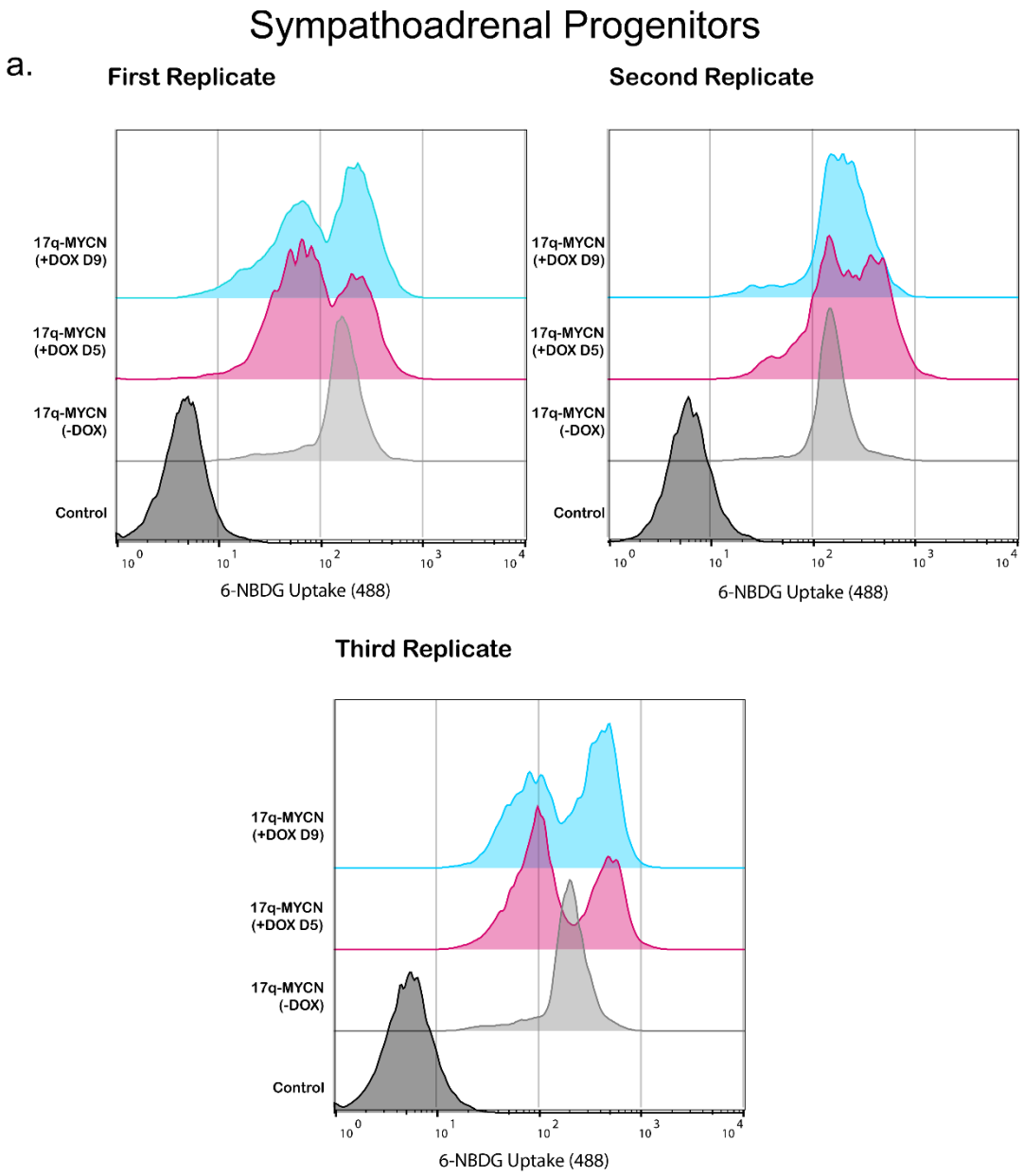

Figure 63. Glucose uptake profile of the 17q-MYCN(-DOX) and 17q-MYCN(+DOX) cells during SAP differentiation. a. Flow cytometry histograms for 6-NBDG uptake. Shown are three biological replicates of glucose uptake assay at SAP stage, with 17q-MYCN(-DOX) (grey), 17q-MYCN(+DOX D5) (Magenta), 17q-MYCN(+DOX D9) (Blue) and the control untreated sample (black).

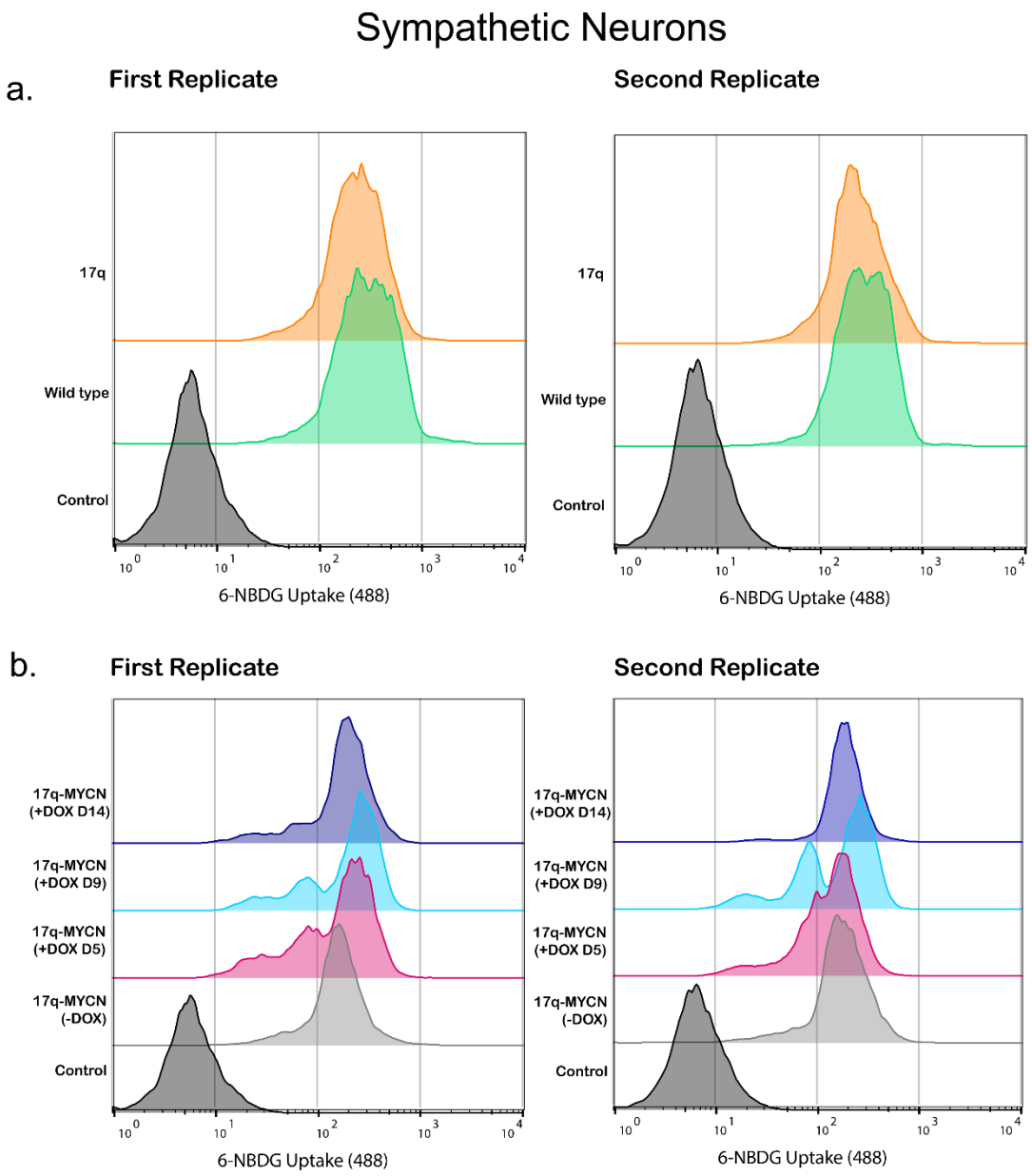

Figure 64. Glucose uptake profile of the wild type, 17q and 17q-MYCN with and without DOX cells during SN differentiation. Flow cytometry histograms for 6-NBDG uptake. Shown are two biological replicates of glucose uptake assay at SN stage **a.** Wild type (green), 17q (orange) and the control untreated sample (black). **b.** 17q-MYCN(-DOX) (grey), 17q-MYCN(+DOX) (magenta), 17q-MYCN(+DOX D9) (Blue), 17q-MYCN(+DOX D14) (Purple) and the control untreated sample (black).

5.2.5 Genome instability

5.2.5.1 MYCN induction in 17q-MYCN cell line results in increased DNA damage

Cells are continuously exposed to potential DNA damage, but one of the most aggressive ones is the called Double-strand breaks (DSB) (Karagiannis and El-Osta, 2004b, Karagiannis and El-Osta, 2004a). A prompt response of the cell to DSBs is the phosphorylation on the Ser-139 of the histone H2AX. To know the level of damage that the different cell lines had along the whole differentiation process, I decided to assess the phosphorylation state of the histone H2AX by using an antibody that would only recognise this particular site (γH2AX antibody). Immunofluorescence images were processed, and only cells that were in the S/G2 phase were analysed as it is during this stage of the cell cycle where damage occurs more frequently (Ichijima et al., 2010).

To verify that the γH2AX antibody was detecting DNA damage, CPT (camptothecin) was used as a control. This drug was selected as it interferes in the DNA replication process, inducing breaks in the DNA(Ferrara and Kmiec, 2004, Avemann et al., 1988). In **Figure 65-a**, immunofluorescence images show wild type NMP cells stained with γH2AX. It can be appreciated at least six cells showing a "whole nuclei" staining (pan-γH2AX), but also other cells showing "speckles" of different sizes inside the nuclei. When cells were treated with CPT for 3 hours, a notorious increase is observed in the number of nuclei showing γH2AX signal.

The phases S/G2 were gated based on the DNA intensity as shown in **Figure 65-b**, the cells that fell within this gate were then analysed for their γH2AX intensity. The wild type and the wild type treated with CPT are shown in **Figure 65-c**. The addition of CPT in the media raises the γH2AX intensity, suggesting that more DNA damage is taking place per nuclei. Traditional γH2AX DNA damage assay quantifies the number of foci per nuclei, but our magnification was not enough to count accurately the foci, therefore we took a similar approach to the flow cytometry-based methods(Johansson et al., 2017), and quantified integrated- intensity (value of each pixel within the nuclei added together) for the comparisons.

To better appreciate the changes in the intensity levels of the γH2AX signal, **Figure 65-d** is presented a relative frequency distribution graph. It can be observed that in cells treated with CPT, more cells showed higher γH2AX intensities per nuclei. Another way of analysing the data is through a Spearman correlation heatmap (**Figure 65-e**). This map is based on the distributions of the intensities, when two conditions equal to 1 it means they are identical. The lower the value the less similar the distributions are. Therefore, when we compare how similar are the wild type and the CPT treated, we conclude that they have a Spearman correlation of 0.67.

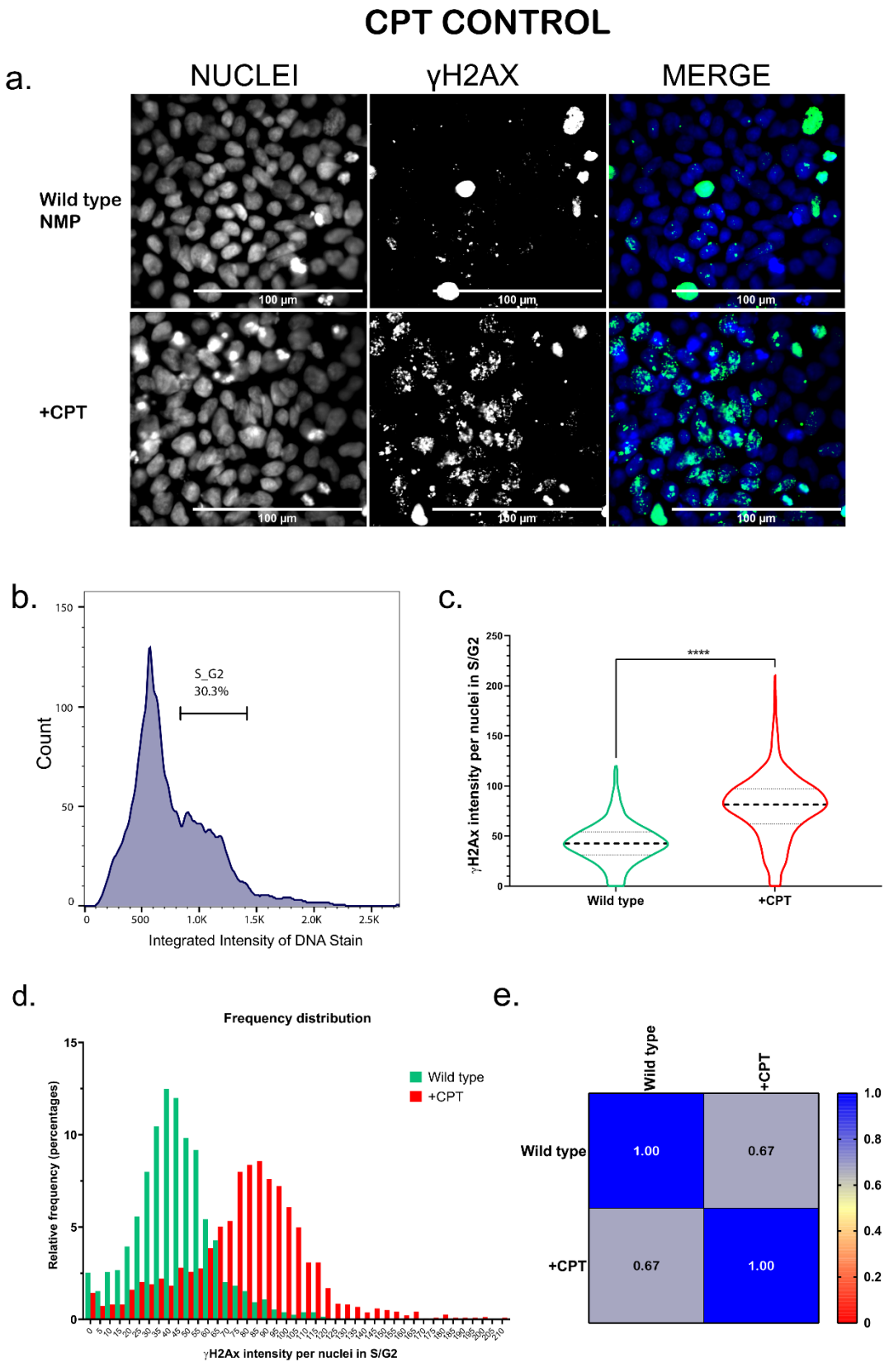
CPT CONTROL
a.
NUCLEI
γH2AX
MERGE
Wild type
NMP
+CPT
100 µm
b.
Count
S_G2
30.3%
Integrated Intensity of DNA Stain
c.
γH2Ax intensity per nuclei in S/G2
****
Wild type
+CPT
d.
Frequency distribution
Wild type
+CPT
Relative frequency (percentages)
γH2Ax intensity per nuclei in S/G2
e.
Wild type
+CPT
1.00
0.67
0.67
1.00

Figure 65. Assessment of DNA damage by γH2AX
a. Immunofluorescence images of the wild type NMP cell line without and with CPT treatment (10ng/ml for 3hrs). Shown is γH2AX (Merge: Hoechst(blue), γH2AX (green). **b.** Cell cycle profile generated from DNA content quantified by Hoechst staining. The bar on the graph depicts the area and the percentage of cells on the S and G2 phases. **c.** Violin plots showing the γH2AX integrated intensity per nuclei of cells in S/G2 for wild type and cells treated with CPT. CPT induced higher levels of DNA damage per nuclei compared to the wild type. (n= 1 biological replicate, >2400 cells analysed per condition, error bars= SD, Kolmogorov-Smirnov test, $p \leq 0.05$= *, $p \leq 0.01$= **, $p \leq 0.001$= ***, $p \leq 0.0001$= ****). **d.** Relative frequency distribution of the γH2AX integrated intensity per nuclei. It can be appreciated that cells treated with CPT showed more cells bearing a higher amount of γH2AX integrated intensity than the control. **e.** Spearman correlation heatmap based on the distributions in **d.** Blue indicates higher similarity, red indicates lower similarity.

DNA damage was assessed at different points during the differentiation process. hPSC and NMP wild type, 17q and 17q-MYCN(-DOX) cells were stained with anti- γH2AX and analysed. In both stages (hPSC and NMP stage) a similar behaviour was observed between the different signals. Interestingly and contra-intuitive, the cells carrying the chromosomal aberrations showed significantly less DNA damage when compared to the wild type (**Figure 66-a,c and Figure 67-a,c**). Spearman correlation heatmaps further corroborated these observations (**Figure 66-b,d and Figure 67-b,d**). The percentage of cells that exhibit "pan- γH2AX" staining was also quantified (**Figure 66-e, Figure67-e**). In both hPSC and NMP stages, wild type cell line presented the highest mean percentage. However, the standard deviations between the replicates were large and had an overlap between the groups, therefore it is difficult to even speculate whether the increase in the mean percentage in the wild type was significant.

I continued to assess the differences in DNA damage between the lines and I began to assess the influence of MYCN overexpression on the level of DNA damage, γH2AX intensity was analysed in the 17q-MYCN cell line. Doxycycline was supplemented from day 5 of the differentiation protocol. Wild type, 17q, 17q-MYCN(-DOX) and 17q-MYCN(+DOX) were analysed at the end of the Neural crest stage (day 9 of the protocol). The Wild type cell line continued to present higher levels of DNA damage when compared to 17q and 17q-MYCN(-DOX). However, when doxycycline was added to induce MYCN expression, a significant increase in DNA damage was observed (**68-a,c,e**). Spearman correlation heatmaps further corroborated these observations (**Figure 68-b,d).** Additionally, when the percentage of "pan-gamma" positive cells was assessed, 17q-MYCN(+DOX) cell line showed a much higher level of damage (**Figure 68-g**). Similar findings were observed during the Sympathoadrenal progenitor stage, although significant differences were found in the "pan-gamma" percentage when doxycycline was added (**Figure 69-a-g**).

During the Sympathetic neuron differentiation stage, the wild type exhibited lower levels of damage similar to those present in 17q and 17q-MYCN(-DOX), contrasting what was observed in the previous stages. However, the overexpression of MYCN continued to elevate the levels of DNA damage and "pan-gamma" percentages (**Figure 70-a-e**).

Certain trends were apparent in all stages of the differentiation. Firstly, the wild type cell line tended to present higher levels of DNA damage when compared to 17q. Secondly, 17q and 17q-MYCN(-DOX) distributions correlated well with each other, visible in the Spearman correlation heatmaps. Finally, the over-expression of MYCN tended to elevate the DNA damage levels in every stage analysed, including those when "pan-gamma" was assessed. Therefore, the over-expression of MYCN is the strongest inducer for DNA damage in the cell culture conditions analysed.

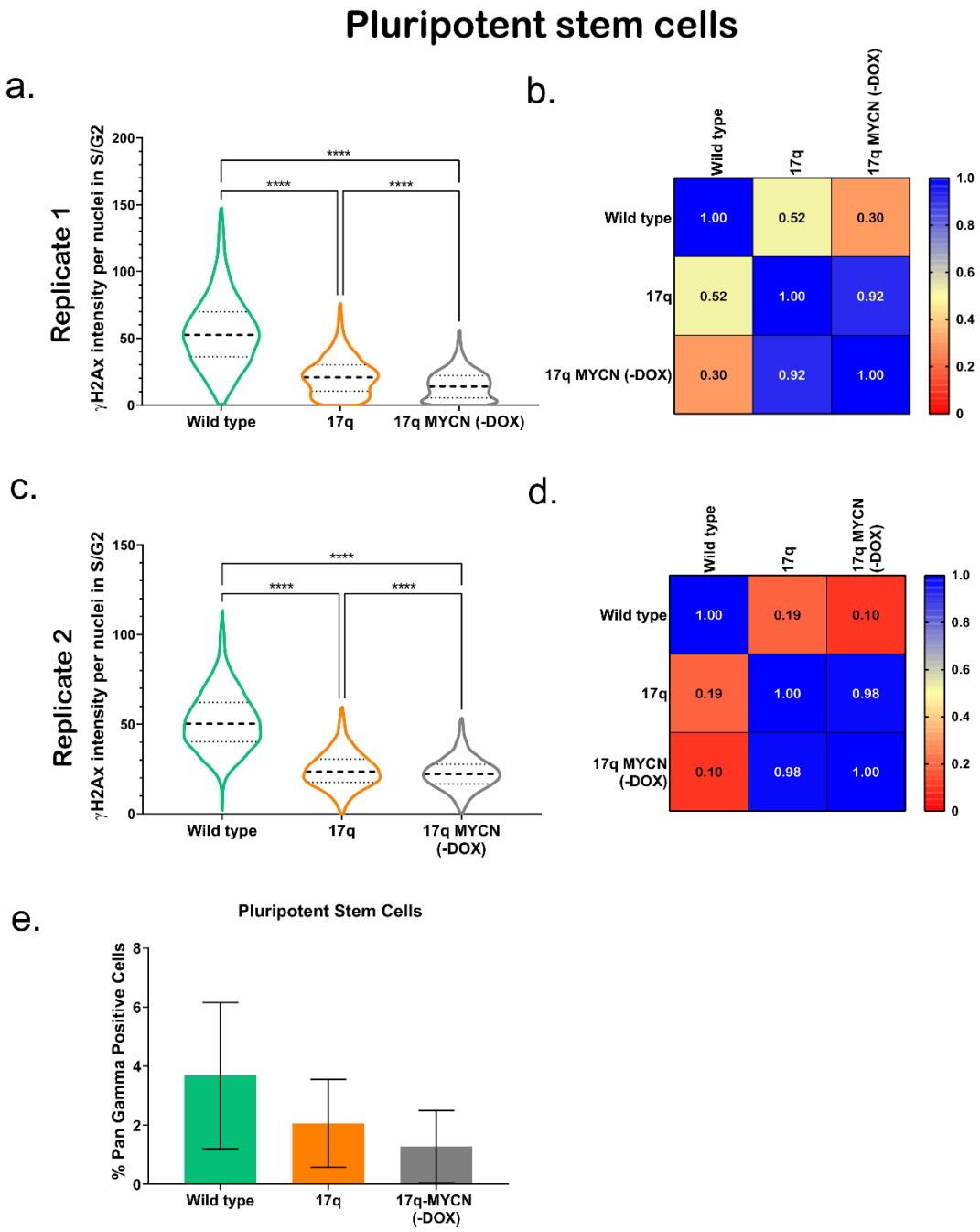

Figure 66. Assessment of the DNA damage on the wild type, 17q and 17q-MYCN(-DOX) pluripotent stem cell population

a,c. Violin plots showing the γH2AX integrated intensity per nuclei of cells in S/G2 for wild type, 17q and 17q-MYCN(-DOX) at the day 0 of differentiation (n= 2 biological replicate, >2000 cells analysed per condition, error bars= SD, Kruskal-Wallis test with Dunn's multiple comparison correction, $p \leq 0.05$= *, $p \leq 0.01$= **, $p \leq 0.001$= ***, $p \leq 0.0001$= ****). **b,d.** Spearman correlation heatmap based on the distributions in **a,c**. Blue indicates higher similarity, red indicates lower similarity. The wild type seems to have an increase of DNA damage compared to the other conditions. **e.** Bar chart showing the percentage of Pan-Gamma cells, n= 2 biological replicates.

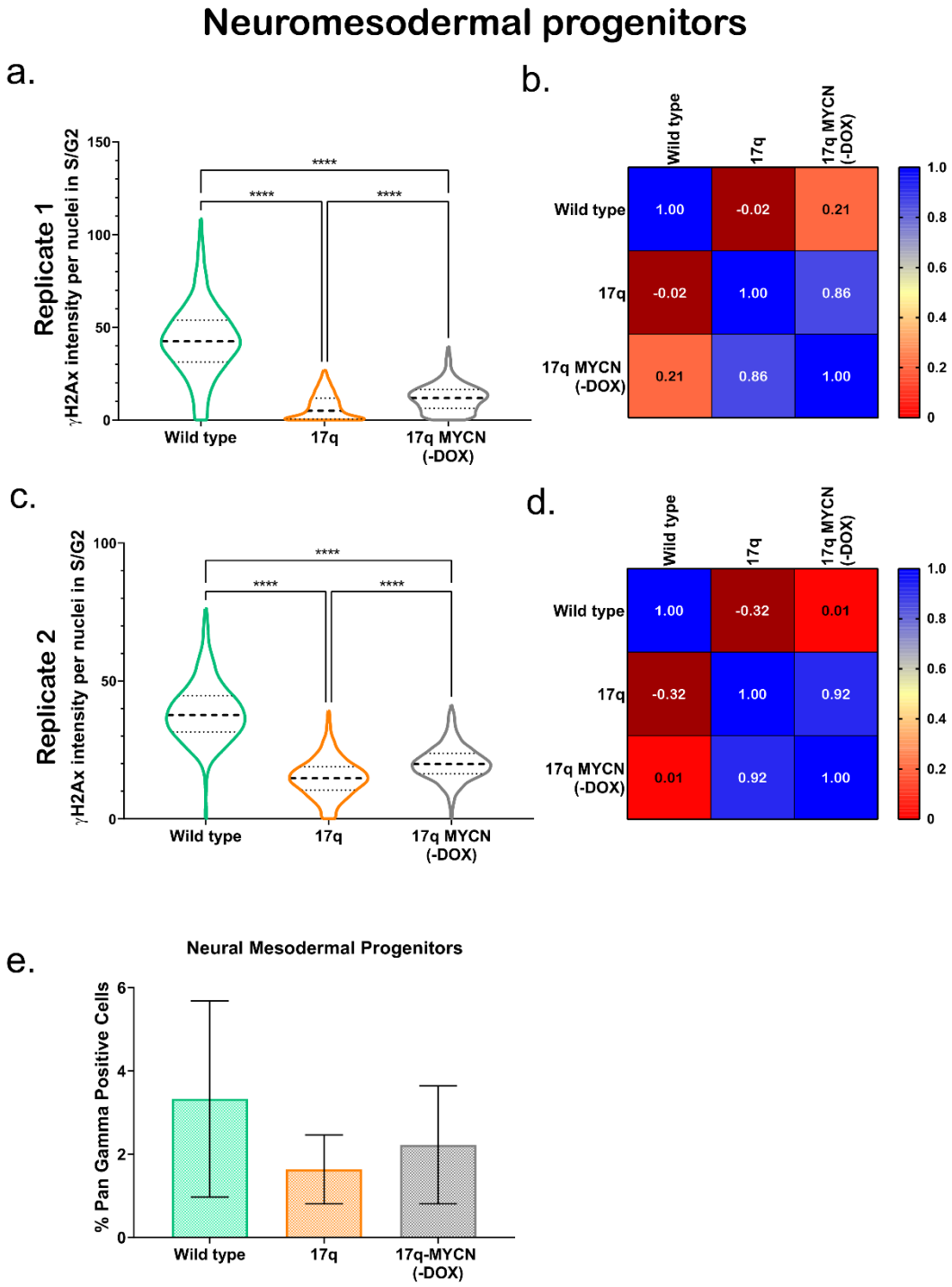

Figure 67. Assessment of the DNA damage on the wild type, 17q and 17q-MYCN(-DOX) at the NMP stage of differentiation

a,c. Violin plots showing the γH2AX integrated intensity per nuclei of cells in S/G2 for wild type, 17q and 17q-MYCN(-DOX) at NMP stage of differentiation (n= 2 biological replicate, >2000 cells analysed per condition, error bars= SD, Kruskal-Wallis test with Dunn's multiple comparison correction, $p \leq 0.05$= *, $p \leq 0.01$= **, $p \leq 0.001$= ***, $p \leq 0.0001$= ****). **b,d.** Spearman correlation heatmap based on the distributions in **a,c**. Blue indicates higher similarity, red indicates lower similarity. The wild type seems to have an increase of DNA damage compared to the other conditions. **e.** Bar chart showing the percentage of Pan-Gamma cells, n= 2 biological replicates.

Neural Crest

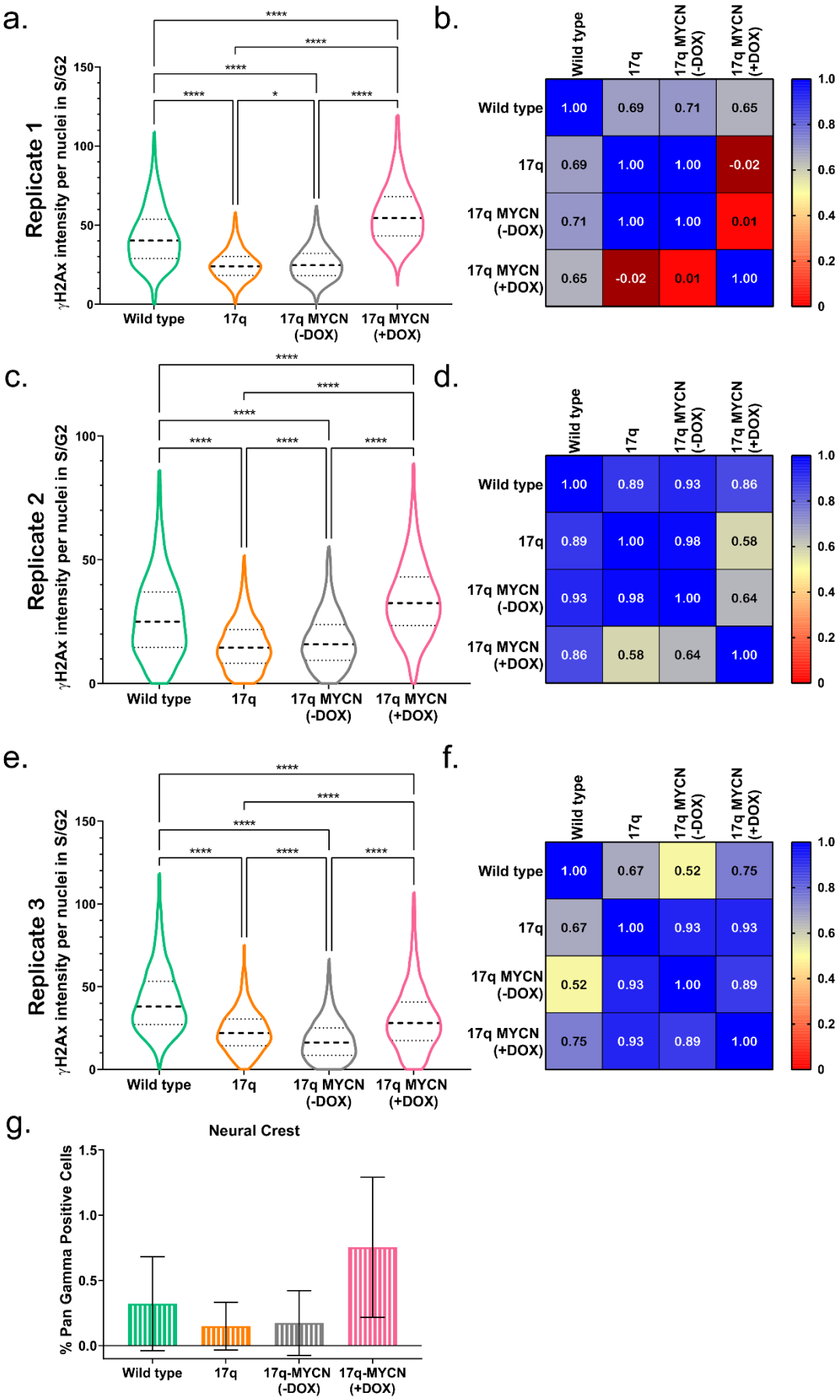

Figure 68. Assessment of the DNA damage on the wild type, 17q and 17q-MYCN(-/+DOX) at the Neural crest stage of differentiation

a,c,e. Violin plots showing the γH2AX integrated intensity per nuclei of cells in S/G2 for wild type, 17q and 17q-MYCN(-DOX) at NC stage of differentiation (n= 3 biological replicate, >2000 cells analysed per condition, error bars= SD, Kruskal-Wallis test with Dunn's multiple comparison correction, $p \leq 0.05$= *, $p \leq 0.01$= **, $p \leq 0.001$= ***, $p \leq 0.0001$= ****). **b,d,f.** Spearman correlation heatmap based on the distributions in **a,c,e.** Blue indicates higher similarity, red indicates lower similarity. The level of damage of the wild type remains higher than the 17q cell line. MYCN overexpression promoted an increase in the level of damage when compared to its control. **g.** Bar chart showing the percentage of Pan-Gamma cells, n= 3 biological replicates. Ordinary One-way Anova with Tukey correction for multiple comparisons.

Sympathoadrenal progenitors

a.

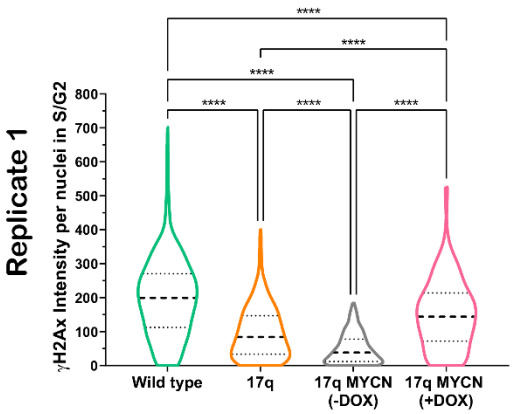

b.

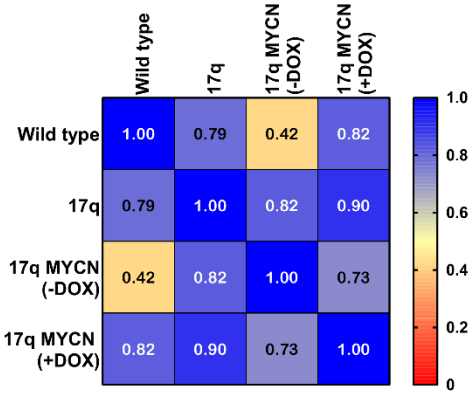

c.

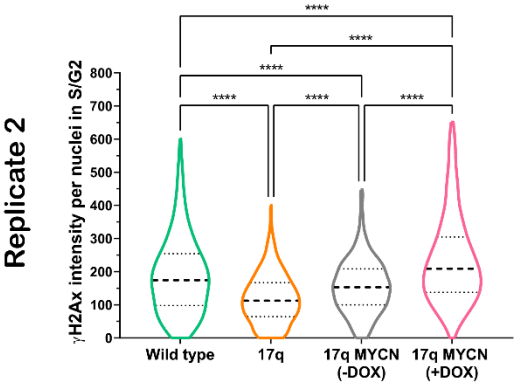

d.

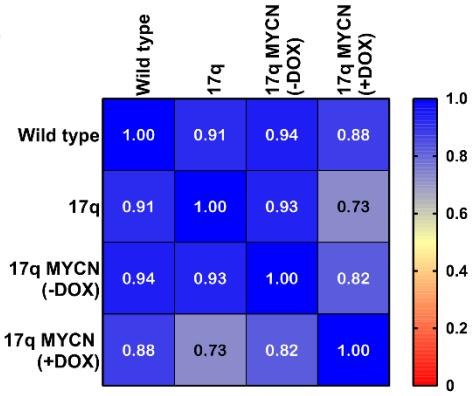

e.

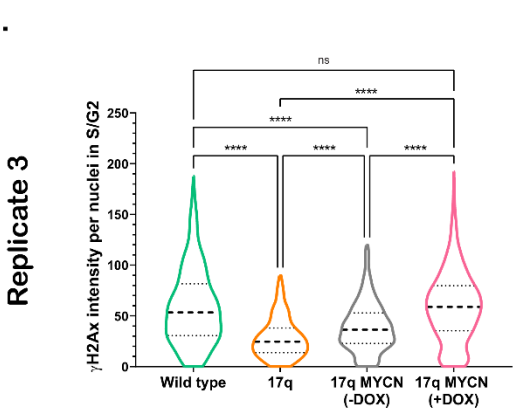

f.

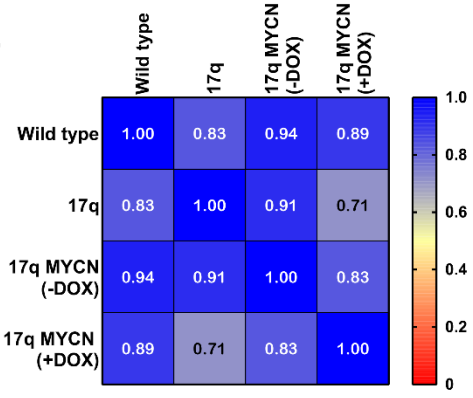

g.

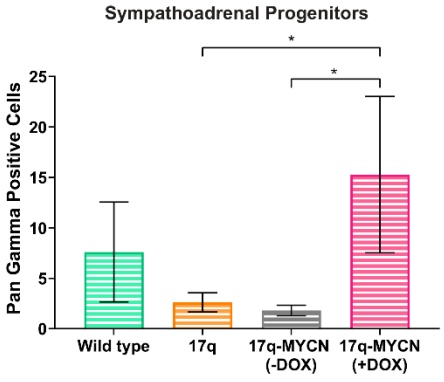

Figure 69. Assessment of the DNA damage on the wild type, 17q and 17q-MYCN(-/+DOX) at the Sympathoadrenal progenitor stage

a,c,e. Violin plots showing the amount of γH2AX foci per nuclei of cells in S/G2 for wild type, 17q and 17q-MYCN(-DOX) at NC stage of differentiation (n= 3 biological replicate, >2000 cells analysed per condition, error bars= SD, Kruskal-Wallis test with Dunn's multiple comparison correction, $p \leq 0.05$= *, $p \leq 0.01$= **, $p \leq 0.001$= ***, $p \leq 0.0001$= ****). **b,d,f.** Spearman correlation heatmap based on the distributions in **a,c,e.** Blue indicates higher similarity, red indicates lower similarity. The level of damage of the wild type remained similar to the observed one in the previous stages. Also, the amount of DNA damage in the 17q-MYCN(+DOX) stayed high, whereas 17q and 17q-MYCN(-DOX) showed more variability but tending to an increase in damage. **g.** Bar chart showing the percentage of Pan-Gamma cells, n= 3 biological replicates. MYCN overexpression increased significantly the percentage of Pan-Gamma positive cells when compared to control. Ordinary One-way Anova with Tukey correction for multiple comparisons ($p \leq 0.05$= *).

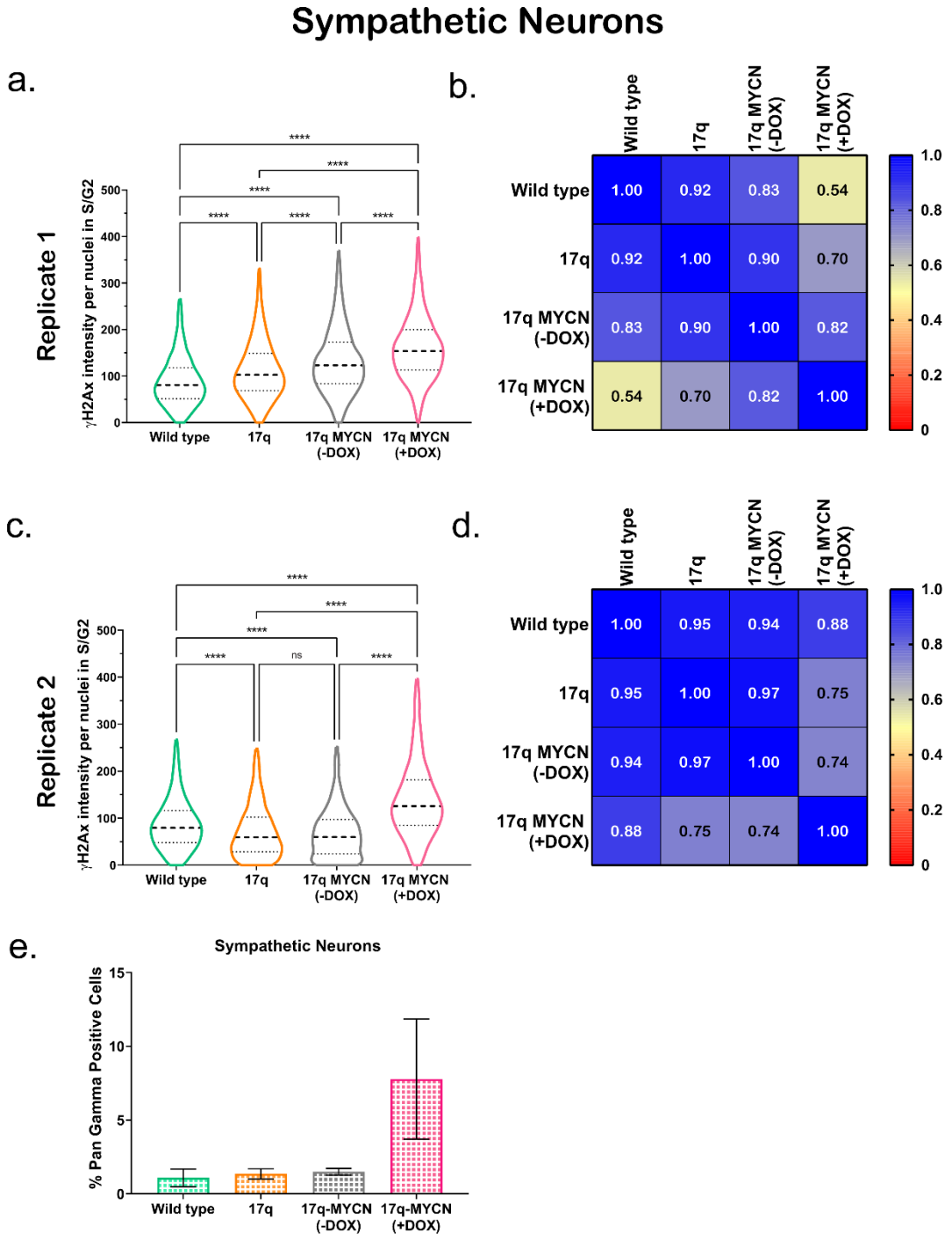

Figure 70. Assessment of the DNA damage on the wild type, 17q and 17q-MYCN(-/+DOX) differentiated into sympathetic neuron cells.

a,c,e. Violin plots showing the amount of γH2AX foci per nuclei of cells in S/G2 for wild type, 17q and 17q-MYCN(-DOX) at NC stage of differentiation (n= 2 biological replicate, >2000 cells analysed per condition, error bars= SD Kruskal-Wallis test with Dunn's multiple comparison correction, $p \leq 0.05$= *, $p \leq 0.01$= **, $p \leq 0.001$= ***, $p \leq 0.0001$= ****). **b,d,f.** Spearman correlation heatmap based on the distributions in **a,c,e.** Blue indicates higher similarity, red indicates lower similarity. The level of damage of the wild type remained similar to the observed one in the previous stages. Also, the amount of DNA damage in the 17q-MYCN(+DOX) stayed high, whereas 17q and 17q-MYCN(-DOX) remained variable. **e.** Bar chart showing the percentage of Pan-Gamma cells, n= 2 biological replicates.

5.3 Discussion

The acquisition of cancer hallmarks remains fundamental in disease initiation and progression, thus assessment of these traits remains vital in assessing *in vitro* based models. I have tested a small range of these features to identify early indications of tumour-like characteristics. The most prevalent feature in tumours is their ability to proliferate indefinitely. Therefore, I assessed this by using two robust approaches. The EdU technique allowed us to visualise the number of cells entering the S phase at different stages of the differentiation protocol, whereas Ki-67 staining provided a broad view of the proportion of cells cycling.

Wild type and 17q cell line showed very little differences during NMP differentiation in terms of cell proliferation when analysed by EdU and Ki-67 assays. However, further during differentiation differences became apparent with higher Ki-67 percentages in the wild type cells in both NC and SAP stages (**Figure 58- c,d**). These changes in Ki-67 and coupled with the lack of differences in cells entering the S phase at NC and SAP stages might indicate a larger proportion of cells in G0 in the 17q cell line as Ki-67 is not present in non-cycling cells (Gerdes et al., 1984).

On the other hand, MYCN overexpression seemed to be a powerful inducer of cell cycle progression, as its expression was enough to increase the number of cells entering the S phase at all stages of differentiation. Ki-67 expression was also enhanced in the presence of MYCN induction. Its influence was the most pronounced during the SAP stage (**Figure 58-e**).

MYCN has been previously reported to induce cells to re-enter the S phase in postmitotic sympathetic neurons(Wartiovaara et al., 2002). MYCN exerts control on the cell cycle through its interactions with Cyclin-dependant Kinase 4 (CDK4), the S-phase kinase-associated protein 2 (SKP2) and inhibition of CDK inhibitors (Muth et al., 2010, Evans et al., 2015, Ryl et al., 2017). Ryl et al, 2017 demonstrated in high-MYCN neuroblastoma cell lines that MYCN blocks the entry into G0 even when DNA damage has occurred.

Cells going through high levels of stress can present deficiencies in their survival and proliferation behaviour. The plating of cells at low densities challenges their ability to overcome this external stress to form a colony(Menyhárt et al., 2016). When assessing all cell lines, we found that the overexpression of MYCN gave a significant advantage to the cells yielding a higher number of colonies (**Figure 59-b**).

Cancer cells require an elevated supply of glucose to fuel their proliferation rates, to do so cancerous cells normally utilise glycolysis as their first source of energy over the alternatives pathways (reviewed in (Liberti and Locasale, 2016, DeBerardinis and Chandel, 2020)). Neuroblastomas high affinity for

glucose uptake has been used to target tumour masses for identification and treatment using a glucose analogue(Dhull et al., 2015). We used a 6-NBDG, a glucose analogue, to assess uptake *in vitro* at the different stages of the protocol. I only observed the most prominent changes at the SAP stage when MYCN was overexpressed from day 5 and day 9. Two apparent populations were present showing higher and lower glucose uptake profiles. Interestingly, the addition of doxycycline at day 14 had minimal effect on the glucose profile. Possible explanations for this could be that cells at the SAP stage might be more dependent on glucose, perhaps due to changes in glucose transport(Ramani et al., 2013, Mendez et al., 2002). The lowest fraction of cells might be undergoing apoptosis. It has been shown that neuroblastoma cells in culture are sensitive to treatment with glucose analogues(Tjaden et al., 2020). Although, it has also been observed that cells undergoing apoptosis do not change their glucose uptake levels (Pradelli et al., 2014). A second possibility could be that cells have acquired metabolic plasticity and switched to a different energy source as has been shown in cancer cells(Bergers and Fendt, 2021). Furthermore, the expression of MYCN has been linked to a switch towards glutaminolysis in neuroblastoma(Wang et al., 2018). Nevertheless, this heterogeneous population seems to mainly exist in the SAP stage and requires further investigation to fully understand this context dependant phenomenon.

The most striking and perhaps the most noticeable feature of the cells were the morphological changes exhibited by MYCN overexpressing cells during the SAP stage of differentiation. Before this stage, all cell lines seemed to display similar morphology. Interestingly, when MYCN was induced at later stages (day 9) the dome-like morphology appeared again. However, when doxycycline was supplied on day 14 this morphology was not observed. As the cells are moving to the SN stage, we see an outgrowth of cells with another morphology distinct to the dome-like and the control neurons.

The presence of genetic instabilities is a common characteristic in cancer (Negrini et al., 2010). This is possibly triggered by DNA damage induced by aberrant expression of oncogenes (Halazonetis et al., 2008). Therefore, we decided to analyse the level of DNA damage during the differentiation by examining the phosphorylation status of the histone H2AX (a mark of double-strand break damage). Overall, an increase in DNA damage was observed on the wild type cell line when compared to the 17q in most of the differentiation, with the exception of the SN stage where wild type showed similar levels of damage to 17q. This disparity between the wild type and 17q might be explained by the presence of an extra copy of BRCA1, which is located in 17q21.31. This gene has been reported to contribute to the repair of DNA damage, especially DSBs and activate the homologous recombination mechanism (reviewed in Yoshida and Miki, 2004)(Yoshida and Miki, 2004). Conversely, the induction of MYCN expression correlated with a significant increase in DNA damage in all stages of differentiation. In this sense, MYCN has been linked to an increase in the replication fork stalling

causing a rise of the DNA damage during the S phase(King et al., 2020). Also, it has been reported to participate in the delay of the resolution of DNA damage, leading to an inefficient repair (Ambrosio et al., 2015).

17q and MYCN are two of the most common aberrations found in Neuroblastoma, therefore it is important to understand their individual contributions in a temporal manner to the onset of cancer-like features. In our analysis, MYCN overexpression on a 17q background showed the strongest influence in initiating cellular dynamics similar to those observed in tumours. In the hallmarks analysed, the addition of doxycycline stimulated an increase in cell proliferation marked by Ki-67 and Edu incorporation in S-phase. The latter could partially explain its notable capacity to form colonies when plated at low density. Although the glucose assay was heterogeneous, it demonstrated that dysregulation was triggered only when MYCN was overexpressed and specific to the SAP stage. Finally, as it has been previously reported, the overexpression of the oncogene MYCN lead to an increase in the DNA breaks, these could give rise to further acquisition of aberrations as seen *in vivo* models(Weiss et al., 1997, Olsen et al., 2017, Cohen et al., 2020). Strikingly, 17q aberration alone did not show any remarkable differences when compared to the wild type. However, we do not discard that 17q could influence hallmarks not assessed in this work, nor that 17q might influence the later stages of development.

6 Final Discussion

Despite the plethora of approaches developed to understand the mechanisms implicated in the onset and progression of neuroblastoma, up to date some key questions remain unanswered. Firstly, although the consensus is the disease is of a neural crest origin(Olsen et al., 2017, Schulte et al., 2013, Montavon et al., 2014, Delloye-Bourgeois and Castellani, 2019, Tomolonis et al., 2018, Jiang et al., 2011, Gonzalez Malagon and Liu, 2018), but for some, this is still a matter of debate (Yang et al., 2020b). Secondly, even though 17q gain is present in above 50% of the tumours and is related to poor prognosis, very little is known about its particular contribution to neuroblastoma aetiology. Finally, although MYCN oncogenic potential is well established, the specific timing of aberrant overexpression to trigger the neuroblastoma phenotype is still not well defined. Current models do not allow for the precise temporal dissection required to answer these questions, partially due to the rapid nature of some of the processes that occur during neural crest specification but also, the difficulty in manipulating the signals of such processes *in vivo*.

In this thesis, I demonstrated how hPSC can be used as a tool to recapitulate the temporal aspects of neurocristopathies, in this case, neuroblastoma *in vitro*. The model allows for the assessment of disease-specific mutations. I showed the first neuroblastoma model specifically aimed to evaluate one of the most common aberrations, 17q gain. In this system, the gain of 17q showed a possible dysregulation in the response to lower levels of WNT signalling during trunk neural crest differentiation, as cells struggle to maintain their axial identity. Moreover, we exploited the system further using a MYCN-inducible hPSC line on a 17q background, finding a susceptible time window that might exist rather than a specific time-point for MYCN initiation of neuroblastoma. To our knowledge, this is the first **fully** *in vitro* model using human cells to dissect the mechanisms of neuroblastoma initiation.

The gain of the 17q chromosome is linked to high-risk neuroblastoma, although the exact mechanisms by which it influences neuroblastoma aetiology are as yet not well understood. Analysis of the influence of 17q aberration during this differentiation protocol suggested a differential response to WNT signalling, but the specifics of this mechanism needs further investigation. Later in differentiation, the 17q cell line showed upregulation in both *ASCL1 and MYCN*, both of which have been reported to be members of the adrenergic core regulatory circuitry in neuroblastoma. In this study, it was found that ASCL1 plays a role in cell growth and the blocking of differentiation (Wang et al., 2019, Wylie et al., 2015). Ideally, cells in our current study should be allowed to mature further. This would allow firstly, to see if ASCL1 remains upregulated and secondly, to see if such upregulation would prevent them to reach a post-mitotic stage.

Our work with MYCN on the 17q background highlighted the powerful effect it possesses on not only the cell fate decisions but also physiological characteristics. What was clear from this data is that the induction of MYCN at day 5 and day 9, roughly corresponding to the neural crest specification and neural crest delamination time points in vivo, behaved in the same manner. Showing not only similarities in their morphology and transcriptional profiles but also both exhibited similar patterns of glucose uptake. Interestingly, the most noticeable changes were observed during the sympathoadrenal progenitor induction corresponding to days 10 to 14. Conversely, when MYCN was induced at a later point of differentiation (day 14), no noticeable changes were observed when compared to non-induced control. This data suggests that during the neural crest stage of differentiation towards the sympathetic lineage a time window might exist where cells are more susceptible to MYCN influence, which manifests later during the sympathoadrenal specification. Future work could be done to further specify the time window of MYCN impact by inducing its expression at closer time intervals. Another advantage that the model offers and that could be explored is the titration of different levels of MYCN induction throughout the process and their effect on the differentiation. With this in mind, we performed a preliminary comparison of MYCN levels between our cell line and some of the most common neuroblastoma cell lines. After data normalisation, our cell line overexpressing MYCN at day 9 of differentiation exhibited equivalent levels of MYCN expression to those observed in several MYCN-amplified neuroblastoma cell lines (**Appendix Figure 1**).

Perhaps, the most remarkable transcriptional change observed was the strong downregulation MYCN overexpression seems to have on SOX10. The specifics of this interaction were not covered in this work, nor could I find any published papers detailing this potential interplay. Interestingly, a recent paper has found SOX10 expression to be absent in a subset of neuroblastoma tumours, suggesting that perhaps the cell of origin of neuroblastoma might not be neural crest(Yang et al., 2020b). To further test this hypothesis, they created a transgenic mouse that overexpresses MYCN upon the expression of SOX10. This resulted in perinatal lethality leading the authors to conclude that the cell of origin could not be SOX10+ neural crest. However, based on our model, MYCN overexpression prior to or coinciding with SOX10 expression leads to the loss or downregulation of SOX10. Therefore, they could, unknowingly, elicited the same response that I observed. It is worth noting that knock-out studies of SOX10 displayed similar perinatal lethality at embryonic day 18.5(Britsch et al., 2001, Mollaaghababa and Pavan, 2003) resulting from fewer migrating neural crest cells plus increased apoptosis during later maturation stages. Therefore, this cannot exclude the possibility that neural crest might still be the cell of origin of neuroblastoma, as regular cancers likely arise from an individual/small population of aberrant cells, not an entire cell lineage.

The precise control mechanisms governing MYCN control over SOX10 expression are not known requiring further analysis. One possible explanation could be through the interactions between SOX10 and N-MYC interacting (NMI) protein which have been reported in glial cells, gliomas and in the spinal cord (Schlierf et al., 2005). To investigate this and other possible mechanisms, a more detailed analysis is needed. We have sent samples for bulk and single-cell RNA-seq, and ATAC-seq which we hope will shed some light on this by comparing with other databases on neuroblastoma tumours, cell lines and normal sympathetic development. Interestingly, single-cell RNA-seq data from three separate groups highlight the common theme of a block in differentiation in neuroblastoma development, although they differ in their specific proposed cell of origin, their studies speak to a similar idea of a time frame, ranging from neural crest EMT-like cells up to chromaffin-like cells. In these studies, MYCN amplified tumours were related to an earlier undifferentiated state similar to EMT-neural crest-like cells (Jansky et al., 2021, Dong et al., 2020, Kildisiute et al., 2021).

Beyond the transcriptional changes, we noticed alterations associated with the hallmarks of cancer such as increased colony-forming capacity, a higher proportion of proliferative cells, dysregulation of glucose uptake, and finally significant increase in DNA damage. It would be interesting to expand the panel of cancer traits assessed using *in vitro* assays detailed in **Figure 71**. With respect to DNA damage, MYCN is associated with chromosomal aberrations (Bown et al., 2001) and in *in vivo* mouse models of MYCN overexpression, gains in chromosome syntenic to human neuroblastoma have been observed (Weiss et al., 1997, Althoff et al., 2015, Cohen et al., 2020). Therefore, it would be interesting to assess in our system if the DNA damage induced by MYCN leads to the development of chromosomal aberrations, possibly related to the gains/losses seen in human neuroblastomas. This could be assessed at the end point of our differentiation by traditional karyotyping by metaphase-spread G banding or more rapidly primers could be designed to assess gains/losses by qPCR similar to the method described in Laing et al 2019 (Laing et al., 2019).

The protocol that has been used in this work was developed to obtain higher efficiencies of trunk neural crest cells and, therefore allowing for further successful differentiation of the sympathoadrenal lineage. We took advantage of this system in order to model neuroblastoma onset and progression while inducing MYCN overexpression in a 17q genetic background. The trunk neural crest generation system is based on the sustained activity of the WNT pathway. This is achieved by inhibiting GSK3-β, which is a key component of the β-catenin destruction complex. This inhibition permits β-catenin to be released and allows its translocation to the nucleus where it will bind and promote the expression of canonical WNT targets (MacDonald et al., 2009). Therefore, we used it to mimic WNT signalling. Nonetheless, by doing this we are also bypassing the participation of the WNT receptors such as Frizzled-2 (FZD2), and the activation of WNT signalling by WNT ligands secreted by the cells, such as

WNT3. In particular, FZD2 and WNT3 expression have associated with high-risk neuroblastoma tumours and both reside in the long arm of chromosome 17(Duffy et al., 2016, Zins et al., 2016). Aside from its role in β-catenin signalling, GSK-3β has other roles such as the post-translational modification of MYCN, which leads to its destabilisation (Suenaga et al., 2014, Otto et al., 2009). The ALK signalling pathway has demonstrated similar inhibition of GSK-3β (Chesler et al., 2006). Fortunately, because our *in vitro* system is adaptable, we could circumvent this issue by the use of recombinant WNT ligands, represented in **Figure 72**.

Another limitation that our system possesses is that 17q is always present throughout the whole differentiation. Although unproved, it is unlikely that 17q or any chromosomal aberrations would be present as early in *in vivo* development. Otherwise, they would be present in other lineages as well. Therefore, assessment of 17q exclusively at certain specific stages during the differentiation is not achievable in this system. However, the system still represents, possibly the only system, which can assess the impact of 17q addition at these early stages of development.

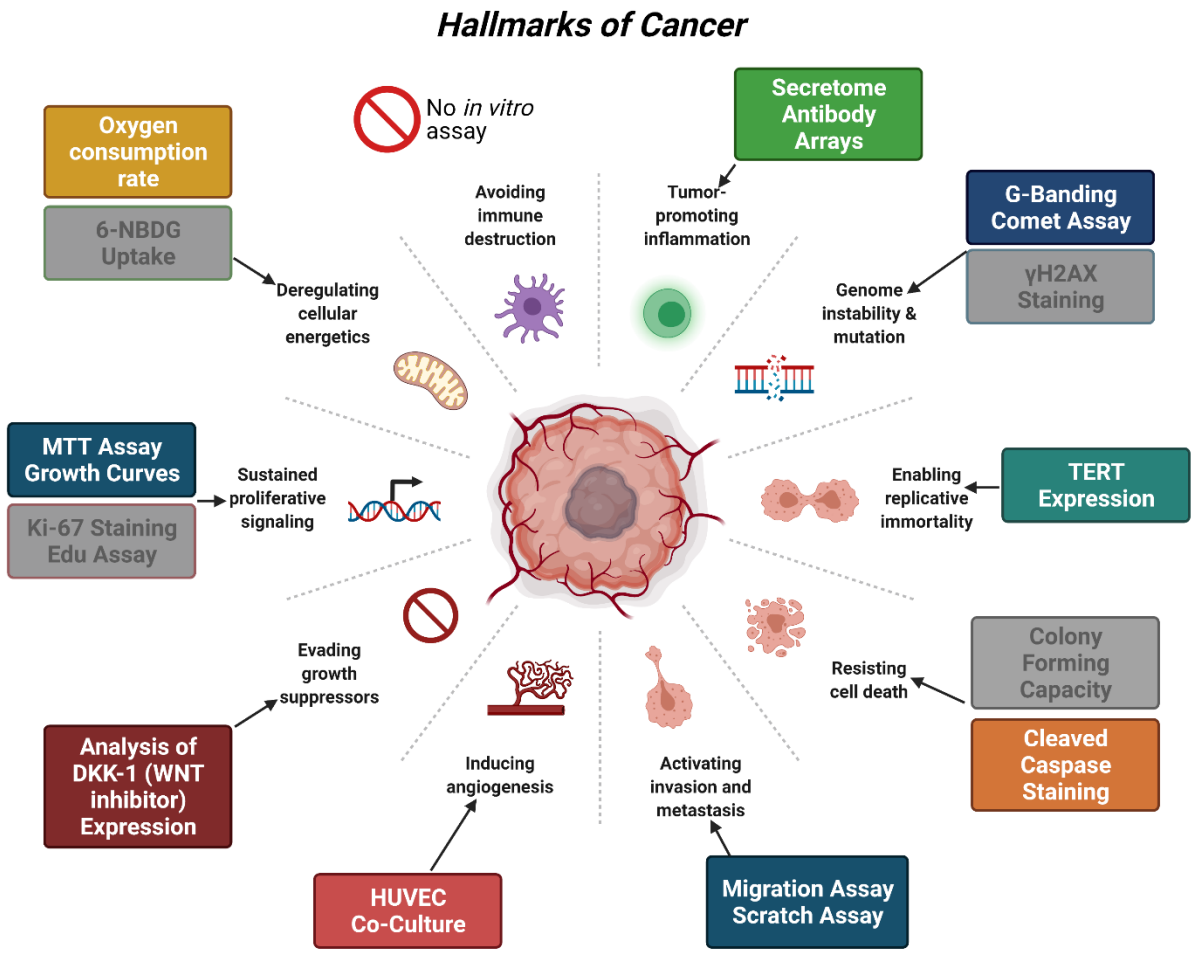

Figure 71. Current Hallmarks of cancer and *in vitro* assays for assessment.

Illustration adapted from Hanahan and Weinberg, 2011. Shown are the different capabilities that allow tumours to proliferate and disseminate successfully. Grey-out boxes on the outside display the assays used in this work to test particular hallmarks. Coloured boxes represent in vitro assays that could be used to assess other cancer hallmarks, approaches reviewed Ward et al, 2014. Created with BioRender.com.

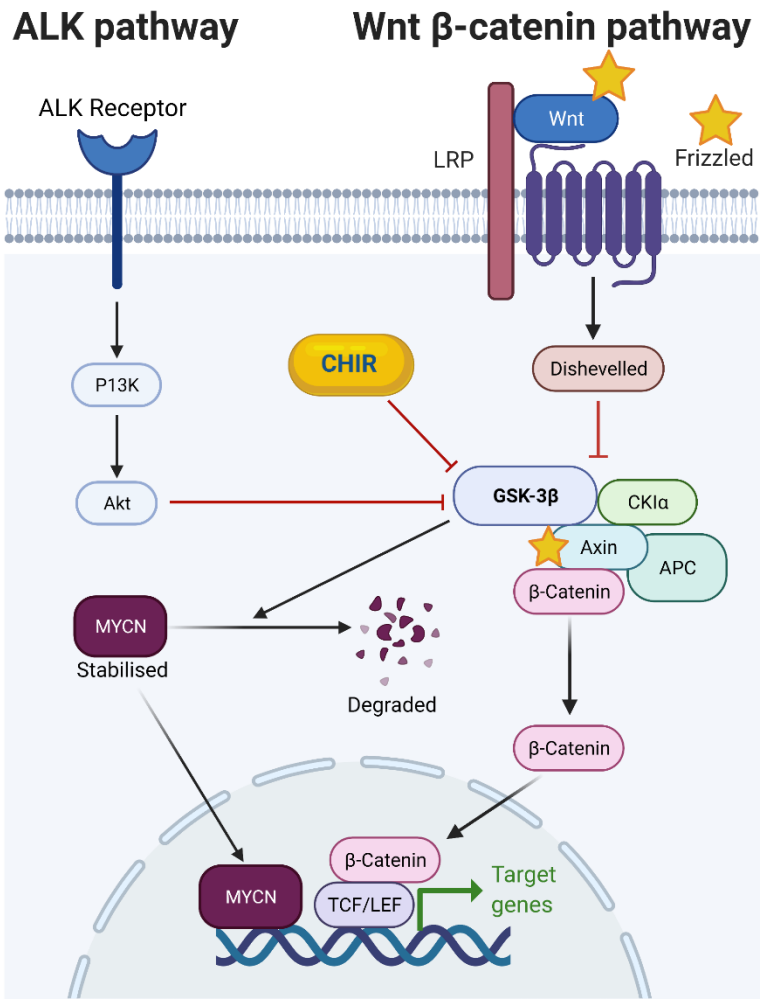

Figure 72: The overlapping actions of CHIR and ALK signalling.

Representation of the WNT signalling and ALK signalling and how GSK-3β inhibition could affect both. Proteins marked with Yellow stars are encoded by genes on the long chromosome 17. Created with BioRender.com

Finally, a disadvantage of the present system is that it is difficult to assess the individual contribution of MYCN in the onset of neuroblastoma-like features in culture. Additionally, the gain of 1q within the 17q-MYCN cell line during transfection added another level of complexity to the analysis, as this acquisition made it harder to dissect the individual contribution that 17q gain had during the differentiation when MYCN was overexpressed. Therefore, in order to resolve these issues, shortly prior to writing this manuscript, we were able to engineer both wild type and 17q cell lines carrying a MYCN-inducible system with an mScarlet reporter (the plasmid was a gift from Miller Huang, Children's Hospital, Los Angeles, USA) (**Appendix Figure 2-a,b**). These cell lines have currently been single-cell sorted and clonal lines established. However, prior to this process and because of the short period of time before submission, we did some preliminary analysis on the mixed population of the wild type cell line and segregate based on mScarlet expression (**Appendix Figure 2-c,d**). Induction of MYCN oncogene was done on day 5 and day 9 of the differentiation protocol and analysis was performed on day 14 (SAP stage). mScarlet expression showed a heterogeneous but generally elevated level of MYCN protein by immunofluorescence analysis (**Appendix Figure 2-e,f**). Both induction conditions showed a significant increase in DNA damage assessed by γH2AX intensity in mScarlet positive cells, in concordance with our previous observations with the 17q-MYCN line (**Appendix Figure 2-g**).

Due to the nature of this defined system on the control of WNT and BMP signalling during Neural crest specification, it is advisable to focus in-depth observations at post-neural crest stages where the system works more "freely" and subtleties within the population possess a higher impact on cell fate. Therefore, if in the future the researchers would want to expand this "window of freedom", pertinent modifications related to the control of neural crest fate should be applied to the protocol. For example, removing DMH1, a selective inhibitor of BMP receptor, might reveal differential responses in BMP signalling during neural crest specification.

Overall, our system offers a dynamic platform for future *in vitro* investigations of neuroblastoma. This system allows the assessment of the individual contribution of high-risk associated traits, in this case, 17q gain and MYCN overexpression. Moreover, it is possible to dissect the differentiation towards the sympathetic lineage in a temporal manner, permitting us not only to analyse in detail potential molecular interactions but also making it possible to test different MYCN expression levels, similar to those observed in different types of neuroblastoma tumours. Equally, MYCN overexpression can be induced at different crucial time points of the differentiation, allowing us to better understand its contribution to cancer initiation. Due to the nature of this platform, it is adjustable for high-content drug screening providing a potent and cost-effective instrument for the identification of clinically relevant treatments. Additionally, it is possible to recreate an environment of cancer-like cells

cohabiting with wild type cell lines, allowing us to investigate how cancer-like cells influence their neighbours. I believe that we have demonstrated the power and feasibility of this tool, and I hope it can be of use to others in the field enabling a better understanding of the ever-evolving and highly elusive mechanisms of neuroblastoma.

7 Appendix

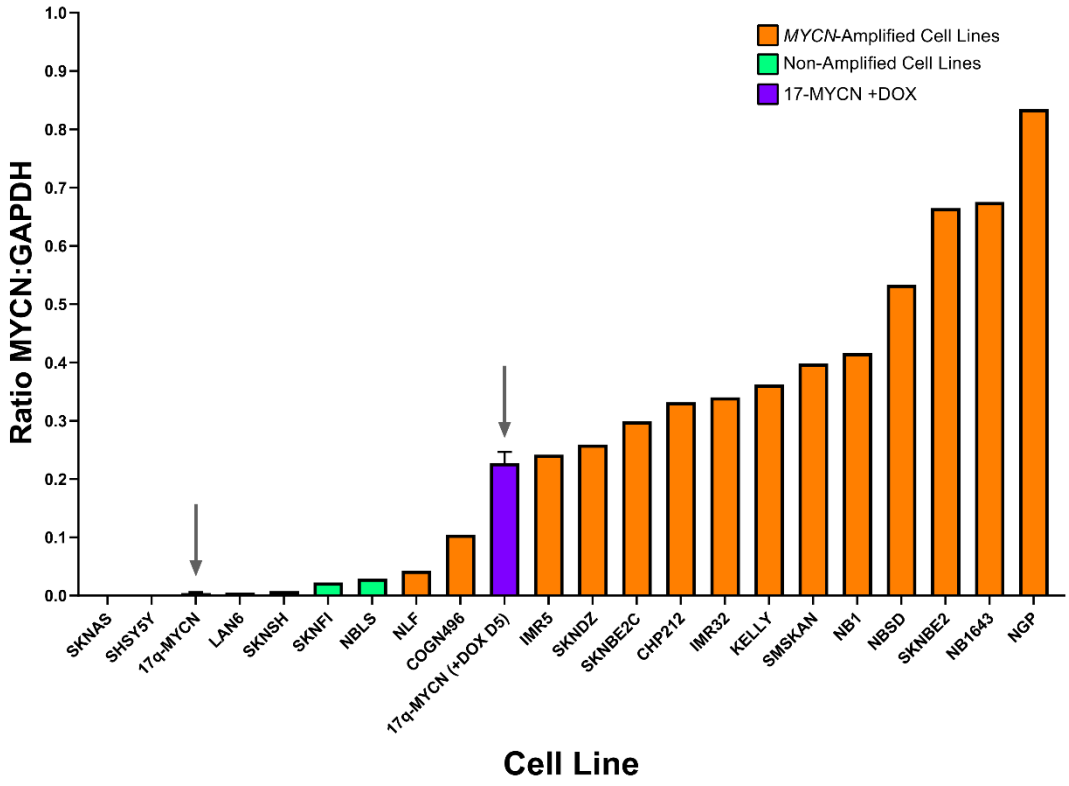

Appendix Figure 1: MYCN expression levels induced in our systems are similar to those assessed in neuroblastoma cell lines.

The bar chart shows the ratio of MYCN to GAPDH of some common neuroblastoma lines assessed by RNA sequencing in Harenza et al 2017 and the 17q-MYCN line at the neural crest stage with and without doxycycline assessed by qPCR. RNA sequencing ratios were calculated using the Fragments per Kilobase per Million (FPKM) values for GAPDH and MYCN. qPCR ratios were calculated using CT values for GAPDH and MYCN, then 2^ΔCT transformed.

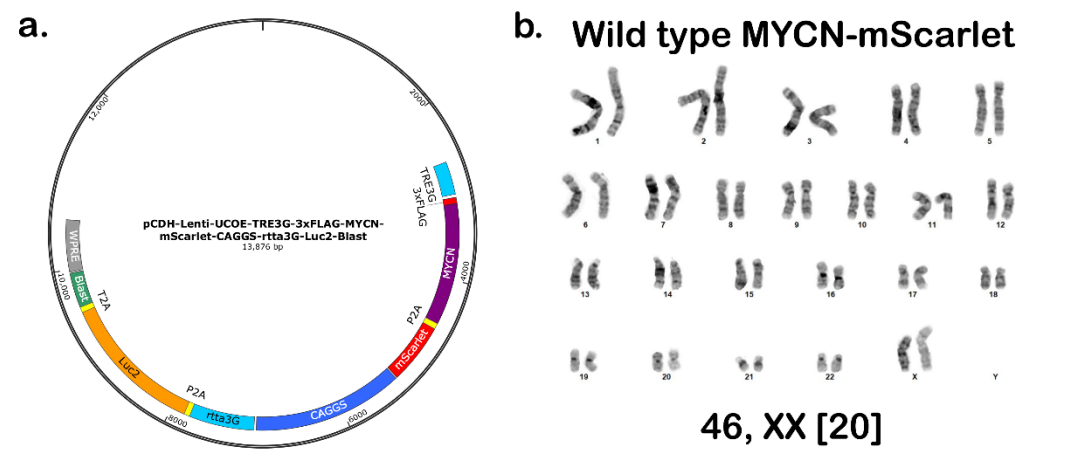
a.
pCDH-Lenti-UCOE-TRE3G-3xFLAG-MYCN-mScarlet-CAGGS-rtta3G-Luc2-Blast
13,876 bp
TRE3G
3xFLAG
MYCN
P2A
mScarlet
CAGGS
rtta3G
P2A
Luc2
T2A
BSD
WPRE
b.
Wild type MYCN-mScarlet
46, XX [20]

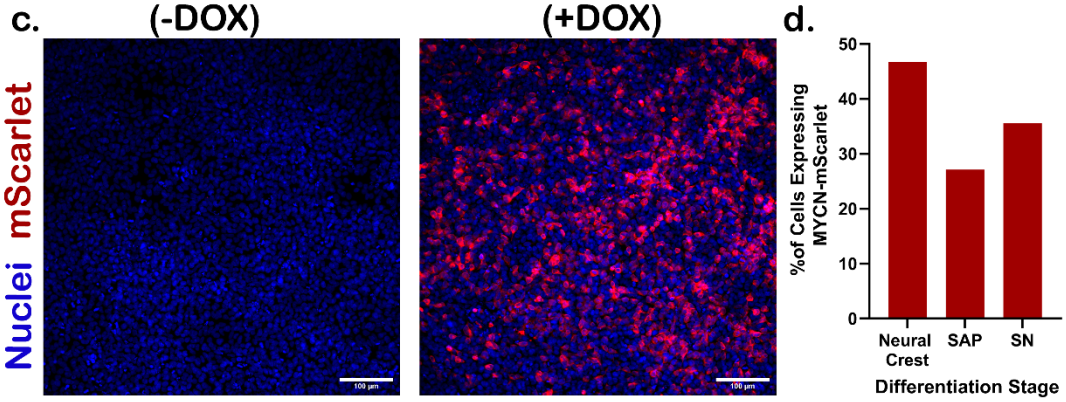
c.
(-DOX)
(+DOX)
Nuclei mScarlet
d.
%of Cells Expressing MYCN-mScarlet
Neural Crest
SAP
SN
Differentiation Stage

SAP Stage:

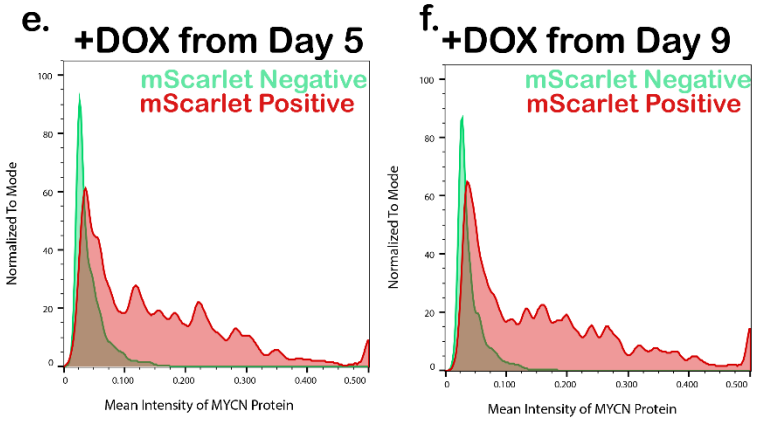
e.
+DOX from Day 5
mScarlet Negative
mScarlet Positive
Normalized To Mode
Mean Intensity of MYCN Protein
f.
+DOX from Day 9
mScarlet Negative
mScarlet Positive
Normalized To Mode
Mean Intensity of MYCN Protein

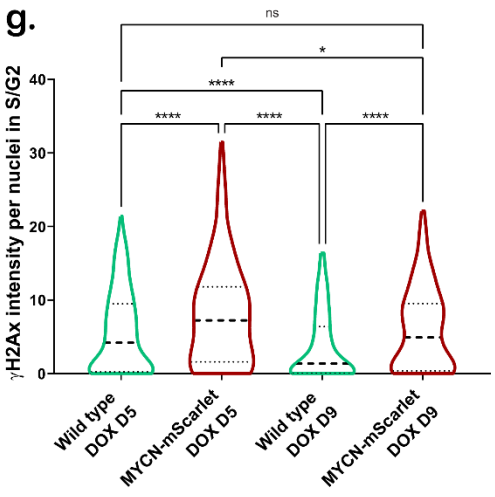
g.
γH2Ax intensity per nuclei in S/G2
ns
*
****
****
****
****
Wild type DOX D5
MYCN-mScarlet DOX D5
Wild type DOX D9
MYCN-mScarlet DOX D9

Appendix Figure 2. Generation and assessment of the DNA damage of a wild type line overexpressing MYCN-mScarlet during sympathetic lineage differentiation.

a. Plasmid construct of inducible MYCN-mScarlet. **b.** Wild type (H7) cell line, carrying the inducible MYCN-mScarlet, karyotype, showing a normal diploid chromosome number (46, XX). In square brackets is shown the number of metaphase spreads analysed. 30 cells examined gives a 95% chance of detecting a 10% population. **c.** Immunofluorescence images, merge: Hoechst(blue), MYCN-mScarlet (magenta). **d.** Bar-chart showing percentage MYCN-mScarlet cells at different stages of differentiation. **e,f.** Histograms of Mean florescent intensity plotted per cell of MYCN Protein from mScarlet negative (green) and mScarlet positive(red) at the SAP stage, day 14 with doxycycline added from **e.** day 5 and **f.** day 9. **g.** Violin plots showing the amount of γH2AX foci per nuclei of cells in S/G2 for wild type, MYCN-mScarlet cells at SAP stage of differentiation with doxycycline added at day 5 or day 9 (n= 1 biological replicate, >2000 cells analysed per condition, error bars= SD. Kruskal-Wallis test with Dunn's multiple comparison correction, $p \leq 0.05$= *, $p \leq 0.01$= **, $p \leq 0.001$= ***, $p \leq 0.0001$= ****).

8 References

ALEXANDER, F. 2000. Neuroblastoma. *Urol Clin North Am,* 27**,** 383-92, vii.

ALI, F. R., MARCOS, D., CHERNUKHIN, I., WOODS, L. M., PARKINSON, L. M., WYLIE, L. A., PAPKOVSKAIA, T. D., DAVIES, J. D., CARROLL, J. S. & PHILPOTT, A. 2020. Dephosphorylation of the Proneural Transcription Factor ASCL1 Re-Engages a Latent Post-Mitotic Differentiation Program in Neuroblastoma. *Molecular Cancer Research,* 18**,** 1759-1766.

ALTHOFF, K., BECKERS, A., BELL, E., NORTMEYER, M., THOR, T., SPRÜSSEL, A., LINDNER, S., DE PRETER, K., FLORIN, A., HEUKAMP, L. C., KLEIN-HITPASS, L., ASTRAHANTSEFF, K., KUMPS, C., SPELEMAN, F., EGGERT, A., WESTERMANN, F., SCHRAMM, A. & SCHULTE, J. H. 2015. A Cre-conditional MYCN-driven neuroblastoma mouse model as an improved tool for preclinical studies. *Oncogene,* 34**,** 3357-3368.

AMBROS, V. 1989. A hierarchy of regulatory genes controls a larva-to-adult developmental switch in C. elegans. *Cell,* 57**,** 49-57.

AMBROS, V. & HORVITZ, H. R. 1984. Heterochronic mutants of the nematode Caenorhabditis elegans. *Science,* 226**,** 409-416.

AMBROSIO, S., AMENTE, S., NAPOLITANO, G., DI PALO, G., LANIA, L. & MAJELLO, B. 2015. MYC impairs resolution of site-specific DNA double-strand breaks repair. *Mutation Research/Fundamental and Molecular Mechanisms of Mutagenesis,* 774**,** 6-13.

AMIEL, J., LAUDIER, B., ATTIÉ-BITACH, T., TRANG, H., DE PONTUAL, L., GENER, B., TROCHET, D., ETCHEVERS, H., RAY, P. & SIMONNEAU, M. 2003. Polyalanine expansion and frameshift mutations of the paired-like homeobox gene PHOX2B in congenital central hypoventilation syndrome. *Nature genetics,* 33**,** 459-461.

AMIN, S., NEIJTS, R., SIMMINI, S., VAN ROOIJEN, C., TAN, S. C., KESTER, L., VAN OUDENAARDEN, A., CREYGHTON, M. P. & DESCHAMPS, J. 2016. Cdx and T Brachyury Co-activate Growth Signaling in the Embryonic Axial Progenitor Niche. *Cell Reports,* 17**,** 3165-3177.

ARTYMOVICH, K. & APPLEDORN, D. M. 2015. A Multiplexed Method for Kinetic Measurements of Apoptosis and Proliferation Using Live-Content Imaging. *In:* MOR, G. & ALVERO, A. B. (eds.) *Apoptosis and Cancer: Methods and Protocols.* New York, NY: Springer New York.

ATTIYEH, E. F., LONDON, W. B., MOSSÉ, Y. P., WANG, Q., WINTER, C., KHAZI, D., MCGRADY, P. W., SEEGER, R. C., LOOK, A. T., SHIMADA, H., BRODEUR, G. M., COHN, S. L., MATTHAY, K. K. & MARIS, J. M. 2005. Chromosome 1p and 11q deletions and outcome in neuroblastoma. *N Engl J Med,* 353**,** 2243-53.

AU, S. L., WONG, C. C., LEE, J. M., FAN, D. N., TSANG, F. H., NG, I. O. & WONG, C. M. 2012. Enhancer of zeste homolog 2 epigenetically silences multiple tumor suppressor microRNAs to promote liver cancer metastasis. *Hepatology,* 56**,** 622-31.

AVEMANN, K., KNIPPERS, R., KOLLER, T. & SOGO, J. M. 1988. Camptothecin, a specific inhibitor of type I DNA topoisomerase, induces DNA breakage at replication forks. *Molecular and cellular biology,* 8**,** 3026-3034.

AVIOR, Y., SAGI, I. & BENVENISTY, N. 2016. Pluripotent stem cells in disease modelling and drug discovery. *Nat Rev Mol Cell Biol,* 17**,** 170-82.

AYBAR, M. J., NIETO, M. A. & MAYOR, R. 2003. Snail precedes slug in the genetic cascade required for the specification and migration of the Xenopus neural crest. *Development,* 130**,** 483-494.

AYRAULT, O., ZHAO, H., ZINDY, F., QU, C., SHERR, C. J. & ROUSSEL, M. F. 2010. Atoh1 inhibits neuronal differentiation and collaborates with Gli1 to generate medulloblastoma-initiating cells. *Cancer research,* 70**,** 5618-5627.

AZUHATA, T., SCOTT, D., TAKAMIZAWA, S., WEN, J., DAVIDOFF, A., FUKUZAWA, M. & SANDLER, A. 2001. The inhibitor of apoptosis protein survivin is associated with high-risk behavior of neuroblastoma. *J Pediatr Surg,* 36**,** 1785-91.

BAE, C. J., PARK, B. Y., LEE, Y. H., TOBIAS, J. W., HONG, C. S. & SAINT-JEANNET, J. P. 2014. Identification of Pax3 and Zic1 targets in the developing neural crest. *Dev Biol,* 386**,** 473-83.

BAGATELL, R., BECK-POPOVIC, M., LONDON, W. B., ZHANG, Y., PEARSON, A. D. J., MATTHAY, K. K., MONCLAIR, T., AMBROS, P. F., COHN, S. L. & INTERNATIONAL NEUROBLASTOMA RISK, G. 2009. Significance of MYCN amplification in international neuroblastoma staging system stage 1 and 2 neuroblastoma: a report from the International Neuroblastoma Risk Group database. *Journal of clinical oncology : official journal of the American Society of Clinical Oncology,* 27**,** 365-370.

BAJPAI, R., CHEN, D. A., RADA-IGLESIAS, A., ZHANG, J., XIONG, Y., HELMS, J., CHANG, C. P., ZHAO, Y., SWIGUT, T. & WYSOCKA, J. 2010. CHD7 cooperates with PBAF to control multipotent neural crest formation. *Nature,* 463**,** 958-62.

BAKER, D., HIRST, ADAM J., GOKHALE, PAUL J., JUAREZ, MIGUEL A., WILLIAMS, S., WHEELER, M., BEAN, K., ALLISON, THOMAS F., MOORE, HARRY D., ANDREWS, PETER W. & BARBARIC, I. 2016. Detecting Genetic Mosaicism in Cultures of Human Pluripotent Stem Cells. *Stem Cell Reports,* 7**,** 998-1012.

BARBARIC, I., BIGA, V., GOKHALE, P. J., JONES, M., STAVISH, D., GLEN, A., COCA, D. & ANDREWS, P. W. 2014. Time-lapse analysis of human embryonic stem cells reveals multiple bottlenecks restricting colony formation and their relief upon culture adaptation. *Stem cell reports,* 3**,** 142-155.

BAREMBAUM, M. & BRONNER, M. E. 2013. Identification and dissection of a key enhancer mediating cranial neural crest specific expression of transcription factor, Ets-1. *Dev Biol,* 382**,** 567-75.

BARROS, L. F., BITTNER, C. X., LOAIZA, A., RUMINOT, I., LARENAS, V., MOLDENHAUER, H., OYARZÚN, C. & ALVAREZ, M. 2009. Kinetic validation of 6-NBDG as a probe for the glucose transporter GLUT1 in astrocytes. *Journal of Neurochemistry,* 109**,** 94-100.

BASCH, M. L., BRONNER-FRASER, M. & GARCÍA-CASTRO, M. I. 2006. Specification of the neural crest occurs during gastrulation and requires Pax7. *Nature,* 441**,** 218-22.

BECKER, J. & WILTING, J. 2018. WNT signaling, the development of the sympathoadrenal-paraganglionic system and neuroblastoma. *Cell Mol Life Sci,* 75**,** 1057-1070.

BEHRENS, J., JERCHOW, B.-A., WÜRTELE, M., GRIMM, J., ASBRAND, C., WIRTZ, R., KÜHL, M., WEDLICH, D. & BIRCHMEIER, W. 1998. Functional Interaction of an Axin Homolog, Conductin, with β-Catenin, APC, and GSK3β. *Science,* 280**,** 596-599.

BEIERLE, E. A., TRUJILLO, A., NAGARAM, A., KURENOVA, E. V., FINCH, R., MA, X., VELLA, J., CANCE, W. G. & GOLUBOVSKAYA, V. M. 2007. N-MYC regulates focal adhesion kinase expression in human neuroblastoma. *J Biol Chem,* 282**,** 12503-16.

BELL, E., LUNEC, J. & TWEDDLE, D. A. 2007. Cell cycle regulation targets of MYCN identified by gene expression microarrays. *Cell Cycle,* 6**,** 1249-56.

BELL, J. L., TURLAPATI, R., LIU, T., SCHULTE, J. H. & HÜTTELMAIER, S. 2015. IGF2BP1 Harbors Prognostic Significance by Gene Gain and Diverse Expression in Neuroblastoma. *Journal of Clinical Oncology,* 33**,** 1285-1293.

BERGERS, G. & FENDT, S.-M. 2021. The metabolism of cancer cells during metastasis. *Nature Reviews Cancer,* 21**,** 162-180.

BERRY, T., LUTHER, W., BHATNAGAR, N., JAMIN, Y., POON, E., SANDA, T., PEI, D., SHARMA, B., VETHAROY, WINSTON R., HALLSWORTH, A., AHMAD, Z., BARKER, K., MOREAU, L., WEBBER, H., WANG, W., LIU, Q., PEREZ-ATAYDE, A., RODIG, S., CHEUNG, N.-K., RAYNAUD, F., HALLBERG, B., ROBINSON, SIMON P., GRAY, NATHANAEL S., PEARSON, ANDREW D. J., ECCLES, SUZANNE A., CHESLER, L. & GEORGE, RANI E. 2012. The ALK^{F1174L} Mutation Potentiates the Oncogenic Activity of MYCN in Neuroblastoma. *Cancer Cell,* 22**,** 117-130.

BETANCUR, P., BRONNER-FRASER, M. & SAUKA-SPENGLER, T. 2010. Genomic code for Sox10 activation reveals a key regulatory enhancer for cranial neural crest. *Proceedings of the National Academy of Sciences,* 107**,** 3570-3575.

BETTERS, E., LIU, Y., KJAELDGAARD, A., SUNDSTRÖM, E. & GARCÍA-CASTRO, M. I. 2010. Analysis of early human neural crest development. *Dev Biol,* 344**,** 578-92.

BHAT, N., KWON, H.-J. & RILEY, B. B. 2013. A gene network that coordinates preplacodal competence and neural crest specification in zebrafish. *Developmental biology,* 373**,** 107-117.

BOWN, N., COTTERILL, S., LASTOWSKA, M., O'NEILL, S., PEARSON, A. D., PLANTAZ, D., MEDDEB, M., DANGLOT, G., BRINKSCHMIDT, C., CHRISTIANSEN, H., LAUREYS, G., SPELEMAN, F., NICHOLSON, J., BERNHEIM, A., BETTS, D. R., VANDESOMPELE, J. & VAN ROY, N. 1999a. Gain of chromosome arm 17q and adverse outcome in patients with neuroblastoma. *N Engl J Med,* 340**,** 1954-61.

BOWN, N., COTTERILL, S., ŁASTOWSKA, M., O'NEILL, S., PEARSON, A. D. J., PLANTAZ, D., MEDDEB, M., DANGLOT, G., BRINKSCHMIDT, C., CHRISTIANSEN, H., LAUREYS, G., NICHOLSON, J., BERNHEIM, A., BETTS, D. R., VANDESOMPELE, J., VAN ROY, N. & SPELEMAN, F. 1999b. Gain of Chromosome Arm 17q and Adverse Outcome in Patients with Neuroblastoma. *New England Journal of Medicine,* 340**,** 1954-1961.

BOWN, N., LASTOWSKA, M., COTTERILL, S., O'NEILL, S., ELLERSHAW, C., ROBERTS, P., LEWIS, I. & PEARSON, A. D. 2001. 17q gain in neuroblastoma predicts adverse clinical outcome. U.K. Cancer Cytogenetics Group and the U.K. Children's Cancer Study Group. *Med Pediatr Oncol,* 36**,** 14-9.

BRESLER, SCOTT C., WEISER, DANIEL A., HUWE, PETER J., PARK, JIN H., KRYTSKA, K., RYLES, H., LAUDENSLAGER, M., RAPPAPORT, ERIC F., WOOD, ANDREW C., MCGRADY, PATRICK W., HOGARTY, MICHAEL D., LONDON, WENDY B., RADHAKRISHNAN, R., LEMMON, MARK A. & MOSSÉ, YAËL P. 2014. ALK Mutations Confer Differential Oncogenic Activation and Sensitivity to ALK Inhibition Therapy in Neuroblastoma. *Cancer Cell,* 26**,** 682-694.

BREWER, G. J., TORRICELLI, J. R., EVEGE, E. K. & PRICE, P. J. 1993. Optimized survival of hippocampal neurons in B27-supplemented Neurobasal, a new serum-free medium combination. *J Neurosci Res,* 35**,** 567-76.

BRINKSCHMIDT, C., CHRISTIANSEN, H., TERPE, H. J., SIMON, R., LAMPERT, F., BOECKER, W. & DOCKHORN-DWORNICZAK, B. 2001. Distal chromosome 17 gains in neuroblastomas detected by comparative genomic hybridization (CGH) are associated with a poor clinical outcome. *Med Pediatr Oncol,* 36**,** 11-3.

BRITSCH, S., GOERICH, D. E., RIETHMACHER, D., PEIRANO, R. I., ROSSNER, M., NAVE, K. A., BIRCHMEIER, C. & WEGNER, M. 2001. The transcription factor Sox10 is a key regulator of peripheral glial development. *Genes & development,* 15**,** 66-78.

BRODEUR, G. M. 2003. Neuroblastoma: biological insights into a clinical enigma. *Nat Rev Cancer,* 3**,** 203-16.

BRODEUR, G. M., PRITCHARD, J., BERTHOLD, F., CARLSEN, N. L., CASTEL, V., CASTELBERRY, R. P., DE BERNARDI, B., EVANS, A. E., FAVROT, M., HEDBORG, F. & ET AL. 1993. Revisions of the international criteria for neuroblastoma diagnosis, staging, and response to treatment. *J Clin Oncol,* 11**,** 1466-77.

BRODEUR, G. M., SEEGER, R. C., SCHWAB, M., VARMUS, H. E. & BISHOP, J. M. 1984. Amplification of N-myc in untreated human neuroblastomas correlates with advanced disease stage. *Science,* 224**,** 1121-4.

BURSTYN-COHEN, T., STANLEIGH, J., SELA-DONENFELD, D. & KALCHEIM, C. 2004. Canonical Wnt activity regulates trunk neural crest delamination linking BMP/noggin signaling with G1/S transition. *Development,* 131**,** 5327-5339.

CAMBRAY, N. & WILSON, V. 2002. Axial progenitors with extensive potency are localised to the mouse chordoneural hinge. *Development,* 129**,** 4855-66.

CAMBRAY, N. & WILSON, V. 2007. Two distinct sources for a population of maturing axial progenitors. *Development,* 134**,** 2829-40.

CANGEMI, G., REGGIARDO, G., BARCO, S., BARBAGALLO, L., CONTE, M., D'ANGELO, P., BIANCHI, M., FAVRE, C., GALLENI, B., MELIOLI, G., HAUPT, R., GARAVENTA, A. & CORRIAS, M. V. 2012. Prognostic value of ferritin, neuron-specific enolase, lactate dehydrogenase, and urinary and

plasmatic catecholamine metabolites in children with neuroblastoma. *OncoTargets and therapy,* 5**,** 417-423.

CARÉN, H., KRYH, H., NETHANDER, M., SJÖBERG, R. M., TRÄGER, C., NILSSON, S., ABRAHAMSSON, J., KOGNER, P. & MARTINSSON, T. 2010. High-risk neuroblastoma tumors with 11q-deletion display a poor prognostic, chromosome instability phenotype with later onset. *Proc Natl Acad Sci U S A,* 107**,** 4323-8.

CARON, H., VAN SLUIS, P., DE KRAKER, J., BÖKKERINK, J., EGELER, M., LAUREYS, G., SLATER, R., WESTERVELD, A., VOÛTE, P. A. & VERSTEEG, R. 1996. Allelic Loss of Chromosome 1p as a Predictor of Unfavorable Outcome in Patients with Neuroblastoma. *New England Journal of Medicine,* 334**,** 225-230.

CARTWRIGHT, P., MCLEAN, C., SHEPPARD, A., RIVETT, D., JONES, K. & DALTON, S. 2005. LIF/STAT3 controls ES cell self-renewal and pluripotency by a Myc-dependent mechanism. *Development,* 132**,** 885-96.

CASTLE, V. P., HEIDELBERGER, K. P., BROMBERG, J., OU, X., DOLE, M. & NUÑEZ, G. 1993. Expression of the apoptosis-suppressing protein bcl-2, in neuroblastoma is associated with unfavorable histology and N-myc amplification. *Am J Pathol,* 143**,** 1543-50.

CATLETT-FALCONE, R., LANDOWSKI, T. H., OSHIRO, M. M., TURKSON, J., LEVITZKI, A., SAVINO, R., CILIBERTO, G., MOSCINSKI, L., FERNÁNDEZ-LUNA, J. L., NUÑEZ, G., DALTON, W. S. & JOVE, R. 1999. Constitutive Activation of Stat3 Signaling Confers Resistance to Apoptosis in Human U266 Myeloma Cells. *Immunity,* 10**,** 105-115.

CAVALIERI, F. & GOLDFARB, M. 1988. N-myc proto-oncogene expression can induce DNA replication in Balb/c 3T3 fibroblasts. *Oncogene,* 2**,** 289-91.

CHAMBERS, S. M., FASANO, C. A., PAPAPETROU, E. P., TOMISHIMA, M., SADELAIN, M. & STUDER, L. 2009. Highly efficient neural conversion of human ES and iPS cells by dual inhibition of SMAD signaling. *Nat Biotechnol,* 27**,** 275-80.

CHARRON, J., MALYNN, B. A., FISHER, P., STEWART, V., JEANNOTTE, L., GOFF, S. P., ROBERTSON, E. J. & ALT, F. W. 1992. Embryonic lethality in mice homozygous for a targeted disruption of the N-myc gene. *Genes Dev,* 6**,** 2248-57.

CHAWENGSAKSOPHAK, K., DE GRAAFF, W., ROSSANT, J., DESCHAMPS, J. & BECK, F. 2004. Cdx2 is essential for axial elongation in mouse development. *Proceedings of the National Academy of Sciences of the United States of America,* 101**,** 7641-7645.

CHEN, D., COX, J., ANNAM, J., WEINGART, M., ESSIEN, G., RATHI, K. S., ROKITA, J. L., KHURANA, P., CUYA, S. M., BOSSE, K. R., PILGRIM, A., LI, D., SHIELDS, C., LAUR, O., MARIS, J. M. & SCHNEPP, R. W. 2020. LIN28B promotes neuroblastoma metastasis and regulates PDZ binding kinase. *Neoplasia,* 22**,** 231-241.

CHEN, G., GULBRANSON, D. R., HOU, Z., BOLIN, J. M., RUOTTI, V., PROBASCO, M. D., SMUGA-OTTO, K., HOWDEN, S. E., DIOL, N. R., PROPSON, N. E., WAGNER, R., LEE, G. O., ANTOSIEWICZ-BOURGET, J., TENG, J. M. & THOMSON, J. A. 2011. Chemically defined conditions for human iPSC derivation and culture. *Nat Methods,* 8**,** 424-9.

CHEN, L., ALEXE, G., DHARIA, N. V., ROSS, L., INIGUEZ, A. B., CONWAY, A. S., WANG, E. J., VESCHI, V., LAM, N., QI, J., GUSTAFSON, W. C., NASHOLM, N., VAZQUEZ, F., WEIR, B. A., COWLEY, G. S., ALI, L. D., PANTEL, S., JIANG, G., HARRINGTON, W. F., LEE, Y., GOODALE, A., LUBONJA, R., KRILL-BURGER, J. M., MEYERS, R. M., TSHERNIAK, A., ROOT, D. E., BRADNER, J. E., GOLUB, T. R., ROBERTS, C. W., HAHN, W. C., WEISS, W. A., THIELE, C. J. & STEGMAIER, K. 2018. CRISPR-Cas9 screen reveals a MYCN-amplified neuroblastoma dependency on EZH2. *J Clin Invest,* 128**,** 446-462.

CHEN, L., IRACI, N., GHERARDI, S., GAMBLE, L. D., WOOD, K. M., PERINI, G., LUNEC, J. & TWEDDLE, D. A. 2010. p53 is a direct transcriptional target of MYCN in neuroblastoma. *Cancer Res,* 70**,** 1377-88.

CHESLER, L., GOLDENBERG, D. D., COLLINS, R., GRIMMER, M., KIM, G. E., TIHAN, T., NGUYEN, K., YAKOVENKO, S., MATTHAY, K. K. & WEISS, W. A. 2008. Chemotherapy-induced apoptosis in a

transgenic model of neuroblastoma proceeds through p53 induction. *Neoplasia,* 10**,** 1268-IN34.

CHESLER, L., SCHLIEVE, C., GOLDENBERG, D. D., KENNEY, A., KIM, G., MCMILLAN, A., MATTHAY, K. K., ROWITCH, D. & WEISS, W. A. 2006. Inhibition of Phosphatidylinositol 3-Kinase Destabilizes Mycn Protein and Blocks Malignant Progression in Neuroblastoma. *Cancer Research,* 66**,** 8139-8146.

COHEN, M. A., ZHANG, S., SENGUPTA, S., MA, H., BELL, G. W., HORTON, B., SHARMA, B., GEORGE, R. E., SPRANGER, S. & JAENISCH, R. 2020. Formation of Human Neuroblastoma in Mouse-Human Neural Crest Chimeras. *Cell Stem Cell,* 26**,** 579-592.e6.

COHN, S. L., PEARSON, A. D., LONDON, W. B., MONCLAIR, T., AMBROS, P. F., BRODEUR, G. M., FALDUM, A., HERO, B., IEHARA, T., MACHIN, D., MOSSERI, V., SIMON, T., GARAVENTA, A., CASTEL, V. & MATTHAY, K. K. 2009. The International Neuroblastoma Risk Group (INRG) classification system: an INRG Task Force report. *J Clin Oncol,* 27**,** 289-97.

COHN, S. L., RADEMAKER, A. W., SALWEN, H. R., FRANKLIN, W. A., GONZALES-CRUSSI, F., ROSEN, S. T. & BAUER, K. D. 1990. Analysis of DNA ploidy and proliferative activity in relation to histology and N-myc amplification in neuroblastoma. *Am J Pathol,* 136**,** 1043-52.

COLE, K. A., HUGGINS, J., LAQUAGLIA, M., HULDERMAN, C. E., RUSSELL, M. R., BOSSE, K., DISKIN, S. J., ATTIYEH, E. F., SENNETT, R., NORRIS, G., LAUDENSLAGER, M., WOOD, A. C., MAYES, P. A., JAGANNATHAN, J., WINTER, C., MOSSE, Y. P. & MARIS, J. M. 2011. RNAi screen of the protein kinome identifies checkpoint kinase 1 (CHK1) as a therapeutic target in neuroblastoma. *Proceedings of the National Academy of Sciences,* 108**,** 3336-3341.

COTTERMAN, R. & KNOEPFLER, P. S. 2009. N-Myc regulates expression of pluripotency genes in neuroblastoma including lif, klf2, klf4, and lin28b. *PLoS One,* 4**,** e5799.

CUSHING, H. & WOLBACH, S. B. 1927. The Transformation of a Malignant Paravertebral Sympathicoblastoma into a Benign Ganglioneuroma. *The American journal of pathology,* 3**,** 203-216.7.

DARDENNE, E., BELTRAN, H., BENELLI, M., GAYVERT, K., BERGER, A., PUCA, L., CYRTA, J., SBONER, A., NOORZAD, Z., MACDONALD, T., CHEUNG, C., YUEN, KA S., GAO, D., CHEN, Y., EILERS, M., MOSQUERA, J.-M., ROBINSON, BRIAN D., ELEMENTO, O., RUBIN, MARK A., DEMICHELIS, F. & RICKMAN, DAVID S. 2016. N-Myc Induces an EZH2-Mediated Transcriptional Program Driving Neuroendocrine Prostate Cancer. *Cancer Cell,* 30**,** 563-577.

DARZYNKIEWICZ, Z., JUAN, G., LI, X., GORCZYCA, W., MURAKAMI, T. & TRAGANOS, F. 1997. Cytometry in cell necrobiology: analysis of apoptosis and accidental cell death (necrosis). *Cytometry,* 27**,** 1-20.

DE BROUWER, S., DE PRETER, K., KUMPS, C., ZABROCKI, P., PORCU, M., WESTERHOUT, E. M., LAKEMAN, A., VANDESOMPELE, J., HOEBEECK, J., VAN MAERKEN, T., DE PAEPE, A., LAUREYS, G., SCHULTE, J. H., SCHRAMM, A., VAN DEN BROECKE, C., VERMEULEN, J., VAN ROY, N., BEISKE, K., RENARD, M., NOGUERA, R., DELATTRE, O., JANOUEIX-LEROSEY, I., KOGNER, P., MARTINSSON, T., NAKAGAWARA, A., OHIRA, M., CARON, H., EGGERT, A., COOLS, J., VERSTEEG, R. & SPELEMAN, F. 2010. Meta-analysis of Neuroblastomas Reveals a Skewed ALK Mutation Spectrum in Tumors with MYCN Amplification. *Clinical Cancer Research,* 16**,** 4353-4362.

DEBERARDINIS, R. J. & CHANDEL, N. S. 2020. We need to talk about the Warburg effect. *Nature Metabolism,* 2**,** 127-129.

DECAESTEKER, B., DE PRETER, K. & SPELEMAN, F. 2019. DREAM target reactivation by core transcriptional regulators supports neuroblastoma growth. *Molecular & Cellular Oncology,* 6**,** 1-3.

DECAESTEKER, B., DENECKER, G., VAN NESTE, C., DOLMAN, E. M., VAN LOOCKE, W., GARTLGRUBER, M., NUNES, C., DE VLOED, F., DEPUYDT, P., VERBOOM, K., ROMBAUT, D., LOONTIENS, S., DE WYN, J., KHOLOSY, W. M., KOOPMANS, B., ESSING, A. H. W., HERRMANN, C., DREIDAX, D., DURINCK, K., DEFORCE, D., VAN NIEUWERBURGH, F., HENSSEN, A., VERSTEEG, R., BOEVA, V.,

SCHLEIERMACHER, G., VAN NES, J., MESTDAGH, P., VANHAUWAERT, S., SCHULTE, J. H., WESTERMANN, F., MOLENAAR, J. J., DE PRETER, K. & SPELEMAN, F. 2018. TBX2 is a neuroblastoma core regulatory circuitry component enhancing MYCN/FOXM1 reactivation of DREAM targets. *Nature Communications,* 9**,** 4866.

DELLOYE-BOURGEOIS, C. & CASTELLANI, V. 2019. Hijacking of Embryonic Programs by Neural Crest-Derived Neuroblastoma: From Physiological Migration to Metastatic Dissemination. *Front Mol Neurosci,* 12**,** 52.

DENHAM, M., HASEGAWA, K., MENHENIOTT, T., ROLLO, B., ZHANG, D., HOUGH, S., ALSHAWAF, A., FEBBRARO, F., IGHANIYAN, S. & LEUNG, J. 2015. Multipotent caudal neural progenitors derived from human pluripotent stem cells that give rise to lineages of the central and peripheral nervous system. *Stem cells,* 33**,** 1759-1770.

DEPINHO, R. A., SCHREIBER-AGUS, N. & ALT, F. W. 1991. myc Family Oncogenes in the Development of Normal and Neoplastic Cells. *In:* VANDE WOUDE, G. F. & KLEIN, G. (eds.) *Advances in Cancer Research.* Academic Press.

DESCHAMPS, J., VAN DEN AKKER, E., FORLANI, S., DE GRAAFF, W., OOSTERVEEN, T., ROELEN, B. & ROELFSEMA, J. 1999. Initiation, establishment and maintenance of Hox gene expression patterns in the mouse. *Int J Dev Biol,* 43**,** 635-50.

DHULL, V. S., SHARMA, P., PATEL, C., KUNDU, P., AGARWALA, S., BAKHSHI, S., BHATNAGAR, V., BAL, C. & KUMAR, R. 2015. Diagnostic value of 18F-FDG PET/CT in paediatric neuroblastoma: comparison with: 131: I-MIBG scintigraphy. *Nuclear Medicine Communications,* 36.

DISKIN, S. J., CAPASSO, M., SCHNEPP, R. W., COLE, K. A., ATTIYEH, E. F., HOU, C., DIAMOND, M., CARPENTER, E. L., WINTER, C., LEE, H., JAGANNATHAN, J., LATORRE, V., IOLASCON, A., HAKONARSON, H., DEVOTO, M. & MARIS, J. M. 2012. Common variation at 6q16 within HACE1 and LIN28B influences susceptibility to neuroblastoma. *Nature Genetics,* 44**,** 1126-1130.

DISKIN, S. J., HOU, C., GLESSNER, J. T., ATTIYEH, E. F., LAUDENSLAGER, M., BOSSE, K., COLE, K., MOSSÉ, Y. P., WOOD, A., LYNCH, J. E., PECOR, K., DIAMOND, M., WINTER, C., WANG, K., KIM, C., GEIGER, E. A., MCGRADY, P. W., BLAKEMORE, A. I., LONDON, W. B., SHAIKH, T. H., BRADFIELD, J., GRANT, S. F., LI, H., DEVOTO, M., RAPPAPORT, E. R., HAKONARSON, H. & MARIS, J. M. 2009. Copy number variation at 1q21.1 associated with neuroblastoma. *Nature,* 459**,** 987-91.

DONG, R., YANG, R., ZHAN, Y., LAI, H. D., YE, C. J., YAO, X. Y., LUO, W. Q., CHENG, X. M., MIAO, J. J., WANG, J. F., LIU, B. H., LIU, X. Q., XIE, L. L., LI, Y., ZHANG, M., CHEN, L., SONG, W. C., QIAN, W., GAO, W. Q., TANG, Y. H., SHEN, C. Y., JIANG, W., CHEN, G., YAO, W., DONG, K. R., XIAO, X. M., ZHENG, S., LI, K. & WANG, J. 2020. Single-Cell Characterization of Malignant Phenotypes and Developmental Trajectories of Adrenal Neuroblastoma. *Cancer Cell,* 38**,** 716-733.e6.

DOTTORI, M., GROSS, M. K., LABOSKY, P. & GOULDING, M. 2001. The winged-helix transcription factor Foxd3 suppresses interneuron differentiation and promotes neural crest cell fate. *Development,* 128**,** 4127-4138.

DRAPER, J. S., SMITH, K., GOKHALE, P., MOORE, H. D., MALTBY, E., JOHNSON, J., MEISNER, L., ZWAKA, T. P., THOMSON, J. A. & ANDREWS, P. W. 2004a. Recurrent gain of chromosomes 17q and 12 in cultured human embryonic stem cells. *Nat Biotechnol,* 22**,** 53-4.

DRAPER, J. S., SMITH, K., GOKHALE, P., MOORE, H. D., MALTBY, E., JOHNSON, J., MEISNER, L., ZWAKA, T. P., THOMSON, J. A. & ANDREWS, P. W. 2004b. Recurrent gain of chromosomes 17q and 12 in cultured human embryonic stem cells. *Nature Biotechnology,* 22**,** 53-54.

DUBOIS, S. G., KALIKA, Y., LUKENS, J. N., BRODEUR, G. M., SEEGER, R. C., ATKINSON, J. B., HAASE, G. M., BLACK, C. T., PEREZ, C., SHIMADA, H., GERBING, R., STRAM, D. O. & MATTHAY, K. K. 1999. Metastatic sites in stage IV and IVS neuroblastoma correlate with age, tumor biology, and survival. *J Pediatr Hematol Oncol,* 21**,** 181-9.

DUFFY, D. J., KRSTIC, A., SCHWARZL, T., HALASZ, M., ILJIN, K., FEY, D., HALEY, B., WHILDE, J., HAAPA-PAANANEN, S., FEY, V., FISCHER, M., WESTERMANN, F., HENRICH, K. O., BANNERT, S., HIGGINS, D. G. & KOLCH, W. 2016. Wnt signalling is a bi-directional vulnerability of cancer cells. *Oncotarget,* 7**,** 60310-60331.

DUNGWA, J. V., UPARKAR, U., MAY, M. T. & RAMANI, P. 2012. Angiogenin up-regulation correlates with adverse clinicopathological and biological factors, increased microvascular density and poor patient outcome in neuroblastomas. *Histopathology,* 60**,** 911-23.

DUNWOODIE, S. L. 2009. The role of hypoxia in development of the Mammalian embryo. *Dev Cell,* 17**,** 755-73.

EILERS, M. & EISENMAN, R. N. 2008. Myc's broad reach. *Genes Dev,* 22**,** 2755-66.

ENVER, T., SONEJI, S., JOSHI, C., BROWN, J., IBORRA, F., ORNTOFT, T., THYKJAER, T., MALTBY, E., SMITH, K., ABU DAWUD, R., JONES, M., MATIN, M., GOKHALE, P., DRAPER, J. & ANDREWS, P. W. 2005. Cellular differentiation hierarchies in normal and culture-adapted human embryonic stem cells. *Hum Mol Genet,* 14**,** 3129-40.

EVANS, A. E., CHATTEN, J., D'ANGIO, G. J., GERSON, J. M., ROBINSON, J. & SCHNAUFER, L. 1980. A review of 17 IV-S neuroblastoma patients at the children's hospital of Philadelphia. *Cancer,* 45**,** 833-839.

EVANS, L., CHEN, L., MILAZZO, G., GHERARDI, S., PERINI, G., WILLMORE, E., NEWELL, D. R. & TWEDDLE, D. A. 2015. SKP2 is a direct transcriptional target of MYCN and a potential therapeutic target in neuroblastoma. *Cancer Lett,* 363**,** 37-45.

FERRARA, L. & KMIEC, E. B. 2004. Camptothecin enhances the frequency of oligonucleotide-directed gene repair in mammalian cells by inducing DNA damage and activating homologous recombination. *Nucleic Acids Research,* 32**,** 5239-5248.

FERRUCCI, F., CIACCIO, R., MONTICELLI, S., PIGINI, P., DI GIACOMO, S., PURGATO, S., ERRIQUEZ, D., BERNARDONI, R., NORRIS, M., HABER, M., MILAZZO, G. & PERINI, G. 2018. MAX to MYCN intracellular ratio drives the aggressive phenotype and clinical outcome of high risk neuroblastoma. *Biochimica et Biophysica Acta (BBA) - Gene Regulatory Mechanisms,* 1861**,** 235-245.

FRANKEN, N. A., RODERMOND, H. M., STAP, J., HAVEMAN, J. & VAN BREE, C. 2006. Clonogenic assay of cells in vitro. *Nat Protoc,* 1**,** 2315-9.

FRIEDMAN, D. L., KADAN-LOTTICK, N. S., WHITTON, J., MERTENS, A. C., YASUI, Y., LIU, Y., MEADOWS, A. T., ROBISON, L. L. & STRONG, L. C. 2005. Increased risk of cancer among siblings of long-term childhood cancer survivors: a report from the childhood cancer survivor study. *Cancer Epidemiol Biomarkers Prev,* 14**,** 1922-7.

FRITH, T. J., GRANATA, I., WIND, M., STOUT, E., THOMPSON, O., NEUMANN, K., STAVISH, D., HEATH, P. R., ORTMANN, D., HACKLAND, J. O., ANASTASSIADIS, K., GOUTI, M., BRISCOE, J., WILSON, V., JOHNSON, S. L., PLACZEK, M., GUARRACINO, M. R., ANDREWS, P. W. & TSAKIRIDIS, A. 2018. Human axial progenitors generate trunk neural crest cells in vitro. *Elife,* 7.

FRITH, T. J. R. & TSAKIRIDIS, A. 2019. Efficient Generation of Trunk Neural Crest and Sympathetic Neurons from Human Pluripotent Stem Cells Via a Neuromesodermal Axial Progenitor Intermediate. *Current Protocols in Stem Cell Biology,* 49**,** e81.

GARCíA-CASTRO, M. N. I., MARCELLE, C. & BRONNER-FRASER, M. 2002. Ectodermal Wnt function as a neural crest inducer. *Science,* 297**,** 848-851.

GEORGE, R. E., LONDON, W. B., COHN, S. L., MARIS, J. M., KRETSCHMAR, C., DILLER, L., BRODEUR, G. M., CASTLEBERRY, R. P. & LOOK, A. T. 2005. Hyperdiploidy Plus Nonamplified MYCN Confers a Favorable Prognosis in Children 12 to 18 Months Old With Disseminated Neuroblastoma: A Pediatric Oncology Group Study. *Journal of Clinical Oncology,* 23**,** 6466-6473.

GEORGOMANOLI, M. & PAPAPETROU, E. P. 2019. Modeling blood diseases with human induced pluripotent stem cells. *Dis Model Mech,* 12.

GERDES, J., LEMKE, H., BAISCH, H., WACKER, H. H., SCHWAB, U. & STEIN, H. 1984. Cell cycle analysis of a cell proliferation-associated human nuclear antigen defined by the monoclonal antibody Ki-67. *The Journal of Immunology,* 133**,** 1710-1715.

GOGOLIN, S., EHEMANN, V., BECKER, G., BRUECKNER, L. M., DREIDAX, D., BANNERT, S., NOLTE, I., SAVELYEVA, L., BELL, E. & WESTERMANN, F. 2013. CDK4 inhibition restores G_1-S arrest in MYCN-amplified neuroblastoma cells in the context of doxorubicin-induced DNA damage. *Cell Cycle,* 12**,** 1091-1104.

GONZALEZ MALAGON, S. G. & LIU, K. J. 2018. ALK and GSK3: Shared Features of Neuroblastoma and Neural Crest Cells. *J Exp Neurosci,* 12**,** 1179069518792499.

GOUTI, M., TSAKIRIDIS, A., WYMEERSCH, F. J., HUANG, Y., KLEINJUNG, J., WILSON, V. & BRISCOE, J. 2014. In Vitro Generation of Neuromesodermal Progenitors Reveals Distinct Roles for Wnt Signalling in the Specification of Spinal Cord and Paraxial Mesoderm Identity. *PLOS Biology,* 12**,** e1001937.

GROVES, A. K. & LABONNE, C. 2014. Setting appropriate boundaries: Fate, patterning and competence at the neural plate border. *Developmental Biology,* 389**,** 2-12.

GUALDRINI, F., CORVETTA, D., CANTILENA, S., CHAYKA, O., TANNO, B., RASCHELLÀ, G. & SALA, A. 2010. Addiction of MYCN amplified tumours to B-MYB underscores a reciprocal regulatory loop. *Oncotarget,* 1**,** 278-288.

GUO, C., WHITE, P. S., WEISS, M. J., HOGARTY, M. D., THOMPSON, P. M., STRAM, D. O., GERBING, R., MATTHAY, K. K., SEEGER, R. C. & BRODEUR, G. M. 1999. Allelic deletion at 11q23 is common in MYCN single copy neuroblastomas. *Oncogene,* 18**,** 4948-4957.

HACKLAND, J. O. S., FRITH, T. J. R., THOMPSON, O., MARIN NAVARRO, A., GARCIA-CASTRO, M. I., UNGER, C. & ANDREWS, P. W. 2017. Top-Down Inhibition of BMP Signaling Enables Robust Induction of hPSCs Into Neural Crest in Fully Defined, Xeno-free Conditions. *Stem Cell Reports,* 9**,** 1043-1052.

HALAZONETIS, T. D., GORGOULIS, V. G. & BARTEK, J. 2008. An Oncogene-Induced DNA Damage Model for Cancer Development. *Science,* 319**,** 1352-1355.

HANAHAN, D. & WEINBERG, R. A. 2000. The Hallmarks of Cancer. *Cell,* 100**,** 57-70.

HANAHAN, D. & WEINBERG, R. A. 2011. Hallmarks of cancer: the next generation. *Cell,* 144**,** 646-74.

HATZI, E., BREIT, S., ZOEPHEL, A., ASHMAN, K., TONTSCH, U., AHORN, H., MURPHY, C., SCHWEIGERER, L. & FOTSIS, T. 2000. MYCN oncogene and angiogenesis: down-regulation of endothelial growth inhibitors in human neuroblastoma cells. Purification, structural, and functional characterization. *Adv Exp Med Biol,* 476**,** 239-48.

HATZI, E., MURPHY, C., ZOEPHEL, A., RASMUSSEN, H., MORBIDELLI, L., AHORN, H., KUNISADA, K., TONTSCH, U., KLENK, M., YAMAUCHI-TAKIHARA, K., ZICHE, M., ROFSTAD, E. K., SCHWEIGERER, L. & FOTSIS, T. 2002. N-myc oncogene overexpression down-regulates IL-6; evidence that IL-6 inhibits angiogenesis and suppresses neuroblastoma tumor growth. *Oncogene,* 21**,** 3552-61.

HENRIQUE, D., ABRANCHES, E., VERRIER, L. & STOREY, K. G. 2015. Neuromesodermal progenitors and the making of the spinal cord. *Development,* 142**,** 2864-2875.

HICKMAN, F. E., STANLEY, E. M. & CARTER, B. D. 2018. Neurotrophin Responsiveness of Sympathetic Neurons Is Regulated by Rapid Mobilization of the p75 Receptor to the Cell Surface through TrkA Activation of Arf6. *The Journal of Neuroscience,* 38**,** 5606-5619.

HIRAI, M., YOSHIDA, S., KASHIWAGI, H., KAWAMURA, T., ISHIKAWA, T., KANEKO, M., OHKAWA, H., NAKAGAWARA, A., MIWA, M. & UCHIDA, K. 1999. 1q23 gain is associated with progressive neuroblastoma resistant to aggressive treatment. *Genes Chromosomes Cancer,* 25**,** 261-9.

HO, R., MINTURN, J. E., SIMPSON, A. M., IYER, R., LIGHT, J. E., EVANS, A. E. & BRODEUR, G. M. 2011. The effect of P75 on Trk receptors in neuroblastomas. *Cancer Lett,* 305**,** 76-85.

HONORÉ, S. M., AYBAR, M. J. & MAYOR, R. 2003. Sox10 is required for the early development of the prospective neural crest in Xenopus embryos. *Dev Biol,* 260**,** 79-96.

HUANG, M. & WEISS, W. A. 2013. Neuroblastoma and MYCN. *Cold Spring Harbor perspectives in medicine,* 3**,** a014415-a014415.
HUANG, R., CHEUNG, N. K., VIDER, J., CHEUNG, I. Y., GERALD, W. L., TICKOO, S. K., HOLLAND, E. C. & BLASBERG, R. G. 2011. MYCN and MYC regulate tumor proliferation and tumorigenesis directly through BMI1 in human neuroblastomas. *Faseb j,* 25**,** 4138-49.
HUBER, K. 2006. The sympathoadrenal cell lineage: Specification, diversification, and new perspectives. *Developmental Biology,* 298**,** 335-343.
HUBER, K. 2015. Segregation of neuronal and neuroendocrine differentiation in the sympathoadrenal lineage. *Cell Tissue Res,* 359**,** 333-41.
HUI, A. B.-Y., LO, K.-W., YIN, X.-L., POON, W.-S. & NG, H.-K. 2001. Detection of multiple gene amplifications in glioblastoma multiforme using array-based comparative genomic hybridization. *Laboratory investigation,* 81**,** 717-723.
ICHIJIMA, Y., YOSHIOKA, K., YOSHIOKA, Y., SHINOHE, K., FUJIMORI, H., UNNO, J., TAKAGI, M., GOTO, H., INAGAKI, M., MIZUTANI, S. & TERAOKA, H. 2010. DNA lesions induced by replication stress trigger mitotic aberration and tetraploidy development. *PLoS One,* 5**,** e8821.
JANOUEIX-LEROSEY, I., SCHLEIERMACHER, G., MICHELS, E., MOSSERI, V., RIBEIRO, A., LEQUIN, D., VERMEULEN, J., COUTURIER, J., PEUCHMAUR, M., VALENT, A., PLANTAZ, D., RUBIE, H., VALTEAU-COUANET, D., THOMAS, C., COMBARET, V., ROUSSEAU, R., EGGERT, A., MICHON, J., SPELEMAN, F. & DELATTRE, O. 2009. Overall Genomic Pattern Is a Predictor of Outcome in Neuroblastoma. *Journal of Clinical Oncology,* 27**,** 1026-1033.
JANSKY, S., SHARMA, A. K., KÖRBER, V., QUINTERO, A., TOPRAK, U. H., WECHT, E. M., GARTLGRUBER, M., GRECO, A., CHOMSKY, E., GRÜNEWALD, T. G. P., HENRICH, K.-O., TANAY, A., HERRMANN, C., HÖFER, T. & WESTERMANN, F. 2021. Single-cell transcriptomic analyses provide insights into the developmental origins of neuroblastoma. *Nature Genetics*.
JASTY, R., VAN GOLEN, C., LIN, H. J., SOLOMON, G., HEIDELBERGER, K., POLVERINI, P., OPIPARI, A., FELDMAN, E. & CASTLE, V. P. 2001. Bcl-2 and M-Myc coexpression increases IGF-IR and features of malignant growth in neuroblastoma cell lines. *Neoplasia,* 3**,** 304-13.
JHO, E.-H., ZHANG, T., DOMON, C., JOO, C.-K., FREUND, J.-N. & COSTANTINI, F. 2002. Wnt/β-Catenin/Tcf Signaling Induces the Transcription of Axin2, a Negative Regulator of the Signaling Pathway. *Molecular and Cellular Biology,* 22**,** 1172-1183.
JIANG, M., STANKE, J. & LAHTI, J. M. 2011. The connections between neural crest development and neuroblastoma. *Curr Top Dev Biol,* 94**,** 77-127.
JOHANSSON, P., FASTH, A., EK, T. & HAMMARSTEN, O. 2017. Validation of a flow cytometry-based detection of γ-H2AX, to measure DNA damage for clinical applications. *Cytometry B Clin Cytom,* 92**,** 534-540.
JOSHI, V. V., CANTOR, A. B., ALTSHULER, G., LARKIN, E. W., NEILL, J. S., SHUSTER, J. J., HOLBROOK, C. T., HAYES, F. A., NITSCHKE, R., DUNCAN, M. H. & ET AL. 1992. Age-linked prognostic categorization based on a new histologic grading system of neuroblastomas. A clinicopathologic study of 211 cases from the Pediatric Oncology Group. *Cancer,* 69**,** 2197-211.
JURÍKOVÁ, M., DANIHEL, Ľ., POLÁK, Š. & VARGA, I. 2016. Ki67, PCNA, and MCM proteins: Markers of proliferation in the diagnosis of breast cancer. *Acta Histochemica,* 118**,** 544-552.
KANG, J., RYCHAHOU, P. G., ISHOLA, T. A., MOUROT, J. M., EVERS, B. M. & CHUNG, D. H. 2008. N-myc is a novel regulator of PI3K-mediated VEGF expression in neuroblastoma. *Oncogene,* 27**,** 3999-4007.
KANG, J. H., RYCHAHOU, P. G., ISHOLA, T. A., QIAO, J., EVERS, B. M. & CHUNG, D. H. 2006. MYCN silencing induces differentiation and apoptosis in human neuroblastoma cells. *Biochem Biophys Res Commun,* 351**,** 192-7.
KARAGIANNIS, T. C. & EL-OSTA, A. 2004a. DNA damage repair and transcription. *Cellular and Molecular Life Sciences CMLS,* 61**,** 2137-2147.

KARAGIANNIS, T. C. & EL-OSTA, A. 2004b. Double-strand breaks: signaling pathways and repair mechanisms. *Cell Mol Life Sci,* 61**,** 2137-47.
KASEMEIER-KULESA, J. C., MCLENNAN, R., ROMINE, M. H., KULESA, P. M. & LEFCORT, F. 2010. CXCR4 controls ventral migration of sympathetic precursor cells. *J Neurosci,* 30**,** 13078-88.
KASEMEIER-KULESA, J. C., MORRISON, J. A., LEFCORT, F. & KULESA, P. M. 2015. TrkB/BDNF signalling patterns the sympathetic nervous system. *Nat Commun,* 6**,** 8281.
KASIM, M., HEß, V., SCHOLZ, H., PERSSON, P. B. & FÄHLING, M. 2016. Achaete-scute homolog 1 expression controls cellular differentiation of neuroblastoma. *Frontiers in molecular neuroscience,* 9**,** 156.
KEMPF, H., OLMER, R., HAASE, A., FRANKE, A., BOLESANI, E., SCHWANKE, K., ROBLES-DIAZ, D., COFFEE, M., GÖHRING, G., DRÄGER, G., PÖTZ, O., JOOS, T., MARTINEZ-HACKERT, E., HAVERICH, A., BUETTNER, F. F. R., MARTIN, U. & ZWEIGERDT, R. 2016. Bulk cell density and Wnt/TGFbeta signalling regulate mesendodermal patterning of human pluripotent stem cells. *Nature Communications,* 7**,** 13602.
KEROSUO, L., NEPPALA, P., HSIN, J., MOHLIN, S., VIECELI, F. M., TÖRÖK, Z., LAINE, A., WESTERMARCK, J. & BRONNER, M. E. 2018. Enhanced expression of MycN/CIP2A drives neural crest toward a neural stem cell-like fate: Implications for priming of neuroblastoma. *Proceedings of the National Academy of Sciences,* 115**,** E7351-E7360.
KHUDYAKOV, J. & BRONNER-FRASER, M. 2009a. Comprehensive spatiotemporal analysis of early chick neural crest network genes. *Dev Dyn,* 238**,** 716-23.
KHUDYAKOV, J. & BRONNER-FRASER, M. 2009b. Comprehensive spatiotemporal analysis of early chick neural crest network genes. *Developmental dynamics : an official publication of the American Association of Anatomists,* 238**,** 716-723.
KILDISIUTE, G., KHOLOSY, W. M., YOUNG, M. D., ROBERTS, K., ELMENTAITE, R., VAN HOOFF, S. R., PACYNA, C. N., KHABIROVA, E., PIAPI, A., THEVANESAN, C., BUGALLO-BLANCO, E., BURKE, C., MAMANOVA, L., KELLER, K. M., LANGENBERG-VERVERGAERT, K. P. S., LIJNZAAD, P., MARGARITIS, T., HOLSTEGE, F. C. P., TAS, M. L., WIJNEN, M., VAN NOESEL, M. M., DEL VALLE, I., BARONE, G., VAN DER LINDEN, R., DUNCAN, C., ANDERSON, J., ACHERMANN, J. C., HANIFFA, M., TEICHMANN, S. A., RAMPLING, D., SEBIRE, N. J., HE, X., DE KRIJGER, R. R., BARKER, R. A., MEYER, K. B., BAYRAKTAR, O., STRAATHOF, K., MOLENAAR, J. J. & BEHJATI, S. 2021. Tumor to normal single-cell mRNA comparisons reveal a pan-neuroblastoma cancer cell. *Sci Adv,* 7.
KIM, J., HOFFMAN, J. P., ALPAUGH, R. K., RHIM, A. D., REICHERT, M., STANGER, B. Z., FURTH, E. E., SEPULVEDA, A. R., YUAN, C.-X., WON, K.-J., DONAHUE, G., SANDS, J., GUMBS, A. A. & ZARET, K. S. 2013. An iPSC line from human pancreatic ductal adenocarcinoma undergoes early to invasive stages of pancreatic cancer progression. *Cell reports,* 3**,** 2088-2099.
KIM, J., LO, L., DORMAND, E. & ANDERSON, D. J. 2003. SOX10 maintains multipotency and inhibits neuronal differentiation of neural crest stem cells. *Neuron,* 38**,** 17-31.
KING, D., LI, X. D., ALMEIDA, G. S., KWOK, C., GRAVELLS, P., HARRISON, D., BURKE, S., HALLSWORTH, A., JAMIN, Y., GEORGE, S., ROBINSON, S. P., LORD, C. J., POON, E., YEOMANSON, D., CHESLER, L. & BRYANT, H. E. 2020. MYCN expression induces replication stress and sensitivity to PARP inhibition in neuroblastoma. *Oncotarget,* 11**,** 2141-2159.
KNOEPFLER, P. S., ZHANG, X. Y., CHENG, P. F., GAFKEN, P. R., MCMAHON, S. B. & EISENMAN, R. N. 2006. Myc influences global chromatin structure. *Embo j,* 25**,** 2723-34.
KNUDSON, A. G., JR. & STRONG, L. C. 1972. Mutation and cancer: neuroblastoma and pheochromocytoma. *Am J Hum Genet,* 24**,** 514-32.
KOCAK, H., ACKERMANN, S., HERO, B., KAHLERT, Y., OBERTHUER, A., JURAEVA, D., ROELS, F., THEISSEN, J., WESTERMANN, F., DEUBZER, H., EHEMANN, V., BRORS, B., ODENTHAL, M., BERTHOLD, F. & FISCHER, M. 2013. Hox-C9 activates the intrinsic pathway of apoptosis and is associated with spontaneous regression in neuroblastoma. *Cell Death & Disease,* 4**,** e586-e586.

KOHL, N. E., KANDA, N., SCHRECK, R. R., BRUNS, G., LATT, S. A., GILBERT, F. & ALT, F. W. 1983. Transposition and amplification of oncogene-related sequences in human neuroblastomas. *Cell,* 35**,** 359-67.

KOHL, N. E., LEGOUY, E., DEPINHO, R. A., NISEN, P. D., SMITH, R. K., GEE, C. E. & ALT, F. W. 1986. Human N-myc is closely related in organization and nucleotide sequence to c-myc. *Nature,* 319**,** 73-7.

KOPPEN, A., AIT-AISSA, R., HOPMAN, S., KOSTER, J., HANEVELD, F., VERSTEEG, R. & VALENTIJN, L. J. 2007a. Dickkopf-1 is down-regulated by MYCN and inhibits neuroblastoma cell proliferation. *Cancer Lett,* 256**,** 218-28.

KOPPEN, A., AIT-AISSA, R., KOSTER, J., VAN SLUIS, P. G., ØRA, I., CARON, H. N., VOLCKMANN, R., VERSTEEG, R. & VALENTIJN, L. J. 2007b. Direct regulation of the minichromosome maintenance complex by MYCN in neuroblastoma. *European Journal of Cancer,* 43**,** 2413-2422.

KRAMER, M., RIBEIRO, D., ARSENIAN-HENRIKSSON, M., DELLER, T. & ROHRER, H. 2016. Proliferation and Survival of Embryonic Sympathetic Neuroblasts by MYCN and Activated ALK Signaling. *The Journal of Neuroscience,* 36**,** 10425-10439.

KRETZNER, L., BLACKWOOD, E. M. & EISENMAN, R. N. 1992. Transcriptional activities of the Myc and Max proteins in mammalian cells. *Curr Top Microbiol Immunol,* 182**,** 435-43.

KRISPIN, S., NITZAN, E., KASSEM, Y. & KALCHEIM, C. 2010. Evidence for a dynamic spatiotemporal fate map and early fate restrictions of premigratory avian neural crest. *Development,* 137**,** 585-595.

KRYH, H., CARÉN, H., ERICHSEN, J., SJÖBERG, R.-M., ABRAHAMSSON, J., KOGNER, P. & MARTINSSON, T. 2011. Comprehensive SNP array study of frequently used neuroblastoma cell lines; copy neutral loss of heterozygosity is common in the cell lines but uncommon in primary tumors. *BMC Genomics,* 12**,** 443.

LAING, O., HALLIWELL, J. & BARBARIC, I. 2019. Rapid PCR Assay for Detecting Common Genetic Variants Arising in Human Pluripotent Stem Cell Cultures. *Curr Protoc Stem Cell Biol,* 49**,** e83.

LAMERS, F., PLOEG, I. V. D., SCHILD, L., EBUS, M. E., KOSTER, J., HANSEN, B. R., KOCH, T., VERSTEEG, R., CARON, H. N. & MOLENAAR, J. J. 2011. Knockdown of survivin (BIRC5) causes apoptosis in neuroblastoma via mitotic catastrophe. *Endocrine-Related Cancer,* 18**,** 657.

LAMERS, F., SCHILD, L., DEN HARTOG, I. J., EBUS, M. E., WESTERHOUT, E. M., ORA, I., KOSTER, J., VERSTEEG, R., CARON, H. N. & MOLENAAR, J. J. 2012. Targeted BCL2 inhibition effectively inhibits neuroblastoma tumour growth. *Eur J Cancer,* 48**,** 3093-103.

LASORELLA, A., BOLDRINI, R., DOMINICI, C., DONFRANCESCO, A., YOKOTA, Y., INSERRA, A. & IAVARONE, A. 2002. Id2 Is Critical for Cellular Proliferation and Is the Oncogenic Effector of N-Myc in Human Neuroblastoma. *Cancer Research,* 62**,** 301-306.

LASORELLA, A., NOSEDA, M., BEYNA, M. & IAVARONE, A. 2000. Id2 is a retinoblastoma protein target and mediates signalling by Myc oncoproteins. *Nature,* 407**,** 592-598.

LASTOWSKA, M., ROBERTS, P., PEARSON, A. D., LEWIS, I., WOLSTENHOLME, J. & BOWN, N. 1997. Promiscuous translocations of chromosome arm 17q in human neuroblastomas. *Genes Chromosomes Cancer,* 19**,** 143-9.

LASTOWSKA, M., VAN ROY, N., BOWN, N., SPELEMAN, F., LUNEC, J., STRACHAN, T., PEARSON, A. D. & JACKSON, M. S. 1998. Molecular cytogenetic delineation of 17q translocation breakpoints in neuroblastoma cell lines. *Genes Chromosomes Cancer,* 23**,** 116-22.

LEE, C.-T., BENDRIEM, RAPHAEL M., KINDBERG, ABIGAIL A., WORDEN, LILA T., WILLIAMS, MELANIE P., DRGON, T., MALLON, BARBARA S., HARVEY, BRANDON K., RICHIE, CHRISTOPHER T., HAMILTON, REBECCA S., CHEN, J., ERRICO, STACIE L., TSAI, S.-YI A., UHL, GEORGE R. & FREED, WILLIAM J. 2015a. Functional Consequences of 17q21.31/WNT3-WNT9B Amplification in hPSCs with Respect to Neural Differentiation. *Cell Reports,* 10**,** 616-632.

LEE, D. F., SU, J., KIM, H. S., CHANG, B., PAPATSENKO, D., ZHAO, R., YUAN, Y., GINGOLD, J., XIA, W., DARR, H., MIRZAYANS, R., HUNG, M. C., SCHANIEL, C. & LEMISCHKA, I. R. 2015b. Modeling familial cancer with induced pluripotent stem cells. *Cell,* 161**,** 240-54.

LEE, G., KIM, H., ELKABETZ, Y., AL SHAMY, G., PANAGIOTAKOS, G., BARBERI, T., TABAR, V. & STUDER, L. 2007. Isolation and directed differentiation of neural crest stem cells derived from human embryonic stem cells. *Nat Biotechnol,* 25**,** 1468-75.

LEE, W.-H., MURPHREE, A. L. & BENEDICT, W. F. 1984. Expression and amplification of the N-myc gene in primary retinoblastoma. *Nature,* 309**,** 458-460.

LESTINI, B. J., GOLDSMITH, K. C., FLUCHEL, M. N., LIU, X., CHEN, N. L., GOYAL, B., PAWEL, B. R. & HOGARTY, M. D. 2009. Mcl1 downregulation sensitizes neuroblastoma to cytotoxic chemotherapy and small molecule Bcl2-family antagonists. *Cancer Biol Ther,* 8**,** 1587-95.

LEUNG, A. W., MURDOCH, B., SALEM, A. F., PRASAD, M. S., GOMEZ, G. A. & GARCÍA-CASTRO, M. I. 2016. WNT/β-catenin signaling mediates human neural crest induction via a pre-neural border intermediate. *Development,* 143**,** 398-410.

LI, J., YANG, Y., PENG, Y., AUSTIN, R. J., VAN EYNDHOVEN, W. G., NGUYEN, K. C., GABRIELE, T., MCCURRACH, M. E., MARKS, J. R., HOEY, T., LOWE, S. W. & POWERS, S. 2002. Oncogenic properties of PPM1D located within a breast cancer amplification epicenter at 17q23. *Nat Genet,* 31**,** 133-4.

LI, Z., TAKENOBU, H., SETYAWATI, A. N., AKITA, N., HARUTA, M., SATOH, S., SHINNO, Y., CHIKARAISHI, K., MUKAE, K., AKTER, J., SUGINO, R. P., NAKAZAWA, A., NAKAGAWARA, A., ABURATANI, H., OHIRA, M. & KAMIJO, T. 2018. EZH2 regulates neuroblastoma cell differentiation via NTRK1 promoter epigenetic modifications. *Oncogene,* 37**,** 2714-2727.

LIBERTI, M. V. & LOCASALE, J. W. 2016. The Warburg Effect: How Does it Benefit Cancer Cells? *Trends in Biochemical Sciences,* 41**,** 211-218.

LIU, N. & ZHU, B. 2017. Chapter 10 - Regulation of PRC2 Activity. *In:* PIRROTTA, V. (ed.) *Polycomb Group Proteins.* Academic Press.

LIU, W., REN, Z., LU, K., SONG, C., CHEUNG, E. C. W., ZHOU, Z. & CHEN, G. 2018a. The Suppression of Medium Acidosis Improves the Maintenance and Differentiation of Human Pluripotent Stem Cells at High Density in Defined Cell Culture Medium. *International journal of biological sciences,* 14**,** 485-496.

LIU, Y., XU, J., CHOI, H. H., HAN, C., FANG, Y., LI, Y., VAN DER JEUGHT, K., XU, H., ZHANG, L., FRIEDEN, M., WANG, L., EYVANI, H., SUN, Y., ZHAO, G., ZHANG, Y., LIU, S., WAN, J., HUANG, C., JI, G., LU, X., HE, X. & ZHANG, X. 2018b. Targeting 17q23 amplicon to overcome the resistance to anti-HER2 therapy in HER2+ breast cancer. *Nat Commun,* 9**,** 4718.

LO, L.-C., JOHNSON, J. E., WUENSCHELL, C. W., SAITO, T. & ANDERSON, D. J. 1991. Mammalian achaete-scute homolog 1 is transiently expressed by spatially restricted subsets of early neuroepithelial and neural crest cells. *Genes & development,* 5**,** 1524-1537.

LOOK, A. T., HAYES, F. A., NITSCHKE, R., MCWILLIAMS, N. B. & GREEN, A. A. 1984. Cellular DNA content as a predictor of response to chemotherapy in infants with unresectable neuroblastoma. *N Engl J Med,* 311**,** 231-5.

LOOK, A. T., HAYES, F. A., SHUSTER, J. J., DOUGLASS, E. C., CASTLEBERRY, R. P., BOWMAN, L. C., SMITH, E. I. & BRODEUR, G. M. 1991. Clinical relevance of tumor cell ploidy and N-myc gene amplification in childhood neuroblastoma: a Pediatric Oncology Group study. *J Clin Oncol,* 9**,** 581-91.

MACARTHUR, I. C., BEI, Y., GARCIA, H. D., ORTIZ, M. V., TOEDLING, J., KLIRONOMOS, F., ROLFF, J., EGGERT, A., SCHULTE, J. H., KENTSIS, A. & HENSSEN, A. G. 2019. Prohibitin promotes de-differentiation and is a potential therapeutic target in neuroblastoma. *JCI Insight,* 5.

MACDONALD, B. T., TAMAI, K. & HE, X. 2009. Wnt/beta-catenin signaling: components, mechanisms, and diseases. *Developmental cell,* 17**,** 9-26.

MALLO, M., WELLIK, D. M. & DESCHAMPS, J. 2010. Hox genes and regional patterning of the vertebrate body plan. *Dev Biol,* 344**,** 7-15.

MAO, L., DING, J., ZHA, Y., YANG, L., MCCARTHY, B. A., KING, W., CUI, H. & DING, H.-F. 2011. HOXC9 Links Cell-Cycle Exit and Neuronal Differentiation and Is a Prognostic Marker in Neuroblastoma. *Cancer Research,* 71**,** 4314-4324.

MARCHAND, F. 1891. *Beiträge zur Kenntniss der normalen und pathologischen Anatomie der Glandula carotica under Nebennieren*, A. Hirschwald.

MARIN NAVARRO, A., DAY, K., KOGNER, P., WILHELM, M. & FALK, A. 2019. Generation of induced pluripotent stem cell lines from two Neuroblastoma patients carrying a germline ALK R1275Q mutation. *Stem Cell Res,* 34**,** 101356.

MARIS, J. M. 2010. Recent advances in neuroblastoma. *The New England journal of medicine,* 362**,** 2202-2211.

MARIS, J. M., HOGARTY, M. D., BAGATELL, R. & COHN, S. L. 2007. Neuroblastoma. *Lancet,* 369**,** 2106-20.

MARTIN, B. L. & KIMELMAN, D. 2008. Regulation of canonical Wnt signaling by Brachyury is essential for posterior mesoderm formation. *Dev Cell,* 15**,** 121-33.

MATTHAY, K. K., MARIS, J. M., SCHLEIERMACHER, G., NAKAGAWARA, A., MACKALL, C. L., DILLER, L. & WEISS, W. A. 2016. Neuroblastoma. *Nature Reviews Disease Primers,* 2**,** 16078.

MCCONVILLE, C. M., DYER, S., REES, S. A., LUTTIKHUIS, M. E., MCMULLAN, D. J., VICKERS, S. J., RAMANI, P., REDFERN, D. & MORLAND, B. J. 2001. Molecular cytogenetic characterization of two non-MYCN amplified neuroblastoma cell lines with complex t(11;17). *Cancer Genet Cytogenet,* 130**,** 133-40.

MCGREW, M. J., SHERMAN, A., LILLICO, S. G., ELLARD, F. M., RADCLIFFE, P. A., GILHOOLEY, H. J., MITROPHANOUS, K. A., CAMBRAY, N., WILSON, V. & SANG, H. 2008. Localised axial progenitor cell populations in the avian tail bud are not committed to a posterior Hox identity. *Development,* 135**,** 2289-99.

MEDDEB, M., DANGLOT, G., CHUDOBA, I., VÉNUAT, A.-M., BÉNARD, J., AVET-LOISEAU, H., VASSEUR, B., LE PASLIER, D., TERRIER-LACOMBE, M.-J., HARTMANN, O. & BERNHEIM, A. 1996. Additional copies of a 25 Mb chromosomal region originating from 17q23.1-17qter are present in 90% of high-grade neuroblastomas. *Genes, Chromosomes and Cancer,* 17**,** 156-165.

MEITINGER, F., OHTA, M., LEE, K.-Y., WATANABE, S., DAVIS, R. L., ANZOLA, J. V., KABECHE, R., JENKINS, D. A., SHIAU, A. K., DESAI, A. & OEGEMA, K. 2020. TRIM37 controls cancer-specific vulnerability to PLK4 inhibition. *Nature,* 585**,** 440-446.

MENDEZ, L. E., MANCI, N., CANTUARIA, G., GOMEZ-MARIN, O., PENALVER, M., BRAUNSCHWEIGER, P. & NADJI, M. 2002. Expression of glucose transporter-1 in cervical cancer and its precursors. *Gynecol Oncol,* 86**,** 138-43.

MENENDEZ, L., YATSKIEVYCH, T. A., ANTIN, P. B. & DALTON, S. 2011. Wnt signaling and a Smad pathway blockade direct the differentiation of human pluripotent stem cells to multipotent neural crest cells. *Proc Natl Acad Sci U S A,* 108**,** 19240-5.

MENYHÁRT, O., HARAMI-PAPP, H., SUKUMAR, S., SCHÄFER, R., MAGNANI, L., DE BARRIOS, O. & GYŐRFFY, B. 2016. Guidelines for the selection of functional assays to evaluate the hallmarks of cancer. *Biochimica et Biophysica Acta (BBA) - Reviews on Cancer,* 1866**,** 300-319.

METZIS, V., STEINHAUSER, S., PAKANAVICIUS, E., GOUTI, M., STAMATAKI, D., IVANOVITCH, K., WATSON, T., RAYON, T., MOUSAVY GHARAVY, S. N., LOVELL-BADGE, R., LUSCOMBE, N. M. & BRISCOE, J. 2018. Nervous System Regionalization Entails Axial Allocation before Neural Differentiation. *Cell,* 175**,** 1105-1118.e17.

MEULEMANS, D. & BRONNER-FRASER, M. 2002. Amphioxus and lamprey AP-2 genes: implications for neural crest evolution and migration patterns. *Development,* 129**,** 4953-4962.

MEYER, N. & PENN, L. Z. 2008. Reflecting on 25 years with MYC. *Nature Reviews Cancer,* 8**,** 976-990.

MICA, Y., LEE, G., CHAMBERS, S. M., TOMISHIMA, M. J. & STUDER, L. 2013. Modeling neural crest induction, melanocyte specification, and disease-related pigmentation defects in hESCs and patient-specific iPSCs. *Cell Rep,* 3**,** 1140-52.

MOBLEY, B. C., KWON, M., KRAEMER, B. R., HICKMAN, F. E., QIAO, J., CHUNG, D. H. & CARTER, B. D. 2015. Expression of MYCN in Multipotent Sympathoadrenal Progenitors Induces Proliferation and Neural Differentiation, but Is Not Sufficient for Tumorigenesis. *PloS one,* 10**,** e0133897-e0133897.

MOLENAAR, J. J., DOMINGO-FERNÁNDEZ, R., EBUS, M. E., LINDNER, S., KOSTER, J., DRABEK, K., MESTDAGH, P., VAN SLUIS, P., VALENTIJN, L. J., VAN NES, J., BROEKMANS, M., HANEVELD, F., VOLCKMANN, R., BRAY, I., HEUKAMP, L., SPRÜSSEL, A., THOR, T., KIECKBUSCH, K., KLEIN-HITPASS, L., FISCHER, M., VANDESOMPELE, J., SCHRAMM, A., VAN NOESEL, M. M., VARESIO, L., SPELEMAN, F., EGGERT, A., STALLINGS, R. L., CARON, H. N., VERSTEEG, R. & SCHULTE, J. H. 2012. LIN28B induces neuroblastoma and enhances MYCN levels via let-7 suppression. *Nature Genetics,* 44**,** 1199-1206.

MOLLAAGHABABA, R. & PAVAN, W. J. 2003. The importance of having your SOX on: role of SOX10† in the development of neural crest-derived melanocytes and glia. *Oncogene,* 22**,** 3024-3034.

MONCLAIR, T., BRODEUR, G. M., AMBROS, P. F., BRISSE, H. J., CECCHETTO, G., HOLMES, K., KANEKO, M., LONDON, W. B., MATTHAY, K. K., NUCHTERN, J. G., VON SCHWEINITZ, D., SIMON, T., COHN, S. L., PEARSON, A. D. J. & FORCE, I. T. 2009. The International Neuroblastoma Risk Group (INRG) staging system: an INRG Task Force report. *Journal of clinical oncology : official journal of the American Society of Clinical Oncology,* 27**,** 298-303.

MONDAL, T., JUVVUNA, P. K., KIRKEBY, A., MITRA, S., KOSALAI, S. T., TRAXLER, L., HERTWIG, F., WERNIG-ZORC, S., MIRANDA, C., DELAND, L., VOLLAND, R., BARTENHAGEN, C., BARTSCH, D., BANDARU, S., ENGESSER, A., SUBHASH, S., MARTINSSON, T., CARÉN, H., AKYÜREK, L. M., KURIAN, L., KANDURI, M., HUARTE, M., KOGNER, P., FISCHER, M. & KANDURI, C. 2018. Sense-Antisense lncRNA Pair Encoded by Locus 6p22.3 Determines Neuroblastoma Susceptibility via the USP36-CHD7-SOX9 Regulatory Axis. *Cancer Cell,* 33**,** 417-434.e7.

MONSORO-BURQ, A.-H., WANG, E. & HARLAND, R. 2005. Msx1 and Pax3 cooperate to mediate FGF8 and WNT signals during Xenopus neural crest induction. *Developmental cell,* 8**,** 167-178.

MONTAVON, G., JAUQUIER, N., COULON, A., PEUCHMAUR, M., FLAHAUT, M., BOURLOUD, K. B., YAN, P., DELATTRE, O., SOMMER, L., JOSEPH, J. M., JANOUEIX-LEROSEY, I., GROSS, N. & MÜHLETHALER-MOTTET, A. 2014. Wild-type ALK and activating ALK-R1275Q and ALK-F1174L mutations upregulate Myc and initiate tumor formation in murine neural crest progenitor cells. *Oncotarget,* 5**,** 4452-66.

MORIKAWA, Y., MASKA, E., BRODY, H. & CSERJESI, P. 2009a. Sonic hedgehog signaling is required for sympathetic nervous system development. *NeuroReport,* 20**,** 684-688.

MORIKAWA, Y., ZEHIR, A., MASKA, E., DENG, C., SCHNEIDER, M. D., MISHINA, Y. & CSERJESI, P. 2009b. BMP signaling regulates sympathetic nervous system development through Smad4-dependent and-independent pathways. *Development,* 136**,** 3575-3584.

MOSS, E. G., LEE, R. C. & AMBROS, V. 1997. The cold shock domain protein LIN-28 controls developmental timing in C. elegans and is regulated by the lin-4 RNA. *Cell,* 88**,** 637-646.

MOSSE, Y. P., LAUDENSLAGER, M., KHAZI, D., CARLISLE, A. J., WINTER, C. L., RAPPAPORT, E. & MARIS, J. M. 2004. Germline PHOX2B mutation in hereditary neuroblastoma. *The American Journal of Human Genetics,* 75**,** 727-730.

MOSSÉ, Y. P., LAUDENSLAGER, M., LONGO, L., COLE, K. A., WOOD, A., ATTIYEH, E. F., LAQUAGLIA, M. J., SENNETT, R., LYNCH, J. E., PERRI, P., LAUREYS, G., SPELEMAN, F., KIM, C., HOU, C., HAKONARSON, H., TORKAMANI, A., SCHORK, N. J., BRODEUR, G. M., TONINI, G. P., RAPPAPORT, E., DEVOTO, M. & MARIS, J. M. 2008. Identification of ALK as a major familial neuroblastoma predisposition gene. *Nature,* 455**,** 930-935.

MUÑOZ-PINEDO, C., EL MJIYAD, N. & RICCI, J. E. 2012. Cancer metabolism: current perspectives and future directions. *Cell Death & Disease,* 3**,** e248-e248.

MURKO, C., VIECELI, F. M. & BRONNER, M. 2018. Transcriptome dataset of trunk neural crest cells migrating along the ventral pathway of chick embryos. *Data in brief,* 21**,** 2547-2553.

MUTH, D., GHAZARYAN, S., ECKERLE, I., BECKETT, E., PÖHLER, C., BATZLER, J., BEISEL, C., GOGOLIN, S., FISCHER, M., HENRICH, K. O., EHEMANN, V., GILLESPIE, P., SCHWAB, M. & WESTERMANN, F. 2010. Transcriptional repression of SKP2 is impaired in MYCN-amplified neuroblastoma. *Cancer Res,* 70**,** 3791-802.

NAKAGAWARA, A., AZAR, C. G., SCAVARDA, N. J. & BRODEUR, G. M. 1994. Expression and function of TRK-B and BDNF in human neuroblastomas. *Mol Cell Biol,* 14**,** 759-67.

NARA, K., KUSAFUKA, T., YONEDA, A., OUE, T., SANGKHATHAT, S. & FUKUZAWA, M. 2007. Silencing of MYCN by RNA interference induces growth inhibition, apoptotic activity and cell differentiation in a neuroblastoma cell line with MYCN amplification. *Int J Oncol,* 30**,** 1189-96.

NEGRINI, S., GORGOULIS, V. G. & HALAZONETIS, T. D. 2010. Genomic instability — an evolving hallmark of cancer. *Nature Reviews Molecular Cell Biology,* 11**,** 220-228.

NEIJTS, R., SIMMINI, S., GIULIANI, F., VAN ROOIJEN, C. & DESCHAMPS, J. 2014. Region-specific regulation of posterior axial elongation during vertebrate embryogenesis. *Developmental Dynamics,* 243**,** 88-98.

NIKITINA, N., SAUKA-SPENGLER, T. & BRONNER-FRASER, M. 2008. Dissecting early regulatory relationships in the lamprey neural crest gene network. *Proceedings of the National Academy of Sciences,* 105**,** 20083-20088.

NIKLASSON, C. U., FREDLUND, E., MONNI, E., LINDVALL, J. M., KOKAIA, Z., HAMMARLUND, E. U., BRONNER, M. E. & MOHLIN, S. 2021. Hypoxia inducible factor-2α importance for migration, proliferation, and self-renewal of trunk neural crest cells. *Developmental Dynamics,* 250**,** 191-236.

NISEN, P. D., ZIMMERMAN, K. A., COTTER, S. V., GILBERT, F. & ALT, F. W. 1986. Enhanced expression of the N-myc gene in Wilms' tumors. *Cancer research,* 46**,** 6217-6222.

OCHIAI, H., TAKENOBU, H., NAKAGAWA, A., YAMAGUCHI, Y., KIMURA, M., OHIRA, M., OKIMOTO, Y., FUJIMURA, Y., KOSEKI, H., KOHNO, Y., NAKAGAWARA, A. & KAMIJO, T. 2010. Bmi1 is a MYCN target gene that regulates tumorigenesis through repression of KIF1Bbeta and TSLC1 in neuroblastoma. *Oncogene,* 29**,** 2681-90.

OH, Y., CHO, G. S., LI, Z., HONG, I., ZHU, R., KIM, M. J., KIM, Y. J., TAMPAKAKIS, E., TUNG, L., HUGANIR, R., DONG, X., KWON, C. & LEE, G. 2016. Functional Coupling with Cardiac Muscle Promotes Maturation of hPSC-Derived Sympathetic Neurons. *Cell Stem Cell,* 19**,** 95-106.

OLIVERA-MARTINEZ, I., HARADA, H., HALLEY, P. A. & STOREY, K. G. 2012. Loss of FGF-Dependent Mesoderm Identity and Rise of Endogenous Retinoid Signalling Determine Cessation of Body Axis Elongation. *PLOS Biology,* 10**,** e1001415.

OLSEN, R. R., OTERO, J. H., GARCÍA-LÓPEZ, J., WALLACE, K., FINKELSTEIN, D., REHG, J. E., YIN, Z., WANG, Y. D. & FREEMAN, K. W. 2017. MYCN induces neuroblastoma in primary neural crest cells. *Oncogene,* 36**,** 5075-5082.

OSAFUNE, K., CARON, L., BOROWIAK, M., MARTINEZ, R. J., FITZ-GERALD, C. S., SATO, Y., COWAN, C. A., CHIEN, K. R. & MELTON, D. A. 2008. Marked differences in differentiation propensity among human embryonic stem cell lines. *Nature Biotechnology,* 26**,** 313-315.

OTTO, T., HORN, S., BROCKMANN, M., EILERS, U., SCHÜTTRUMPF, L., POPOV, N., KENNEY, A. M., SCHULTE, J. H., BEIJERSBERGEN, R., CHRISTIANSEN, H., BERWANGER, B. & EILERS, M. 2009. Stabilization of N-Myc is a critical function of Aurora A in human neuroblastoma. *Cancer Cell,* 15**,** 67-78.

PASINI, D., BRACKEN, A. P., HANSEN, J. B., CAPILLO, M. & HELIN, K. 2007. The polycomb group protein Suz12 is required for embryonic stem cell differentiation. *Mol Cell Biol,* 27**,** 3769-79.

PFISTER, S., REMKE, M., BENNER, A., MENDRZYK, F., TOEDT, G., FELSBERG, J., WITTMANN, A., DEVENS, F., GERBER, N. U., JOOS, S., KULOZIK, A., REIFENBERGER, G., RUTKOWSKI, S., WIESTLER, O. D., RADLWIMMER, B., SCHEURLEN, W., LICHTER, P. & KORSHUNOV, A. 2009. Outcome Prediction in Pediatric Medulloblastoma Based on DNA Copy-Number Aberrations

of Chromosomes 6q and 17q and the MYC and MYCN Loci. *Journal of Clinical Oncology,* 27**,** 1627-1636.

PLANTAZ, D., VANDESOMPELE, J., VAN ROY, N., ŁASTOWSKA, M., BOWN, N., COMBARET, V., FAVROT, M., DELATTRE, O., MICHON, J. & BENARD, J. 2001. Comparative genomic hybridization (CGH) analysis of stage 4 neuroblastoma reveals high frequency of 11q deletion in tumors lacking MYCN amplification. *International journal of cancer,* 91**,** 680-686.

PLOUHINEC, J. L., ROCHE, D. D., PEGORARO, C., FIGUEIREDO, A. L., MACZKOWIAK, F., BRUNET, L. J., MILET, C., VERT, J. P., POLLET, N., HARLAND, R. M. & MONSORO-BURQ, A. H. 2014. Pax3 and Zic1 trigger the early neural crest gene regulatory network by the direct activation of multiple key neural crest specifiers. *Dev Biol,* 386**,** 461-72.

POMP, O., BROKHMAN, I., BEN-DOR, I., REUBINOFF, B. & GOLDSTEIN, R. S. 2005. Generation of peripheral sensory and sympathetic neurons and neural crest cells from human embryonic stem cells. *Stem Cells,* 23**,** 923-30.

PRADELLI, L. A., VILLA, E., ZUNINO, B., MARCHETTI, S. & RICCI, J. E. 2014. Glucose metabolism is inhibited by caspases upon the induction of apoptosis. *Cell Death & Disease,* 5**,** e1406-e1406.

RAABE, E. H., LAUDENSLAGER, M., WINTER, C., WASSERMAN, N., COLE, K., LAQUAGLIA, M., MARIS, D. J., MOSSE, Y. P. & MARIS, J. M. 2008. Prevalence and functional consequence of PHOX2B mutations in neuroblastoma. *Oncogene,* 27**,** 469-76.

RAMANI, P., HEADFORD, A. & MAY, M. T. 2013. GLUT1 protein expression correlates with unfavourable histologic category and high risk in patients with neuroblastic tumours. *Virchows Archiv,* 462**,** 203-209.

RANDOLPH, L. N., BAO, X., ZHOU, C. & LIAN, X. 2017. An all-in-one, Tet-On 3G inducible PiggyBac system for human pluripotent stem cells and derivatives. *Sci Rep,* 7**,** 1549.

REBBAA, A., CHOU, P. M. & MIRKIN, B. L. 2001. Factors secreted by human neuroblastoma mediated doxorubicin resistance by activating STAT3 and inhibiting apoptosis. *Mol Med,* 7**,** 393-400.

REISSMANN, E., ERNSBERGER, U., FRANCIS-WEST, P. H., RUEGER, D., BRICKELL, P. M. & ROHRER, H. 1996. Involvement of bone morphogenetic protein-4 and bone morphogenetic protein-7 in the differentiation of the adrenergic phenotype in developing sympathetic neurons. *Development,* 122**,** 2079-2088.

RHEINBAY, E., SUVÀ, M. L., GILLESPIE, S. M., WAKIMOTO, H., PATEL, A. P., SHAHID, M., OKSUZ, O., RABKIN, S. D., MARTUZA, R. L. & RIVERA, M. N. 2013. An aberrant transcription factor network essential for Wnt signaling and stem cell maintenance in glioblastoma. *Cell reports,* 3**,** 1567-1579.

RICKMAN, D. S., SCHULTE, J. H. & EILERS, M. 2018. The Expanding World of N-MYC-Driven Tumors. *Cancer Discov,* 8**,** 150-163.

RODRIGO ALBORS, A., HALLEY, P. A. & STOREY, K. G. 2018. Lineage tracing of axial progenitors using Nkx1-2CreER^{T2} mice defines their trunk and tail contributions. *Development,* 145**,** dev164319.

ROHRER, H. 2011. Transcriptional control of differentiation and neurogenesis in autonomic ganglia. *European Journal of Neuroscience,* 34**,** 1563-1573.

ROUAH, E., WILSON, D. R., ARMSTRONG, D. L. & DARLINGTON, G. J. 1989. N-myc amplification and neuronal differentiation in human primitive neuroectodermal tumors of the central nervous system. *Cancer research,* 49**,** 1797-1801.

RYCHLIK, J. L., GERBASI, V. & LEWIS, E. J. 2003. The interaction between dHAND and Arix at the dopamine beta-hydroxylase promoter region is independent of direct dHAND binding to DNA. *J Biol Chem,* 278**,** 49652-60.

RYL, T., KUCHEN, E. E., BELL, E., SHAO, C., FLÓREZ, A. F., MÖNKE, G., GOGOLIN, S., FRIEDRICH, M., LAMPRECHT, F., WESTERMANN, F. & HÖFER, T. 2017. Cell-Cycle Position of Single MYC-Driven Cancer Cells Dictates Their Susceptibility to a Chemotherapeutic Drug. *Cell Syst,* 5**,** 237-250.e8.

SAITO, D., TAKASE, Y., MURAI, H. & TAKAHASHI, Y. 2012. The Dorsal Aorta Initiates a Molecular Cascade That Instructs Sympatho-Adrenal Specification. *Science,* 336**,** 1578-1581.

SALIC, A. & MITCHISON, T. J. 2008. A chemical method for fast and sensitive detection of DNA synthesis in vivo. *Proceedings of the National Academy of Sciences,* 105**,** 2415-2420.

SATO, T., SASAI, N. & SASAI, Y. 2005. Neural crest determination by co-activation of Pax3 and Zic1 genes in Xenopus ectoderm. *Development,* 132**,** 2355-2363.

SAUKA-SPENGLER, T. & BRONNER-FRASER, M. 2008. A gene regulatory network orchestrates neural crest formation. *Nat Rev Mol Cell Biol,* 9**,** 557-68.

SAVELYEVA, L., CORVI, R. & SCHWAB, M. 1994. Translocation involving 1p and 17q is a recurrent genetic alteration of human neuroblastoma cells. *Am J Hum Genet,* 55**,** 334-40.

SAWAI, S., SHIMONO, A., WAKAMATSU, Y., PALMES, C., HANAOKA, K. & KONDOH, H. 1993. Defects of embryonic organogenesis resulting from targeted disruption of the N-myc gene in the mouse. *Development,* 117**,** 1445-55.

SCHLEIERMACHER, G., JANOUEIX-LEROSEY, I., RIBEIRO, A., KLIJANIENKO, J., COUTURIER, J., PIERRON, G., MOSSERI, V., VALENT, A., AUGER, N., PLANTAZ, D., RUBIE, H., VALTEAU-COUANET, D., BOURDEAUT, F., COMBARET, V., BERGERON, C., MICHON, J. & DELATTRE, O. 2010. Accumulation of Segmental Alterations Determines Progression in Neuroblastoma. *Journal of Clinical Oncology,* 28**,** 3122-3130.

SCHLEIERMACHER, G., MICHON, J., HUON, I., D'ENGHIEN, C. D., KLIJANIENKO, J., BRISSE, H., RIBEIRO, A., MOSSERI, V., RUBIE, H., MUNZER, C., THOMAS, C., VALTEAU-COUANET, D., AUVRIGNON, A., PLANTAZ, D., DELATTRE, O. & COUTURIER, J. 2007a. Chromosomal CGH identifies patients with a higher risk of relapse in neuroblastoma without MYCN amplification. *Br J Cancer,* 97**,** 238-46.

SCHLEIERMACHER, G., MICHON, J., HUON, I., D'ENGHIEN, C. D., KLIJANIENKO, J., BRISSE, H., RIBEIRO, A., MOSSERI, V., RUBIE, H., MUNZER, C., THOMAS, C., VALTEAU-COUANET, D., AUVRIGNON, A., PLANTAZ, D., DELATTRE, O., COUTURIER, J. & ON BEHALF OF THE SOCIÉTÉ FRANÇAISE DES CANCERS DE, L. E. 2007b. Chromosomal CGH identifies patients with a higher risk of relapse in neuroblastoma without MYCN amplification. *British Journal of Cancer,* 97**,** 238-246.

SCHLEIERMACHER, G., MICHON, J., RIBEIRO, A., PIERRON, G., MOSSERI, V., RUBIE, H., MUNZER, C., BÉNARD, J., AUGER, N., COMBARET, V., JANOUEIX-LEROSEY, I., PEARSON, A., TWEDDLE, D. A., BOWN, N., GERRARD, M., WHEELER, K., NOGUERA, R., VILLAMON, E., CAÑETE, A., CASTEL, V., MARQUES, B., DE LACERDA, A., TONINI, G. P., MAZZOCCO, K., DEFFERRARI, R., DE BERNARDI, B., DI CATALDO, A., VAN ROY, N., BRICHARD, B., LADENSTEIN, R., AMBROS, I., AMBROS, P., BEISKE, K., DELATTRE, O. & COUTURIER, J. 2011. Segmental chromosomal alterations lead to a higher risk of relapse in infants with MYCN-non-amplified localised unresectable/disseminated neuroblastoma (a SIOPEN collaborative study). *Br J Cancer,* 105**,** 1940-8.

SCHLEIERMACHER, G., MOSSERI, V., LONDON, W. B., MARIS, J. M., BRODEUR, G. M., ATTIYEH, E., HABER, M., KHAN, J., NAKAGAWARA, A., SPELEMAN, F., NOGUERA, R., TONINI, G. P., FISCHER, M., AMBROS, I., MONCLAIR, T., MATTHAY, K. K., AMBROS, P., COHN, S. L. & PEARSON, A. D. 2012. Segmental chromosomal alterations have prognostic impact in neuroblastoma: a report from the INRG project. *Br J Cancer,* 107**,** 1418-22.

SCHLIERF, B., LANG, S., KOSIAN, T., WERNER, T. & WEGNER, M. 2005. The High-mobility Group Transcription Factor Sox10 Interacts with the N-myc-interacting Protein Nmi. *Journal of Molecular Biology,* 353**,** 1033-1042.

SCHMITTGEN, T. D. & LIVAK, K. J. 2008. Analyzing real-time PCR data by the comparative C(T) method. *Nat Protoc,* 3**,** 1101-8.

SCHNEPP, R. W., KHURANA, P., ATTIYEH, E. F., RAMAN, P., CHODOSH, S. E., OLDRIDGE, D. A., GAGLIARDI, M. E., CONKRITE, K. L., ASGHARZADEH, S. & SEEGER, R. C. 2015. A LIN28B-RAN-AURKA signaling network promotes neuroblastoma tumorigenesis. *Cancer cell,* 28**,** 599-609.

SCHOENWOLF, G. C., CHANDLER, N. B. & SMITH, J. L. 1985. Analysis of the origins and early fates of neural crest cells in caudal regions of avian embryos. *Dev Biol,* 110**,** 467-79.
SCHULTE, J. H. & EGGERT, A. 2015. Neuroblastoma. *Crit Rev Oncog,* 20**,** 245-70.
SCHULTE, J. H., LINDNER, S., BOHRER, A., MAURER, J., DE PRETER, K., LEFEVER, S., HEUKAMP, L., SCHULTE, S., MOLENAAR, J., VERSTEEG, R., THOR, T., KÜNKELE, A., VANDESOMPELE, J., SPELEMAN, F., SCHORLE, H., EGGERT, A. & SCHRAMM, A. 2013. MYCN and ALKF1174L are sufficient to drive neuroblastoma development from neural crest progenitor cells. *Oncogene,* 32**,** 1059-65.
SCHWAB, M., ALITALO, K., KLEMPNAUER, K. H., VARMUS, H. E., BISHOP, J. M., GILBERT, F., BRODEUR, G., GOLDSTEIN, M. & TRENT, J. 1983. Amplified DNA with limited homology to myc cellular oncogene is shared by human neuroblastoma cell lines and a neuroblastoma tumour. *Nature,* 305**,** 245-8.
SCHWAB, M. & BISHOP, J. M. 1988. Sustained expression of the human protooncogene MYCN rescues rat embryo cells from senescence. *Proceedings of the National Academy of Sciences,* 85**,** 9585-9589.
SCHWAB, M., VARMUS, H. E. & BISHOP, J. M. 1985. Human N-myc gene contributes to neoplastic transformation of mammalian cells in culture. *Nature,* 316**,** 160-162.
SCULLY, D., KEANE, E., BATT, E., KARUNAKARAN, P., HIGGINS, D. F. & ITASAKI, N. 2016. Hypoxia promotes production of neural crest cells in the embryonic head. *Development,* 143**,** 1742-1752.
SEDELNIKOVA, O. A., PILCH, D. R., REDON, C. & BONNER, W. M. 2003. Histone H2AX in DNA damage and repair. *Cancer Biol Ther,* 2**,** 233-5.
SEDELNIKOVA, O. A., ROGAKOU, E. P., PANYUTIN, I. G. & BONNER, W. M. 2002. Quantitative detection of (125)IdU-induced DNA double-strand breaks with gamma-H2AX antibody. *Radiat Res,* 158**,** 486-92.
SEEGER, R. C., BRODEUR, G. M., SATHER, H., DALTON, A., SIEGEL, S. E., WONG, K. Y. & HAMMOND, D. 1985. Association of multiple copies of the N-myc oncogene with rapid progression of neuroblastomas. *N Engl J Med,* 313**,** 1111-6.
SELLECK, M. & BRONNER-FRASER, M. 1995. Origins of the avian neural crest: the role of neural plate-epidermal interactions. *Development,* 121**,** 525-538.
SERBEDZIJA, G. N., FRASER, S. E. & BRONNER-FRASER, M. 1990. Pathways of trunk neural crest cell migration in the mouse embryo as revealed by vital dye labelling. *Development,* 108**,** 605-12.
SHAH, N. M., GROVES, A. K. & ANDERSON, D. J. 1996. Alternative neural crest cell fates are instructively promoted by TGFbeta superfamily members. *Cell,* 85**,** 331-43.
SHEN, X., LIU, Y., HSU, Y.-J., FUJIWARA, Y., KIM, J., MAO, X., YUAN, G.-C. & ORKIN, S. H. 2008. EZH1 Mediates Methylation on Histone H3 Lysine 27 and Complements EZH2 in Maintaining Stem Cell Identity and Executing Pluripotency. *Molecular Cell,* 32**,** 491-502.
SHIMADA, H., AMBROS, I. M., DEHNER, L. P., HATA, J., JOSHI, V. V. & ROALD, B. 1999. Terminology and morphologic criteria of neuroblastic tumors: recommendations by the International Neuroblastoma Pathology Committee. *Cancer,* 86**,** 349-63.
SHIN, M., CHO, Y. S., PARK, Y.-J., KI-WOONG, S., HYUN, S. H., CHOI, J. Y. & LEE, K.-H. 2020. ¹⁸F-FDG Avidity and Correlation with Histopathologic and Cytogenetic Prognostic Factors in Neuroblastoma. *Journal of Nuclear Medicine,* 61**,** 115-115.
SIMÕES-COSTA, M. S., MCKEOWN, S. J., TAN-CABUGAO, J., SAUKA-SPENGLER, T. & BRONNER, M. E. 2012. Dynamic and differential regulation of stem cell factor FoxD3 in the neural crest is Encrypted in the genome. *PLoS Genet,* 8**,** e1003142.
SLACK, A., CHEN, Z., TONELLI, R., PULE, M., HUNT, L., PESSION, A. & SHOHET, J. M. 2005. The p53 regulatory gene MDM2 is a direct transcriptional target of MYCN in neuroblastoma. *Proc Natl Acad Sci U S A,* 102**,** 731-6.
SMALL, M. B., HAY, N., SCHWAB, M. & BISHOP, J. M. 1987. Neoplastic transformation by the human gene N-myc. *Molecular and cellular biology,* 7**,** 1638-1645.

SMITH, K. N., SINGH, A. M. & DALTON, S. 2010. Myc represses primitive endoderm differentiation in pluripotent stem cells. *Cell stem cell,* 7**,** 343-354.

SOLDATOV, R., KAUCKA, M., KASTRITI, M. E., PETERSEN, J., CHONTOROTZEA, T., ENGLMAIER, L., AKKURATOVA, N., YANG, Y., HÄRING, M., DYACHUK, V., BOCK, C., FARLIK, M., PIACENTINO, M. L., BOISMOREAU, F., HILSCHER, M. M., YOKOTA, C., QIAN, X., NILSSON, M., BRONNER, M. E., CROCI, L., HSIAO, W. Y., GUERTIN, D. A., BRUNET, J. F., CONSALEZ, G. G., ERNFORS, P., FRIED, K., KHARCHENKO, P. V. & ADAMEYKO, I. 2019. Spatiotemporal structure of cell fate decisions in murine neural crest. *Science,* 364.

SONG, L., ARA, T., WU, H. W., WOO, C. W., REYNOLDS, C. P., SEEGER, R. C., DECLERCK, Y. A., THIELE, C. J., SPOSTO, R. & METELITSA, L. S. 2007. Oncogene MYCN regulates localization of NKT cells to the site of disease in neuroblastoma. *J Clin Invest,* 117**,** 2702-12.

SPEIZER, L., HAUGLAND, R. & KUTCHAI, H. 1985. Asymmetric transport of a fluorescent glucose analogue by human erythrocytes. *Biochim Biophys Acta,* 815**,** 75-84.

SPITZ, R., HERO, B., ERNESTUS, K. & BERTHOLD, F. 2003. Deletions in chromosome arms 3p and 11q are new prognostic markers in localized and 4s neuroblastoma. *Clin Cancer Res,* 9**,** 52-8.

STALLINGS, R. L., CARTY, P., MCARDLE, L., MULLARKEY, M., MCDERMOTT, M., BREATNACH, F. & O'MEARA, A. 2004. Molecular cytogenetic analysis of recurrent unbalanced t(11;17) in neuroblastoma. *Cancer Genet Cytogenet,* 154**,** 44-51.

STAMOS, J. L. & WEIS, W. I. 2013. The β-catenin destruction complex. *Cold Spring Harbor perspectives in biology,* 5**,** a007898-a007898.

STANTON, L. W., SCHWAB, M. & BISHOP, J. M. 1986. Nucleotide sequence of the human N-myc gene. *Proceedings of the National Academy of Sciences of the United States of America,* 83**,** 1772-1776.

STARBORG, M., GELL, K., BRUNDELL, E. & HÖÖG, C. 1996. The murine Ki-67 cell proliferation antigen accumulates in the nucleolar and heterochromatic regions of interphase cells and at the periphery of the mitotic chromosomes in a process essential for cell cycle progression. *J Cell Sci,* 109 (Pt 1)**,** 143-53.

STARK, B., JEISON, M., GLASER-GABAY, L., BAR-AM, I., MARDOUKH, J., ASH, S., ATIAS, D., STEIN, J., ZAIZOV, R. & YANIV, I. 2003. der(11)t(11;17): a distinct cytogenetic pathway of advanced stage neuroblastoma (NBL) - detected by spectral karyotyping (SKY). *Cancer Lett,* 197**,** 75-9.

STEIN, J. M., MUMMERY, C. L. & BELLIN, M. 2020. Engineered models of the human heart: directions and challenges. *Stem Cell Reports*.

STEVENTON, B. & MARTINEZ ARIAS, A. 2017. Evo-engineering and the cellular and molecular origins of the vertebrate spinal cord. *Developmental Biology,* 432**,** 3-13.

STEWART, R. A., ARDUINI, B. L., BERGHMANS, S., GEORGE, R. E., KANKI, J. P., HENION, P. D. & LOOK, A. T. 2006. Zebrafish foxd3 is selectively required for neural crest specification, migration and survival. *Developmental Biology,* 292**,** 174-188.

STIGLIANI, S., COCO, S., MORETTI, S., OBERTHUER, A., FISCHER, M., THEISSEN, J., GALLO, F., GARAVENT, A., BERTHOLD, F., BONASSI, S., TONINI, G. P. & SCARUFFI, P. 2012. High genomic instability predicts survival in metastatic high-risk neuroblastoma. *Neoplasia (New York, N.Y.),* 14**,** 823-832.

STILLER, C. A. & PARKIN, D. M. 1992. International variations in the incidence of neuroblastoma. *Int J Cancer,* 52**,** 538-43.

STRENGER, V., KERBL, R., DORNBUSCH, H. J., LADENSTEIN, R., AMBROS, P. F., AMBROS, I. M. & URBAN, C. 2007. Diagnostic and prognostic impact of urinary catecholamines in neuroblastoma patients. *Pediatr Blood Cancer,* 48**,** 504-9.

SUBRAMANIAM, M. M., PIQUERAS, M., NAVARRO, S. & NOGUERA, R. 2009. Aberrant copy numbers of ALK gene is a frequent genetic alteration in neuroblastomas. *Hum Pathol,* 40**,** 1638-42.

SUENAGA, Y., ISLAM, S. M. R., ALAGU, J., KANEKO, Y., KATO, M., TANAKA, Y., KAWANA, H., HOSSAIN, S., MATSUMOTO, D., YAMAMOTO, M., SHOJI, W., ITAMI, M., SHIBATA, T., NAKAMURA, Y., OHIRA, M., HARAGUCHI, S., TAKATORI, A. & NAKAGAWARA, A. 2014. NCYM, a Cis-Antisense

Gene of MYCN, Encodes a De Novo Evolved Protein That Inhibits GSK3β Resulting in the Stabilization of MYCN in Human Neuroblastomas. *PLOS Genetics,* 10**,** e1003996.
SUSANTO, E., MARIN NAVARRO, A., ZHOU, L., SUNDSTRÖM, A., VAN BREE, N., STANTIC, M., MOSLEM, M., TAILOR, J., RIETDIJK, J., ZUBILLAGA, V., HÜBNER, J.-M., WEISHAUPT, H., WOLFSBERGER, J., ALAFUZOFF, I., NORDGREN, A., MAGNALDO, T., SIESJÖ, P., JOHNSEN, J. I., KOOL, M., TAMMIMIES, K., DARABI, A., SWARTLING, F. J., FALK, A. & WILHELM, M. 2020. Modeling SHH-driven medulloblastoma with patient iPS cell-derived neural stem cells. *Proceedings of the National Academy of Sciences,* 117**,** 20127-20138.
SZEWCZYK, K., WIECZOREK, A., MŁYNARSKI, W., JANCZAR, S., WOSZCZYK, M., GAMROT, Z., CHABER, R., WYSOCKI, M., POGORZAŁA, M., BIK-MULTANOWSKI, M. & BALWIERZ, W. 2019. Unfavorable Outcome of Neuroblastoma in Patients With 2p Gain. *Front Oncol,* 9**,** 1018.
TAKAHASHI, K., TANABE, K., OHNUKI, M., NARITA, M., ICHISAKA, T., TOMODA, K. & YAMANAKA, S. 2007. Induction of Pluripotent Stem Cells from Adult Human Fibroblasts by Defined Factors. *Cell,* 131**,** 861-872.
TAKEMOTO, T., UCHIKAWA, M., KAMACHI, Y. & KONDOH, H. 2006. Convergence of Wnt and FGF signals in the genesis of posterior neural plate through activation of the Sox2 enhancer N-1. *Development,* 133**,** 297-306.
TCHIEU, J., ZIMMER, B., FATTAHI, F., AMIN, S., ZELTNER, N., CHEN, S. & STUDER, L. 2017. A Modular Platform for Differentiation of Human PSCs into All Major Ectodermal Lineages. *Cell Stem Cell,* 21**,** 399-410.e7.
TELIAS, M. & BEN-YOSEF, D. 2014. Modeling neurodevelopmental disorders using human pluripotent stem cells. *Stem Cell Rev Rep,* 10**,** 494-511.
TERADA, Y., JO, N., ARAKAWA, Y., SAKAKURA, M., YAMADA, Y., UKAI, T., KABATA, M., MITSUNAGA, K., MINEHARU, Y., OHTA, S., NAKAGAWA, M., MIYAMOTO, S., YAMAMOTO, T. & YAMADA, Y. 2019. Human Pluripotent Stem Cell-Derived Tumor Model Uncovers the Embryonic Stem Cell Signature as a Key Driver in Atypical Teratoid/Rhabdoid Tumor. *Cell Rep,* 26**,** 2608-2621.e6.
THEISSEN, J., OBERTHUER, A., HOMBACH, A., VOLLAND, R., HERTWIG, F., FISCHER, M., SPITZ, R., ZAPATKA, M., BRORS, B., ORTMANN, M., SIMON, T., HERO, B. & BERTHOLD, F. 2014. Chromosome 17/17q gain and unaltered profiles in high resolution array-CGH are prognostically informative in neuroblastoma. *Genes Chromosomes Cancer,* 53**,** 639-49.
THÉVENEAU, E., DUBAND, J.-L. & ALTABEF, M. 2007. Ets-1 Confers Cranial Features on Neural Crest Delamination. *PLOS ONE,* 2**,** e1142.
THOMSON, J. A., ITSKOVITZ-ELDOR, J., SHAPIRO, S. S., WAKNITZ, M. A., SWIERGIEL, J. J., MARSHALL, V. S. & JONES, J. M. 1998. Embryonic stem cell lines derived from human blastocysts. *Science,* 282**,** 1145-7.
TJADEN, B., BAUM, K., MARQUARDT, V., SIMON, M., TRAJKOVIC-ARSIC, M., KOURIL, T., SIEBERS, B., LISEC, J., SIVEKE, J. T., SCHULTE, J. H., BENARY, U., REMKE, M., WOLF, J. & SCHRAMM, A. 2020. N-Myc-induced metabolic rewiring creates novel therapeutic vulnerabilities in neuroblastoma. *Scientific Reports,* 10**,** 7157.
TOMOLONIS, J. A., AGARWAL, S. & SHOHET, J. M. 2018. Neuroblastoma pathogenesis: deregulation of embryonic neural crest development. *Cell Tissue Res,* 372**,** 245-262.
TROCHET, D., BOURDEAUT, F., JANOUEIX-LEROSEY, I., DEVILLE, A., DE PONTUAL, L., SCHLEIERMACHER, G., COZE, C., PHILIP, N., FRÉBOURG, T. & MUNNICH, A. 2004. Germline mutations of the paired–like homeobox 2B (PHOX2B) gene in neuroblastoma. *The American Journal of Human Genetics,* 74**,** 761-764.
TSAKIRIDIS, A., HUANG, Y., BLIN, G., SKYLAKI, S., WYMEERSCH, F., OSORNO, R., ECONOMOU, C., KARAGIANNI, E., ZHAO, S., LOWELL, S. & WILSON, V. 2014. Distinct Wnt-driven primitive streak-like populations reflect in vivo lineage precursors. *Development,* 141**,** 1209-1221.
TSUBOTA, S., KISHIDA, S., SHIMAMURA, T., OHIRA, M., YAMASHITA, S., CAO, D., KIYONARI, S., USHIJIMA, T. & KADOMATSU, K. 2017. PRC2-Mediated Transcriptomic Alterations at the

Embryonic Stage Govern Tumorigenesis and Clinical Outcome in MYCN-Driven Neuroblastoma. *Cancer Research,* 77**,** 5259-5271.

TZOUANACOU, E., WEGENER, A., WYMEERSCH, F. J., WILSON, V. & NICOLAS, J.-F. 2009a. Redefining the Progression of Lineage Segregations during Mammalian Embryogenesis by Clonal Analysis. *Developmental Cell,* 17**,** 365-376.

TZOUANACOU, E., WEGENER, A., WYMEERSCH, F. J., WILSON, V. & NICOLAS, J. F. 2009b. Redefining the progression of lineage segregations during mammalian embryogenesis by clonal analysis. *Dev Cell,* 17**,** 365-76.

URBACH, A., SCHULDINER, M. & BENVENISTY, N. 2004. Modeling for Lesch-Nyhan disease by gene targeting in human embryonic stem cells. *Stem Cells,* 22**,** 635-41.

VALLI, E., TRAZZI, S., FUCHS, C., ERRIQUEZ, D., BARTESAGHI, R., PERINI, G. & CIANI, E. 2012. CDKL5, a novel MYCN-repressed gene, blocks cell cycle and promotes differentiation of neuronal cells. *Biochim Biophys Acta,* 1819**,** 1173-85.

VALSESIA-WITTMANN, S., MAGDELEINE, M., DUPASQUIER, S., GARIN, E., JALLAS, A. C., COMBARET, V., KRAUSE, A., LEISSNER, P. & PUISIEUX, A. 2004. Oncogenic cooperation between H-Twist and N-Myc overrides failsafe programs in cancer cells. *Cancer Cell,* 6**,** 625-30.

VAN DEN AKKER, E., FORLANI, S., CHAWENGSAKSOPHAK, K., DE GRAAFF, W., BECK, F., MEYER, B. I. & DESCHAMPS, J. 2002. Cdx1 and Cdx2 have overlapping functions in anteroposterior patterning and posterior axis elongation. *Development,* 129**,** 2181-2193.

VAN ROY, N., CHENG, N. C., LAUREYS, G., OPDENAKKER, G., VERSTEEG, R. & SPELEMAN, F. 1995. Molecular cytogenetic analysis of 1;17 translocations in neuroblastoma. *Eur J Cancer,* 31a**,** 530-5.

VAN ROY, N., LAUREYS, G., VAN GELE, M., OPDENAKKER, G., MIURA, R., VAN DER DRIFT, P., CHAN, A., VERSTEEG, R. & SPELEMAN, F. 1997. Analysis of 1;17 translocation breakpoints in neuroblastoma: implications for mapping of neuroblastoma genes. *European Journal of Cancer,* 33**,** 1974-1978.

VANNESTE, D., TAKAGI, M., IMAMOTO, N. & VERNOS, I. 2009. The Role of Hklp2 in the Stabilization and Maintenance of Spindle Bipolarity. *Current Biology,* 19**,** 1712-1717.

VARLEY, J. E. & MAXWELL, G. D. 1996. BMP-2 and BMP-4, but not BMP-6, increase the number of adrenergic cells which develop in quail trunk neural crest cultures. *Exp Neurol,* 140**,** 84-94.

VARLEY, J. E., WEHBY, R. G., RUEGER, D. C. & MAXWELL, G. D. 1995. Number of adrenergic and islet-1 immunoreactive cells is increased in avian trunk neural crest cultures in the presence of human recombinant osteogenic protein-1. *Dev Dyn,* 203**,** 434-47.

VIRCHOW, R. 1864. Hyperplasie der Zirbel und der Nebennieren. *Die Krankhaften Geschwulste,* 2**,** 1864-1865.

VISVADER, J. E. 2011. Cells of origin in cancer. *Nature,* 469**,** 314-322.

VISWANATHAN, S. R., POWERS, J. T., EINHORN, W., HOSHIDA, Y., NG, T. L., TOFFANIN, S., O'SULLIVAN, M., LU, J., PHILLIPS, L. A. & LOCKHART, V. L. 2009. Lin28 promotes transformation and is associated with advanced human malignancies. *Nature genetics,* 41**,** 843-848.

VOGEL, K. S. & WESTON, J. A. 1990. The sympathoadrenal lineage in avian embryos. I. Adrenal chromaffin cells lose neuronal traits during embryogenesis. *Dev Biol,* 139**,** 1-12.

WAKAMATSU, Y., WATANABE, Y., NAKAMURA, H. & KONDOH, H. 1997. Regulation of the neural crest cell fate by N-myc: promotion of ventral migration and neuronal differentiation. *Development,* 124**,** 1953-1962.

WANG, L., TAN, T. K., DURBIN, A. D., ZIMMERMAN, M. W., ABRAHAM, B. J., TAN, S. H., NGOC, P. C. T., WEICHERT-LEAHEY, N., AKAHANE, K., LAWTON, L. N., ROKITA, J. L., MARIS, J. M., YOUNG, R. A., LOOK, A. T. & SANDA, T. 2019. ASCL1 is a MYCN- and LMO1-dependent member of the adrenergic neuroblastoma core regulatory circuitry. *Nature Communications,* 10**,** 5622.

WANG, L. L., SUGANUMA, R., IKEGAKI, N., TANG, X., NARANJO, A., MCGRADY, P., LONDON, W. B., HOGARTY, M. D., GASTIER-FOSTER, J. M., LOOK, A. T., PARK, J. R., MARIS, J. M., COHN, S. L.,

SEEGER, R. C. & SHIMADA, H. 2013a. Neuroblastoma of undifferentiated subtype, prognostic significance of prominent nucleolar formation, and MYC/MYCN protein expression: a report from the Children's Oncology Group. *Cancer,* 119**,** 3718-26.

WANG, L. L., TESHIBA, R., IKEGAKI, N., TANG, X. X., NARANJO, A., LONDON, W. B., HOGARTY, M. D., GASTIER-FOSTER, J. M., LOOK, A. T., PARK, J. R., MARIS, J. M., COHN, S. L., SEEGER, R. C., ASGHARZADEH, S. & SHIMADA, H. 2015. Augmented expression of MYC and/or MYCN protein defines highly aggressive MYC-driven neuroblastoma: a Children's Oncology Group study. *British journal of cancer,* 113**,** 57-63.

WANG, M., ZHOU, C., SUN, Q., CAI, R., LI, Y., WANG, D. & GONG, L. 2013b. ALK amplification and protein expression predict inferior prognosis in neuroblastomas. *Experimental and Molecular Pathology,* 95**,** 124-130.

WANG, T., LIU, L., CHEN, X., SHEN, Y., LIAN, G., SHAH, N., DAVIDOFF, A. M., YANG, J. & WANG, R. 2018. MYCN drives glutaminolysis in neuroblastoma and confers sensitivity to an ROS augmenting agent. *Cell Death & Disease,* 9**,** 220.

WANG, Y.-C., CHEN, Y.-L., YUAN, R.-H., PAN, H.-W., YANG, W.-C., HSU, H.-C. & JENG, Y.-M. 2010. Lin-28B expression promotes transformation and invasion in human hepatocellular carcinoma. *Carcinogenesis,* 31**,** 1516-1522.

WARTIOVAARA, K., BARNABÉ-HEIDER, F., MILLER, F. D. & KAPLAN, D. R. 2002. N-myc Promotes Survival and Induces S-Phase Entry of Postmitotic Sympathetic Neurons. *The Journal of Neuroscience,* 22**,** 815-824.

WEISS, W. A., ALDAPE, K., MOHAPATRA, G., FEUERSTEIN, B. G. & BISHOP, J. M. 1997. Targeted expression of MYCN causes neuroblastoma in transgenic mice. *The EMBO journal,* 16**,** 2985-2995.

WESTERMARK, U. K., WILHELM, M., FRENZEL, A. & HENRIKSSON, M. A. 2011. The MYCN oncogene and differentiation in neuroblastoma. *Seminars in Cancer Biology,* 21**,** 256-266.

WILSON, V. & BEDDINGTON, R. S. 1996. Cell fate and morphogenetic movement in the late mouse primitive streak. *Mech Dev,* 55**,** 79-89.

WONG, M., SUN, Y., XI, Z., MILAZZO, G., POULOS, R. C., BARTENHAGEN, C., BELL, J. L., MAYOH, C., HO, N., TEE, A. E., CHEN, X., LI, Y., CIACCIO, R., LIU, P. Y., JIANG, C. C., LAN, Q., JAYATILLEKE, N., CHEUNG, B. B., HABER, M., NORRIS, M. D., ZHANG, X. D., MARSHALL, G. M., WANG, J. Y., HÜTTELMAIER, S., FISCHER, M., WONG, J. W. H., XU, H., PERINI, G., DONG, Q., GEORGE, R. E. & LIU, T. 2019. JMJD6 is a tumorigenic factor and therapeutic target in neuroblastoma. *Nature Communications,* 10**,** 3319.

WOOLSTON, C. & MARTIN, S. 2011. Analysis of Tumor and Endothelial Cell Viability and Survival Using Sulforhodamine B and Clonogenic Assays. *In:* STODDART, M. J. (ed.) *Mammalian Cell Viability: Methods and Protocols.* Totowa, NJ: Humana Press.

WRIGHT, J. H. 1910. NEUROCYTOMA OR NEUROBLASTOMA, A KIND OF TUMOR NOT GENERALLY RECOGNIZED. *The Journal of experimental medicine,* 12**,** 556-561.

WU, J., FAN, Y. & TZANAKAKIS, E. S. 2015. Increased culture density is linked to decelerated proliferation, prolonged G1 phase, and enhanced propensity for differentiation of self-renewing human pluripotent stem cells. *Stem cells and development,* 24**,** 892-903.

WU, L. C., WANG, Z. W., TSAN, J. T., SPILLMAN, M. A., PHUNG, A., XU, X. L., YANG, M. C., HWANG, L. Y., BOWCOCK, A. M. & BAER, R. 1996. Identification of a RING protein that can interact in vivo with the BRCA1 gene product. *Nat Genet,* 14**,** 430-40.

WU, Z.-Q., BRABLETZ, T., FEARON, E., WILLIS, A. L., HU, C. Y., LI, X.-Y. & WEISS, S. J. 2012. Canonical Wnt suppressor, Axin2, promotes colon carcinoma oncogenic activity. *Proceedings of the National Academy of Sciences,* 109**,** 11312-11317.

WYLIE, L. A., HARDWICK, L. J., PAPKOVSKAIA, T. D., THIELE, C. J. & PHILPOTT, A. 2015. Ascl1 phospho-status regulates neuronal differentiation in a Xenopus developmental model of neuroblastoma. *Disease models & mechanisms,* 8**,** 429-441.

WYMEERSCH, F. J., HUANG, Y., BLIN, G., CAMBRAY, N., WILKIE, R., WONG, F. C. & WILSON, V. 2016. Position-dependent plasticity of distinct progenitor types in the primitive streak. *Elife,* 5**,** e10042.

XU, H., FIRULLI, A. B., ZHANG, X. & HOWARD, M. J. 2003. HAND2 synergistically enhances transcription of dopamine-beta-hydroxylase in the presence of Phox2a. *Dev Biol,* 262**,** 183-93.

YAMAGUCHI, T. P., TAKADA, S., YOSHIKAWA, Y., WU, N. & MCMAHON, A. P. 1999. T (Brachyury) is a direct target of Wnt3a during paraxial mesoderm specification. *Genes Dev,* 13**,** 3185-90.

YANG, C.-L., SERRA-ROMA, A., GUALANDI, M., BODMER, N., NIGGLI, F., SCHULTE, J. H., BODE, P. K. & SHAKHOVA, O. 2020a. Lineage-restricted sympathoadrenal progenitors confer neuroblastoma origin and its tumorigenicity. *Oncotarget,* 11**,** 2357-2371.

YANG, C. L., SERRA-ROMA, A., GUALANDI, M., BODMER, N., NIGGLI, F., SCHULTE, J. H., BODE, P. K. & SHAKHOVA, O. 2020b. Lineage-restricted sympathoadrenal progenitors confer neuroblastoma origin and its tumorigenicity. *Oncotarget,* 11**,** 2357-2371.

YOGEV, O., ALMEIDA, G. S., BARKER, K. T., GEORGE, S. L., KWOK, C., CAMPBELL, J., ZAROWIECKI, M., KLEFTOGIANNIS, D., SMITH, L. M., HALLSWORTH, A., BERRY, P., MÖCKLINGHOFF, T., WEBBER, H. T., DANIELSON, L. S., BUTTERY, B., CALTON, E. A., DA COSTA, B. M., POON, E., JAMIN, Y., LISE, S., VEAL, G. J., SEBIRE, N., ROBINSON, S. P., ANDERSON, J. & CHESLER, L. 2019. In Vivo Modeling of Chemoresistant Neuroblastoma Provides New Insights into Chemorefractory Disease and Metastasis. *Cancer Research,* 79**,** 5382-5393.

YOSHIDA, K. & MIKI, Y. 2004. Role of BRCA1 and BRCA2 as regulators of DNA repair, transcription, and cell cycle in response to DNA damage. *Cancer Science,* 95**,** 866-871.

YOUNG, T., ROWLAND, J. E., VAN DE VEN, C., BIALECKA, M., NOVOA, A., CARAPUCO, M., VAN NES, J., DE GRAAFF, W., DULUC, I. & FREUND, J.-N. 2009. Cdx and Hox genes differentially regulate posterior axial growth in mammalian embryos. *Developmental cell,* 17**,** 516-526.

YU, J., VODYANIK, M. A., SMUGA-OTTO, K., ANTOSIEWICZ-BOURGET, J., FRANE, J. L., TIAN, S., NIE, J., JONSDOTTIR, G. A., RUOTTI, V. & STEWART, R. 2007. Induced pluripotent stem cell lines derived from human somatic cells. *science,* 318**,** 1917-1920.

ZHANG, M., VANDANA, J. J., LACKO, L. & CHEN, S. 2020. Modeling cancer progression using human pluripotent stem cell-derived cells and organoids. *Stem Cell Research,* 49**,** 102063.

ZHAO, X., D, D. A., LIM, W. K., BRAHMACHARY, M., CARRO, M. S., LUDWIG, T., CARDO, C. C., GUILLEMOT, F., ALDAPE, K., CALIFANO, A., IAVARONE, A. & LASORELLA, A. 2009. The N-Myc-DLL3 cascade is suppressed by the ubiquitin ligase Huwe1 to inhibit proliferation and promote neurogenesis in the developing brain. *Dev Cell,* 17**,** 210-21.

ZHU, S., LEE, J.-S., GUO, F., SHIN, J., PEREZ-ATAYDE, A. R., KUTOK, J. L., RODIG, S. J., NEUBERG, D. S., HELMAN, D. & FENG, H. 2012. Activated ALK collaborates with MYCN in neuroblastoma pathogenesis. *Cancer cell,* 21**,** 362-373.

ZIMMERMAN, L. B., DE JESÚS-ESCOBAR, J. M. & HARLAND, R. M. 1996. The Spemann organizer signal noggin binds and inactivates bone morphogenetic protein 4. *Cell,* 86**,** 599-606.

ZINS, K., SCHÄFER, R., PAULUS, P., DOBLER, S., FAKHARI, N., SIOUD, M., AHARINEJAD, S. & ABRAHAM, D. 2016. Frizzled2 signaling regulates growth of high-risk neuroblastomas by interfering with β-catenin-dependent and β-catenin-independent signaling pathways. *Oncotarget,* 7**,** 46187-46202.